

THESIS

SPECTRAL GAMMA RAY CHARACTERIZATION OF THE ELKO FORMATION,  
NEVADA—A CASE STUDY FOR A SMALL LACUSTRINE BASIN

Submitted by

Erin M. McGowan

Department of Geosciences

In partial fulfillment of the requirements

For the Degree of Master of Science

Colorado State University

Fort Collins, Colorado

Summer 2015

Master's Committee:

Advisor: Sven O. Egenhoff

Derek Schutt

Gamze Cavdar

Robert Amerman

Copyright by Erin M. McGowan 2015

All Rights Reserved

## ABSTRACT

### SPECTRAL GAMMA RAY CHARACTERIZATION OF THE ELKO FORMATION, NEVADA—A CASE STUDY FOR A SMALL LACUSTRINE BASIN

Handheld gamma ray spectrometry is a cost-effective and time-efficient means of furthering understanding of lake facies and small-scale lake systems. Spectral and total gamma ray data were recorded every foot vertically through a succession *in situ* at four outcrops along a NNW-to-SSE transect representing the lower to middle Eocene Elko Formation in northeast Nevada, USA. The lacustrine Elko Formation consists of, from oldest to youngest, four major units: 1) a basal conglomerate, 2) an overlying carbonate, 3) a fine-grained organic-rich mudstone with intercalated carbonate mudstones, and 4) volcanoclastics. These units comprise fourteen sedimentological facies identifiable in outcrop. In this study, these fourteen facies have been reduced to eight that are discernable by spectral gamma ray (SGR) signals. Each recorded interval in the Elko Formation succession was assigned to one of these eight facies. These eight facies comprise five siliciclastic (plant-bearing mudstone, clay-dominated mudstone, microbial-mat-bearing mudstone, ash-bearing mudstone, and conglomerate) facies, two carbonate (calcareous mudstone and fossiliferous mudstone-wackestone) facies, and one volcanic tuff facies.

In conjunction with SGR, outcrop observation, X-ray diffraction (XRD), thin section observation, and total organic carbon (TOC) analyses allowed a thorough understanding of facies composition and its SGR signal. The primary controls of SGR components [potassium (K), uranium (U), and thorium (Th)] reflect K-bearing volcanic minerals (feldspars and micas), U-enriched organic material, and clay abundance (illite and montmorillonite; potentially derived

from volcanic ash), respectively. High radioactivity, with signals above 120 American Petroleum Institute (API) units, was demonstrated for five facies (plant-bearing mudstone, clay-dominated mudstone, microbial-mat-bearing mudstone, ash-bearing mudstone, and volcanic tuff) in contrast to the remaining three facies (calcareous mudstone, fossiliferous mudstone-packstone, and conglomerate) exhibiting low radioactivity of less than or equal to 120 API. Distribution of radioactive minerals across the outcrops was largely found to be not only a function of general lithologic composition, but also the paleogeographic locations of the outcrops within the lake basin, due to the differing contributions of organic debris and volcanic constituents. This distribution of radioactive minerals across each outcrop supports a recent depositional model of north-to-south diachronous deposition of the Elko Formation (Horner, 2015).

The microbial-mat-bearing mudstone facies was a traceable, deep-lake sediment throughout the basin by which outcrops could be assigned to more proximal or more distal positions within the paleo-lake by applying Th/U ratios. The proximal outcrop data show a low Th/U ratio (below 2.5), as opposed to the distal outcrop data that have a high Th/U ratio (2.5–4). These data confirm that most likely Th/U ratios reflect the increase in the amount of clay with distance from the proximal outcrops.

Thin section microscopy and scanning electron microscope (SEM) analyses allowed for recognition of eight diagenetic cements reflecting a strongly varying diagenetic history in the Elko Formation sedimentary rocks. One calcite, four stages of dolomite, two types of silica, and one zeolite cement were identified. The calcite, dolomite, and silica cements were typically formed sequentially as listed above, whereas the zeolites formed independently. Intraparticle, interparticle, matrix, shelter, and fracture porosity types are also present, each forming post-deposition, except for interparticle and matrix porosity within volcanoclastics. Calcite, dolomite,

and silica cements were found succeeding shelter and fracture porosity, whereas the timing of zeolite cement in matrix porosity was unclear. Overall, cement phases and porosity were found to be minimal, and therefore, probably had only a minor influence on the overall gamma ray signal of the Elko Formation sedimentary rocks.

SGR characterization of each of the eight facies across a proximal-to-distal transect of the Elko continental-lacustrine sedimentary basin reflects the strong influence that climate and tectonics have on depositional changes in a small-scale lake. Applying gamma ray techniques to the small-scale lake system of the Elko Formation was found to be a useful tool and provides a framework to apply to lacustrine studies as a predictive tool in future exploration.

## ACKNOWLEDGEMENTS

I'm thankful to my advisor, Dr. Sven Egenhoff for the many hours of editing, reviewing, and feedback on this study, as well as helping to improve my writing.

I'm incredibly grateful to Noble Energy for providing financial support to carry out this research over the past two years —as well as the feedback and genuine interest in the project: Thank you Rob Amerman, Morgan Hocker, Donald Burch, Rick Stucker, and Wendell Bond. From the last field season, thanks to Jon Bowman for arranging a track-hoe for field excavations. I would also like further thank Donald Burch for the time he spent to helping guide this project and giving me insightful suggestions.

Many thanks to Heather Lowers at the USGS for her assistance with the SEM and EDS analyses as well as Joe Taglieri from Atoka Geochemical for his XRD services. Each greatly enhanced this work and are much appreciated.

I'm also thankful to the Tomera family for allowing us to study the Elko succession on their property and even to excavate the outcrop. Will Horner, Sven Egenhoff, and Rob Amerman, thank you for the enthusiasm and help in the field.

I would also like to express my gratitude to my committee members, Dr. Sven Egenhoff, Dr. Gamze Cavdar, and Dr. Rob Amerman for their comments and suggestions to improve the quality of my thesis. CSU sedimentology group, thank you for your support and laughs to make this a great place to work.

Finally, a big thank you to my family and Travis Moss for their love, continuous support, and patience.

## TABLE OF CONTENTS

ABSTRACT.....	ii
ACKNOWLEDGEMENTS.....	v
1.0 INTRODUCTION .....	1
2.0 GEOLOGICAL SETTING .....	5
2.1 Regional Tectonism and Volcanism .....	5
2.2 Paleogeography and Paleontology.....	7
2.3 Basin Extents and Shape.....	7
2.4 Stratigraphy.....	8
3.0 REVIEW OF PREVIOUS LITERATURE.....	12
3.1 Elko Formation .....	12
3.2 Gamma Radiation and Spectral Gamma Ray: Potassium, Thorium, and Uranium.....	21
3.3 Gamma Ray Spectrometer Measurements.....	23
4.0 METHODOLOGY .....	25
4.1 Study Area .....	25
4.2 Gamma Ray Spectrometer Tool.....	26
4.3 Field Methods .....	27
4.4 Thin section, Total Organic Carbon, X-Ray Diffraction/Fluorescence.....	30
5.0 RESULTS .....	32
5.1 Total Gamma Ray Data .....	32
5.2 Spectral Gamma Ray Measurements .....	36
5.2.1 Facies 1/2: Plant-Bearing Mudstone (Fig. 13A).....	39
5.2.2 Facies 3: Clay-Dominated Mudstone (Fig. 13B).....	39
5.2.3 Facies 4: Calcareous Mudstone (Fig. 13C).....	39
5.2.4 Facies 5: Microbial-Mat-Bearing-Mudstone (Fig. 13D) .....	39
5.2.5 Facies 6: Ash-Bearing Mudstone (Fig. 13E) .....	40
5.2.6 Facies 8/13: Fossiliferous mudstone-packstone (Fig. 13F) .....	40
5.2.7 Facies 10–12: Volcanic Tuff (Fig. 13G).....	40
5.2.8 Facies 14: Conglomerate (Fig. 13H).....	41
5.2.9 Cumulative Data (Fig. 13I) .....	41

5.3 Th/U by Outcrop .....	46
5.4 X-Ray Diffraction and Total Organic Carbon .....	47
6.0 INTERPRETATION.....	50
6.1 Gamma Ray Log Signature.....	50
6.2 Spectral Gamma Ray (SGR) Signature.....	50
6.2.1 Outcrop Trends .....	53
6.2.2 Facies 1/2: Plant-Bearing Mudstone.....	54
6.2.3 Facies 3: Clay-Dominated Mudstone.....	55
6.2.4 Facies 4: Calcareous Mudstone .....	56
6.2.5 Facies 5: Microbial-Mat-Bearing Mudstone.....	56
6.2.6 Facies 6: Ash-Bearing Mudstone.....	57
6.2.7 Facies 8/13: Fossiliferous mudstone-packstone.....	58
6.2.8 Facies 10-12: Volcanic Tuff .....	59
6.2.9 Facies 14: Conglomerate.....	59
6.3 Th/U Trends and Basin Application .....	60
6.4 X-Ray Diffraction and Total Organic Carbon .....	61
7.0 DIAGENESIS .....	63
7.1 Carbonate .....	63
7.1.1 Calcite .....	63
7.1.2 Dolomite .....	63
7.2 Quartz.....	64
7.3 Zeolites.....	65
7.4 Porosity .....	67
7.4.1 Interparticle Porosity.....	67
7.4.2 Intraparticle Porosity.....	67
7.4.3 Shelter Porosity .....	68
7.4.4 Matrix Porosity .....	68
7.4.5 Fracture Porosity .....	68
7.5 Relative Timing .....	70
7.5.1 Calcite .....	70
7.5.2 Dolomite .....	70

7.5.3 Quartz.....	70
7.5.4 Zeolite .....	71
7.5.5 Porosity .....	72
8.0 DISCUSSION .....	74
8.1 Pitfalls of gamma ray spectrometry .....	74
8.2 Comparison of gamma ray readings with similar previous studies .....	75
8.3 Diagenetic effect on gamma ray readings.....	76
8.4 Application of Th/U ratios to analyze lacustrine basin extents .....	78
8.5 Assigned facies .....	79
8.6 Interpretation of SGR data .....	80
8.7 Comparison to Noble Energy EOS-3 core SGR data .....	81
9.0 CONCLUSIONS.....	84
REFERENCES .....	88
APPENDICES .....	96
APPENDIX 1: OUTCROP GAMMA RAY DATA.....	97
APPENDIX 2: GAMMA RAY DATA SUMMARY STATISTICS .....	122
APPENDIX 3: GAMMA RAY MEASUREMENT ACCURACY EXPERIMENTS .....	133
APPENDIX 4: TOC ANALYSES.....	137
APPENDIX 5: X-RAY DIFFRACTION ANALYSES.....	138
APPENDIX 6: FREQUENCY DISTRIBUTION CHARTS .....	139
APPENDIX 7: SCANNING ELECTRON MICROSCOPE ANALYSES.....	147
APPENDIX 8: GAMMA RAY CURVES.....	172
APPENDIX 9: CROSS-PLOTS (K, U, & TH VS. TOTAL GAMMA RAY) .....	181

## 1.0 INTRODUCTION

With increasing interest in unconventional resources aided by new technologies, it is becoming apparent how little is known about lacustrine facies aside from the Green River Formation of Colorado, Utah, and Wyoming (Burton et al., 2014; Carroll and Bohacs, 2001; Fischer and Roberts, 1991; Surdam and Stanley, 1979 and others). Emphasis thus far has been focused on black shale marine systems, but organic-rich lake basins are gaining popularity as exploration targets not only in China, Indonesia, and Brazil (Carroll and Bohacs, 2001; Hanson et al., 2001; Katz and Lin, 2014). As the attractiveness of these unconventional reservoirs intensifies, the necessity of characterizing lacustrine black shale facies, understanding their depositional environments, and predicting their varying gamma ray signatures for non-cored wells becomes equally important.

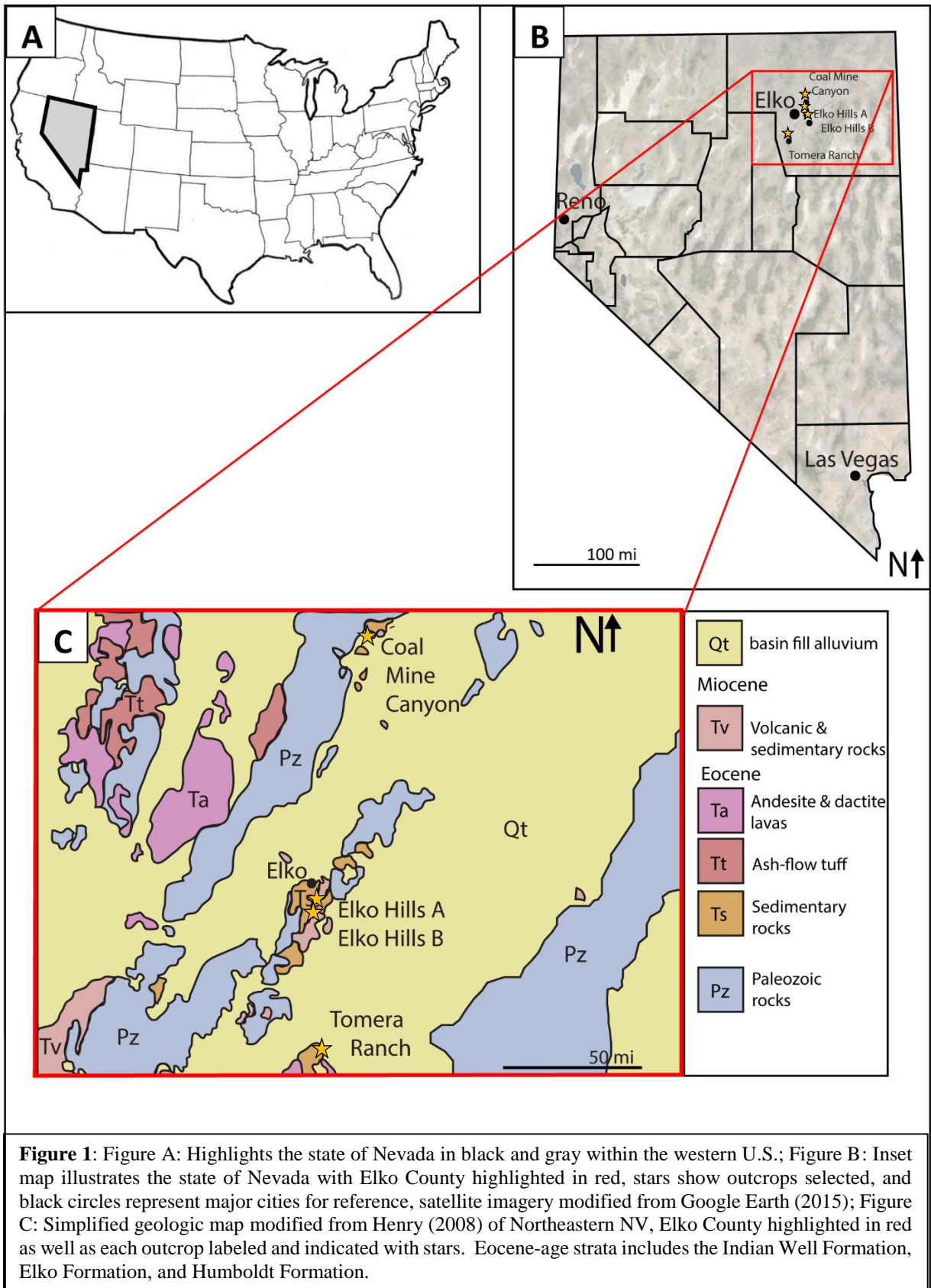
For the past several decades, initial exploration in potential hydrocarbon reservoirs consisted of measuring natural gamma radiation to differentiate between shale and non-shale intervals, while the spectral gamma ray (SGR) technique was used to subdivide the homogenous marine black shale intervals by fine-scale changes in potassium (K), uranium (U), and thorium (Th) distribution that reflected minute mineralogic differences (Fertl and Chilingarian, 1990; Blum et al., 1997; IAEA, 2003). Gamma ray curves have been a valuable tool used to correlate exposures in outcrop to the subsurface (Aigner et al., 1995). Handheld gamma ray spectrometry has been conducted in several outcrop studies with varying objectives such as sequence stratigraphic analysis and reservoir characterization in seemingly homogeneous lithologies (i.e. black shales) (Aigner et al., 1995), optimizing stratigraphic mapping and correlating stratigraphic sections within a basin (Chamberlain, 1984; Slatt et al., 1992), and applying integrated geochemical

analyses and mineralogy to better understand the gamma ray log signature and related facies (Wignall and Myers, 1988; Krystyniak, 2003; Aufill, 2007; Guagliardi et al., 2013).

Thorium-to-uranium (Th/U) ratios within marine basins have proved exceptionally useful in determining sediment provenance, sequence stratigraphic surfaces, facies descriptions, and basin analysis, but remain uninvestigated in lacustrine settings (Adams and Weaver, 1958; Bohacs, 1998; Ehrenberg and Svånå, 2001). With the lack of SGR research in lacustrine systems, examining the log character for non-marine systems in greater detail provides the necessary step to furthering knowledge of less explored unconventional hydrocarbon reservoirs containing vast reserves such as those found in East Asia and South America (Katz and Lin, 2014).

This study aims at providing a detailed description of the mineralogical composition and its influence on the log signature using the Elko Formation of northeastern Nevada, USA, as an example for a small lacustrine basin. This investigation is also intended to guide future studies, especially for relatively small lacustrine systems and the heterogenetic distribution of facies. The objectives of this research are: 1) assess the utility of SGR as a predictive exploration tool for a small lacustrine basin 2) quantifying a range for cumulative API units, and as K, Th, and U spectra for the eight main facies described for the upper Elko Formation, 3) assess the contribution of diagenetic phases, and its overall effect on the gamma ray signal, 4) analyzing proximal versus distal microbial-mat-bearing mudstone facies of the lake basin by quantifying the amount of terrigenous material and sediment influx through Th/U ratios, and 5) evaluate the previous depositional model by Horner (2015) constructed for the Elko Formation. In order to conduct this research, a portable, handheld gamma ray spectrometer was used to directly measure gamma radiation *in situ* at all four available outcrops: Coal Mine Canyon, Elko Hills A, Elko Hills B, and Tomera Ranch (Fig. 1). These outcrops represent the upper Elko Formation in northeastern,

Nevada from NNW to SSE, respectively, and provide a proximal-to-distal transect necessary to improve understanding of the distribution of facies within small-lake systems.



## 2.0 GEOLOGICAL SETTING

### 2.1 Regional Tectonism and Volcanism

In the late Paleozoic and early Mesozoic, northeastern Nevada experienced compressional tectonic movements as a result of oceanic plate subduction under the North American craton during a ~100 Ma time-span, creating the Antler orogen prominent in present-day Idaho, California, and Nevada (DeCelles, 2004; Henry, 2008). In northeastern Nevada, the Antler Orogeny formed the Roberts Mountains thrust where deep-water siliciclastics were pushed over shelf and slope rocks west of the present-day location of the thrust (Johnson and Pendergast, 1981). In the late Cretaceous, northeastern Nevada underwent compression from the Sevier Orogeny until ~66 Ma (DeCelles, 2004) resulting in crustal thickening (50–60 km thick) by the early Cenozoic (Coney and Harms, 1984).

By the mid to late Cenozoic, tectonism was predominately extensional in northeastern Nevada and these tectonic movements affected the hinterland of the Sevier orogenic belt, which stretched from present-day Canada to Mexico (Coney and Harms, 1984; DeCelles, 2004). The low-relief hinterland region was believed to be an eroding highland composed of largely metamorphic rocks (Fouch et al., 1979). There is some evidence of lacustrine deposition in the area as early as the Aptian during the Late Cretaceous (Vandervoort and Schmitt, 1990).

Extension occurred during the exhumation of the RMEH metamorphic core complex beginning at ~55 Ma, resulting in Eocene-age sedimentary basins, including the lacustrine Elko Basin (Satarugsa and Johnson, 2000; Henry, 2008). Isostatic uplift formed and rotated a new system of normal and listric faults within the hanging wall, subsequently forming the Elko Basin as an intermontane asymmetric depression in the system of half grabens of the Ruby Mountains

detachment fault (Solomon et al., 1979; McGrew and Snee, 1994; Haynes, 2003; Henry, 2008). The lacustrine Elko Basin began to subside and diachronous clastic sedimentation of the Elko Formation progressively filled this paleo-lake from north to south as subsidence increased. Magmatism initiated in the present-day state of Washington and successively moved southward to the Challis volcanic field in Idaho beginning at 45 Ma (Christiansen and Yeats, 1992) followed by production of rhyolitic ash-flow tuffs from the Tuscarora field near Elko, initiating at 39 Ma (Henry and John, 2013). In northeast Nevada, compression and coeval magmatism is assumed to have increased elevations by ~2 km in the middle Eocene-early Oligocene, then decreasing by the middle Miocene, although both their timing and the resulting elevations are debated (Horton et al., 2004).

With nearby volcanism continuing in the Tuscarora field, clastic deposition declined in the Elko Basin and normal faulting tilted the basin by less than 15 degrees into east and separated the basin into southeast-dipping fault blocks (Henry and Faulds, 1999; Haynes, 2003). Evidence of volcanic activity is recognized throughout the late stages of the Elko Basin and overlying strata by air-fall tuff and ash, specifically plagioclase from andesite dated by  $^{40}\text{Ar}/^{39}\text{Ar}$  methods at  $38.1 \pm 2.5$  Ma, and dacite lava from local domal sources (Haynes, 2003; Henrici and Haynes, 2006). However, a hiatus from volcanism lasted from the late Eocene (35 Ma) until the middle Miocene (~16.5 Ma; Coats, 1964). During the early Miocene, disruption and extension of the Elko Basin resulted in widespread normal faulting as exhibited by the horst-and-graben systems of the Basin and Range region today (Solomon, 1981). As a result of continued extension during the middle to late Miocene, the upper crust was stretched by ~10%.

## 2.2 Paleogeography and Paleontology

Paleogeographic reconstructions and paleontologic data characterize the Eocene climate as temperate with seasonal cold periods, and basin development at elevations akin to the present (Axelrod and Bailey, 1969; Wingate, 1983; Haynes, 2003; Henrici and Haynes, 2006) (Fig. 2). *Botryococcus* algal matter discovered in the Coal Mine Canyon section throughout the microbial-mat-bearing mudstones suggesting fresh to slightly saline lacustrine conditions (Wingate, 1983). Abundant plant fossils (conifers, alders, elms) provide evidence of the swampy vegetation and forests that likely outlined the lake basin with particularly high fossil abundance in the Coal Mine Canyon and Elko Hills outcrops (Wingate, 1983; Haynes, 2003).

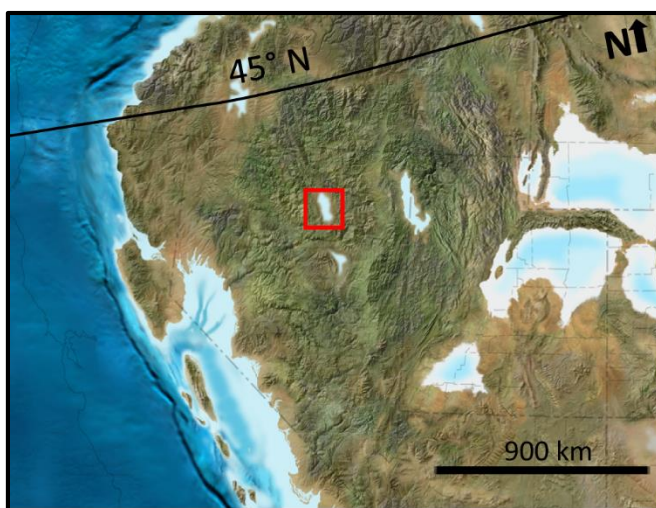


**Figure 2:** Paleogeographic reconstruction of Western North America during the Eocene Epoch 50 Ma (48-52 Ma). (Modified from R. Blakey's website: [http://cpgeosystems.com/images/SWNA\\_50Ma-sm.jpg](http://cpgeosystems.com/images/SWNA_50Ma-sm.jpg) (2014). The approximate position of the Elko Basin in present-day northeastern NV is indicated by a red box.

## 2.3 Basin Extents and Shape

Although outcrops of the Elko Formation have been found in an area encompassing at least 28,000 km<sup>2</sup>, there is an unresolved debate regarding the possibilities that the Elko Formation was deposited in multiple, smaller, discontinuous lake basins (Smith et al., 1976; Solomon, 1992; Christiansen and Yeats, 1992; Wallace et al., 2008), one large lake basin with similar lake facies throughout (Smith et al., 1976; Solomon, 1992, Henry, 2008; Horner, 2015), or one large basin

separated by paleotopographic highs that created sub-basins each containing differing lake facies (Haynes, 2003; Henrici and Haynes, 2006). With the precise boundary of the basin undetermined, the shape of the Elko Basin is also debated.

Geographic landforms and exposures of lacustrine shale were used to estimate rough constraints on the extent of the basin. Smith et al. (1976) and Solomon and Moore (1982*a* and *b*) believe that the lake was bounded by the Ruby Mountains to the east, and by the Adobe Range to the west. However, Henry and Faulds (1999) and Haynes (2003) suggest that the western boundary is farther to the west within the Tuscarora Mountains, where age-equivalent strata was found, but not confirmed, as part of the Elko Formation. Elko Formation outcrops scattered throughout the region suggest an east–west extent of ~100 km, and a north–south extent of ~190 km (Solomon, 1992; Haynes, 2003; Henrici and Haynes, 2006) (Fig. 3). The original lake was likely narrower than the present distribution of the outcrops, but have been stretched due to the impact of Miocene Basin and Range extension (Solomon, 1981).

## **2.4 Stratigraphy**

Following Smith et al. (1976) and Solomon et al. (1979), the Elko Formation consists of conglomerate, sandstone, limestone, black shale, mudstone, siltstone, and volcanic tuff (Fig. 4). Intervals of cherty limestone and conglomerate underlie these rocks (Smith et al., 1976). Coats (1987) named these the “Tertiary cherty limestone” located exclusively in the Pinon Range and Elko Hills, and the “Tertiary conglomerate” present across the entire basin. Smith et al. (1976), Solomon and Moore (1982*a* and *b*), and Moore et al. (1983) do not define either the “Tertiary cherty limestone” or the “Tertiary conglomerate” as part of the Elko Formation, whereas Jaeger (1987), Solomon et al. (1979), Ketner and Alpha (1992), and Haynes (2003) do include these units as the basal part of the Elko Formation.

According to Haynes (2003), basal sandy pebble conglomerates overlying Paleozoic rock comprise the lower member of the Elko Formation and are interpreted as alluvial fan and braided stream deposits due to their range in clast size and lack of mud. Overlying the sandy pebble conglomerate, the succession fines upwards into the middle and upper members composed of cherty limestone and fine-grained, deep-lake sediment, respectively, assumed to reflect the lake level deepening from initial basin extension and subsidence between the Adobe Range and East Humboldt Range (Haynes, 2003). With regional subsidence outpacing sedimentation, the initiation of an open-lacustrine system is reflected by the subsequent succession of black shale and siltstone deposition overlying the limestone and interbedded shale (Haynes, 2003).

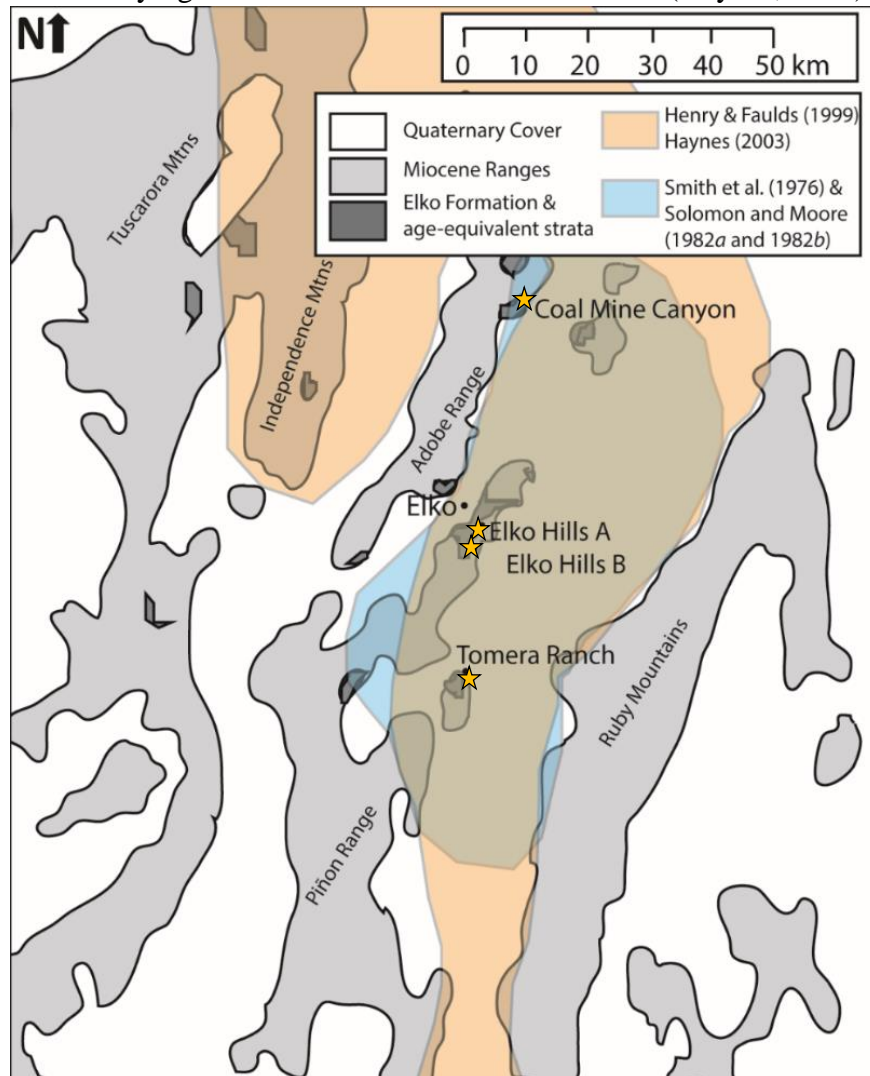


**Figure 3 (previous page):** Map modified from Henrici and Haynes (2006) showing known outcrops of the Elko Formation, age-equivalent rocks, and opposing views of the Elko Basin extents. Henry and Faulds (1999) and Haynes (2003) believe the Elko Basin encompasses the area highlighted in orange, contradicting Smith et al. (1976) and Solomon and Moore (1982*a* and *b*) that claim the Elko Basin is the region highlighted in blue. The area of overlap is highlighted in gray-green and represents the basin extents agreed upon by both Henry and Faulds (1999), Haynes (2003), Smith et al. (1976), and Solomon and Moore (1982*a* and 1982*b*).

The fine-grained lacustrine sediment became less predominant with an increase in volcanism from the Challis field in southern Idaho at 45 Ma (Henry, 2008) and with additional volcanoclastic input thought to originate from the Tuscarora Volcanic Field located northwest of Elko. Continued volcanism associated with the intrusion of local rhyolite domes beginning at  $38.6 \pm 0.1$  Ma, based on U-Pb Zircon dates (Haynes, 2003; Henry and John, 2013) and contributed to the final phase of the filling of the lake basin, with clastic deposition of the Elko Formation declining around  $38.9 \pm 0.3$  Ma, indicated by U-Pb Zircon dates from an andesite (Haynes, 2003; Coats, 1987). The volcanoclastic Indian Well Formation dated at  $37.6 \pm 1.3$  Ma, based on  $^{40}\text{Ar}/^{39}\text{Ar}$  dating of biotite, to  $33.2 \pm 0.7$  Ma determined by sanidine dating (Smith and Ketner, 1976), directly overlies the Elko Formation, separated by a low-angle unconformity (Solomon et al., 1979; Haynes, 2003). Dark brown to black blocky andesite followed the deposition of the Indian Well Formation composed of plagioclase, orthopyroxene, and clinopyroxene phenocrysts within a glass matrix, interpreted to be a brecciated flow deposit (Haynes, 2003). Unconformably overlying the andesite interval, is the Humboldt Formation consisting of fine-grained lacustrine sediment including silt, shale, claystone, and volcanic tuff, found deposited only in present-day valleys formed by Basin and Range extension during the Miocene (Haynes, 2003). Most recently, Quaternary-age sediment has been deposited overlying the Humboldt Formation and is predominantly fine- to coarse-grained siliciclastics interpreted as alluvium and fluvial deposits.

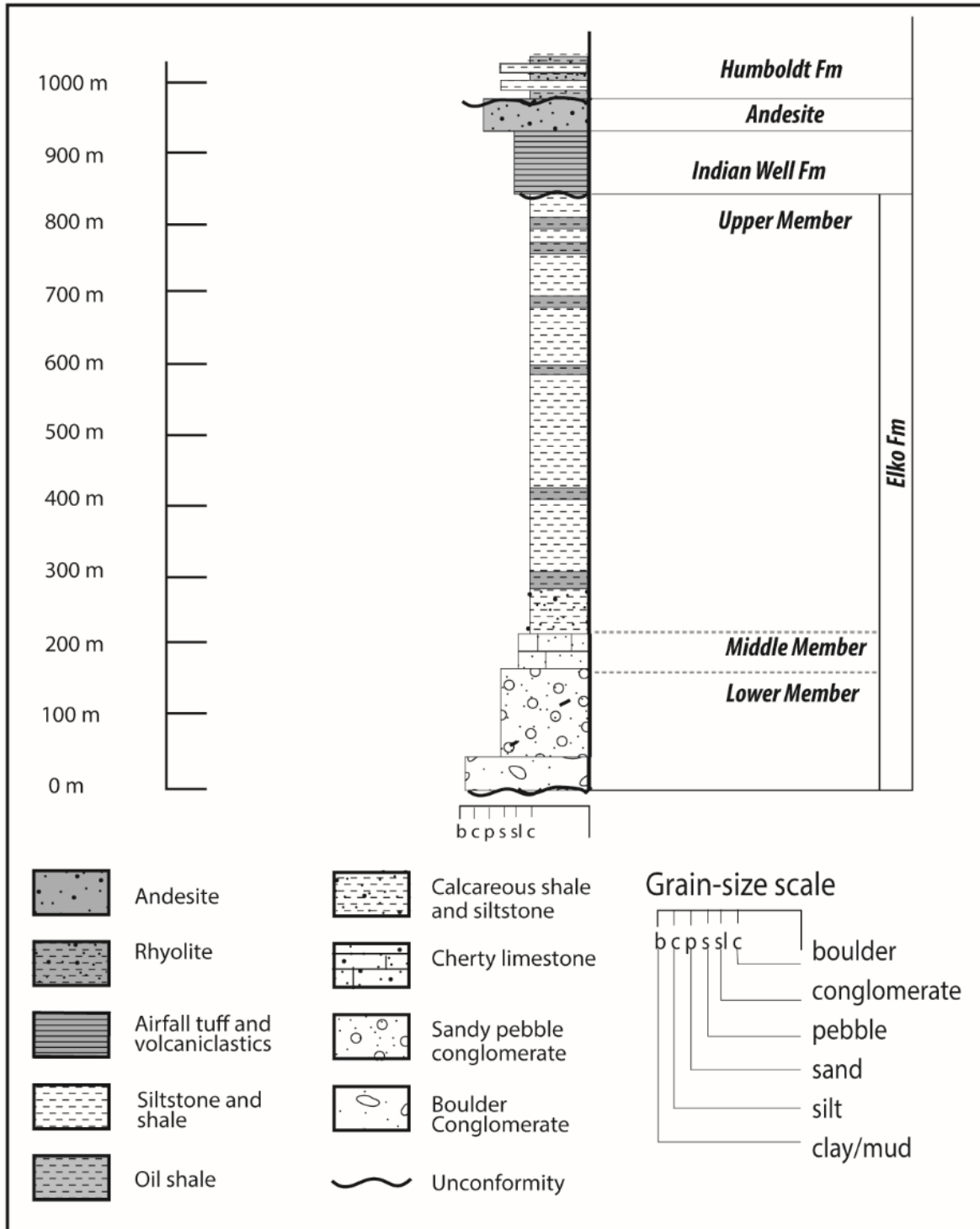


**Figure 4:** General stratigraphy displaying fining-upward from basal conglomerate based on several locations modified from Henrici and Haynes (2006).

### **3.0 REVIEW OF PREVIOUS LITERATURE**

#### **3.1 Elko Formation**

Until Horner (2015), studies on the sedimentology of the Elko Formation, NV have been essentially non-existent. In combination, the work of Solomon et al. (1979) and Haynes (2003), discussed previously, provided a broad framework for the Elko lacustrine basin, but their studies lack facies identification, facies architecture, or a depositional model. The sedimentological and the depositional models of Horner (2015) were an important resource for this investigation; therefore, an overview of the study is presented here in order to gain a better understanding of the facies comprising the Elko Formation and their correlation to gamma ray readings.

The Elko Formation broadly consists of, in ascending stratigraphic order, basal coarse-grained siliciclastics and carbonates, fine-grained organic-rich siliciclastics and carbonates, and fine- to coarse-grained volcanoclastics. Based on Horner's (2015) of the four outcrops described in Chapter 1, these intervals comprise fourteen facies (Table 1A), which were grouped into five facies associations (FAs). Ten facies (F1, F2, F3, F3B, F5, F6, F7, F9, F13, and F14) are siliciclastic, two facies (F4, F8, and F13) are calcareous, and three facies (F10, F11, and F12) are volcanoclastic. Facies were further grouped according to facies associations (FAs) (Table 1B), based on temporal and spatial relationships between facies in each of the four outcrops. FA1 is composed of siliciclastic mudstones and conglomerates and is interpreted to reflect a continental-lacustrine setting. FA2 is composed of massive coal-rich mudstones, interpreted as a proximal, low-energy, swamp system. FA3 is made up of microbial-mat-bearing mudstones and carbonates, interpreted as a limnetic, "open-water" lacustrine sedimentation. Extrabasinal airfall tuff including sedimentation of microbial-mat-bearing mudstones overlying FA3 comprises FA4 and represents

the initiation of airborne sedimentation in the limnetic portion of the lake. FA5 consists of carbonates and volcaniclastics. FA5 represents an increase in volcanism outpacing lake subsidence, terminating lacustrine sedimentation by removing any available accommodation space, essentially filling the lake.

**Table 1A: Sedimentary Facies (Horner, 2015)**

	<b>Facies</b>	<b>Facies Thickness</b>	<b>Description and Sedimentary Structures</b>	<b>Composition</b>	<b>Interpretation</b>
<b>1</b>	Bituminous Coal	1-3 cm	Massive fabric with distinct “blocky” texture Beds are often lenticular (10-20 cm length) Vertically associated with lignite facies	90-95% terrigenous plant material or macrophytes 5-10% fine to medium silt-size detrital quartz	Fine grain size (clay and silt) suggests low energy conditions (initial suspension settling of plant material and <i>in situ</i> development of subbituminous coal?)
<b>2</b>	Lignite	15-125 cm	Massive fabric Broken to whole fossil leaves and woody detritus occur on bedding planes Locally contains slip surfaces with parallel striations (i.e. slickensides) Contains abundant root traces	60-80% terrigenous plant material or macrophytes 10-35% siliciclastic clay matrix 5-10% fine to medium silt-size detrital quartz	Fine grain size (clay and silt) suggests low energy depositional conditions (initial suspension settling and <i>in situ</i> development of lignite?) Broken to whole fossil leaves and woody detritus on bedding planes suggest deposition through suspension settling for organic matter Slickensides denote contracting and swelling of expansive clay minerals (e.g. Gray and Nickelsen 1989; Retallack, 1990)
<b>3A</b>	Massive, siliciclastic mudstone	5-215 cm	No internal structure Variegated colors (grey, green, brown) Commonly unconsolidated Silt-rich clastic dykes commonly disrupt bedding Locally contains wispy organic material	70-85% siliciclastic clay matrix 5-15% fine to medium silt-size detrital quartz or volcanic lithoclasts 0-15% organic material	Fine-grain size (clay and silt) suggest low-energy conditions upon deposition Structureless fabric and dispersed silt grains indicate deposition after deceleration of fluid mud flows (Plint, 2014) or syndimentary liquefaction and/or fluidization, likely triggered by tectonism (Sims, 2013)
<b>3B</b>	Massive, root-bearing siliciclastic mudstone	15-400 cm	Massive fabric with irregular, patchy distribution of clay-rich and organic-rich zones Commonly unconsolidated Contains abundant root traces Breaks apart in peds Locally contains slip surfaces with parallel striations (i.e. slickensides)	60-70% siliciclastic clay matrix 20-30% fine to medium silt-size detrital quartz 0-10% organic material	Fine-grain size (clay and silt) suggests low-energy conditions upon deposition Subangular to subround silt grains indicate aeolian or water-lain deposition Peds and root traces suggest moderate to strong paleosol development in a terrestrial environment Massive fabric attributed to bioturbation and/or pedoturbation (Renault and Gierlowski-Kordesch, 2010) Slickensides denote contracting and swelling of expansive clay minerals (e.g. Gray and Nickelsen 1989; Retallack, 1990)
<b>4</b>	Calcareous mudstone	0.1-200 cm	Discontinuous to continuous undulating to planar-laminations of uneven to even thickness mm apart Quartz silt is often dispersed in carbonate mud laminae Coarse silt to sand-rich laminae often scour underlying carbonate mud laminae Laminae contain no internal structures  Clastic dykes, micro-normal faults, and water-escape structures commonly disrupt laminae and form convolute bedding Mm-scale stromatolites occur locally	60-90% carbonate mud and/ or microcrystalline dolomite matrix 10-40% fine to coarse silt-size detrital quartz  * 100% diagenetically altered to chert in middle member Elko Formation	Non-erosive, planar-laminae of even thickness suggest phases of suspension-settling of carbonate mud Undulating to planar laminae of uneven thickness and basal erosional scours suggest instances bedload transport (Schieber et al., 2013)  Clastic dykes, slumps, micro-normal faults, and water-escape structures indicate fluidization and/or liquefaction, likely triggered by a tectonic source (Sims, 2013)

5	Laminated, microbial mat-bearing mudstone	10-225 cm	Contain "wavy-crinkly" organic-rich laminae of sub-mm thickness and planar clay laminae of ~1-2 mm thickness Medium-silt to fine-sand grains are dispersed and often surrounded by sub-mm organic-rich laminae Clay generally occurs in lenses Locally contain ostracods (~1 mm), bivalves (3-5 mm), gastropods (~1 cm), fish (up to 1cm), leaves, and wood detritus, and pollen spores Extremely fissile in outcrop	40-80% organic-rich mud mats 10-40% siliciclastic clay matrix 5-20% fine to medium silt-size detrital quartz and/ or volcanic lithoclasts	In-situ growth of benthic cyanobacterial microbial mats Lenticular clay laminae indicate instances of bedload transport of clay-sized material independent of microbial mats Microbial mats baffle isolated quartz silt, organic detritus, and volcanic silt grains from suspension and are most prevalent during periods of non-sedimentation
6	Massive, ash-bearing mudstone	0.1-125 cm	No internal structure Locally contains fossil wood detritus and other amorphous organic detritus on bedding planes Vesicular in places Vertically associated with microbial mat-bearing organic rich mudstone	60-80% clay matrix 0-20% organic detritus 0-20% fine to coarse silt-size quartz 0-20% fine to coarse silt-size plagioclase	Fine grain size (clay and silt) suggests low-energy processes (suspension settling of ash, clay, and silt after volcanic events?) Vesicular texture attributed to gas expansion formed during rapid cooling of ash Organic detritus on bedding planes suggest deposition of organic matter through suspension along with ash
7	Laminated silt to sand-bearing siliciclastic mudstone	2-125 cm	Discontinuous to continuous planar laminae of uneven to even thickness (sub-mm to 3mm thick) Massive structure within laminae is predominant Coarse-tail grading of siliciclastic silt to sand locally occurs in 3mm thick, continuous, poorly sorted mudstone laminae	60-80% siliciclastic clay matrix 20-40% fine to medium silt-size detrital quartz 0-40% fine to medium sand-size detrital quartz	Sub-mm thick laminae of even thickness suggest periods of suspension settling Planar-laminae of uneven thickness with silt to sand-size grains suggest instances of bedload transport Few continuous laminae of coarse-tail graded, poorly sorted silt in a mud matrix indicates debris flows as a possible transport mechanism (Fisher, 1971)
8	Fossiliferous wackestone	5-60 cm	Massive fabric Contains broken to whole ostracods (~1 mm) and/ or gastropods (~1 cm) Clastic dykes (consist of massive siltstone) and water-escape structures in places Commonly interbedded with microbial mat-bearing organic-rich mudrock (F5)	70-90% micrite and/or microcrystalline dolomite matrix 10-30% carbonate shells 0-10% medium to coarse silt-size detrital quartz	Transport of carbonate mud either through suspension (Flügel, 2004), or bedload processes (Schieber et al., 2013)
9	Siliciclastic sandstone	0.2-50 cm	No internal structure Commonly occurs as distinct sandstone laminae (~5 mm thick) in carbonaceous mudstone facies Poorly-sorted with angular to sub-angular grains Scours underlying mudrock units Lenticular in places Contains clastic dykes and vertical water escape structures	40-80% fine to coarse sand-size detrital quartz 0-30% fine to coarse sand-size volcaniclastic lithoclasts 20-60% siliciclastic clay matrix	Erosional scours of underlying sediment, local lenticular bedding, and sand-size grains suggest high-energy, bedload transport Clastic-dykes and water-escape structures suggest fluidization and/or liquefaction, likely triggered by tectonic activity (Sims, 2013)
10	Vitric tuff	10-350 cm	Massive fabric Remnant gas bubbles between triple junctions of glass shards Vitric groundmass alters to clay in places Skeletal plagioclase in places (selective dissolution) Contains broken to whole fossil leaves and charcoal fragments on bedding planes in places Rarely contains welding features	60-80% vitric groundmass 10-20% plagioclase phenocrysts 0-5% quartz phenocrysts 0-5% biotite phenocrysts	Vitric groundmass indicates rapid-cooling of volcanic material (air-fall deposition into lake) Rare welding features that are also associated with fossil leaves and charcoal denote instances of air-fall deposition onto subaerial areas

<b>11</b>	Crystal tuff	1-225 cm	No internal structure Vitric groundmass often partly altered to clay Skeletal plagioclase in places (selective dissolution) Rarely contains siliceous spherulite crystals (~1mm)	30-50% vitric to bentonite groundmass 30-40% plagioclase phenocrysts 15-25% quartz phenocrysts 0-5% biotite phenocrysts 0-5% sand-size lithoclasts	Initial air-fall transport and rapid deposition from suspension as indicated by massive fabric Spherulites likely formed from devitrification of volcanic glass (Lofgren, 1971)
<b>12</b>	Lithic tuff	25-300 cm	Massive fabric Groundmass almost entirely altered to clay Skeletal plagioclase in places (selective dissolution) Locally contains gravel-size lithoclasts	50-80% bentonite matrix 20-40% lithoclasts 0-10% plagioclase phenocrysts 0-5% biotite phenocrysts 0-5% charcoal and organic detritus	Initial air-fall transport and rapid deposition from suspension as indicated by massive fabric Charcoal fragments and local gravel-size lithoclasts indicate instances of reworking of sediments
<b>13</b>	Clast-bearing packstone	10-50 cm	Massive fabric Contains clasts of massive to well-laminated carbonate mudstone in places (1-2 cm) Contains shell-debris and lithoclasts in places Commonly heavily dolomitized	20-50% carbonate mud and/ or microcrystalline dolomite matrix 0-40% indistinguishable, round, dolomitized grains with dark rims 0-10% bioclasts (broken ostacods) 0-10% silt to sand-size detrital quartz	Overall coarse grain size suggests high-energy conditions Massive to well-laminated carbonate mudrock clasts represent rip-up clasts Poorly sorted bioclasts and rip-up clasts suspended in matrix suggest high-energy, erosive currents, likely storm or tectonically driven, as possible modes of transport Lack of internal structure indicates rapid deposition and/or liquefaction
<b>14</b>	Siliciclastic conglomerate	50-90 cm	Poorly-sorted angular to sub-rounded grains Unconsolidated in outcrop No internal structure No matrix or cement	40-60% pebble-size lithoclasts 20-40% sand-size detrital quartz 10-30% sand to pebble-size chert *Clasts are boulder-sized in lower Elko Member	Sand to pebble-size grains suggests high energy, bedload transport

**Table 1B:** Facies Associations and corresponding facies (Horner, 2015)

<b>Facies Association</b>	<b>Facies</b>
<b>Facies Association 1</b> Siliciclastic mudstones and conglomerates	<b>Facies 3A:</b> Massive siliciclastic mudstone <b>Facies 14:</b> Siliciclastic conglomerate <b>Facies 9:</b> Siliciclastic sandstone
<b>Facies Association 2</b> Massive coal-rich mudstones	<b>Facies 2:</b> Lignite <b>Facies 3A:</b> Massive siliciclastic mudstone <b>Facies 3B:</b> Massive root-bearing siliciclastic mudstone <b>Facies 1:</b> Bituminous coal
<b>Facies Association 3</b> Microbial-mat-bearing mudstones and carbonates	<b>Facies 5:</b> Laminated, microbial mat-bearing mudstone <b>Facies 3A:</b> Massive, siliciclastic mudstone <b>Facies 4:</b> Calcareous mudstone <b>Facies 8:</b> Fossiliferous wackestone <b>Facies 7:</b> Laminated, silt- to sand-bearing siliciclastic mudstone <b>Facies 13:</b> Clast-bearing packstone <b>Facies 9:</b> Siliciclastic sandstone <b>Facies 10:</b> Vitric tuff
<b>Facies Association 4</b> Microbial-mat-bearing mudstones and volcanoclastics	<b>Facies 5:</b> Laminated microbial-mat-bearing mudstone <b>Facies 6:</b> Massive ash-bearing mudstone <b>Facies 3A:</b> Massive siliciclastic mudstone <b>Facies 4:</b> Calcareous mudstone <b>Facies 10:</b> Vitric tuff
<b>Facies Association 5</b> Carbonates and volcanoclastics	<b>Facies 4:</b> Calcareous mudstone <b>Facies 10:</b> Vitric tuff <b>Facies 11:</b> Crystal tuff <b>Facies 12:</b> Lithic tuff <b>Facies 13:</b> Clast-bearing packstone

The four outcrops within the study area of the Elko Formation are located along a NNW–SSE transect through this continental-lacustrine depositional system. The five FAs are represented in four different depositional zones, from proximal to distal, in lake evolution indicated by heterogeneity of facies throughout the upper Elko Formation, sediment cyclicity, and fossil content (Fig. 5A). These four distinct zones are: (1) alluvial-fluvial (2) palustrine-lacustrine (3) littoral-lacustrine (4) limnetic-lacustrine and represent the four depositional environments of the Elko lacustrine basin from proximal-to-distal.

Deposition in the alluvial-fluvial environment is characterized by subangular, gravel- to pebble-size sediment, representing FA1. Large grain-size and scour features suggest this sediment is likely sourced from paleohighs during this time, thought to be sourced via braided streams to alluvial fans from near the surrounding modern Adobe Range for the Coal Mine Canyon (CMC) and Elko Hills localities and the modern Pinon Range for the Tomera Ranch (TR) section. Exclusive to the CMC section, the proximal palustrine-lacustrine environment represents a shallow-restricted swamp system, based on the presence of paleosols and coal beds (FA2). The

littoral-lacustrine carbonate depozone is recognized by the presence of cherty limestone (FA3) and was located only on margins during early to middle lake development as well as during late lake stages that show interbedded volcanoclastics and carbonates. The most distal depositional zone is represented by a limnetic-lacustrine environment (FA4). During deposition in the limnetic-lacustrine environment, the proximal outcrops of the CMC and TR sections exhibit the laminated microbial-mat-bearing mudstone interbedded with carbonates, suggesting cyclicity of fluctuating lake level likely as a result of climate and tectonics. In contrast, the Elko Hills outcrops record the thickest microbial-mat-bearing mudstone (F5) and lack of carbonate intervals, suggesting that this was the deep, central portion of the lake basin and less affected by variation in lake-level. Rare beds of siliciclastic sandstone (F10) and clast-bearing packstone (F13) occur within this limnetic-lacustrine environment, reflecting storm events inferred from erosional scours and rip-up clasts. Massive fabrics of calcareous mudstone (F4) also contain evidence of soft-sediment deformation and normal micro-faults, implying active extensional tectonism during the formation of the Elko lake.

Horner (2015) combined new ( $\text{Ar}^{40}/\text{Ar}^{39}$ ) dates with previously acquired radiometric age dates ( $^{40}\text{K}/^{40}\text{Ar}$  and  $^{235}\text{U}/^{207}\text{Pb}$ ; Solomon et al., 1979; Haynes, 2003) to divide the Elko Formation into four chronostratigraphic intervals and develop a facies architecture. The age dates indicated that the succession represents a continental-lacustrine sedimentary system with a depocenter shifting from north to south, recording significant lateral changes in accommodation space and distinct facies trends. The northernmost outcrop (Coal Mine Canyon) has an age of  $48.24 \pm 0.02$  Ma, based on K-Ar radiometric dating (Horner, 2015) of a biotite-rich tuff near the base of the measured tuff (rocks stratigraphically lower, but still considered part of the Elko Formation do not

contain volcanic rocks that can be dated radiometrically, but are assumed to be older). In contrast, the biotite-rich tuff previously thought to be a similar chronostratigraphic interval at the TR section, was dated at  $43.5 \text{ Ma} \pm 0.02 \text{ Ma}$ , based on K-Ar radiometric dating (Horner, 2015). Airfall tuff toward the top of the central section (Elko Hills) was dated at  $\sim 38.9 \pm 0.3 \text{ Ma}$ , based on U/Pb of Haynes (2003).

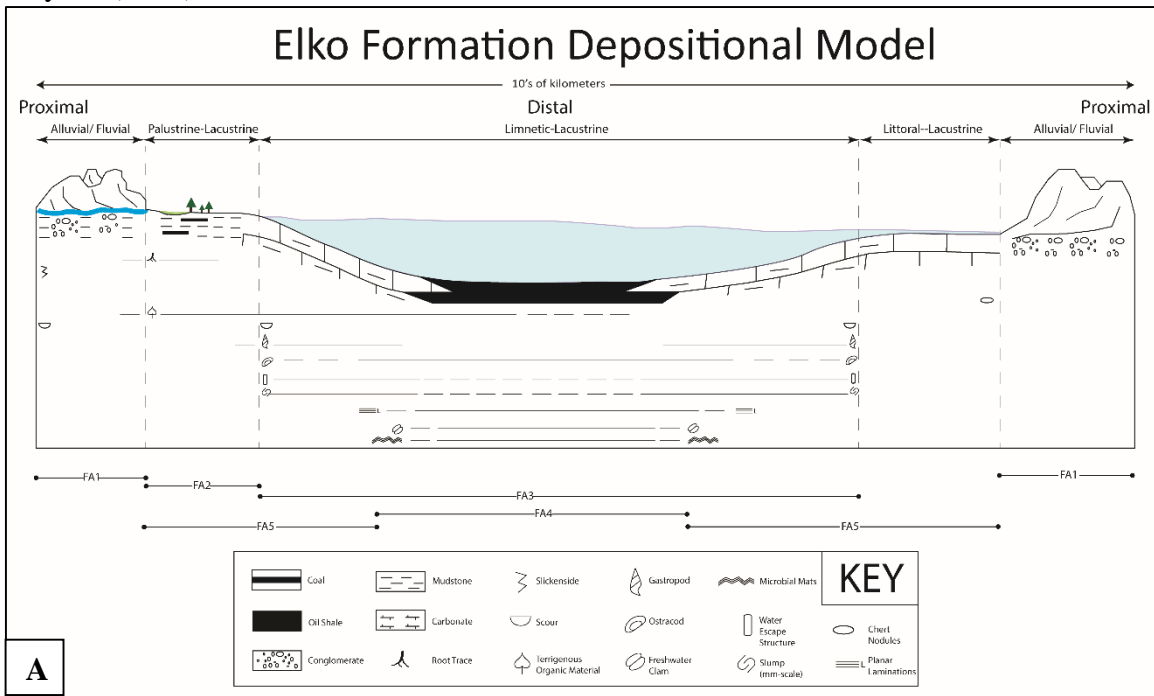


**Figure 5A:** Sedimentologic sketch of the depositional model of the Elko Formation based on Horner (2015).

Given that these radiometric ages are younger from north–south for these similar lake facies and lateral organic-rich microbial-mat-bearing mudstone (F5) thickness also changes from north–south, Horner (2015) interpreted that the depocenter is shifted from north–south. This is schematically shown in four time intervals reflecting the entire lake evolution (Fig. 5B). Time 1 exhibits northernmost deposition of alluvial-fluvial and palustrine-lacustrine sediment (FA1 and FA2, respectively) during  $\sim 53.0\text{--}50.0 \text{ Ma}$ . Time 2 ( $\sim 50.0\text{--}48.5 \text{ Ma}$ ) represents an increase in subsidence in the northernmost outcrop and the initial deposition of littoral-lacustrine (FA3) and limnetic-lacustrine sedimentation (FA4) in the CMC section evidenced by deep-lake fine-grained

sediment. Time 2 also marks the onset of minor input of volcanic ash at the CMC outcrop and the littoral-lacustrine carbonates (FA3) in both of the central Elko Hills outcrops and in the southern TR section. Time 3 (~48.5–43.5 Ma) denotes a shift in subsidence from the north to the central Elko Hills sections and southern extents of the basin. As a result, the depocenter shifted to the central and southern parts of the basin depositing limnetic-lacustrine facies there (FA3 and FA4). Time 3 also records a continued increase in volcanism, while shallow-water carbonates and mixed alluvial and volcanoclastics are deposited at the CMC section (FA5). Time 4 (~43.5–37.5 Ma) represents the shift of the deep-lake limnetic-lacustrine depocenter to the TR outcrop in the south, with an increase in accommodation space due to subsidence. FA5 deposition is also recorded toward the end of time 4, where microbial-mat-bearing mudstones (F5) are capped by volcanoclastics at all four outcrops which subsequently filled the lake.

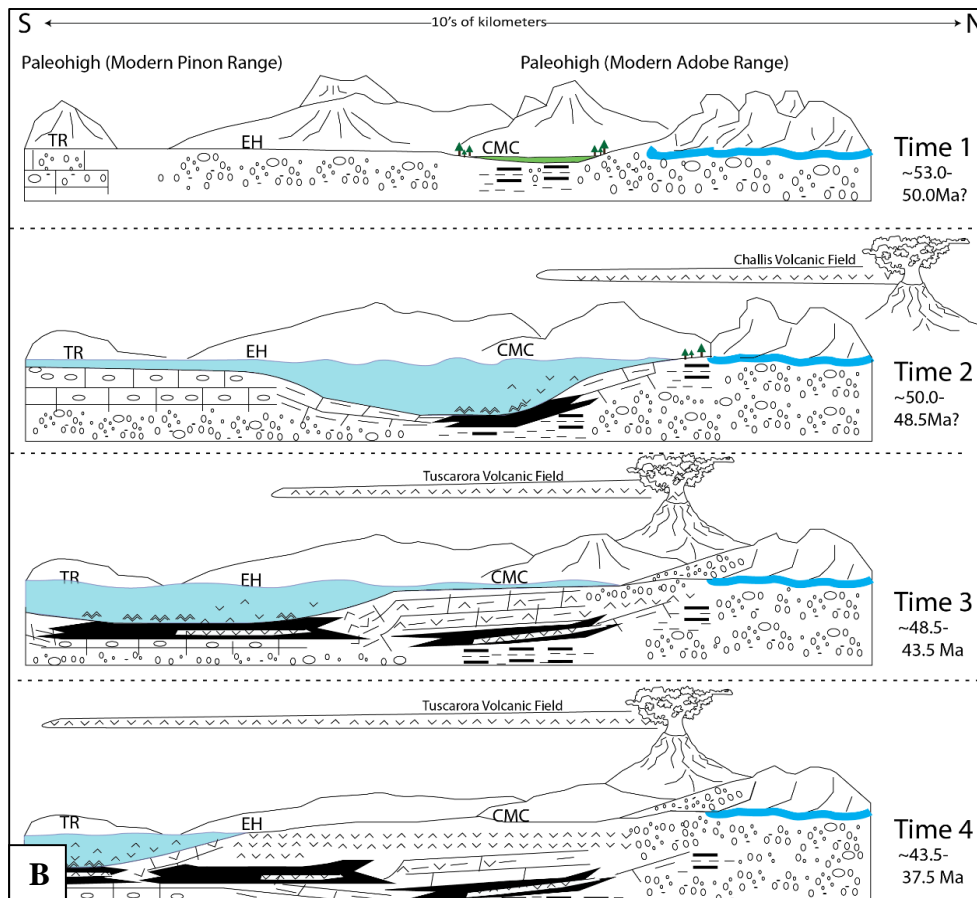


**Figure 5B (previous page):** Sedimentologic sketch of the Elko Formation based on Horner (2015), displaying a shifting depocenter of the Elko Formation in four time intervals from 53–32.5 Ma.

### 3.2 Gamma Radiation and Spectral Gamma Ray: Potassium, Thorium, and Uranium

Gamma ray log signatures have been recorded to differentiate between shale and non-shale lithologies, representing high and low gamma radiation, respectively (Fig. 6) (Ellis and Singer, 2008). Organic-rich black shale contains large amounts of clay and organic matter, resulting in high radioactivity due to radioactive isotopes being readily adsorbed as compared to carbonate and sandstone lithologies which typically lack this composition (Chamberlain, 1984).

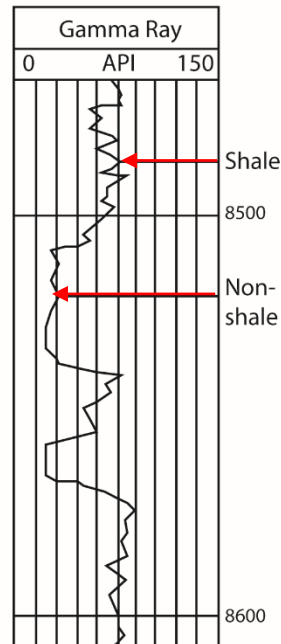


**Figure 6:** Example of a typical gamma ray log, modified from Ellis and Singer (2008). The horizontal scale at the top represents ascending API values to the right and is typically plotted from 0 to 150 API units, vertically the scale shows the depth decreasing toward the top. In an ideal log, shale is easily distinguished from non-shale by a strong reflection or “kick” toward the right and may exceed 150 API.

Spectral gamma ray (SGR) measurements as opposed to total gamma radiation allow for detection of high amounts of individual contributions of potassium (K), thorium (Th), and uranium (U) (Ellis and Singer, 2008). Controls on the absolute and relative contributions of K, Th, and U are complex and not only involve the original rock constituents (including depositional and geochemical properties) but also the effect of weathering (Cowan and Myers, 1988). Richness of

K, U, and Th are a direct product of the mineral composition of the Earth's crust and average abundances of K, U, and Th are estimated to be 2–2.5 wt. %, 2–3 ppm, and 8–12 ppm, respectively. These are only elements with radioactive isotopes that show sufficient gamma ray emission to be adequately measured (IAEA, 2003; Guagliardi et al., 2013). As each of these isotopes decay, the energy released contributes to the total gamma ray log and SGR allows for differentiating the contributions individually (Ehrenberg and Svåná, 2001).

Radioactive decay of potassium is measured directly through the breakdown of its isotope  $^{40}\text{K}$  and is found in greater abundance in comparison to thorium and uranium, therefore, is represented in weight percent (wt. %) (Ellis and Singer, 2008). Typically, K is found to be abundant in orthoclase (K-feldspar), mica (biotite), illite, as well as glauconite with minor amounts found in kaolinite (Fabricius et al., 2003). As K-bearing minerals do not weather easily, K can be transported without changes to its chemical composition, however, leaching through soil in a highly weathered regolith may result in low K readings (Guagliardi et al., 2013).

Thorium isotope  $^{232}\text{Th}$  is a common trace element estimated by its daughter products,  $^{208}\text{Tl}$  and  $^{228}\text{Ac}$ . Due to its low natural abundance it is therefore recorded in parts per million (ppm) (Blum et al., 1997; IAEA, 2003). Commonly, Th is found in heavy minerals, such as monazite, zircon, and rutile, and is also found to be related to clay minerals, although the reason remains unclear (Hassan et al., 1976). Following Adams and Weaver (1958) and Fabricius et al. (2003), Th is assumed to be fixed to clays by adsorption and is practically insoluble.

Uranium is estimated by the daughter products of the isotope  $^{238}\text{U}$ , such as  $^{214}\text{Bi}$ , and similar to Th, recorded in ppm due to its naturally low average abundance (IAEA, 2003). U has a soluble uranyl ion form which allows it to have greater mobility and transport than K and Th, and is known to precipitate under reducing conditions (Fabricius et al., 2003). This radioactive element

is thought to be precipitated as uranium salts, which readily adsorb to the clay or organic material components in marine shale (Swanson, 1961; Ellis and Singer, 2008). Following Svendsen and Hartley (2001), intervals of rocks with high carbonate content can have greater concentrations of U from U substitution. It has also been found to be abundant in volcanic rocks (Dickson and Scott, 1997); accessory minerals such as zircon, zirconite, and monazite; and as Fe-oxide or hydroxide coatings on mineral grains (Dickson and Scott, 1997; Fabricius et al., 2003). Swanson (1961) and Ehrenberg and Svånå (2001) describe the amount of U found in carbonaceous shale as having a positive correlation to the amount of organic matter, whereas for noncarbonaceous shale the uranium is contained in heavy minerals such as zircon and monazite.

Generally, relationships between Th and U are used to determine basin trends and differences in lateral extent from the margins toward the central, distal basin with the assumption that the distal basin exhibits a greater abundance of U-bearing organic-rich marine mudstones (Adams and Weaver, 1958; Bohacs, 1998). In marine systems, Th/U has been used to assess 1) rock type and mineralogy 2) effects of oxidation and weathering and 3) the position in the basin, based on the amount of terrigenous influence and relationship between clay and organic-matter content (Adams and Weaver, 1958).

### **3.3 Gamma Ray Spectrometer Measurements**

Gamma radiation from potassium ( $^{40}\text{K}$ ), thorium ( $^{208}\text{Tl}$ ), and uranium ( $^{238}\text{U}$  and  $^{235}\text{U}$ ) is measured by Bismuth Germanate oxide (BGO) scintillation crystals. These crystals within the detector absorb gamma rays from the sediment, resulting as a light flash. The intensity of the flash corresponds to the energy within the crystal and gets converted by a Photo-Multiplier Tube into a voltage pulse. From the voltage pulse, the amplitude correlates to the amount of energy absorbed from the gamma radiation, and as a result equates to a single reading composed of individual

contribution of radioactivity from K, Th, and U. The total energy absorbed is subdivided into K, U, and Th based upon each isotope's characteristic energy emissions set by the IAEA: 1360–1560 keV, 1660–1860 keV, and 2420–2820 keV, respectively (RSI Technical Note, 2009). This instrument also internally auto-stabilizes spectrum channels as well as takes into account the surrounding background radiation, eliminating the need for outside test sources for calibration. Auto-stabilizing differs from calibrating in that auto-stabilizing refers to tuning the K, Th, and U channels to measure energy emissions from each, which can shift from change of temperature or significant gamma ray emissions change. Calibrating uses stripping ratios (interference between K, Th, and U isotopes) to ensure that the correct proportions of each are recorded, and conducts internal computations to convert raw data to assay readings (units from counts to voltage of energy) (Radiation Solutions Inc., 2008). It is important to note that the spectrometer detector measures an average value for a bowl-shaped section of the rock where it is measuring up to 12 cm (5 in.) depth penetrating into the outcrop surface (Fig. 7). Thus, there is an inherent uncertainty of the amount of interference or overlap between each reading interval.

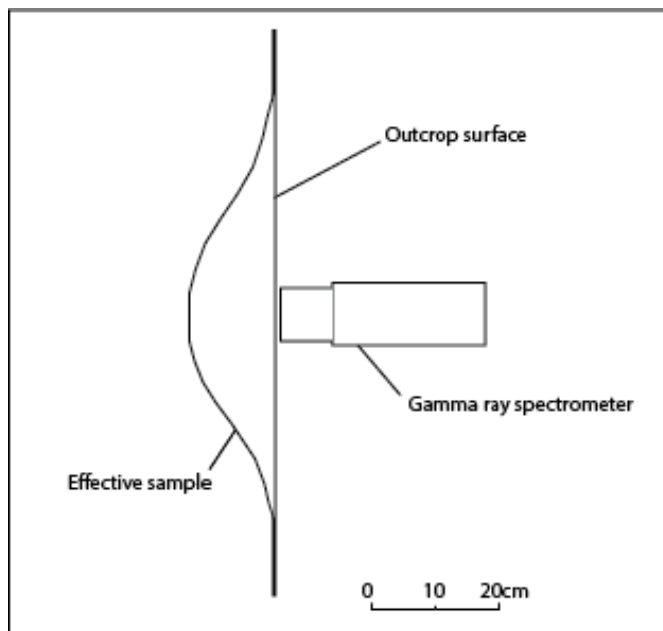


**Figure 7:** Scheme of a handheld gamma ray spectrometer on an outcrop outlining the bowl-shaped reading extents, modified from Løvburg et al. (1971) and Myers and Wignall (1987).

## 4.0 METHODOLOGY

### 4.1 Study Area

SGR measurements were acquired at four outcrops within a ~100-km radius of Elko, Nevada. The four outcrops will be referred to as Coal Mine Canyon (CMC), Elko Hills A (EHA), Elko Hills B (EHB), and Tomera Ranch (TR) in this study and form a NNW–SSE transect (Fig. 1). The Elko Formation naturally forms very poorly exposed outcrops and although other outcrops of the Elko Formation have been identified in an area greater than 28,000 km<sup>2</sup>, each of the four investigated outcrops were formerly trenched by the USGS in the 1970s, providing the best exposures and were therefore chosen for this study (Smith et al., 1976; Moore et al., 1983; Solomon, 1992). Due to intense weathering at the four outcrops, the EHA, EHB, and CMC were dredged out up to 2 ft. into the section by shoveling. As the TR outcrop had been even more heavily weathered, an excavator was used to expose the rocks up to 6 ft. in depth (Fig. 8).



**Figure 8:** Tomera Ranch outcrop being trenched by an excavator unveiling fresh outcrop surface 3-6 ft. into the formation.

## 4.2 Gamma Ray Spectrometer Tool

Colorado State University provided a portable gamma ray spectrometer constructed by Radiation Solutions Company. The RS-230 handheld gamma ray spectrometer has a 2-sq. in. detector pad, 103-cm<sup>3</sup> Bismuth Germanate oxide (BGO) detector, and a 1024-channel spectrum (Radiation Solutions Inc., 2008). Gamma radiation of potassium (<sup>40</sup>K), thorium (<sup>232</sup>Th), and uranium (<sup>238</sup>U and <sup>235</sup>U) is measured by scintillation crystals within the detector. Spectral gamma ray (SGR) signals were recorded as assay point measurements in order to collect K, Th, and U abundance readings based on their emission peaks [in weight percent (wt. %), parts per million (ppm)/counts per minute (cpm), and ppm/cpm, respectively)] at a specific position on the surface of an outcrop (Fig. 9). These assay readings were logged within the instrument as well as documented by hand from the gamma ray screen in order to correlate them to previously documented stratigraphy from Horner (2015).



**Figure 9:** This figure shows the RS-230 handheld gamma ray spectrometer recording an assay point reading on the surface of an outcrop.

### 4.3 Field Methods

Previously conducted gamma ray spectrometer outcrop studies have applied a variety of reading times and intervals of measurement designed for each specific scope and timeline of the study. Distance between assay measurements varies from 2in. –5 ft. (Chamberlain, 1984; Slatt et al., 1992; Bessa and Hesselbo, 1997). Reading times at these intervals can be as long as four hours, or for practical reasons, as little as two minutes (Blum et al., 1997; Cassidy, 1981; Guagliardi et al., 2013). Ideally, the longer the spectrometer is fixed in place to record a value, the greater the accuracy of the measurement (IAEA, 2003). A 120-second (s) time interval was selected and applied to the first three outcrops (EHA, EHB, and CMC) investigated based on studies by Blum et al. (1997), Guagliardi et al. (2013), and Cassidy (1981). After additional experimenting for precision, an interval time of 180 s was implemented at the TR section. These precision experiments entailed conducting 50 measurements on each specific subject (room background radiation, granite, and a 2-sq. in. piece of core collected from the Elko Formation ~4 mi from the EHA outcrop) at reading times of 30 s, 60 s, 120 s, 180 s, and 300 s. The standard deviation was calculated for each reading time set, and it was concluded that the use of a reading time of 180 s was ideal. Readings taken at this time interval were sufficient in precision, yet still represented a realistic time to be used for almost 1000 data points in outcrop field work (see experiment in Appendix 3). In the same fashion, assay point readings were recorded every 0.5-ft. at EHA, EHB, and CMC, based on the distribution of lithology and size of outcrop. The TR section was adjusted to 1-ft. intervals after observing little to no change within a 0.5-ft. interval range.

Once raw SGR data was collected within the spectrometer's internal memory, it was imported into Radiation Solutions software as well as Microsoft Excel for data management. Each

individual assay point was broken down into K wt.%, Th (ppm), and U (ppm) and was used to estimate API units by applying Equation 1 (Doveton and Merriam, 2004; Ellis and Singer, 2008).

$$\gamma API = 4 Th + 8 U + 16 K \quad (Eq. 1)$$

Total gamma ray readings (API) and SGR values (K, U, or Th) were then plotted against vertical outcrop successions using Microsoft Excel (Fig. 10). Once gamma ray curves were constructed, each reading was assigned to a specific facies for log characterization with measurements using detailed notes and stratigraphy documented by Horner (2015). SGR data was also normalized 100% to plot ternary diagrams for data analysis as well as frequency diagrams calculated based on the number of measurements acquired.

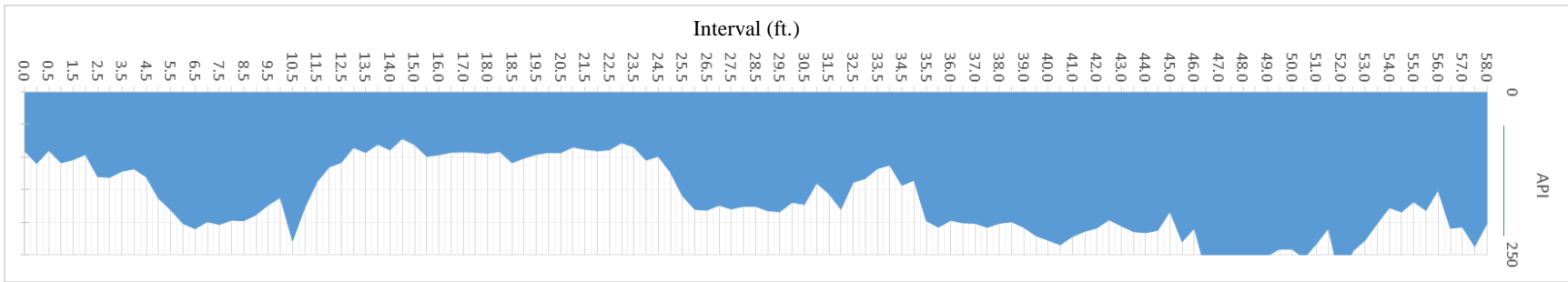


**Figure 10:** Example of a gamma ray curve constructed from gamma ray spectrometer data gathered at the Elko Hills B section. Stratigraphic section is plotted on the y-axis from 0 to 58 ft., while API values are plotted on the x-axis from 0 to 250, right to left.

#### **4.4 Thin section, Total Organic Carbon, X-Ray Diffraction/Fluorescence**

80 thin sections were prepared for this study. Mudstone samples were sent to Wagner Petrographics, in Lindon, Utah, polished to 20  $\mu\text{m}$  thickness, and infused with red fluorescent epoxy. Coarse-grained siliciclastic, volcanic, and carbonate samples were sent to Spectrum Petrographics in Vancouver, Washington. Preparation of the coarse-grained samples involved polishing to 30- $\mu\text{m}$  (siliciclastic and volcanic) or 40- $\mu\text{m}$  thickness (carbonate), and both were impregnated with blue epoxy to allow for porosity to be easily distinguished. Visual observation and thin section photos were carried out using a Nikon Eclipse *Ci-L* petrographic microscope with Nikon DS-Fi2 camera provided at Colorado State University and applying both plane polarized and cross polarized light. This step in analysis proved crucial in identification of fine-scale components (organic matter, sedimentary structures), distinguishing and estimating mineral constituents, and categorizing detrital or diagenetic features. Thin sections were also used to document micron-scale diagenetic cements using a JEOL 5800V scanning electron microscope (SEM) equipped with an energy dispersive spectrometer (EDS) at the USGS in Denver, CO. Rock cements were documented based on the Flügel (2004) scheme of classifying of carbonate cements, whereas the Choquette and Pray (1970) scheme was applied to classify types of porosity.

A total of ten samples were used in total organic carbon (TOC) analyses provided by Weatherford Laboratories in Houston, Texas. Sample preparation included acidization to remove carbonate minerals. The remaining dried sediment could then be oxidized, and TOC determined by measuring the amount of oxidized carbon released from the dried sediment as  $\text{CO}_2$ , using a LECO Carbon Analyzer. TOC analysis provided an estimate of organic content within the sample to be compared to the amount of uranium influence indicated by the SGR log.

X-Ray diffraction (XRD) was conducted at Atoka Geochemical in Centennial, CO, using an Olympus BTX profiler and Delta Professional Geochemical Analyzer. The purpose of XRD analysis was to quantify the inorganic mineral content (recorded as wt. %), including relative abundance of clay and non-clay types.

## 5.0 RESULTS

### 5.1 Total Gamma Ray Data

Organic-rich marine mudstones typically are easily identified in gamma ray logs as high-API values and are commonly referred to as “hot shales” (Dypvik and Eriksen, 1983). The gamma ray signature of the lacustrine Elko Formation is less straightforward, due to its heterogenetic lithologies and depositional influences. The Elko Formation gamma ray measurement results and gamma ray log signature will be described for each of the four outcrops (CMC, EHA, EHB, and TR) separately.

Although eight of the 14 facies were identified by Horner (2015) in the Elko Formation, only eight facies are considered in this study (Figs. 11A–L). These eight facies, some of which comprise two or more of Horner’s (2015) facies, were selected based on an adequate number of samples gathered from outcrop as well as by facies that were discernable from a gamma ray signal.

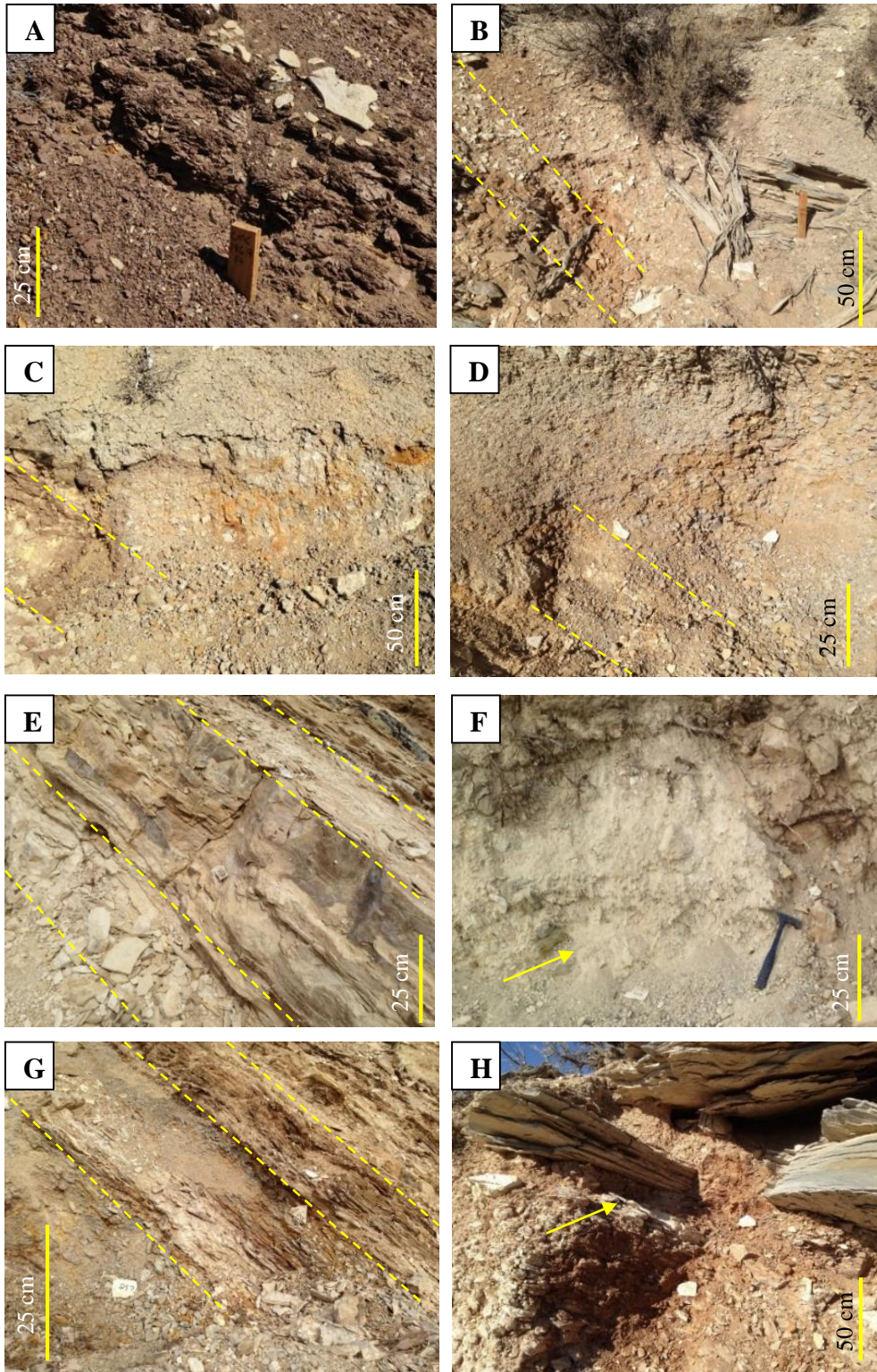
Horner (2015) described bituminous coal (F1) and lignite (F2) separately, based on their differing lithological characteristics, however, in this study, these two facies were jointly classified as *plant-bearing mudstone* (F1/2) due to the fact that the intervals of coal were never thicker than 12 cm and occurred infrequently throughout the succession.

Horner (2015) also identified massive, siliciclastic mudstone (F3A) and massive, root-bearing siliciclastic mudstone (F3B), but are combined into one facies, *clay-dominated mudstone* (F3), for the purpose of this study, as only two F3B samples were collected. Laminated, silt-to-sand-bearing siliciclastic mudstone (F7) and siliciclastic sandstone (F9) were not included in this study, due to these facies only occurring in laminae up to 5 millimeters thick and were, therefore, too small to be read by the gamma ray spectrometer without interference from the adjacent

laminae. One sample of clast-bearing packstone (F13) was combined with fossiliferous wackestone (F8) and, in this study, renamed *fossiliferous mudstone-packstone* (F8/13) to include ostracod and gastropod bearing-lithologies. Horner (2015) also differentiated three volcanoclastic facies (F10, F11, and F12) identifiable only by thin-section observation. For each of these three volcanoclastic facies, gamma ray signals could not be differentiated and were therefore grouped into one well log facies, *volcaniclastics* (F10–12) in this study. Calcareous mudstone (F4), microbial-mat-bearing mudstone (F5), ash-bearing mudstone (F6), and conglomerate (F14) remain as identified by Horner (2015).

**Table 2:** Facies Revised

<b>Horner (2015) Facies</b>	<b>Revised Facies for this Study</b>
F1, F2	Plant-bearing mudstone (F1/2)
F3A, F3B	Clay-dominated mudstone (F3)
F4	Calcareous mudstone (F4)
F5	Microbial-mat-bearing mudstone (F5)
F6	Ash-dominated mudstone (F6)
F8, F13	Fossiliferous mudstone-packstone (F8/13)
F10, F11, F12	Volcaniclastics (F10–12)
F7, F9	Not included
F14	Conglomerate (F14)



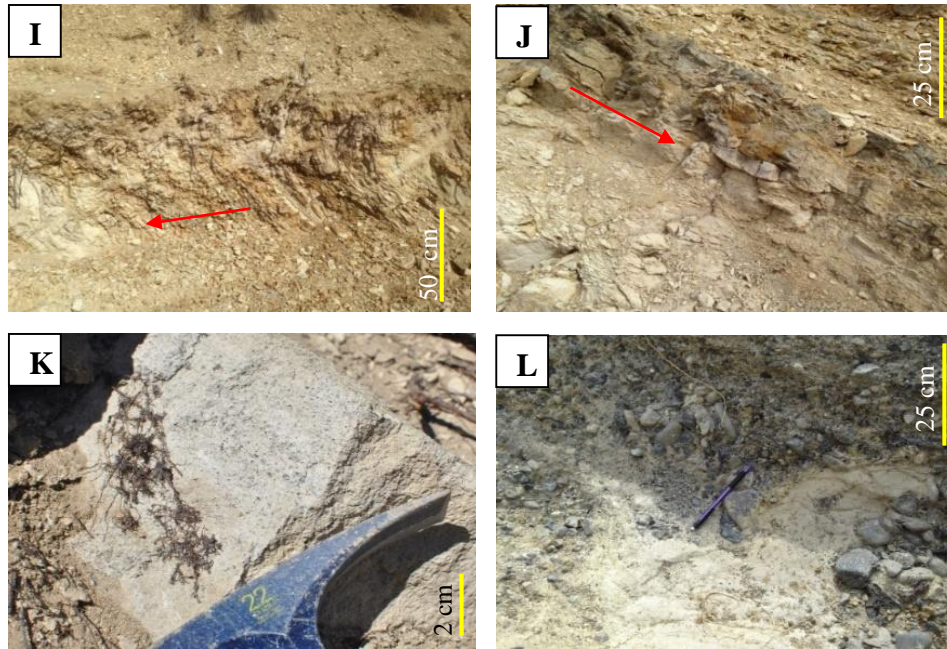


**Figure 11A-L (begins on previous page):** **A)** Plant-bearing mudstone (F1/2) from the CMC section at 186.9 ft. **B)** Plant-bearing mudstone (F1/2) highlighted between dashed yellow lines at the Elko Hills B outcrop at 48.5 ft., with an overall lighter color from the overlying volcanic interval. **C)** Clay-dominated mudstone (F3) at the CMC section between 82 and 84 ft., highlighted by yellow dashed lines. **D)** Clay-dominated mudstone (F3) between 40 and 43ft. at the Elko Hills B outcrop, marked by yellow dashed lines. **E)** Calcareous mudstone (F4) from 249 to 250 ft. at the CMC section. **F)** Heavily weathered, ashy calcareous mudstone (F4, yellow arrow) at the TR outcrop from 404 to 406 ft. **G)** Microbial-mat-bearing mudstone (F5) between 257 and 258 ft. at the CMC section highlighted between the yellow dashed lines. **H)** Elko Hills B outcrop displaying microbial-mat-bearing mudstone (F5) from 44 to 48 ft., which is weathered grey-blue in color (yellow arrow). **I)** Ash-dominated mudstone (F6) between 258 and 259 ft. from the TR outcrop (red arrow). **J)** Fossiliferous mudstone-packstone (F8/13, red arrow) at 239 ft. at the CMC outcrop. **K)** Volcanic tuff (F10–12) found at the TR section with visible accessory minerals. **L)** Conglomerate (F14) at ~35 to 40ft. at the CMC, section displaying sand- to pebble-size, angular-subrounded lithoclasts.

## 5.2 Spectral Gamma Ray Measurements

Fig. 12 displays 10–15 ft. sections as an overview of the gamma ray signature within and between outcrops, including an example of each of the eight facies that could be defined/differentiated by both outcrop and well-log analyses. Complete gamma ray logs, each spectral curve (K, U, and Th), and total API for each outcrop are included in Appendix 8. Ranges for the total gamma ray (ppm), total API, most frequent API value range, K wt. %, U (ppm), and Th (ppm) measurements are summarized in Tables 2–5. All raw data recorded, calculated summary statistics, and frequency distribution charts (calculated per measurement) for all four outcrops including the measurements mentioned above can be found in Appendices 1, 2, and 6, respectively. Gamma ray measurements herein are shown in ternary diagrams with each point representative of one measurement of the total gamma ray (ppm) that can be subdivided into the percentage of K wt. %, U (ppm), and Th (ppm) and have been normalized to 100%. (Figs. 13A–I). Introducing the range of data as well as identifying SGR contributions for each facies within each outcrop allows for a better context for understanding the mineralogical and geochemical signal controlling the gamma ray signature.

412 measurements were acquired every 0.5–2 ft. at the CMC outcrop, along the 210 ft. of measured section that comprises the eight facies applicable to this study. The EHA and EHB sections exhibit lack F4 and F8/13. 120 SGR readings were acquired every 0.5 ft. in outcrop A and 88 in outcrop B, along 58.5 and 44 ft. of section, respectively. 357 readings at the TR outcrop along 425 ft. of section every 1–2 ft. comprised all eight facies.

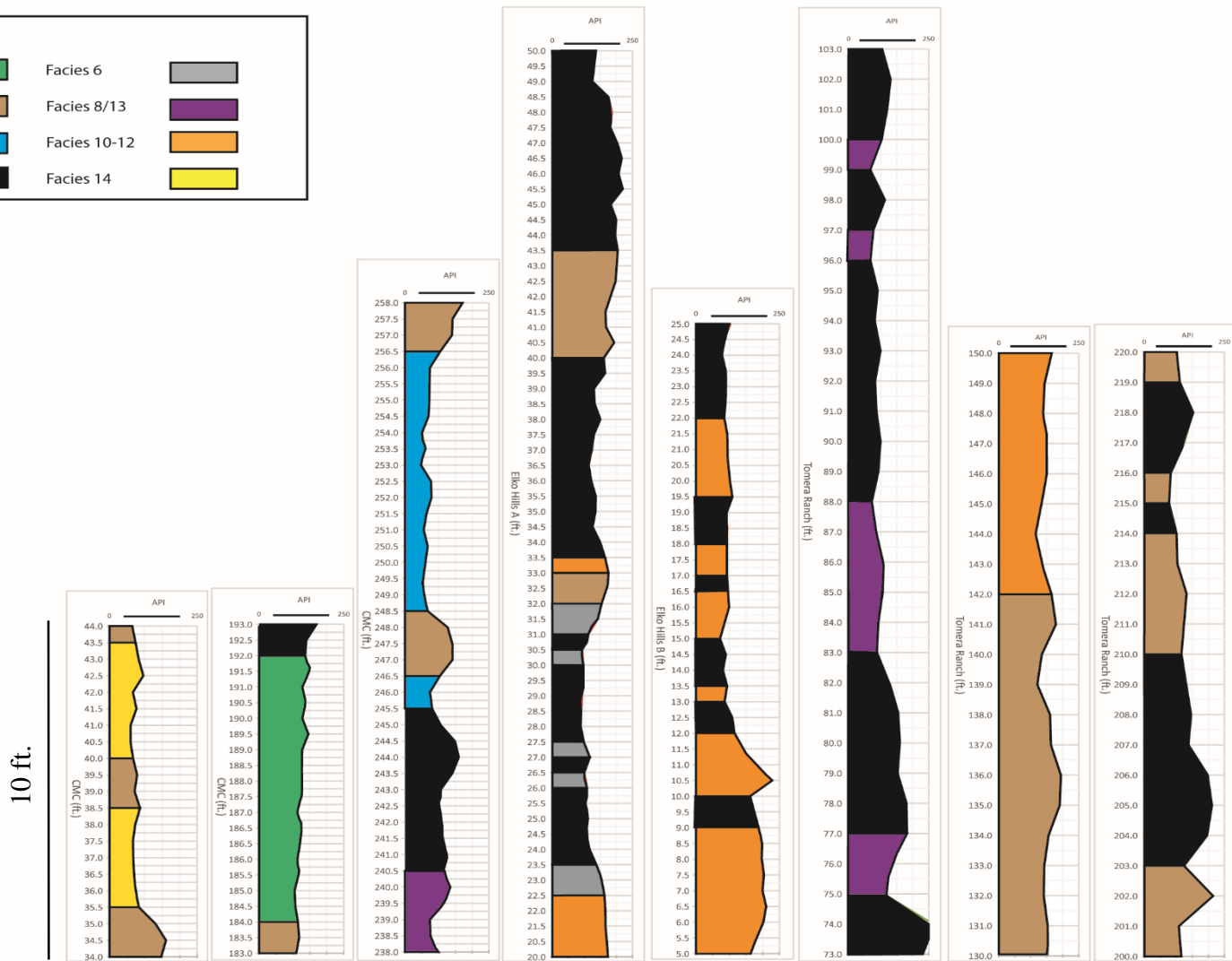
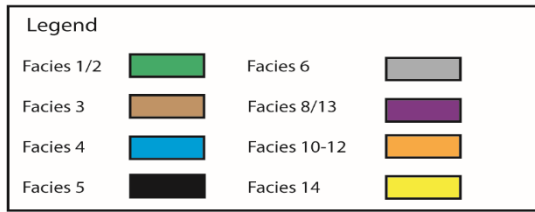


**Figure 12:** Eight curves displaying gamma ray measurements in API units plotted against height in the stratigraphic section in ft. Each interval is color-coded to represent the facies of that specific stratigraphic portion. Gamma ray curves are labeled for their outcrop of origin. The total gamma ray scale, measured in API, shown at the top of each chart ranges from 0 to 250 API units from left to right, respectively, and the vertical section descending from top to bottom in 0.5 or 1 ft. increments. For complete gamma ray curves refer to each of the sections in Appendix 8.

**Table 3A:**

CMC	Total GR [ppm]	Total API	Most Frequent API Range	K wt. %	U [ppm]	Th [ppm]
Facies 1/2	50–147	71–212	120–130	0.5–2.0	3.0–16.8	8.5–19
Facies 3	48–170	65–247	120–140	0.0–2.2	3.1–16.0	3.0–29
Facies 4	242–804	34–112	75–85	0.0–0.7	2.2–11.3	1.3–7.3
Facies 5	416–1149	54–178	70–130	0.0–1.4	2.3–18.9	2.7–15.4
Facies 6	32–71	46–103	60–90	0.0–0.8	3.5–8.6	2.4–15.0
Facies 8/13	50–92	74–135	80–120	0.0–0.6	6.8–14.8	3.2–7.5
Facies 10–12	85–145	126–214	135–150	0.0–0.0	13.4–24.4	2.1–14.2
Facies 14	42–68	60–96	70–75	0.5–1.5	3.4–7.5	3.4–6.7

**Table 3B:**

Elko Hills A	Total GR [ppm]	Total API	Most Frequent API Range	K wt. %	U [ppm]	Th [ppm]
Facies 1/2	1460–1821	190–228	200–210	2.8–5.8	6.0–9.6	13.5–24.6
Facies 3	1230–1562	154–199	180–200	1.9–4.0	5.1–8.1	12.6–25.4
Facies 5	63–159	89–220	100–150	1.4–4.8	3.2–11.6	7.6–22.3
Facies 6	779–1445	97–163	100–140	1.6–3.3	4.0–7.5	9.2–15.9
Facies 10–12	1357–1885	166–237	180–210	2.6–4.7	4.8–10.9	14.2–27.3

**Table 3C:**

Elko Hills B	Total GR [ppm]	Total API	Most Frequent API Range	K wt. %	U [ppm]	Th [ppm]
Facies 1/2	1496–1620	198–208	200–210	3.8–5.2	7.2–9.6	14.6–16.0
Facies 3	955–1934	124–235	180–200	1.9–5.5	5.8–15.0	7.1–25.3
Facies 5	51–136	72–189	90–120	0.9–3.8	3.0–8.0	6.5–19.1
Facies 6	676–1032	91–132	100–140	1.3–2.5	3.5–6.0	8.7–13.9
Facies 10–12	697–2645	93–304	210–250	1.2–4.5	3.0–21.3	8.3–27.3

**Table 3D:**

Tomera Ranch	Total GR [ppm]	Total API	Most Frequent API Range	K wt. %	U [ppm]	Th [ppm]
Facies 3	55–208	77–300	120–140	1.1–4.8	3.3–31.5	3.2–16.5
Facies 4	508–1419	17–183	75–85	0.14–5.5	1.5–13.6	0.1–17.3
Facies 5	454–4268	38–607	100–160	0.6–6.2	2.8–67.1	0.0–15.5
Facies 6	23–251	33–364	100–150	0.5–3.4	2.7–39.3	1.0–9.2
Facies 8/13	17–127	25–183	80–120	0.24–4.0	2.6–16.3	0.0–9.7
Facies 10–12	56–214	80–305	150–180	0.7–6.0	1.4–27.5	4.6–26.9

**Table 3A-3D:** Each table represents one of the four outcrops and their respective measurement ranges for each facies as total gamma ray (ppm), total API, most frequent API value range, K, U, and Th.

### **5.2.1 Facies 1/2: Plant-Bearing Mudstone (Fig. 13A)**

Plant-bearing mudstone (F1/2) gamma ray readings range most frequently from 120–130 API units at CMC and 200–210 API units at the Elko Hills outcrops (Tables 3A–3D). F1/2 values are typically  $\leq 10\%$  K for CMC, and values for EHA and EHB range between 10 and 20% K. CMC, EHA, and EHB values range between 30 and 50% U (there are several data points with higher values at CMC and EHA than at EHB), and between 50–70% Th. SGR ranges for each facies generally cluster by outcrop and are highlighted by polygons in Fig. 13A–G.

### **5.2.2 Facies 3: Clay-Dominated Mudstone (Fig. 13B)**

API values for the clay-dominated mudstone (F3) at the CMC and TR outcrop most frequently range from 120–140 units, while the Elko Hills sections show values between 180 and 200 units (Tables 3A–3D). F3 values are typically from 0–20% K for each of the CMC and TR sections range with the CMC outcrop providing the lowest values. The EHA and EHB sections display readings ranging from 10–20% K, 35–70% U (with five samples above 50%), and between 50–75% Th. Both the CMC and TR sections also exhibit U and Th values predominantly ranging from 30–70%.

### **5.2.3 Facies 4: Calcareous Mudstone (Fig. 13C)**

Calcareous mudstone (F4) has a frequent API range from 75–85 units. The CMC and TR sections show a wide range of values for F4 (Table 3A and 3D). The CMC outcrop has  $<10\%$  K, between 40 and 70% U, and between 40 and 60% Th. The TR section shows F4 data between 10 and 40% K, 40 and 60% U, and 40–60% Th.

### **5.2.4 Facies 5: Microbial-Mat-Bearing-Mudstone (Fig. 13D)**

Microbial-mat-bearing mudstone (F5) has most frequent API values for the CMC section readings are typically between 70 and 130 units, while EHA and EHB outcrops are between 100

and 150 units, and 90 and 120 units, respectively (Tables 3A–3D). The TR locality shows API values between 100 and 160 units. The CMC and TR sections show K values ranging from 0–30% with the CMC outcrop displaying low to zero values, and the TR section displaying data points predominantly from 5–30%. The CMC and TR sections also show similar U and Th values with a majority of the data ranging from 30–70%. High U values, though, are exclusively found in the TR section. The EHA and EHB sections show readings from 10–20% K, 35–65% U (with five readings above 50%), and between 50 and 75% Th.

### **5.2.5 Facies 6: Ash-Bearing Mudstone (Fig. 13E)**

Ash-bearing mudstone (F6) gamma ray values for the CMC outcrop are between 60 and 90 units, EHA and EHB are both between 100 and 140 units, while the TR section ranges from 100 to 150 units (Table 3A–3D). Ash-bearing mudstone (F6) data as two separate clusters distinguishing the Elko Hills’ outcrops into one group and CMC and TR outcrops into another. Both of the Elko Hills sections show 10–20% K, 30–50% U, and 50–70% Th. CMC and TR show values of  $\leq 10\%$  K,  $\geq 50\%$  U, and  $\leq 50\%$  Th.

### **5.2.6 Facies 8/13: Fossiliferous mudstone-packstone (Fig. 13F)**

Fossiliferous mudstone-packstone (F8/13) data is similar for both of the CMC and TR outcrops despite a few outliers. Commonly, API values are frequently between 80 and 120 units (Table 3A and 3D). K values are typically  $\leq 10\%$ , U shows readings between 50 and 95%, and Th  $\leq 50\%$ . Less than five outliers for each the TR and CMC sections show U values higher than 80% and K values at 0%, respectively.

### **5.2.7 Facies 10–12: Volcanic Tuff (Fig. 13G)**

Volcanic tuff (F10–12) API ranges between 135 and 150 units, 180 and 210 units, 210–250 units, and 150–180 units at the CMC, EHA, EHB, and TR sections, respectively (Tables 3A–

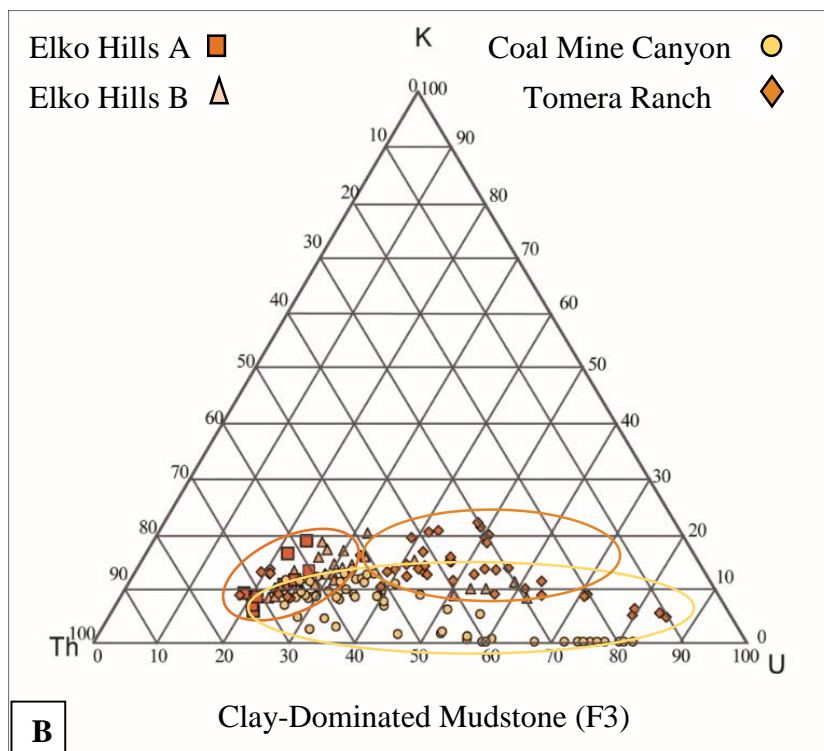
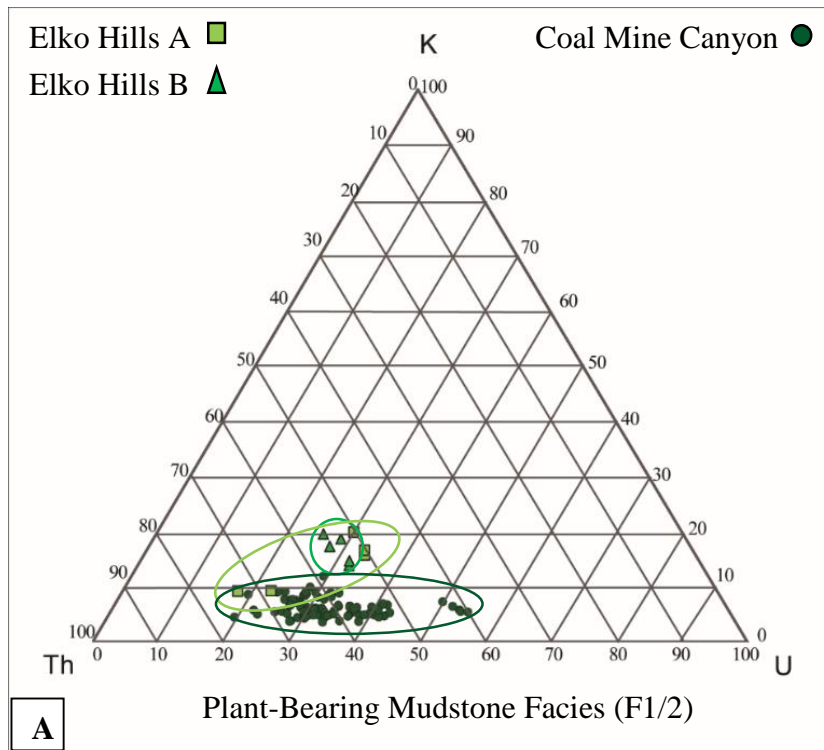
3D). Readings are similar for all four outcrops with the exception of little to no K at the CMC location and 10 readings higher than 20% K for the TR section. Typically, data shows  $\leq 35\%$  K, 20 to 60% U, and 40 to 70% Th.

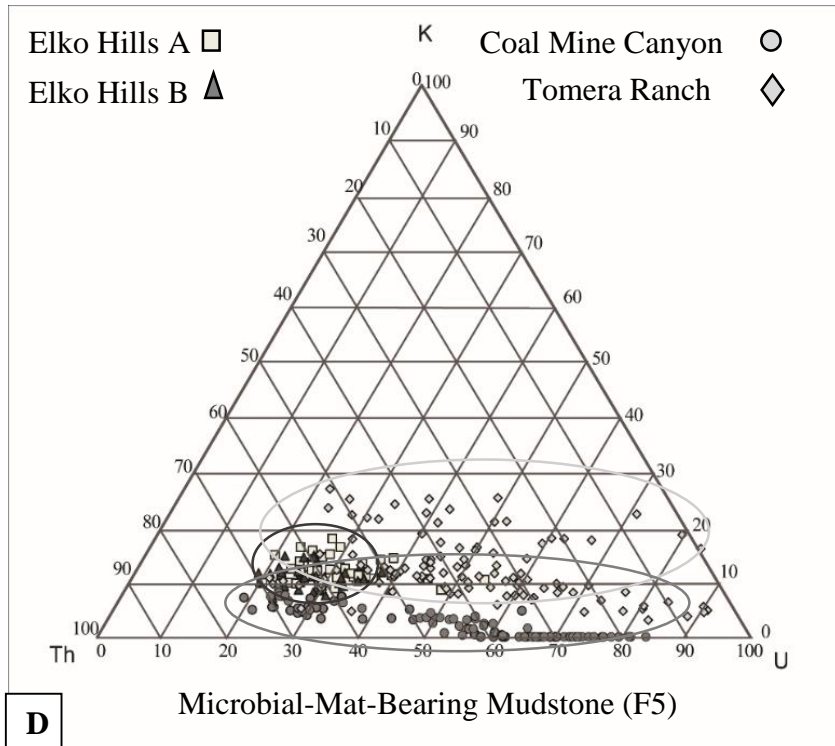
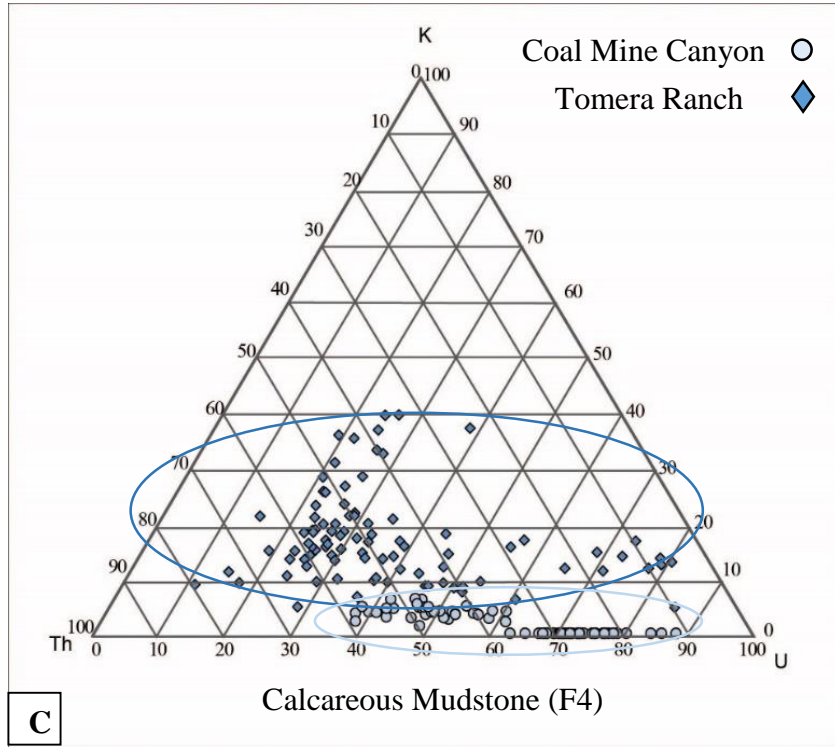
#### **5.2.8 Facies 14: Conglomerate (Fig. 13H)**

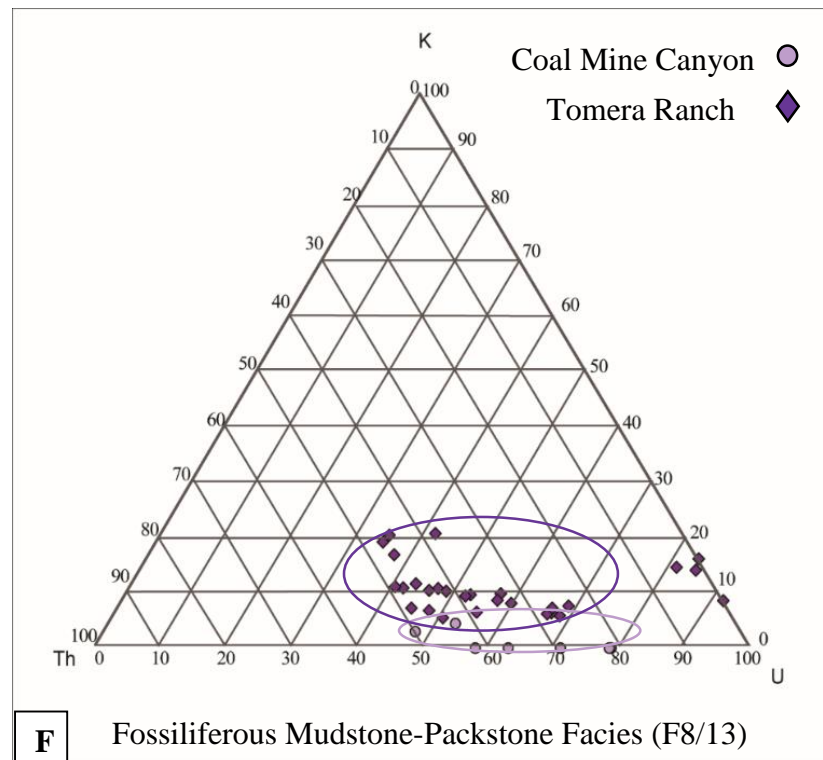
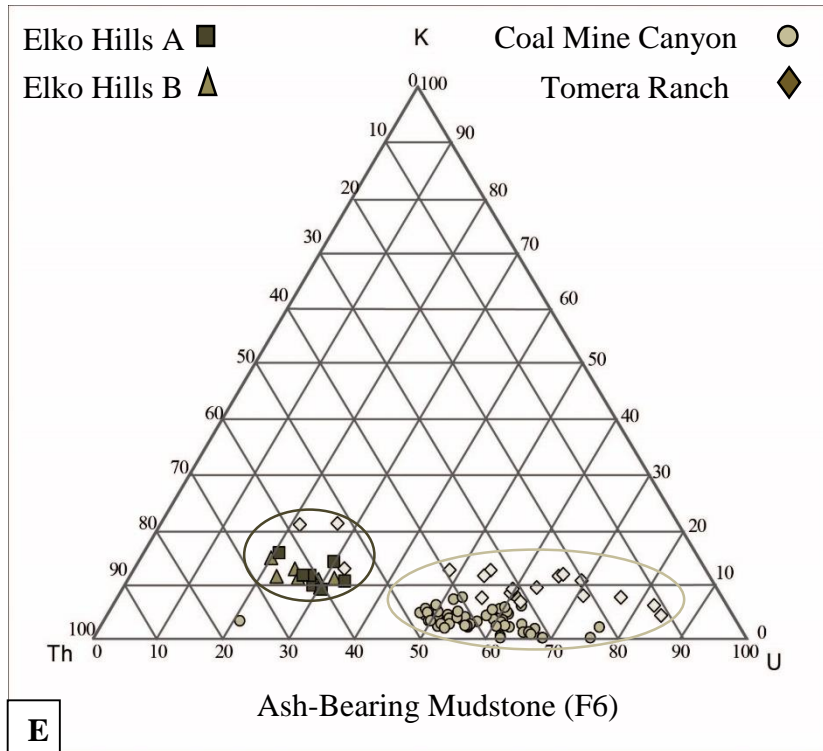
Table 2 shows that most frequently, the conglomerate (F14) interval ranges between 70 and 75 total API units (Table 3A). SGR data for the conglomerate facies (F14) which is only present at the CMC outcrop appear consistent with  $< 20\%$  K, 40 to 70% U, and 30 to 60% Th.

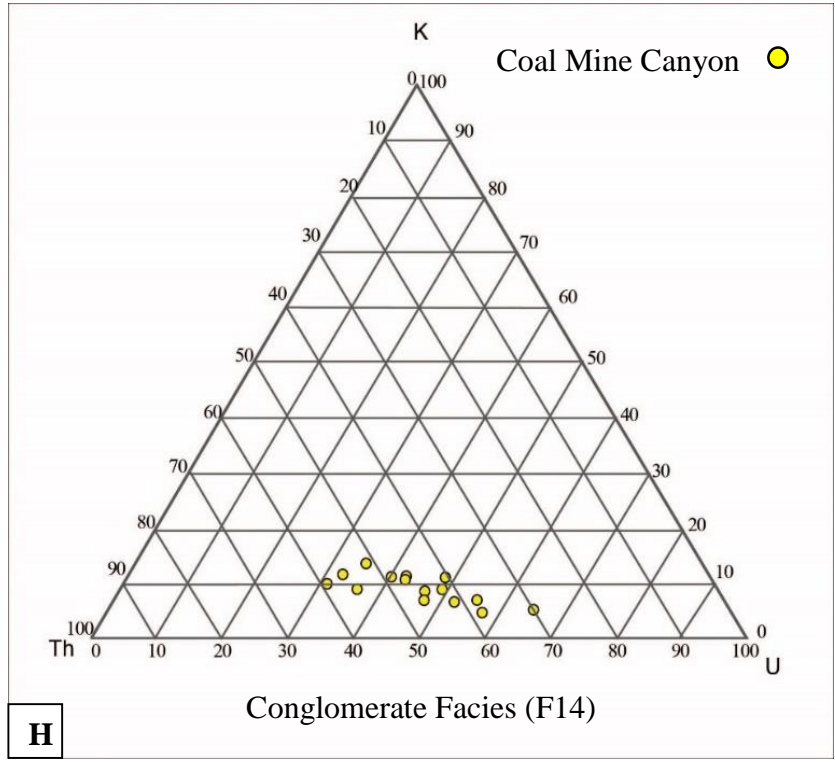
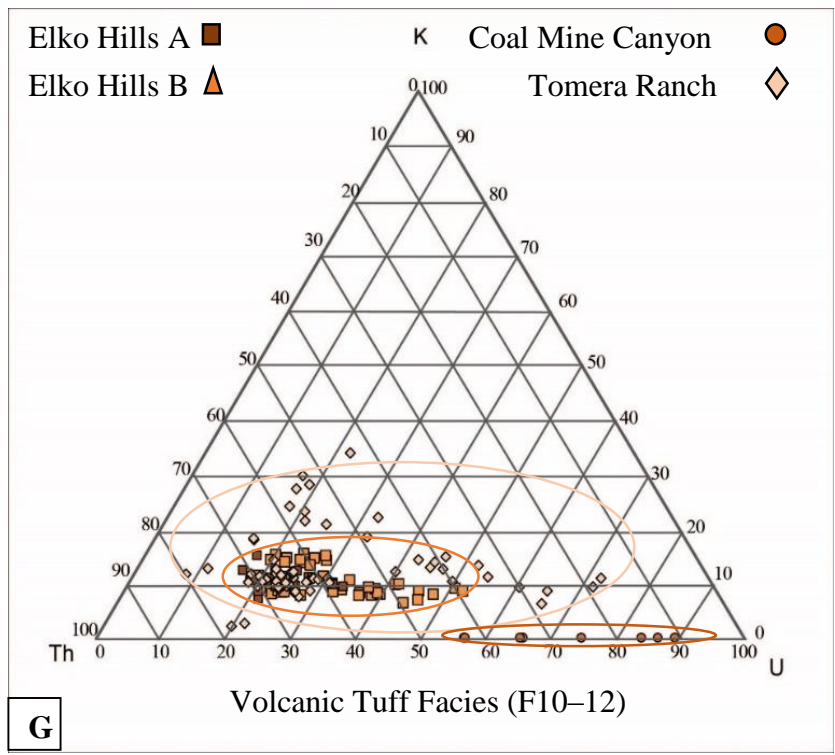
#### **5.2.9 Cumulative Data (Fig. 13I)**

Fig. 14I includes all gamma ray points collected from each of the four outcrops, independent of facies. The CMC outcrop data shows the lowest K readings ( $\leq 10\%$ ) as opposed to TR which has the highest K contribution with values of up to 40%. The EHA and EHB outcrop data cluster between 5% and 20% K. U values at CMC and TR typically range from 30% to 70%, however, few data points exceed this range. The EHA and EHB outcrops show U values ranging between 30 and 60%. Th values for CMC and TR range from 30-70%, whereas the Elko Hills Th values range between 50–70%.









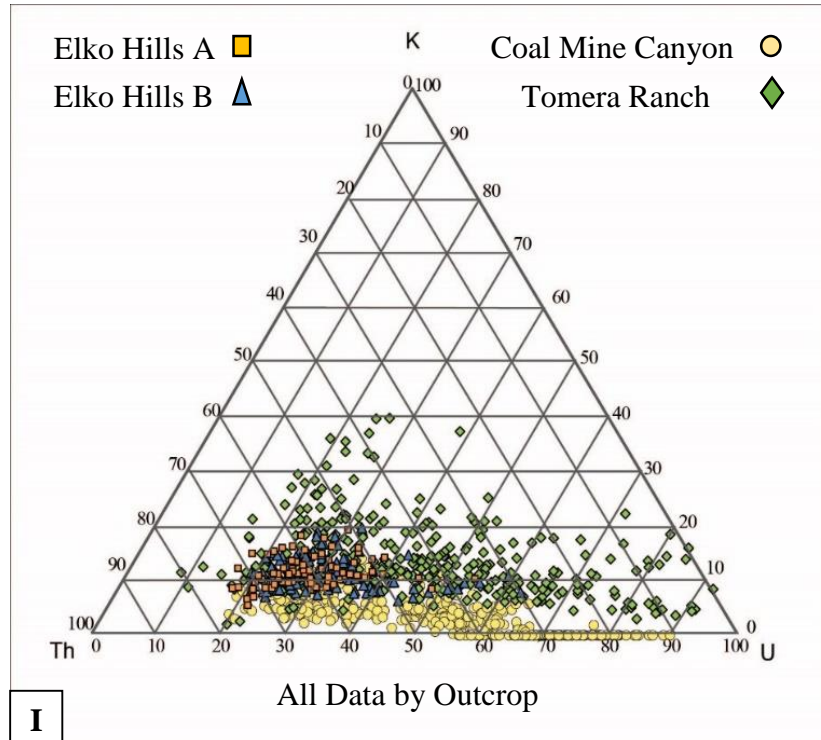


**Figure 13A–I:** Ternary diagrams constructed from (Graham and Midgley, 2000) template. A–H) Each ternary diagram A–H is representative for each of the total eight facies (F1/2, F3, F4, F5, F6, F8/13, F10–12, and F14). Each diagram includes data color-coded representing facies following the color scheme with differing hues as in figure 12. Representative outcrop symbols, as well as polygons color-coded by outcrop symbols are shown to highlight data groupings by outcrop. I) Total data collected at all localities. Each outcrop is represented by symbol and color-coding, independent of facies.

### 5.3 Th/U by Outcrop

As Adams and Weaver (1958) as well as Bohacs (1998) applied Th/U ratios to marine mudstone, to distinguish proximal from distal depositional environments. The microbial-mat-bearing mudstone (F5) of the Elko Formation, which is similar in appearance and composition to the marine examples, is considered to be ideal for applying this method (cf. Ch. 3, p. 9). Th/U ratios were calculated for all intervals assigned to F5 and for each of the four outcrops. Differences in F5 Th/U ratios are subtle and range from 0.5 to 4, but can be separated into two groups which are characterized by 1) a low Th/U ratio <2.5 at EHA and EHB, and 2) a high Th/U ratio between 2.5 and 4 at CMC and TR (Figs. 14A–D).

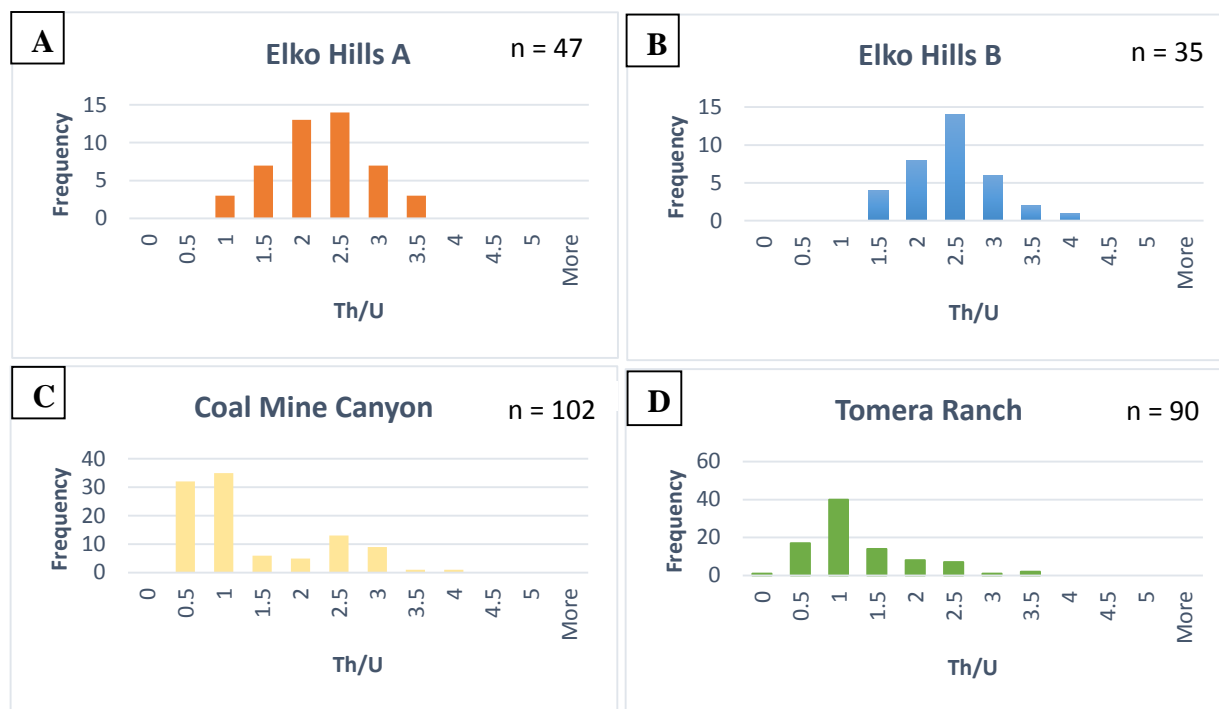


**Figure 14A–D:** Frequency diagrams for the Th/U representing the microbial-mat-bearing facies for each outcrop. Similar to the overall Th, U trend, the Elko Hills outcrops have slightly higher ratios between 2.5 and 4, while Tomera Ranch and Coal Mine Canyon are below 2.5.

#### 5.4 X-Ray Diffraction and Total Organic Carbon

XRD samples are from five plant-bearing mudstones (F1/2), four clay-dominated mudstones (F3), four calcareous mudstones (F4), thirteen microbial-mat-bearing mudstones (F5), two ash-bearing mudstones (F6), three fossiliferous mudstone-packstones (F8/13), nine volcanic tuffs (F10–12), and two conglomerates (F14). 29 of the samples were taken from the CMC outcrop, and 15 from the TR section. The remaining 13 samples were collected at the EHA and EHB outcrops.

Each of the siliciclastic mudstone facies (F1/2, F3, F5, and F6) are predominantly composed of varying amounts of quartz, clay (illite, chlorite, and montmorillonite), and feldspar (K-feldspar and albite/plagioclase), with minor amounts of volcanic (cristobalite) and carbonate minerals (calcite and dolomite). Illite makes up 50% and albite/plagioclase up to 15% of the F1/2

samples. F1/2 also contains up to 30% quartz in the Elko Hills examples, as opposed to 10% or less in the CMC outcrop.

F3 samples are composed primarily of clay (>50% illite and minor amounts of chlorite) and up to 20% feldspar (albite/plagioclase). F3 also contains 30% or more quartz in the Elko Hills, but less than 10% in the CMC and TR samples.

Up to 50% of F5 is made up of quartz at the Elko Hills sections as opposed to less than 25% in CMC and TR outcrops. The second largest component of F5 is illite up to 50%, but is typically closer to 30%. The remaining rock volume is feldspar, which makes up less than 30% of the total rock, with minor amounts of carbonate and additional clays (montmorillonite and chlorite).

Quartz comprises up to 50% of the F6 samples from the Elko Hills, with the remaining 50% made up of feldspars and clay (illite and minor amounts of chlorite).

At the CMC and TR sections, F4 and F8/13 contain at least 50% calcite or dolomite, ~20% illite, with varying amounts of quartz and feldspars (<15%). Feldspars and clays comprise the majority of the F10–12 samples from all sections with typically low amounts of quartz (<10%), up to 12% clinoptilolite (type of zeolite), and trace amounts of pyrite. The conglomerate facies at the CMC section only, is composed of more than 50% quartz, 20% clay (illite), and low amounts of albite/plagioclase feldspars (<10%).

In addition to the minerals discussed above, trace amounts of cristobalite were found in F1/2, F3, F4, and F5 as well as clinoptilolite and additional unidentified zeolites in F5 and F6.

Ten of the samples were also evaluated for quantitative analysis of total organic carbon (TOC) measured as wt. % (Appendix 4). These samples included one of F1/2, one of F4, and eight of F5, ranging from 0.5–31% TOC. The F4 sample contains less than 1% TOC, and the F1/2

measures greater than 25% TOC. The remaining eight F5 samples range from 0.48–31.4%, with  $\frac{3}{4}$  of them greater than 4.

## 6.0 INTERPRETATION

### 6.1 Gamma Ray Log Signature

Radioactivity is emitted from a variety of sources, alone or in combination, including uranium adsorbed to organic matter, clay (illite, chlorite, and montmorillonite), and K-bearing minerals (particularly volcanic). This radioactivity can be identified by high API measurements on gamma ray logs (Fabricius et al., 2003). Plant-bearing mudstone (F1/2), clay-dominated mudstone (F3), microbial-mat-bearing mudstone (F5), ash-bearing mudstone (F6) and volcanic tuff (F10–12) display high API values, with readings commonly between 120 and 230 API units. Calcareous mudstone (F4), fossiliferous mudstone-packstone (F8/13), and conglomerate (F14) characteristically lack these radioactive components, resulting in low API measurements, typically at or below 120 API units.

### 6.2 Spectral Gamma Ray (SGR) Signature

In this study, SGR was analyzed in conjunction with detailed outcrop observations, linear regressions between total gamma ray and contributions of potassium (K), uranium (U), and thorium (Th) for each facies (Appendix 9), and XRD analyses for characterizing each facies by recognizing relationships between mineral composition and abundance or scarcity of K, U, and Th (Ellis and Singer, 2008). Distinct controls were interpreted for high K, U, or Th values and are described herein.

Similar to marine systems, Th and K readings show a high correlation with each other at the CMC and EHA sections with  $R^2$  values of 0.50 for each (Fig. 15) (cf. Bohacs, 1998; Ehrenberg and Svånå, 2001). These  $R^2$  values, as well as coupled K and Th logs where the curves trace each other (Appendix 8), suggest that K and Th isotopes a result from the same composition, likely

emitted from clays containing both K-bearing minerals and adsorbed Th. However, at the EHB and TR outcrops, the much lower  $R^2$  values suggest that K contribution is likely reflecting a greater abundance of K-bearing volcanic minerals in addition to clay. The same is most likely the case for parts of the section where the K log does not trace the Th curve and represents separate components being detected which emit K and Th (Fig. 16). K and Th are independent of each other in an interval of plant-bearing mudstone (F1/2) from 35.0–37.5 ft. and clay-dominated mudstone (F3) from 37.5–45 ft., where both curves do trace each other. The interval showing high K values between 4 and 5% from 36–40.5 ft. (Fig. 16) corresponds to a stratigraphic portion of the succession with high amounts of volcanic material, in addition to clay, that stretches from ~39–40 ft. The same stratigraphic part of the succession is also characterized by high quantities of feldspar in addition to illite and montmorillonite, according to the XRD analyses, which could all be potentially adding radioactivity (Appendix 5). The larger amount of volcanic minerals correlates well with the increase in volcanism during deposition of the EHB and TR sections (cf. Horner 2015). Fig. 16 also gives an example of a high Th content at 41–44 ft., which coincides with an increase of clay (illite and montmorillonite) and volcanic ash, and a decrease of K-bearing volcanic minerals (K-feldspar) recorded from outcrop observations.

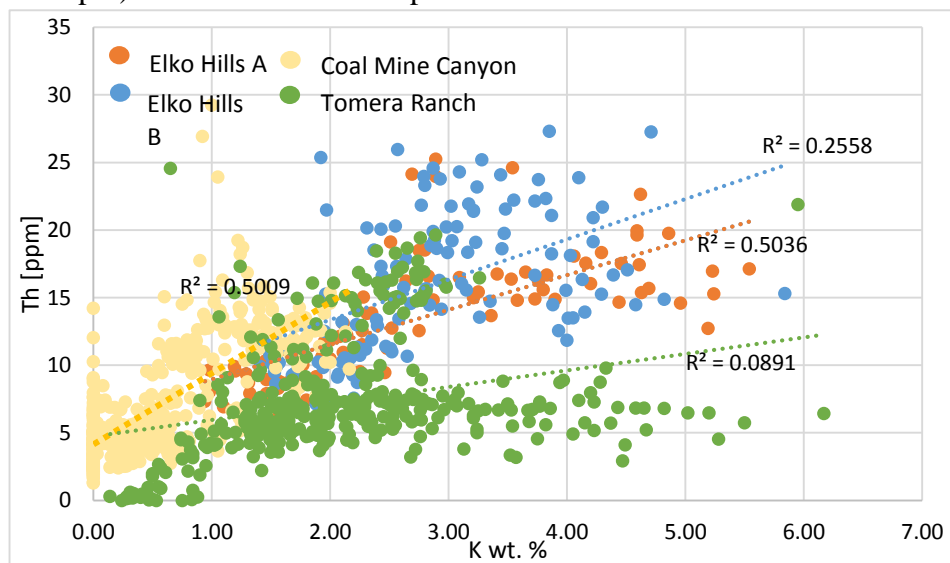


**Figure 15 (previous page):** Cross-plot displaying the relationship between the K (wt. %) against Th (ppm) at each outcrop.

Although origins are unable to be distinguished, clays such as illite and montmorillonite may have initially been volcanic ash which have been altered to clays. Even though poorly understood, this is particularly believed to be the case in the central, Elko Hills outcrops where water levels were deepest during deposition of sediment potentially facilitating alteration of volcanic material (Hazlett et al., 1992) and thorium uptake through cation exchange, adsorption, and surface precipitation (cf. Godelitsas et al., 1996). Thus, Th will be assumed to be a product of, or combination of each clay and volcanic ash, within this study.

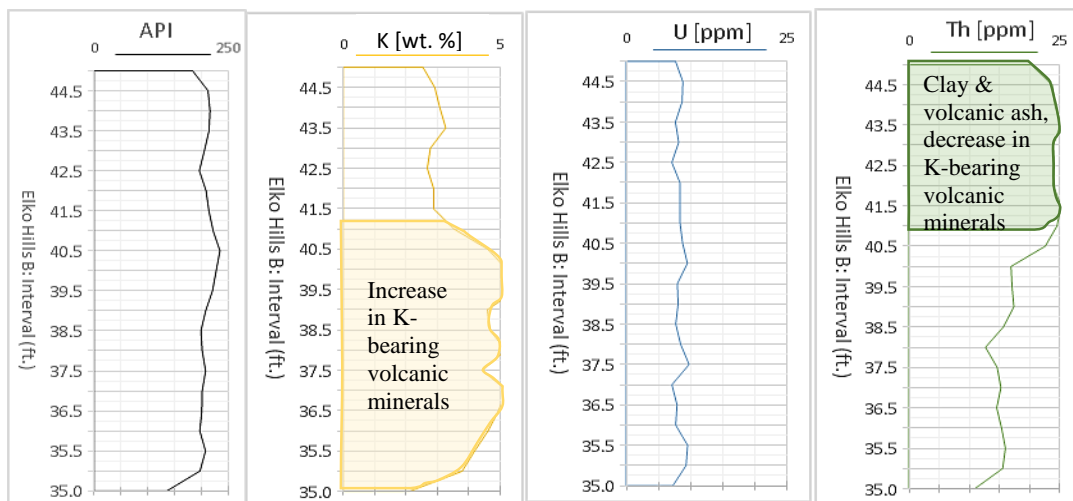


**Figure 16:** Four individual curves plotting API, K, U, and Th from 35 to 45 ft. at the Elko Hills B outcrop, left to right. K % curve shows the high K values at 37 to 40.5 ft. highlighted in yellow. Th (ppm) curve shows high Th reflection from 40.5 to 44 ft. highlighted in green.

Similar to the relationship between U and organic-rich shale in marine systems, high U readings closely correspond with F5 or F1/2 intervals in this study that contain significant amounts of organic matter (cf. Myers and Wignall, 1987). Fig. 17 shows a suite of curves with a U spike at 73–74 ft. and relatively consistent K and Th values that change independently from the U value. High-U readings are characteristically found in stratigraphic intervals which contain high amounts of microbial-mat-bearing mudstones (F5), however, some atypical readings occur. Following

Adams and Weaver (1958), a lack of U in exceptionally weathered outcrops is possible through weathering and leaching. This is generally uncommon, but evident in Elko Formation intervals in the Elko Hills sections such as at 36.7 ft. in the Elko Hills B outcrop (Fig. 16), where TOC analyses confirms 28.80 wt. % organic matter due to the lignite and coal, but lack a high-U response. In contrast, high-U concentrations are known to have occurred in the Elko Formation at the TR section where TOC data showed only 0.48 wt. % organic matter at 275 ft. (Appendix 8, 251–286 ft.). In this example, it is likely that weathering caused U to be adsorbed to iron or aluminum oxides or hydroxides as coatings on grains of the sediment (Adams and Weaver, 1958).

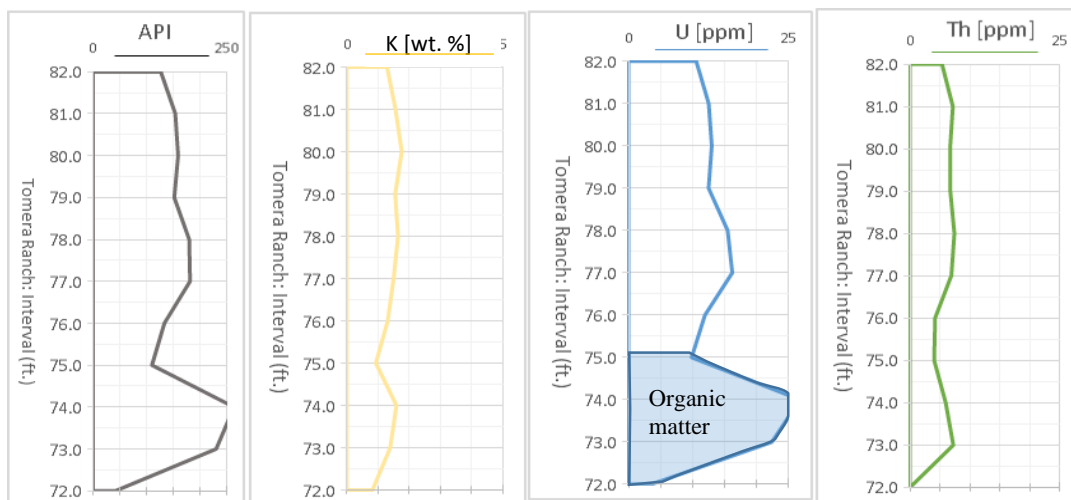


**Figure 17:** Four curves displaying API, K, U, and Th from Tomera Ranch at 72.0 to 82.0 ft., left to right. This shows a high reflection in U highlighted in blue, with relatively consistent K and Th reflections in the same stratigraphic interval.

### 6.2.1 Outcrop Trends

Overall trends at each outcrop were recognized in the distribution of K, U, and Th spectra, independent of facies. Proximal facies in the CMC and TR sections show similar SGR readings as do the SGR values of basinal facies in the EHA and EHB sections.

U-contribution, although relatively consistent throughout the basin, shows slightly higher values at the TR and CMC localities in comparison to both Elko Hills outcrops. This is likely due

to U-enrichment within calcareous mudstone (F4) and fossiliferous mudstone-packstone (F8/13) at CMC and heavy minerals and organic content at the TR section. The abundant, U-enriched organic and woody debris in contact with lake water resulted in high U values and influenced most of the facies at CMC, especially fossiliferous mudstone-packstone (F8/13) and calcareous mudstones (F4). This is likely due to the mobile uranyl ion form of U, which allows transport and precipitates as uranium salts under reducing conditions (Ch. 3).

Th values were higher in the EHA and EHB outcrops in comparison to the CMC and TR localities, probably indicating an abundance of weathered clay from volcanic ash, as well as suggesting the influence of lake water facilitating the subaqueous alteration of the sediment.

K values were low or zero at CMC, but were similar between both the Elko Hills and the TR outcrops. As K values were attributed to feldspars and K-bearing volcanoclastic minerals, these values fit well to the depositional model by Horner (2015) where CMC is the oldest of the four outcrops and volcanism may have only occurred in short pulses toward the later stages of CMC outcrop deposition and as a result did not influence high-K values as it did for the EHA, EHB, and TR sections. It should also be noted that K-bearing volcanic minerals within the minimal volcanoclastic facies (F10–12) samples at the CMC outcrop also exhibit partial to complete dissolution of these minerals, which could also attribute to the lack in high-K readings (Ch. 7.0). These outcrop trends are apparent and effect the eight facies described below.

### **6.2.2 Facies 1/2: Plant-Bearing Mudstone**

High K and Th readings (3.5–5.5 wt. % and 14–16 ppm, correspondingly) are likely due to reworked volcanic tuff (F10–12) stratigraphically overlying the F1/2 intervals at both Elko Hills outcrops, introducing an abundance of volcanic minerals and volcanic ash (Appendix 6; Figs. 23B and 23D). As a result, the Elko Hills sections show nearly two times the API values (200–210 API

units) of the CMC section (120–130 API units) (Appendix 6, Figs. 23A and 23E). The CMC outcrop has similar U values as the Elko Hills sections, and they range between 6 and 10 ppm with several values up to 18 ppm, likely due to the close proximity to the restricted paleo-swamp system active during the time of deposition of F1/2 (Appendix 6; Figs. 23C and 23G). This paleo-swamp system is likely contributing abundant plant debris and, therefore, organic material, adding to higher-U values at the CMC outcrop (cf. Horner, 2015). Following Swanson (1961), peat, lignite, and wood debris all readily extract and fix U from solution, which is consistent with the characteristic abundant plant debris for this facies at CMC.

### **6.2.3 Facies 3: Clay-Dominated Mudstone**

SGR measurements for clay-dominated mudstone (F3) show a lateral trend, where values from both the CMC and TR localities located close to the basin margin are between 120–140 API units, and values from the two Elko Hills outcrops, thought to represent the basin center are between 180–200 API units (Appendix 6, Figs. 23H and 23M). The CMC section shows low to zero K signals, likely due to short pulses of, or at times total lack of, volcanism during deposition, whereas Elko Hills and TR show similar K values between 2 and 3.5 wt. % (Appendix 6, Figs. 23J and 23N). The contribution of the K signal is likely a product of volcanic minerals (K-feldspar, mica), at Elko Hills and TR, as indicated by XRD analyses (Appendix 5). U responses, typically between 10 and 12 ppm, are likely due to higher amount of organic material deposited in the basin center by interbedded microbial-mat-bearing mudstone (F5) intervals between the clay-dominated mudstone (F3), whereas the CMC and TR location responses are between 6 and 8 ppm, suggesting a lack in U-enriched organic material (Appendix 6, Figs. 23K and 23O). Larger Th values (16–22 ppm) in EHA and EHB suggest greater amounts of volcanic ash and clay than the CMC and TR sections displaying 6–8 ppm (Appendix 6, Figs. 23L and 23P).

#### **6.2.4 Facies 4: Calcareous Mudstone**

Due to an overall lack of clay, volcanic minerals, and organic matter, calcareous mudstone (F4) displays API values commonly within 75–85 API units (Appendix 6, Fig. 23Q). Frequency diagrams show that the CMC readings reflect little to no K-bearing minerals, whereas TR has at least 2 wt. % K (Appendix 6, Fig. 23R), indicating that the TR outcrop was most likely affected by synsedimentary volcanism. Very low-K values in the CMC section can be attributed to the short pulses of volcanism during the deposition of F4, as previously mentioned in Ch. 6.2.1. The small amount of K-bearing minerals that were deposited were interpreted as preferentially dissolved as evidenced by the intraparticle porosity formed by partial to complete dissolution of feldspar grains observed in thin section (see Ch. 7.0). U values are almost double at CMC in comparison to TR, which could be due to the close proximity of the source of organic debris facilitating U-enrichment near the CMC section as opposed to TR (Appendix 6, Fig. 23S) (cf. Ehrenberg and Svånå, 2001; Horner, 2015). Th concentrations are also slightly higher at the TR section than at the CMC locality (4–6 ppm versus 6–8 ppm, respectively), most likely indicating higher amounts of clay and volcanic ash at TR versus the CMC section (Appendix 6, Fig. 23T).

#### **6.2.5 Facies 5: Microbial-Mat-Bearing Mudstone**

Microbial-mat-bearing mudstone (F5) is present in each outcrop with a high variability in API ranges due to localized differences in deposition and weathering and the effect on U abundance. The Elko Hills' sections exhibit the thickest microbial-mat-bearing mudstone intervals and the highest API values, ranging between 100 and 150 units at the EHA location, and 90–120 units at the EHB outcrop, likely due to the great amount of organic matter produced from the thickest microbial-mats in the center of the basin (Appendix 6, Fig. 23U). The CMC outcrop and TR recorded values from 70–130 API units, which is an uncharacteristically low value for this

facies. This is likely due to the fact that microbial-mats are interbedded with limestone in this CMC locality and influences the gamma ray readings (see Ch. 3.0). The TR outcrop exhibits a similarly uncharacteristic minimum of SGR readings as well as an atypical maximum value of 606 API units in these rocks, but values most frequently range from 100–160 API units (Appendix 6, Fig. 23Y). These extremely high values at the TR section are a result of a 17-ft. section which underwent intense oxidation exhibiting iron-oxide and hydroxide coatings on grains to which U isotopes readily adsorb (Adams and Weaver, 1958) (Appendix 8, 251–286 ft.). The Elko Hills sections show high Th readings (12–14 ppm), suggesting a great abundance of clay (or clay derived from volcanic ash), which correlates with the increase in volcanism during the time of deposition of this facies (Appendix 6, Figs. 23X and 23BB). U values are most frequently between 4 and 8 ppm for all four outcrops. Weathering and leaching may have played a role in the few U values greater than 8 ppm in the Elko Hills (Appendix 6, Figs. 23W and 23AA). Consistent K values between the Elko Hills and TR localities range from 2–3 wt. % and also confirm an active volcanic influence during deposition (Appendix 6, Figs. 23V and 23Z).

#### **6.2.6 Facies 6: Ash-Bearing Mudstone**

At the CMC location, frequency diagrams show that API values range from 60–90 units, whereas they show readings between 100 and 140 units at EHA and EHB, and between 100 and 150 units at the TR outcrop. Each outcrop's API value range is a function of fluctuating amounts of plant material, volcanic minerals, and clay components (Appendix 6, Figs. 23CC and 23GG) (cf. Horner, 2015). Both the CMC and TR locations show low amounts of K and Th, which most likely reflects the minimum overall gamma ray values that F6 shows at these outcrops, suggesting that weathering leached and removed these elements (Appendix 6, Figs. 23HH and 23JJ). In contrast, XRD data shows feldspar and zeolites from volcanic glass are present in the Elko Hills

outcrops, most likely contributing to their elevated K and Th values (Appendix 5; Appendix 6, Fig. 23DD). U values decrease from north to south (6–8 ppm at CMC and EHA and EHB, and 4–6 ppm at TR), suggesting that the organics in this facies are mainly from the paleo-swamp system near the CMC outcrop. This could be due to the mobile U ions from organic debris and woody material abundant in the paleo-swamp, decreasing as distance from the CMC section increases (Appendix 6, Figs. 23EE and 23II). U shows a wider range of data at TR than at the other three sections, likely due to the iron-oxide and hydroxide oxidation coatings covering the grains. These coatings most likely adsorbed U in some stratigraphic intervals similar to F5 (cf. Adams and Weaver, 1958).

#### **6.2.7 Facies 8/13: Fossiliferous mudstone-packstone**

Fossiliferous mudstone-packstone (F8/13) is present in the TR and CMC sections, commonly interbedded with F5, which likely provides U-bearing organic matter mainly contributing to total values between 80 and 120 API units (Appendix 6, Fig. 23KK). The significant SGR contrast between these outcrops is the lack of a K signal (<1% in the CMC section as opposed to 1.5% in the TR section), but strong U signal (8–10 ppm versus 6–8 ppm) at the CMC outcrop (Appendix 6, Figs. 23LL–23NN). This coupled U-enrichment and K-depletion suggests diagenetic alteration, in addition to volcanism being a very minor influence of K at this location. The notably high amounts of U could be due to the amount of time the rock was in contact with mobile uranyl ions in groundwater (Adams and Weaver, 1958), evidenced by the heavily diagenetically-altered samples as well as close proximity to the source of wood debris and organics at the CMC locality. Similar U-enrichment of wackestones were also reported in Ehrenberg and Svåná (2001) and were found to be a result of diagenesis.

### **6.2.8 Facies 10-12: Volcanic Tuff**

F10–12 combines lithic, crystal, and vitric tuffs, all three facies showing consistently high API values (> 120 API units) due to the overall quantity of radioactive K-bearing minerals (illite, feldspars, and biotite), reworked clays, volcanic ash, and other accessory minerals from volcanism (Appendix 6, Figs. 23OO and 23SS). Both Elko Hills outcrops show higher values for Th readings compared to the readings at the CMC and TR sections (22–26 ppm for both of the Elko Hills sections and 20–22 ppm for both of the CMC and TR sections, respectively), which suggest deposition of volcanic glass in deep water may play a role in facilitating volcanic glass and ash alteration to clays, increasing the Th contribution (Appendix 6, Figs. 23RR and 23VV). As a product of volcanic glass, zeolite crystals in aqueous solution facilitate the adsorption of Th through a process of ion-exchange, adsorption, and surface precipitation (Godelitsas et al., 1996), which could be the case for the Elko Hills sections in the central, “deep” water portion of the lake. The K signal from F10–12 at the CMC section is very low due to weathering of K-minerals evidenced by thin section observation and therefore most likely does not contribute much to the low API values at that locality (Appendix 6, Figs. 23PP and 23TT).

### **6.2.9 Facies 14: Conglomerate**

Conglomerate (F14) API readings at the CMC locality, the only place where this facies outcrops, most frequently range between 70 and 75 API units (Appendix 6, Fig. 23WW). These low API readings are here interpreted as a result of the lack of clay or volcanic minerals. K and Th readings range between 1 and 1.5 % and 4 and 6 ppm, respectively, and are likely the result of plagioclase and illite contents, respectively, based on XRD analyses (Appendix 6, Figs. 23XX and 23ZZ, Appendix 5). The U-contribution to the F14 rocks likely resulted from the contact with

groundwater and the re-distribution of U from U-bearing plant debris which is directly overlying the alluvial and fluvial conglomerate (Appendix 6, Fig. 23YY) (cf. Horner, 2015).

### **6.3 Th/U Trends and Basin Application**

Although this technique has not been previously applied to a lacustrine basin, general trends of Th and U distribution could be interpreted and applied in a similar manner as in marine systems to gain a better understanding of basin extent by lateral changes in Th/U. As clay and clay derived from volcanic ash are identified as the main control for Th values, and the U signal closely corresponds to the amount of U-bearing organic matter, Th/U allows for interpreting central portions of the lake by the amount of clay and organic matter distribution. Ideally, high amounts of Th indicate large quantities of clay in the central portion of the lake (as well as volcanic ash altered to clay) and less detrital and carbonate material in contrast to the lake margins. High abundance of fine-grained sediment such as clay is typically associated with the low-energy, “deep” portion of a basin (Bohacs, 1998). Consequently, in the Elko Basin, as the distance from the margin increases, the Th/U ratio increases as well. Low ratio values (<2.5) are indicative of proximal lake environments, while high ratios (2.5–4) suggest more central, basinward portions of the lake. XRD data confirm that compositional differences are in fact responsible for these lateral changes in Th/U in the microbial-mat-bearing mudstones (F5), as the EHA and EHB sections are composed of higher percentages of quartz and clay (chlorite and illite) in contrast to the CMC and the TR sections. The CMC and the TR outcrops instead display higher amounts of calcite, dolomite, and feldspars in comparison to the Elko Hills sections. The central, basinward portion of the lacustrine Elko Basin represented by the Elko Hills localities may, therefore, reflect the higher abundance of clay from water-lain ash and tuff, which may have been altered to clays (Hazlett et al., 1992). Th/U can be used to quantify and differentiate microbial-mat-bearing

mudstones (F5) between proximal and “distal” lake outcrops which would be valuable in recognizing unknown basin localities. Th/U ratios would be useful, for example, if applied to the Elko basin when drilling exploratory wells as well as a potentially applicable to future small-scale lake basins.

#### **6.4 X-Ray Diffraction and Total Organic Carbon**

XRD analyses show similar clay (illite) contents within plant-bearing mudstone (F1/2) and clay-dominated mudstone (F3) across all outcrops, but a high quartz and feldspar content only within the Elko Hills sections. Due to the stratigraphic position of the mudstones, deposited intermittently between times of volcanism, the source of quartz is likely from the overlying and interbedded volcanic tuff (F10–12) intervals. Four microbial-mat-bearing mudstone (F5) samples from the Elko Hills outcrops and eight F5 samples from CMC and TR sections contain traces of calcite and dolomite. The carbonate content in the TR and the CMC sections is due to being interbedded with carbonate [calcareous mudstones (F4) or fossiliferous mudstone-packstone (F8/13)], whereas the carbonate content in the Elko Hills sections likely was brought in from the margins during a change in lake level or during a storm event.

Illite is the most dominant clay mineral throughout all Elko Formation sections with low amounts of montmorillonite and kaolinite, which could be a result of weathering from volcanic glass or K-feldspar. Montmorillonite and kaolinite contents throughout the Elko Formation suggest that alteration from volcanic glass to bentonite occurred (Compton et al., 1999). Clinoptolite and unidentified zeolites were also prevalent in the Elko Hills and TR outcrops, but was not found in examples from the CMC section. These types of zeolites could indicate a different volcanic source with varying mineral composition or represent a product of alteration with burial depth and increase in temperature (Ogihara, 2000). Another volcanic mineral, cristobalite, was found

primarily in the TR and CMC sections, but not in the Elko Hills localities, which could represent a volcanic interval that did not outcrop in the Elko Hills sections or had never been deposited at those locations. XRD analyses contributed evidence to SGR curves, but independently would not be suffice in interpreting position of the Elko Basin based on examining inorganic content within facies.

TOC analyses confirmed that abundant organic matter typically correlated with high U values for seven out of the ten samples. Seven samples (F5 as well as F1/2) analyzed for TOC with characteristic U values show high amounts of organic content (Appendix 4, Elko Hills 24, 48.5; CMC 214; TR 73, 122, 204, and 209.5). The other three samples also showed high U readings, yet coupled with very low TOC contents confirmed by XRD analyses. These samples were a product of weathering, U-enrichment, or masked by clay. One example of F5 from the TR section at 275 ft. showed the highest U values out of all collected assay data, but showed very low organic matter content (0.48% TOC), confirming U values as a product of U-bearing iron oxides or hydroxides for this example. Another example analyzed was from calcareous mudstone (F4) (CMC 252 ft.), which had <1% TOC, despite its high U signal, concluding this carbonate interval experienced U-enrichment from U-rich groundwater. A Microbial-mat-bearing mudstone (F5) example from the Elko Hills B section at 36.7 ft. (refer to Ch. 6.2) had high organic content, however, it did not show a high U reading. It is therefore likely that the K and Th values were high enough to mask the U value of the rock or that U was leached from the outcrop exposure due to the soluble and mobile form of U (Adams and Weaver, 1958).

## **7.0 DIAGENESIS**

The facies of the Elko Formation exhibit a plethora of diagenetic phases and evidence of alteration, especially at the Coal Mine Canyon (CMC) and Tomera Ranch (TR) localities. All sediments contain authigenic cements, several of them independent of primary lithofacies. Thin section observation, X-ray diffraction (XRD) analyses, and scanning electron microscope analysis including investigations with an attached energy dispersive spectrometer (SEM-EDS) were conducted in order to identify cement phases and porosity types (see Ch. 4 Methodology). Diagenetic phases and porosity types are described below.

### **7.1 Carbonate**

#### **7.1.1 Calcite**

XRD analyses show that calcite cement is sparse, being present in <5% of the rock volume, typically within the clay-dominated mudstone (F3), calcareous mudstone (F4), fossiliferous mudstone-packstone (F8/13), and microbial-mat-bearing mudstone (F5). One type of sparry calcite cement is recognized and is present only at the CMC outcrop. This sparry calcite generally fills voids between crinkly and wavy mud laminae in F3 and is recognized by equigranular crystals, ~0.08 mm in width (Fig. 18C). Calcite crystals are white to off-white in plane light and high birefringence pastel colors in cross-polarized light.

#### **7.1.2 Dolomite**

A total of four generations (I–IV) of dolomite cement were found, three microcrystalline and one bladed cement, and each of the four generations is best distinguished from the other dolomites both under plane and cross-polarized light (Fig. 18B). Dolomite cement is typically found within fossiliferous mudstone-packstone (F8/13) in the internal void of ostracod skeletal

grains, associated with chalcedonic quartz and found within calcareous mudstone (F4), which were both observed in the CMC and TR sections. Dolomite also occurs within the microbial-mat-bearing mudstone (F5) and the clay-dominated mudstone (F3) that are found at all localities. Based on XRD analyses (Appendix 5), the calcareous mudstone (F4) and fossiliferous mudstone-packstone (F8/13) contain dolomite up to 60% in some cases, however, most samples contain less than 30% dolomite and the clay-dominated mudstone (F3) and microbial-mat-bearing mudstone (F5) contain <5% dolomite. SEM-EDS analyses (Appendix 7) confirm that the four types of dolomite show an increase in the amount of magnesium from dolomite I to III, with dolomite IV values being similar to dolomite III. Dolomite I–III are microcrystalline dolomite, displaying each a similar inclusion-poor crystal fabric, but each of them also has a specific, identifying coloring in addition to the successive increase in magnesium. Dolomite I is irregularly shaped, cloudy and relatively colorless to light brown with an average of 7.73 wt. % Mg. Dolomite II forms an isopachous rim up to 0.10 mm in width and is light brown with yellow undertones with an average of 7.99 wt. % Mg. Dolomite III also forms an isopachous rim, up to 0.02 mm in width displaying a light tan color with yellow undertones and the highest average wt. % Mg of 17.81. Dolomite IV exhibits colorless subhedral to euhedral bladed crystals up to 0.05 mm in length and 0.02 mm wide, and contains a similar average Mg wt. % as dolomite III of 17.00.

## **7.2 Quartz**

Quartz is found primarily within the fossiliferous mudstone-packstone (F8/13) and calcareous mudstone (F4) at the CMC and TR sections. Based on XRD analysis, F8/13 samples from CMC and TR typically contain up to 5% quartz, with the exception of almost 50% in one F4 sample from the CMC section. Two generations of chalcedonic quartz cement have been identified: radial and cryptocrystalline (Fig. 18A). Both types of chalcedony fill shelter porosity

within F8/13 and, less commonly, fractures. The first generation forms cryptocrystalline chalcedonic cement, in places present as an isopachous rim that can be up to 0.003 mm thick. Cryptocrystalline chalcedonic fabric is recognized by its radial habit under cross-polarized light (Fig. 18A). The more predominant second generation (present with or without the first generation), radial chalcedony, exhibits a well-defined radial habit identifiable under cross-polarization and reaches up to 0.01 mm in both length and width (Figs. 18A and 18B).

### **7.3 Zeolites**

White or off-white acicular zeolite crystals are typically 0.01 mm wide and up to 0.05 mm long occurring on the outer margin of roundish voids in a volcanic glass matrix in volcanic tuff (F10–12) exclusively at the Elko Hills and TR localities, and in two microbial-mat-bearing mudstone samples, according to XRD analyses (Figs. 18D and 18E). Zeolite cements including clinoptilolite comprise up to 10–15% of F10–12 and ~2–8 % of F5 based on XRD data (Appendix 5).

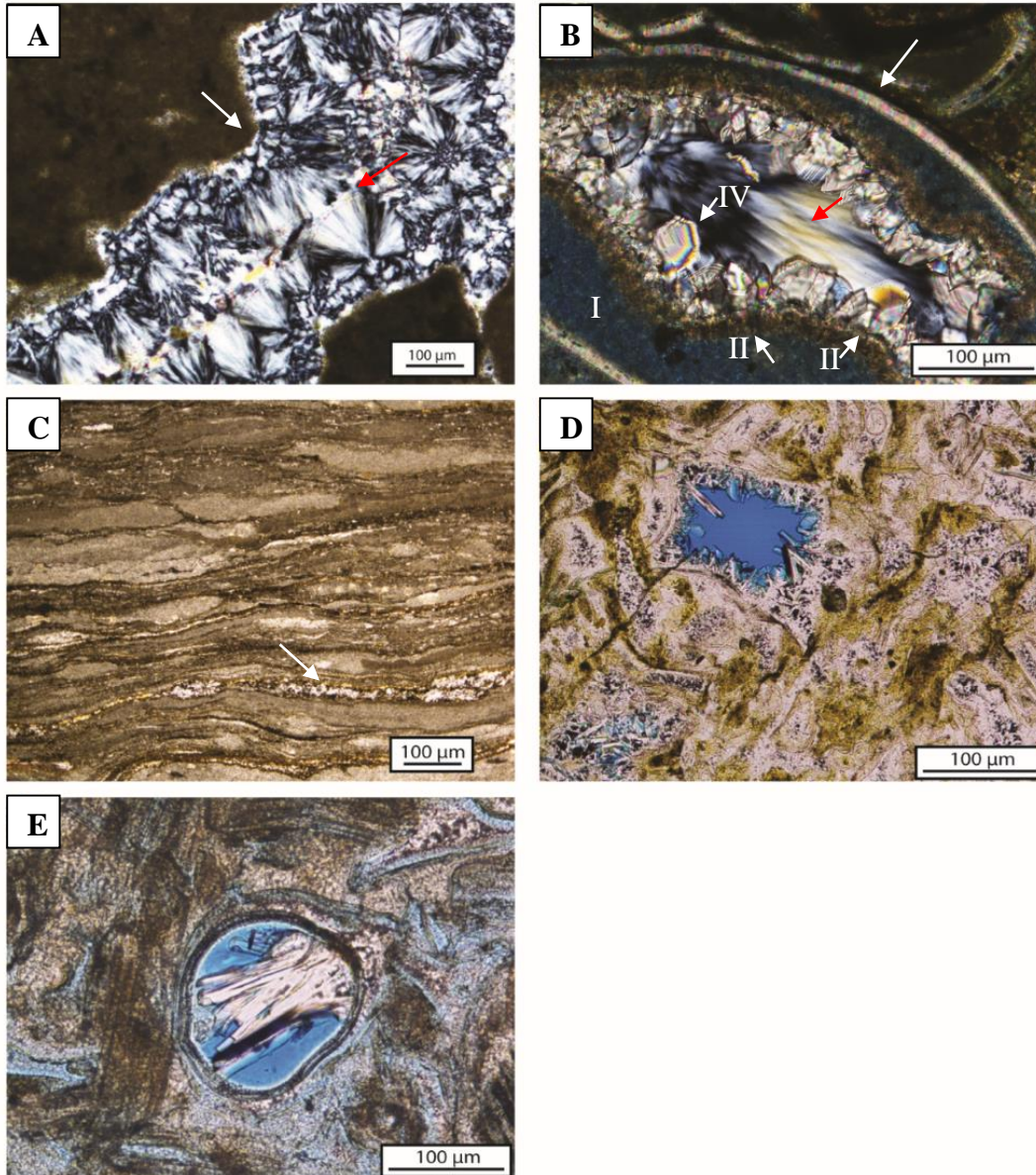


**Figure 18:** **A)** Fracture in the fossiliferous mudstone-packstone (F8/13) filled with two generations of chalcedonic cement, the cryptocrystalline isopachous cement at the margin of the fracture (white arrow) and the radial fabric infilling most of the fracture opening (red arrow). **B)** Example of calcite ostracod shell (white arrow) with dolomite cements I-IV each labeled in fossiliferous mudstone-packstone (F8/13). Radial chalcedony is also marked by a red arrow. **C)** Sparry calcite cement filling in elongate voids, marked by the white arrow in clay-dominated mudstone (F3). **D)** An example from volcanic tuff (F10–12), acicular zeolite cement precipitating into angular voids. **E)** Zeolite cement precipitating in a sphere-shaped void in volcanic tuff (F10–12).

## **7.4 Porosity**

Five types of porosity were recognized in thin section, categorized by applying the Choquette and Pray (1970) classification scheme originally developed for carbonate rocks (for all except matrix porosity) (see Ch. 4.0 methodology). Most porosity types were present within carbonate and volcanic tuff facies [calcareous mudstone (F4), fossiliferous mudstone-packstone (F8/13), and volcanic tuff (F10–12)], but were also infrequently found within siliciclastic facies [plant-bearing mudstone (F5), conglomerate (F14), ash-bearing mudstone (F6), and clay-dominated mudstone (F3)]. With the exception of the conglomerate (F14), porosity was found to be low overall (<3%) with pore sizes ranging from 0.1 to 1 mm wide, and very low connectivity.

### **7.4.1 Interparticle Porosity**

Interparticle porosity is rare in Elko Formation sediments, and predominantly found in volcanic tuff (F10–12) and conglomerate (F14) as open porosity. Pores are typically sub-millimeter-size to millimeter-size and irregularly-shaped between volcanoclastic grains in F10–12, and between clasts in F14 (Fig. 19A). Conglomerate (F14) with up to 30% porosity is only present at CMC and shows moderate to high connectivity of pore spaces. F10–12 displays up to 10% porosity, with very low to no connectivity (Fig. 19B).

### **7.4.2 Intraparticle Porosity**

Intraparticle porosity is present exclusively in volcanic tuff (F10–12) within volcanic minerals as open porosity. F10–12 shows up to 15% intraparticle porosity, found in the Elko Hills and TR outcrops. Pores are irregularly shaped, angular, and range from 0.001 to 0.5 mm with little to no connectivity (Fig. 19B and 19C).

### **7.4.3 Shelter Porosity**

The fossiliferous mudstone-packstone (F8/13) in the CMC and TR sections displays open and minus-cement (original porespace, later filled by cement) shelter porosity (<3%). Shelter porosity in the Elko Formation consists of various forms, often roundish to irregular and is shown underlying randomly-oriented whole and fragmented ostracod shells which are up to 1 mm in length. Individual pores are generally less than 0.5 mm in length, are partly filled with silica and carbonate cements, and show little to no connectivity (Fig. 19D).

### **7.4.4 Matrix Porosity**

In the Elko Formation, matrix porosity is typical of volcanic tuff (F10–12), calcareous mudstone (F4), and fossiliferous mudstone-packstone (F8/13), and generally comprises <3% of the rock as open porosity. Herein, matrix porosity is identified as the voids between either the volcanic glass shards mainly composing the volcanoclastics (F10–12) or voids within carbonate mud in either the calcareous mudstone (F4) or fossiliferous mudstone-packstone (F8/13). Matrix porosity consists of irregularly shaped sub-millimeter micro-pores (Fig. 19B). These micro-pores have moderate to low connectivity.

### **7.4.5 Fracture Porosity**

Fracture porosity is rare and found independent of outcrop location predominantly in clay-dominated mudstone (F3), microbial-mat-bearing mudstone (F5), fossiliferous mudstone-packstone (F8/13), and volcanic tuff (F10–12) as open and minus-cement porosity. Most fractures are sub-vertical and less than 0.3 mm in width, however, some are oriented parallel to bedding, especially within F3 or F5 (Figs. 18A and 19E). In cases of F8/13, fracture width is irregular, variable, but less than 0.5 mm in size, and filled in by silica cement, whereas within F5 and F3 fractures appear regular, unfilled, and less than 0.005 mm in width.

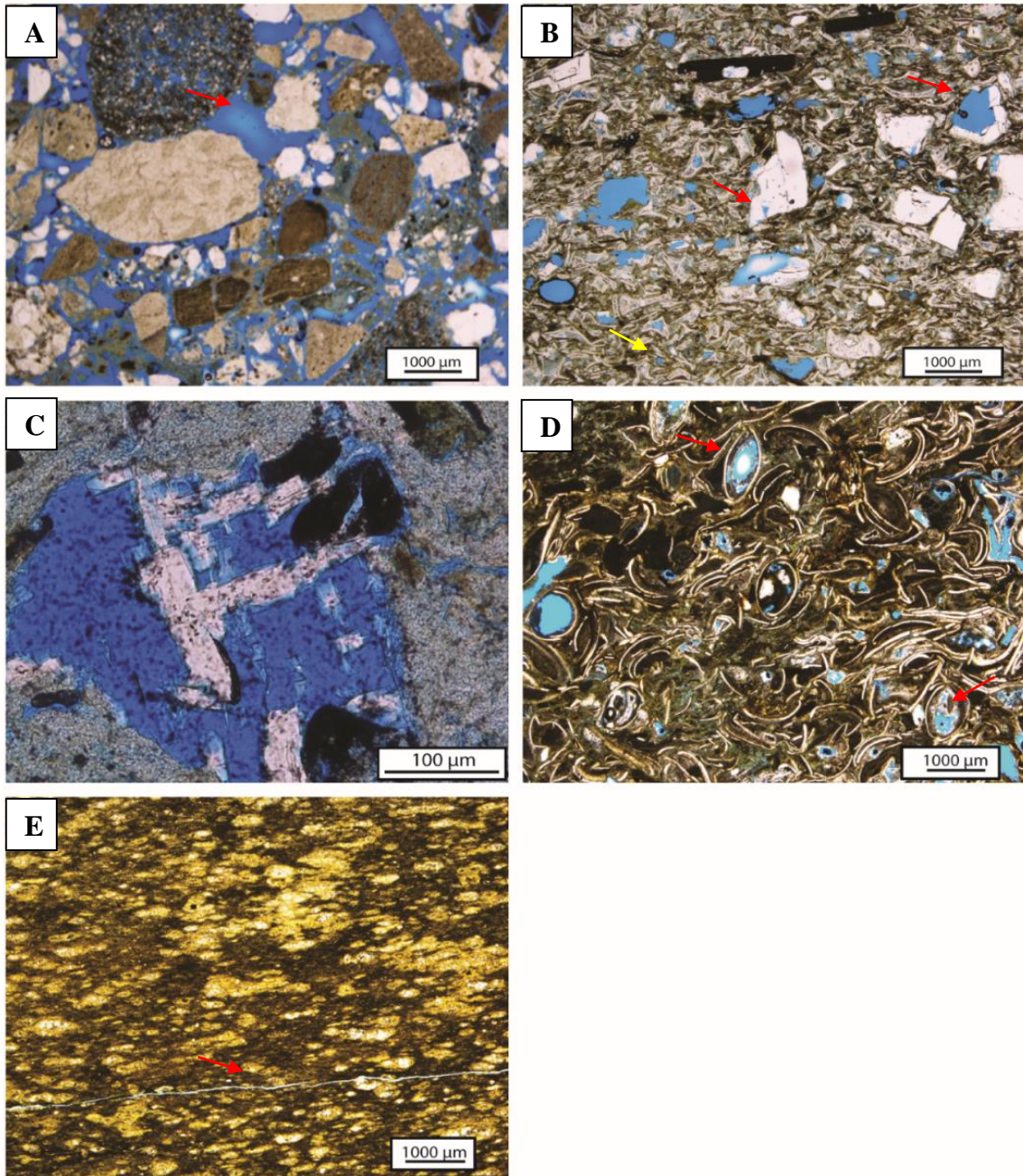


**Figure 19:** **A)** Conglomerate (F14) displaying interparticle porosity (blue-stained areas), marked by red arrow **B)** Volcanic tuff (F10–12) with intraparticle porosity (red arrows) and matrix porosity (yellow arrow). **C)** F10–12 shows intraparticle porosity within volcanic grains. **D)** Fossiliferous mudstone-packstone (F8/13) displaying shelter porosity (marked by red arrows). **E)** Fracture porosity within F5 (red arrow).

## **7.5 Relative Timing**

Textural relationships and overgrowth of diagenetic components can be used to determine their relative timing within the Elko Formation (Fig. 20). Based on this method, the interpretation and succession of the diagenetic cements and porosities within this Tertiary unit are described below.

### **7.5.1 Calcite**

It is likely that the calcite present in the Elko Formation precipitated as a result of an introduction of calcite-rich waters in this meteoric environment (cf. Moore, 2001). Because microcracks likely formed by dewatering of sediment (cf. Flügel, 2004), calcite is also assumed to be a product of post-deposition and burial, although the timing of its formation is unclear.

### **7.5.2 Dolomite**

Each of the four types of dolomite cement is considered post-depositional in origin, generally found succeeding one another, precipitating into shelter porosity in fossiliferous mudstone-packstone (Fig. 18B). Based on overgrowth relationships and SEM analyses (Appendix 7), dolomite I reflects the first generation, typically found precipitating directly on microcrystalline calcite ostracod shells. Dolomite II, III, and IV followed sequentially by overgrowth and represent the second, third, and fourth generation of dolomite cement, respectively.

### **7.5.3 Quartz**

Both generations of chalcedonic quartz, cryptocrystalline and radial, are authigenic and most likely reflect two generations of silica-enriched fluids that migrated through the rocks during burial. Following microcrystalline dolomite I–IV, chalcedonic quartz cement precipitated into shelter or fracture porosity. It is likely that the rock was lithified in order to be fractured, so the precipitation of silica cements most likely occurred at significant depth during burial. In the Elko

Formation sediment, cryptocrystalline chalcedony cement is typically found as a precursor to radial chalcedony. Cryptocrystalline and radial chalcedony likely represent *length-fast* and *length-slow* chalcedony, respectively. *Length-slow* (or “quartzine”) indicates a slower polarized light component produced by the fibers parallel to crystal length formed by replacement of carbonate minerals, whereas *length-fast* indicates fibers perpendicular to the c-axis of the crystals (Folk and Pittman, 1971). Silica precipitation probably originated from silica-enriched groundwater where sources of silica were most likely dissolved quartz or feldspar grains (cf. Yang et al., 2015), or volcanic minerals (i.e. cristobalite) (cf. Schubel and Simonson, 1990; Heaney, 1993).

#### **7.5.4 Zeolite**

Acicular zeolite cement predominantly occurs in the volcanic tuffs (F10–12) as well as two microbial-mat-bearing mudstones (F5) based on XRD analyses, and represents a product of post-deposition and burial, infilling primary matrix porespace and vesicles. Vesicles appear as unfilled spheres sub-millimeter in size, forming between volcanic grains, likely as a product of devitrification (cf. Gondé et al., 2011). XRD analyses (Appendix 5) identifies clinoptolite as well as other unidentifiable zeolites within the Elko Hills and TR sections, reflecting the increase in volcanism during the time of sediment deposition. Following Ogiwara (2000), burial diagenesis allows clinoptolite to form from volcanic glass via cation exchange of K, Na, or Ca. In lake systems, volcanic glass is assumed to increase the pH of neutral water creating an alkaline-rich system. When volcanic glass shards react with highly alkaline water, they produce a gel, which over time crystallizes as zeolite cement (Leggo et al., 2001). Burial diagenesis alters clinoptolite further to analcime and/or heulandite (Utada, 2001) which most likely comprises the unidentified zeolites found in both the Elko Hills and TR sections. As acicular zeolite cement precipitates

mainly into the matrix porosity and vesicles within F10–12, the timing of the zeolite cements remains unclear within the sediments of the Elko Formation.

### **7.5.5 Porosity**

Two of the five types of porosity are primary, shelter and interparticle, i.e., porosity formed during deposition (cf. Choquette and Pray, 1970). Although matrix porosity is typically found as secondary porosity in the Elko Formation, it is too considered primary in the volcanic tuff (F10–12), occurring only within welded to poorly welded glass shards and ash formed during deposition. Interparticle porosity is mainly present within conglomerate (F14) as a product of deposition of gravel-size clasts, while the shelter porosity in the Elko Formation formed in fossiliferous mudstone-packstone (F8/13) from ostracod and skeletal grains shielding infill of sediment during burial. Intraparticle, matrix [in calcareous mudstone (F4), ash-bearing mudstone (F6), and fossiliferous mudstone-packstone (F8/13)], and fracture porosity were most likely created after deposition and are herein considered secondary that may have formed at any time throughout the diagenetic history of the Elko Formation.

In the volcanic tuffs (F10–12), the amount of intraparticle porosity varies as a result of partial or complete dissolution of feldspar grains. Preferential dissolution of feldspar grains can be facilitated through acidic waters at low temperatures, altering the feldspar to kaolinite, and eventually smectite so that secondary porosity can develop (Yang et al., 2015). Secondary matrix porosity appears to be a product of dissolution from mixing of meteoric and acidic waters common in vadose or phreatic environments (Moore, 2001). In the Elko Formation, it is likely that these two types of water were saturated either with volcanic minerals within calcareous mudstone (F4) on the one hand, and from fossiliferous mudstone-packstone (F8/13) on the other hand. Fracture porosity in microbial-mat-bearing mudstone (F5), clay-dominated mudstone (F3), fossiliferous

mudstone-packstone (F8), and volcanic tuff (F10–12) is interpreted as a product of burial and compaction, and in places could indicate active tectonism since found near micro-normal faults (Horner, 2015).

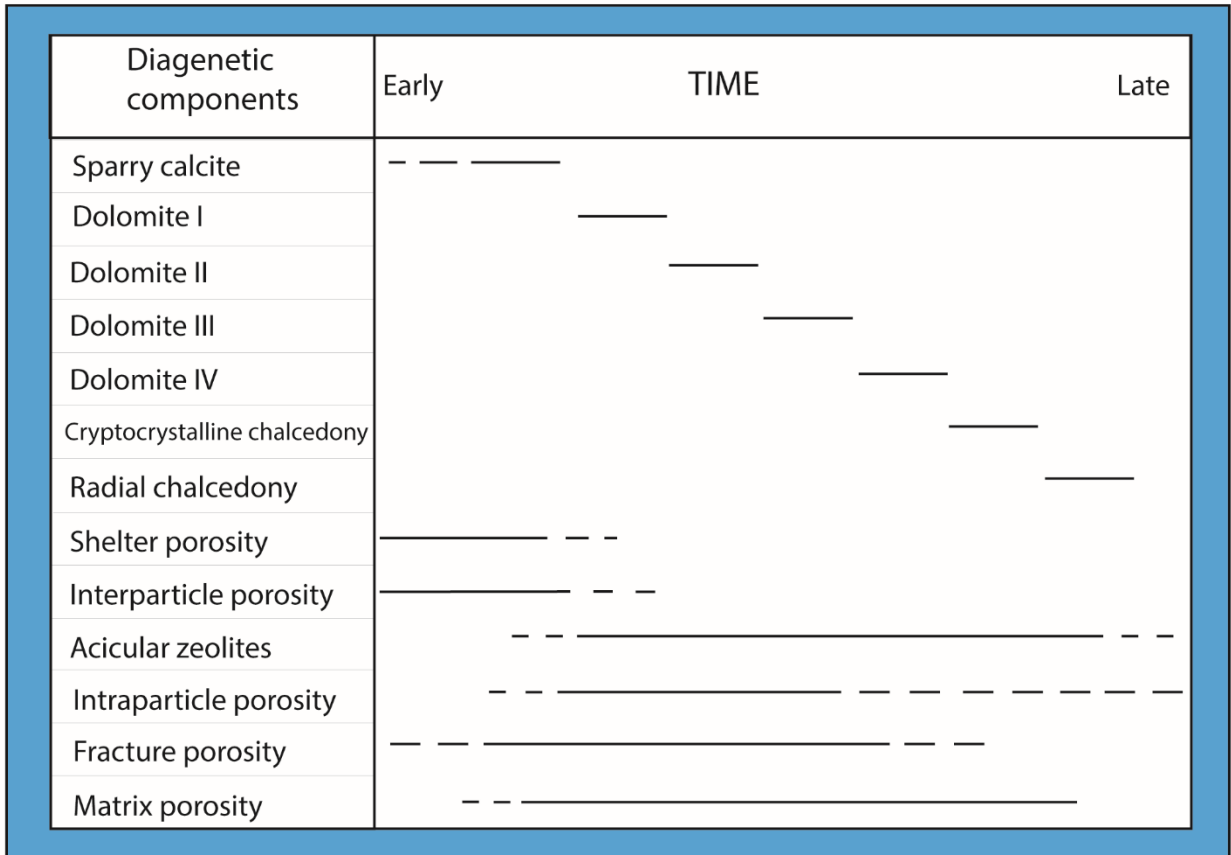


**Figure 20:** Relative timing of diagenetic components in the Elko Formation.

## 8.0 DISCUSSION

### 8.1 Pitfalls of gamma ray spectrometry

One of the purposes of compiling 979 spectral gamma ray (SGR) readings with a portable spectrometer was to evaluate the effectiveness of this methodology as an *in-situ*, time-efficient, and cost-effective means of characterizing the gamma ray signal of the upper Elko Formation. In accordance with Serra (1984) and Blum et al. (1997), collected SGR data proved useful to further understand sediment composition, diagenesis, and origin, by understanding the inorganic or organic constituents which were the source of radioactive elements (K, U, and Th). SGR data represents a direct method to characterize the gamma ray signature of facies based on their potassium (K), thorium (Th), and uranium (U) abundance derived from their geochemical and radiometric attributes (Slatt et al., 1992; Ehrenberg and Svånå, 2001; Guagliardi et al., 2013). Although the gamma ray spectrometer was useful in characterizing the eight facies of the Elko Formation, issues arose, specifically that data is missing from covered intervals and there was inherent uncertainty of reading interference between facies in close proximity.

For SGR data collection, an ideal situation would be a planar, unweathered outcrop surface, as it presents the least amount of disruption for the most accurate readings (Myers and Wignall, 1987). Most of the time, artifacts of weathering were avoided, except at the TR section where most likely uranium adsorbed onto iron oxides on the sediment surface greatly affected the data and gave anomalous high U readings in a 35-ft. interval (cf. Adams and Weaver, 1958; Dickson and Scott, 1997) (Appendix 8, TR at 251–286 ft.). Intervals covered by vegetation, or modern soil that could not be excavated, resulted in intervals of missing data. Lastly, interference between facies is a potential source of error, due to the radius in which the gamma ray spectrometer detector takes

readings. This could result in false facies readings to be influenced by radioactivity from an over- or underlying facies in close proximity to the target facies. This interference was often unavoidable due to the nature of the detector and the stratigraphic interval thickness in some places. Due to these variables, frequency distribution diagrams were useful to narrow down the range of values for an assigned facies, eliminating uncommon and likely anomalous values (Appendix 6). Nevertheless, of these potential and actual reading errors, only the U adsorption would potentially lead to unexpectedly *high* SGR readings. As weathering crusts are generally obvious and oxidation visibly alters the rock in outcrop and would be noted during fieldwork, it is speculated that most of the measured and documented values are too low rather than too high. This should be taken into account when recovering core from an oil well, which may in places show higher readings than the outcrops because of the lack of weathering.

## **8.2 Comparison of gamma ray readings with similar previous studies**

In the present study of Elko Formation strata, SGR detects K, U, and Th that predominantly reflects the amount of K-bearing volcanic minerals (feldspars, mica, and illite), organic material, and clay abundance, respectively. Previous studies (Adams and Weaver, 1958; Ehrenberg and Svånå, 2001; Svendsen and Hartley, 2001; Fabricius et al., 2003; Guagliardi et al., 2013) reported similar findings despite their research being based on marine successions. In these studies, K and Th are typically associated with clays, and K with feldspar, while U abundance is driven by the amount of organic matter and phosphate in the rocks. One of the few lacustrine examples (Bohacs, 1998) showed similarities between controls of K and Th, but did contrast with what components of the rock affected the U readings. Although his results were not based on a specific alkaline lake system, he determined that detrital volcanoclastic sands, heavy minerals, and volcanic ash controlled K, U, and Th contributions, respectively (Bohacs, 1998). Following Bohacs (1998), the

composition of the lacustrine Elko Formation suggests that volcanic minerals, including feldspars, did contribute to the majority of the K readings, especially within the Elko Hills and TR outcrops. As the water-lain ash was likely altered to clays (cf. Hazlett et al., 1992), the contribution of the Th values could potentially be considered from volcanic ash as well (cf. Bohacs, 1998). In contrast to Bohacs (1998), the Elko Formation is rich in organic matter, and variations in the amount of organic matter corresponds to the U readings. Bohacs (1998) found that heavy minerals influenced the U readings at least as much as the organic content of the sediment based on the assumption that freshwater systems exhibit a low concentration of organic material. The palustrine-lacustrine environment and microbial-mats of the Elko Formation provided substantial amounts of organic material which allowed for mobile U isotopes to be fixed (cf. Fabricius et al., 2003). Therefore, a low concentration of U in lake systems may generally explain low SGR U-readings, but these may not apply to all facies within a lake, especially in small-lake systems.

### **8.3 Diagenetic effect on gamma ray readings**

It was expected that the various types of diagenesis may strongly influence SGR readings, even of the same facies, because the signal may have been heavily altered by calcite-filled fractures e.g in clay-dominated mudstone (F3) or microbial-mat-bearing mudstone (F5). Such calcite-filled fractures in great amounts could lower an otherwise high gamma ray reading as carbonate typically shows low SGR signals. Nevertheless, in this study, significant volumes of highly-altered rock were absent and suggests that diagenesis did not change the gamma ray signature of the Elko Formation strata significantly. As diagenetic phases make up a maximum of <10% of the rock volume at most, it was not found in enough abundance to interfere with or give false low gamma ray readings for facies with typically high radioactivity. Most alteration occurred within the carbonate facies [calcareous mudstones (F4) and fossiliferous mudstone-packstone (F8/13)].

Some alteration occurred in the microbial-mat-bearing mudstone (F5) and clay-dominated mudstone (F3), where dolomite replaces calcite; however, this replacement would not affect the gamma ray signal as the readings would remain relatively low. However, 17 ft. of carbonate facies (F4 and F8/13) interbedded with microbial-mat-bearing mudstone (F5) at the CMC outcrop (Appendix 8, 229–246 ft.) exhibit higher than typical U readings. The 17-ft. interval of the CMC section was likely subject to U-enrichment due to its close proximity to the palustrine-lacustrine swamp source likely providing abundant readily available U adsorbed to organic material, whereas the proximal TR section furthest from the swamp source did not show any similarly U-enriched intervals. Diagenetic transfer of U from overlying organic matter-rich material is most likely the cause of high U values coinciding with low K values in this part of the CMC succession (in comparison to the same facies at the TR section). Low K readings in this stratigraphic interval, only in the CMC section, are likely from K-depletion in which feldspars have been dissolved partly or completely in early stages of weathering (Yang et al., 2015). K-depletion supports heavy alteration throughout this carbonate facies interval in addition to the minor volcanoclastic input during deposition. A similar pattern reflecting enrichment of U in a carbonate interval was reported from Ehrenberg and Svåná (2001) in a study focusing on spectral gamma ray signatures of stratigraphic surfaces in a shallow-water carbonate environment. Ehrenberg and Svåná (2001) found that a carbonate interval that likely experienced subaerial exposure during a sea level lowstand also showed high U readings. In their model, mobile, oxidized U from U-enriched groundwater became fixed to the argillaceous strata deposited during the sea-level lowstand. Although, the carbonate facies in this CMC section could have been subaerially exposed, there is no direct evidence to support this.

#### **8.4 Application of Th/U ratios to analyze lacustrine basin extents**

As shown in this study, as distance from margins increases, the Th/U ratio increases as well for the Elko Formation microbial-mat-bearing mudstone (F5), ranging between 0 and 4. In contrast, previous studies conducted on marine environments show that the Th/U ratio decreases as distance from the basin margins increases and displays larger extremes of Th/U ratios, ranging from less than 0.02 to greater than 21 (Koczy, 1949; Adams and Weaver, 1958; Bohacs, 1998; Doveton and Merriam, 2004). These studies have shown that for mudstones in a marine basin, U values are high in the central part of the basin where low-energy, less-oxygenated conditions exist as opposed to the basin margins which would not have the same concentration of organic matter. In contrast, Th values of mudstones are low in the central part of the basin, where little clastic, terrigenous material would be transported (Adams and Weaver, 1958; Bohacs, 1998).

The Elko Formation is a small-lake system with an unknown, but likely shallow depth within the photic zone, based on the presence of microbial mats (Horner, 2015). The concept behind the Th/U ratios is to understand the basin extent of the Elko Formation by distribution of organic and inorganic sediment composition. The usage of the Th/U ratio, though, differs from its marine counterparts. Although average values for Th and U vary slightly between vertical stratigraphic intervals of microbial-mat-bearing mudstones (F5), each individual outcrop exhibits similar Th/U ratios overall with regards to their proximal or distal position in the basin. Th values, rather than U as in marine systems, are the greater control of the Th/U ratios in the Elko Formation due to the alteration of volcanic ash to clay in the central portions of the basin, as well as Th not having a soluble and mobile form equivalent to U. The central Elko Hills locations show Th/U ratios that are consistently higher ( $> 2.5$ – $4$ ) than Th/U ratios at the more proximal CMC and TR sections ( $< 2.5$ ; Fig. 14A–D in Ch. 5). Although the Th/U ratio is not as dramatically different as

for cases described by Adams and Weaver (1958) and is typically  $<4$ , low magnitude ratios are likely directly linked to the size of the lake, water depth, and relatively low U values of organic-rich microbial mats, and lacustrine mudstones in general, as opposed to marine mudstones, which in some examples exceed a ratio of 20. The influence of water depth in the central portions of the lake may play an integral part in the volcanic ash altering into clay, thereby increasing the amount of Th adsorption, whereas in the shallow-water margins, this would be less likely (cf. Godelitsas et al., 1996) (refer to Ch. 6.2).

### **8.5 Assigned facies**

Earlier studies applied handheld gamma ray spectrometers to outcrops exclusively in marine systems focusing on economic black shale, resulting in readings which could be easily discerned from other lithologies due to their overall high radioactivity (greater than 200 API). (Krystinak, 2003; Afill, 2007). In contrast, handheld gamma ray spectrometer application to the Elko Formation lacustrine strata focused on the economically important microbial-mat-bearing mudstone (F5) as well as on seven additional facies. General composition of these eight facies were at times complicated by small amounts of radioactive materials, specifically K-bearing volcanic minerals or U-bearing wood debris, which recorded values outlying the most commonly recorded ranges. Frequency distribution charts (Appendix 6) enabled distinction between SGR readings of these facies, and also emphasized the outcrop position in the basin and the influence that lake position had on the distribution of these radioactive materials.

Based on thin section and XRD analyses, facies of the Elko Hills and TR sections and intervals in close proximity to the volcanic tuff (F10–12) were found to likely have been influenced by K-bearing and heavy minerals, such as these present in the microbial-mat-bearing mudstone (F5), clay-dominated mudstone (F3), and plant-bearing mudstone (F1/2). Another significant

constituent of the rock that could also have influenced facies by U-enrichment was the woody debris. The ash-bearing mudstone (F6), clay-dominated mudstone (F3), fossiliferous mudstone-packstone (F8/13), and calcareous mudstone (F4) that were deposited in close proximity to the palustrine-lacustrine depozone all showed elevated SGR signals due to the organic-rich paleo-swamp near the CMC section which was probably the source of the organic matter. The influence of the position of the outcrop within the lake basin is likely due to the fact that the Elko Basin is a small-lake system as opposed to a large lake or marine environment. Small lakes exhibit depositional environments strongly affected by small-scale changes from climate and tectonics, especially its influence on subsidence and accommodation. Therefore, variations in climate and tectonics have a strong effect on gamma ray readings in lacustrine strata as opposed to marine systems which are generally more static and are controlled by eustatic processes (Bohacs et al., 2000).

### **8.6 Interpretation of SGR data**

Interpretation of SGR data suggests that K, U, and Th were primarily sourced from K-bearing volcanic minerals (K-feldspar and mica), U-enriched organic material, and clays (illite and montmorillonite), respectively. This information provides a guide to analyzing subsurface SGR curves of the Elko Formation with a relatively low level of uncertainty, by constraining the causes of high-K, high-K combined with high-Th, and high-U values.

High-K values independent of high-Th values, strongly suggest heavy K-bearing minerals associated with volcanism. When high-K values are recorded at the same interval as high-Th values, this indicates a greater probability that both high-K and high-Th are associated with non-volcanic clays. High-U values, regardless of high-K or high-Th values being present, is most likely

an indication of U-enriched organic matter. It typically, but not always, occurs with high-Th values.

### **8.7 Comparison to Noble Energy EOS-3 core SGR data**

Noble Energy core data, including TOC and XRD analyses, was available for comparison in this study. Facies were assigned to core SGR measurements based on core descriptions previously recorded, as well as available XRD analysis data.

SGR data acquired by wireline logging was found to be difficult to compare to the outcrop data, due to the higher resolution of the wireline tool versus as compared to the handheld gamma ray spectrometer. In general, values in API units were found to be slightly lower for the core, in contrast to outcrop measurements.

However, more detailed analysis was found to be inconclusive. For example: similarities between K and Th values between the core and EHA and EHB data for F5 were found (Figs. 21A–C; Appendix 6, Figs. 23U-23BB, respectively), however, U values in the core data were much lower. SGR data for F4 showed similarities between K and U values in comparison to the TR section, but Th was much lower in core (Figs. 22A–C). This could be due to a number of issues: the effect of deposition where the core was acquired, the difference between tools utilized to collect data, or the difference between fresh, unaltered core versus exposed outcrop section.

Although quantitative comparisons between overall total gamma radiation and SGR values were not able to be made between the core and outcrop, similar trends between the XRD analyses data and high-K, high-U, and high-Th values recorded on the core SGR curves did to correlate with K-bearing minerals (K-feldspar, mica), TOC-rich intervals, and total clays (illite, montmorillonite), respectively, and these trends can still be applied to better understanding the core log of the Elko Formation or future SGR data gathered.

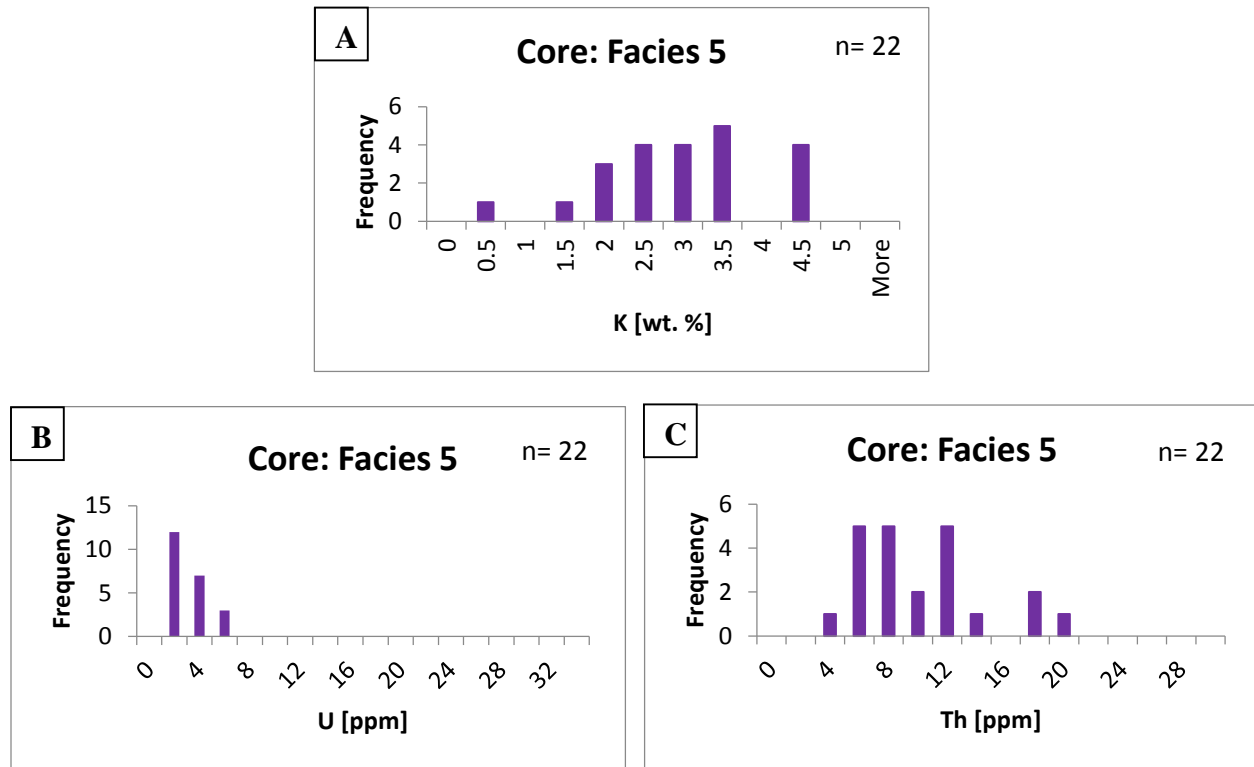


**Figure 21:** SGR frequency diagrams for the microbial-mat-bearing mudstones (F5).

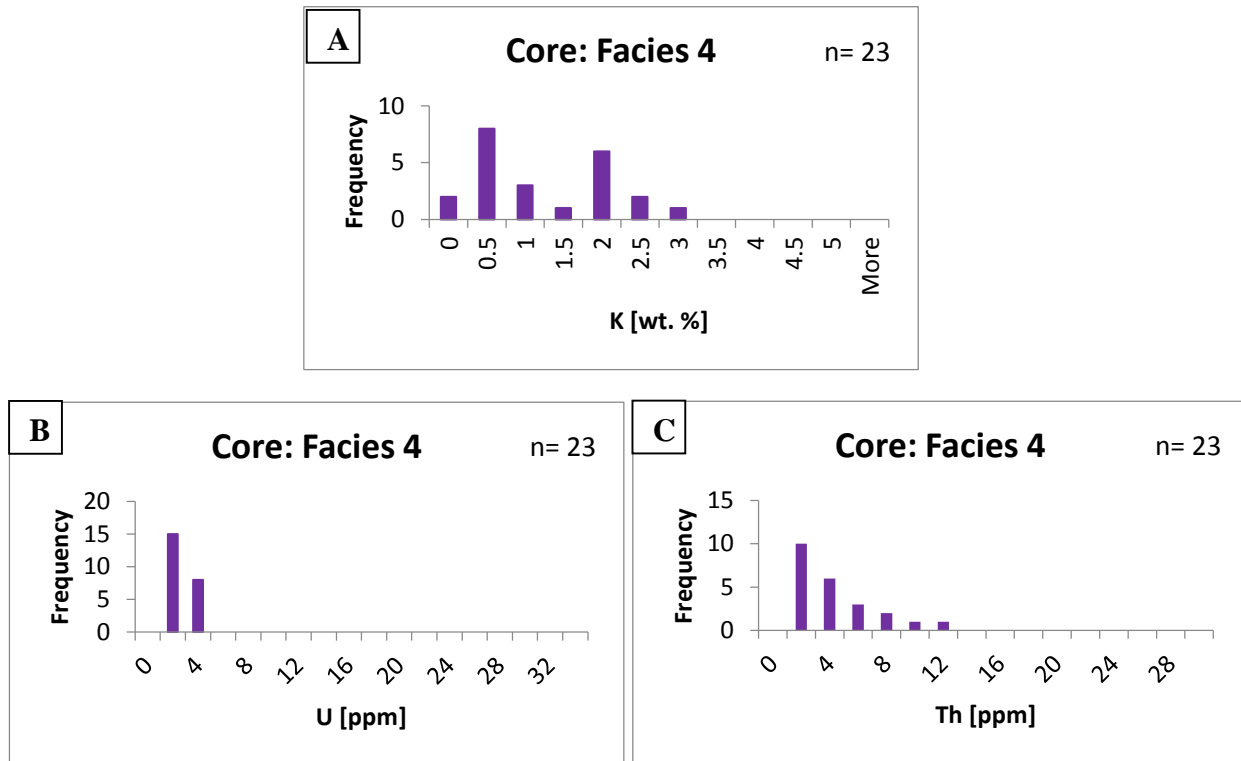


Figure 22: SGR frequency diagrams for the calcareous mudstones (F4).

## 9.0 CONCLUSIONS

1. Handheld, gamma ray spectrometry was found to overall be useful in application to studying the Elko Formation lake facies. Nine-hundred and seventy-nine gamma ray measurements were taken over ~700 ft. of stratigraphic sections measured by Horner (2015) from four Elko Formation outcrops forming a NNW-to-SSE transect in northeastern Nevada. At the northernmost outcrop, Coal Mine Canyon (CMC), 412 measurements were acquired every 0.5 to 2 ft. along 210-ft. of section at 2-minute reading intervals. At the two central outcrops, Elko Hills A (EHA) and Elko Hills B (EHB), 120 and 88 readings were acquired, respectively, every 0.5 ft. along 58.5 and 44 ft. of section, respectively, at 2-minute reading intervals. At the southernmost outcrop, Tomera Ranch (TR) 357 measurements were acquired, along 425-ft. of section, every 1 to 2 ft. at 3-minute reading intervals.
2. From fourteen sedimentological facies identified for the Elko Formation by Horner (2015), eight facies (most of which were combinations of the original fourteen facies) were discernable from a spectral gamma ray signature. These eight facies were assigned to each gamma ray reading, based on an interval thickness of at least 0.5 ft. and an adequate number of measurements. Five of the eight facies used in this study were siliciclastic, including: plant-bearing mudstone, clay-dominated mudstone, microbial-mat-bearing mudstone, ash-bearing mudstone, and conglomerate. The remaining three facies were comprised of two carbonate facies (calcareous mudstone and fossiliferous mudstone-packstone), and one volcanic tuff facies. Facies associations from Horner (2015) could be applied to predict

SGR readings, since facies trends were largely dependent on the specific outcrop being analyzed and its basin position (see conclusion #5).

3. Five out of eight Elko Formation facies [(plant-bearing mudstone (F1/2), clay-dominated mudstone (F3), microbial-mat-bearing mudstone (F5), ash-bearing mudstone (F6), and volcanic tuff (F10–12)] demonstrated high API values above 120 API units. The remaining three facies of the Elko Formation [(calcareous mudstone (F4), fossiliferous mudstone-packstone (F8/13), and conglomerate (F14)] represent low API readings at, or lower than 120 API units.
4. The relative contributions of potassium (K), uranium (U), and thorium (Th) within Elko Formation strata, independent of facies, were found to reflect K-bearing volcanic minerals (feldspars, mica, illite), U-enriched organic matter, and volcanic ash/clay abundance (illite, montmorillonite, chlorite), respectively. This was found to be especially useful for this study, as well as for any future SGR data gathered.
5. Spectral gamma ray readings for the microbial-mat-bearing mudstone (F5) were used to identify basin trends to be identified between all four outcrops studied. The CMC section and the TR outcrop were recognized as proximal and EHA and EHB sections were interpreted as central, basinward outcrops. Within the microbial-mat bearing mudstone (F5), the CMC outcrop data exhibited low K values (<1.5 %), due to the lack of active volcanism during deposition. The TR and Elko Hills sections both had K values from 1–5%. Overall, the range of K values increased from north to south across the four outcrops, which is thought to be linked to the increase in volcanism during the NNW-to-SSE, diachronous deposition of the Elko Formation. The CMC and TR microbial-mat-bearing mudstone outcrop data had low values for Th, commonly between 6 and 8 ppm. The Elko

Hills sections had high Th values, which suggests alteration to clay of water-lain, ash-fall tuff in the central parts of the basin, typically between 10 and 12 ppm. The CMC and TR outcrop data showed similar values for U as the Elko Hills and here generally between 6 and 8 ppm.

6. Th/U ratios of the microbial-mat-bearing mudstone (F5) at each outcrop of the Elko Formation were used to interpret proximal versus distal environments within the deep-lake facies. Low Th/U ratios ( $<2.5$ ) at the CMC and TR sections represent lake strata deposited relatively close to the basin margins, while high Th/U ratios (2.5–4) at the Elko Hills sections, represent the “distal” part of the basin. As distance from the margins increases, the Th/U ratio increases in contrast to marine environments.
7. SGR values used to identify basin trends, as well as application of Th/U, supports the depositional model by Horner (2015), which interprets the CMC and TR outcrops as representing proximal parts of the basin and the Elko Hills sections representing the central basin. This study also supports Horner’s (2015) model of the Elko Formation sediments as diachronous, NNW–SSE deposition across the basin.
8. Eight diagenetic cements in the Elko Formation are were identified: one calcite cement, four phases of dolomite cement, two silica cements, and one zeolite cement. Open and occluded pores found include intraparticle, interparticle, matrix, shelter, and fracture porosity. Calcite, dolomite, and silica cements were formed sequentially and fill in shelter and fracture porosity. Zeolite cement timing is unclear throughout the diagenetic history of the Elko Formation.

9. The eight cements identified in the Elko Formation comprise <10 vol% and it is, therefore, unlikely that they heavily influence the gamma ray signal of Elko Formation sedimentary strata.
10. Comparison between core log data and SGR data acquired by the handheld, gamma ray spectrometer proved inconclusive due to either a difference in tool resolution, variability in deposition between the core and outcrop locations, or contrast between SGR readings from unaltered core versus potentially weathered and altered outcrop exposures.
11. Similar, non-quantitative trends were observed in the core log and the outcrop SGR logs, suggesting similar sources of high-K, high-U, and high-Th values from K-bearing minerals (K-feldspar and mica), U-enriched organic matter, and clays (illite and montmorillonite), respectively.
12. Following Horner (2015), the central Elko Hills sections represent the deep-lake setting and would likely be the most economic source of oil within the basin, unless they prove not brittle enough for hydraulic fracturing, versus to the proximal CMC and TR sections. As these Elko Hills outcrops were deposited during the lake stage with the highest water-level, and with the best preservation of organic matter and thickest microbial-mat-bearing mudstones, facies in the subsurface most similar to these outcrops would be an ideal target for drilling.

## REFERENCES

- Adams, J.A.S., and Weaver, C.E., 1958, Thorium-To-Uranium Ratios as indicators of sedimentary processes: example of concept of geochemical facies: *American Association of Petroleum Geologists Bulletin*, v. 42, p. 387-430.
- Aigner, T., Schauer, M., Junghans, W.-D., and Reinhardt, L., 1995, Outcrop gamma-ray logging and its applications: examples from the German Triassic: *Sedimentary Geology*, v. 100, p. 47-61, doi: 10.1016/0037-0738(95)00102-6.
- Auffill, M.G., 2007, Outcrop-Based Correlation Of Magnetic Susceptibility With Spectral Gamma-Ray Spectrometry In The Woodford Shale of South-Central Oklahoma, Master's thesis, Oklahoma State University, Stillwater, Oklahoma, 255 p.
- Axelrod, D. I., and Bailey, H.P., 1969, Paleotemperature analysis of tertiary floras: *Palaeogeography, Palaeoclimatology, Palaeoecology*, v. 6, p. 163–195, doi:10.1016/0031-0182(69)90013-3.
- Blum, P., Rabaute, A., Gaudon, P., and Allan, J.F., 1997. Analysis of natural gamma-ray spectra obtained from sediment cores with the shipboard scintillation detector of the Ocean Drilling Program: example from Leg 156 *in* Shipley, T.H., Ogawa, Y., Blum, P., and Bahr, J.M. (eds.), *Proc. ODP, Sci. Results*, 156: College Station, TX (Ocean Drilling Program), p.183–195, doi:10.2973/odp.proc.sr.156.024.1997.
- Bessa, J.L., and Hesselbo, S.P., 1997, Gamma-ray character and correlation of the Lower Lias, SW Britain: *Proceedings of the Geologists' Association*, v. 108, p. 113-129, doi:10.1016/S0016-7878(97)80034-X.
- Blakey, R., 2014, Paleogeographic reconstruction of Western North America during the Eocene Epoch (48-52 Ma), map: [http://cpgeosystems.com/images/SWNA\\_50Ma-sm.jpg](http://cpgeosystems.com/images/SWNA_50Ma-sm.jpg), accessed 1/2014.
- Bohacs, K.M., 1998, Contrasting Expressions of Depositional Sequences in Mudrocks from Marine to non Marine Environs: Contrasting Expressions *in* Schieber J., Zimmerle W., Sethi, P.S., Eds., *Shales and Mudstones I*, Schweizerbart'sche Verlagsbuchhandlung, Stuttgart, p. 33–78.
- Bohacs, K. M., Carroll, A. R., Neal, J. E., and Mankiewicz, P. J., 2000, Lake-basin type, source potential, and hydrocarbon character: an integrated-sequence-stratigraphic geochemical framework *in* E. H. Gierlowski-Kordesch and Kelts, K. R. (eds.), *Lake basins through space and time: AAPG Studies in Geology* v. 46, p. 3-34.
- Burton, D., Woolf, K., and Sullivan, B., 2014, Lacustrine depositional environments in the Green River Formation, Uinta Basin: Expression in outcrop and wireline logs: *American*

- Association of Petroleum Geologists Bulletin, v. 98, no. 9, p. 1699-1715, doi: 10.1306/03201413187
- Carroll, A.R., and Bohacs, K.M., 2001, Lake-type controls on petroleum source rock potential in nonmarine basins: American Association of Petroleum Geologists, v. 85, no. 6, p.1033-1053, doi: 10.1306/8626CA5F-173B-11D7-8645000102C1865D.
- Cassidy, J., 1981, Techniques of field gamma-ray spectrometry: Mineralogical Magazine, v. 44, p. 391-398.
- Chamberlain, A.K., 1984, Surface Gamma-Ray Logs: A Correlation Tool for Frontier Areas: American Association of Petroleum Geologists Bulletin, v. 68, no. 8, p. 1040-1043.
- Choquette, P.W., and Pray, L.C., 1970, Geologic nomenclature and classification of porosity in sedimentary carbonates: American Association of Petroleum Geologists Bulletin, v. 54, p. 207-250.
- Christiansen, R.L., and Yeats, R.S., 1992, Post-Laramide geology of the U.S. Cordilleran region *in* Geological Society of America Special Publication, The geology of North America: The Cordilleran Orogen; conterminous U.S., Burchfiel, B.C., Lipman, P.W., and Zoback, M.L. (eds.), p. 261-406.
- Coats, R.R., 1964, Geology of the Jarbidge quadrangle, Nevada-Idaho: U.S. Geological Survey Bulletin 1141-M, 24 p.
- Coats, R.R., 1987, Geology of Elko County, Nevada: Nevada Bureau of Mines and Geology Bulletin, v. 101, 112 p.
- Compton, J.S., Conrad, M.E., and Vennemann, T.W., 1999, Stable isotope evolution of volcanic ash layers during diagenesis of the Miocene Monterey Formation, California: Clay and Minerals, v. 47, no. 2, p. 84-95.
- Coney, P.J., and Harms, T.A., 1984, Cordilleran metamorphic core complexes: Cenozoic extensional relics of Mesozoic compression, *Geology*, v. 12, p. 550-554, doi: 10.1130/0091-7613(1984).
- Cowan, D.R., and Myers, K.J., 1988, Surface Gamma Ray Logs: A Correlation Tool for Frontier Areas: Discussion: American Association of Petroleum Geologists Bulletin, v. 72, no. 5, p. 634-636.
- DeCelles, P.G., 2004, Late Jurassic to Eocene Evolution of the Cordilleran Thrust Belt and Foreland Basin System, Western U.S.A.: *American Journal of Science*, v. 304, p. 105-168, doi: 10.2475/ajs.304.2.105.
- Dickson, B.L., and Scott, K.M., 1997, Interpretation of aerial gamma-ray surveys-adding the geochemical factors: *Journal of Australian Geology and Geophysics*, v. 17 (2), p. 187-200.

- Doveton, J.H., and Merriam, D.F., 2004, Borehole petrophysical chemostratigraphy of Pennsylvanian black shales in the Kansas subsurface: *Chemical Geology*, v. 206, p.249-258, doi: 10.1016/j.chemgeo.2003.12.027.
- Dypvik, H., and Eriksen, D.O., 1983, Natural radioactivity of clastic sediments and the contributions of U, Th and K: *Journal of Petroleum Geology*, v. 5, no. 4, p. 409-416, doi: 10.1111/j.1747-5457.1983.tb00592.x.
- Ehrenberg, S.N., and Svånå, T. A., 2001, Use of spectral gamma-ray signature to interpret stratigraphic surfaces in carbonate strata: an example from the Finnmark carbonate platform (Carboniferous-Permian), Barents Sea: *American Association of Petroleum Geologists*, v. 85, p. 295-308.
- Ellis, D.V., and Singer, J.M., 2008, *Well Logging for Earth Scientists*, New York, Springer, 699 p.
- Fabricius, I.L., Fazladic, L.D., Steinholm, A., and Korsbech, U, 2003, The use of spectral natural-gamma ray analysis in reservoir evaluation of siliciclastic sediments: a case study from the Middle Jurassic of the Harald Field, Danish Central Graben: *Geological Survey of Denmark and Greenland Bulletin*, v. 1, p. 349-366.
- Fertl, W.H., and Chilingarian, G.V., 1990, Hydrocarbon resource evaluation in the Woodford Shale using well logs, *Journal of Petroleum Science and Engineering*, v. 4, p. 347-357.
- Fisher, R. V., 1971, Features of Coarse-Grained, High-Concentration Fluids and Their Deposits: *Journal of Sedimentary Research*, v. 41, no. 4, p. 916-927, doi: 10.1306/74D723B5-2B21-11D7-8648000102C1865D.
- Fischer, A.G., and Roberts, L.T., 1991, Cyclicity of the Green River Formation (Lacustrine Eocene) of Wyoming: *Journal of Sedimentary Petrology*, v. 61, no. 7, p.1146-1154, doi: 10.1306/D4267852-2B26-11D7-8648000102C1865D.
- Flügel, E., 2004, *Microfacies of Carbonate Rocks: Analysis, Interpretation and Application*: Springer – Verlag Berlin Heidelberg, 1006 p.
- Folk, R.L., and Pittman, J.S., 1971, Length-slow chalcedony: A new testament for vanished evaporites: *Journal of Sedimentary petrology*, v. 41, no. 4, p. 1045-1058.
- Fouch, T.D., Hanley, J.H., and Forester, R.M., 1979, Preliminary correlation of Cretaceous and Paleogene lacustrine and related nonmarine sedimentary and volcanic rocks in parts of the eastern Great Basin of Nevada and Utah: *Rocky Mountain Association of Geologists Basin and Range Symposium and Great Basin field conference*, p. 305-312.
- Godelitsas, A., Misaelides, P., Charistos, D., and Filippidis, A., 1996, Interaction of HEU-type Zeolite Crystals with Thorium Aqueous Solutions: *Chemie der Erde*, v. 56, p. 143-156.

- Gondé, C., Martel, C., Pichavant, M., and Bureau, H., 2011, In situ bubble vesiculation in silicic magmas: *American Mineralogist*, v. 96, p. 111-124, doi: 10.2138/am.2011.3546.
- Google Earth 7.1, 2015, state of Nevada, 40°49'16.73" N 115° 45'46.63" W, elevation 1970 m. Image Landsat layer.
- Graham, D.J., and Midgley, N.G., 2000, Graphical representation of particle shape using triangular diagrams: an excel spreadsheet method: *Earth Surface Processes and Landforms*, v. 25, n. 13, p. 1473-1477.
- Gray, M.B., and Nickelsen, R.P., 1989, Pedogenic slickensides, indicators of strain and deformation processes in redbed sequences of the Appalachian foreland: *Geology*, v. 17, no. 1, p. 72-75, doi: 10.1130/0091-7613(1989)017<0072:PSIOSA>2.3.CO;2.
- Guagliardi, I., Buttafuoco, G., Apollaro, C., Bloise, A., De Rosa, R., and Cicchella, D., 2013, Using gamma-ray Spectrometry and Geostatistics for Assessing Geochemical Behavior of Radioactive Elements in the Lese Catchment (southern Italy), *International Journal of Environmental Research*, v. 7(3), p. 645-658.
- Hanson, A.D., Ritts, B.D., Zinniker, D., Moldowan, J.M, and Biffi, U., 2001, Upper Oligocene lacustrine source rocks and petroleum systems of the northern Qaidam basin, northwest China: *American Association of Petroleum Geologists Bulletin*, v. 85, no. 4, p. 601-619, doi: 10.1306/8626C95B-173B-11D7-8645000102C1865D.
- Hassan, M., Hossin, A., and Combaz, A., 1976, Fundamentals of the differential gamma ray log: SPWLA seventeenth annual logging symposium, p. 1-18.
- Haynes, S. R., 2003, Development of the Eocene Elko Basin, Northeastern Nevada : implications for paleogeography and regional tectonism, Unpublished Master's Thesis, The University of British Columbia, Vancouver, Canada, 159 p.
- Hazlett, D.P., Bregar, J.E., and Hersch, J.B., 1992, Petroleum potential of southern Huntingdon Valley and results of the Anadarko Cherry Spring Federal *in* Trexler, J.H, Jr, and others (eds.), *Structural Geology and Petroleum Potential of Southwest Elko County, Nevada: 1992 Fieldtrip Guidebook*, Nevada Petroleum Society, Inc., Reno, Nevada, p. 25-38.
- Heaney, P.J., 1993, A proposed mechanism for the growth of chalcedony: *Contributions of Mineralogy and Petrology*, v. 115, no. 1, p. 66-74, doi: 10.1007/BF00712979.
- Henrici, A.C., and Haynes, S.R., 2006, *Elkobatrachus Brocki*, A new Pelobatid (amphibian: anura) from the Eocene Elko Formation of Nevada: *Annals of Carnegie Museum*, v. 75. no. 1, p. 11-35, doi:10.2992/0097-4463(2006)75[11:EBANPA]2.0.CO;2.
- Henry, C.D., and Faulds, J. E., 1999, Geologic map of the Emigrant Pass quadrangle, Eureka County, Nevada: Nevada Bureau of Mines and Geology, Open File Report 99-9, scale 1:24,000.

- Henry, C.D., 2008, Ash-flow tuffs and paleovalleys in northeastern Nevada: Implications for Eocene paleogeography and extension in the Sevier hinterland, northern Great Basin: *Geosphere*, v. 4, no. 1, p. 1–35, doi:10.1130/GES00122.1.
- Henry, C.D., and John, D.A., 2013, Magmatism, ash-flow tuffs, and calderas of the ignimbrite flareup in the western Nevada volcanic field, Great Basin, USA: *Geosphere*, v. 9, no. 4, p. 951-1008, doi: 10.1130/GES00867.1.
- Horner, W.H., 2015, Tertiary Lake Sedimentation in the Elko Formation, Nevada-The Evolution of a Small Lake System in an Extensional Setting: Unpublished Master's thesis, Colorado State University, Fort Collins, 99 p.
- Horton, T.W., Sjostrom, D.J., Abruzzese, M.J., Poage, M.A., Waldbauer, J.R., Hren, M., Wooden, J., and Chamberlain, C.P., 2004, Spatial and temporal variation of Cenozoic surface elevation in the Great Basin and Sierra Nevada, *American Journal of Science*, v. 304, p. 862-888, doi: 10.2475/ajs.304.10.862.
- International Atomic Energy Agency (IAEA), 2003, Guidelines for radioelement mapping using gamma ray spectrometry data, 179 p.
- Jaeger, K. B., 1987, Structural geology and stratigraphy of the Elko Hills, Elko County, Nevada. Unpublished Master's thesis, University of Wyoming, Laramie. 70 p.
- Johnson, J.G., and Pendergast, A., 1981, Timing and mode of emplacement of the Roberts Mountains allochthon, Antler orogeny, *Geological Society of America Bulletin*, v. 92, no. 9, p. 1648-1658, doi: 10.1130/0016-7606(1981)92<648:TAMOEO>2.0.CO;2.
- Katz, B., and Lin F., 2014, Lacustrine basin unconventional resource plays: key differences: *Marine and Petroleum Geology*, v. 56, p. 255-265, doi:10.1016/j.marpetgeo.2014.02.013.
- Ketner, K. B., and Alpha, A. G., 1992, Mesozoic and Tertiary rocks near Elko, Nevada--evidence for Jurassic to Eocene folding and low-angle faulting, *U.S. Geological Survey Bulletin*, 1988-C, 24 p.
- Koczy, F.F., 1949, The Thorium content of Cambrian Alum Shales of Sweden: *Sveriges Geology Undersokning, Ser. C, Avhandl. och Uppsat. no. 509, Arsbok*, v. 43, no. 7, 12 p.
- Krystyniak, A.M., 2003, Outcrop-Based Gamma-Ray Characterization of the Woodford Shale of South Central Oklahoma, Master's thesis, Lake Superior State University, Sault Sainte Marie, Michigan, 160 p.
- Leggo, P.J., Choeme, J.J., Demant, A., and Lee, W.T., 2001, The role of argillic alteration in the zeolitization of volcanic glass: *Mineralogical Magazine*, v. 65, no. 5, p. 653-663.
- Lofgren, G., 1971, Spherulitic textures in glassy and crystalline rocks: *Journal of Geophysical Research*, 76(23), p. 5635-5648, doi: 10.1029/JB076i023p05635.

- Løvburg, L., Wollenberg, H., Sørensen, P., and Hansen, J., 1971, Field Determination of Uranium and Thorium by Gamma-Ray Spectrometry, Exemplified by Measurements in the Ilímeaussag Alkaline Intrusion, South Greenland: *Economic Geology*, v. 66, p. 368-384.
- McGrew, A.J., and Snee, L.W., 1994,  $^{40}\text{Ar}/^{39}\text{Ar}$  thermochronologic constraints on the tectonothermal evolution of the northern East Humboldt Range metamorphic core complex, Nevada: *Tectonophysics* v. 238, p. 425-450.
- Moore, S.W., Madrid, H.B., and Server, T.G., 1983, Results of Oil-Shale Investigations in Northeastern Nevada: United States Department of the Interior Geological Survey Open File Report 83-586, 111 p.
- Moore, C.H. (ed.), 2001, Carbonate Reservoirs—Porosity Evolution and Diagenesis in a Sequence Stratigraphic Framework: *Developments in Sedimentology*, Elsevier, p. 185-244.
- Muntean, J. L., Tarnocai, C. A., Coward, M., Rouby, D., and Jackson A., 2001, Styles and restorations of Tertiary extension in north-central Nevada *in* Shaddrick, D. R., Zbinden, E. A., Mathewson, D. C., and Prens, C. (eds.), *Regional tectonics and structural control of ore: the major gold trends of northern Nevada*, Geological Society of Nevada Special Publication no. 33, p. 55-69.
- Myers, K.J., and Wignall, P.B., 1987, Understanding Jurassic Organic-rich mudrocks—new concepts using gamma ray spectrometry and palaeoecology: examples from the Kimmerage Clay of Dorset and the Jet Rock of Yorkshire *in* Leggett, J.K., and Zuffa, G.G. (eds.), *Marine Clastic Sedimentology*, p. 172-189, doi: 10.1007/978-94-009-3241-8\_9.
- Ogihara, S., 2000, Composition of clinoptilolite formed from volcanic glass during burial diagenesis; *Clays and Clay Minerals*, v. 48, no. 1, p. 106-110.
- Plint, A., 2014, Mud dispersal across a Cretaceous prodelta: Storm-generated, wave-enhanced sediment gravity flows inferred from mudstone microtexture and microfacies: *Sedimentology*, v. 61, no. 3, p. 609–647, DOI: 10.1111/sed.12068.
- Radiation Solutions Inc., 2008, User's manual for RS-125 Super-spec and RS-230 BGO super-spec gamma ray spectrometer, rev. 1.7: Radiation Solutions, Inc., Ontario, Canada, 35 p.
- Radiation Solutions Inc. (RSI), 2009, Spectrum Stabilization and Calibration for the RSI RS-125 and RS-230 Handheld Spectrometers: RSI Technical Note #-RSG-703, Radiation Solutions Inc., 6 p.
- Renault, R.W., and Gierlowski-Kordesch, E.H., 2010, Lakes *in* Dalrymple, R. and James, N. (eds.), *Facies Models*, 4th Edition, Geological Association of Canada, Toronto, p. 541-575.
- Retallack, G. J., 1990, *Soils of the Past: An Introduction to Paleopedology*: Boston, Unwin Hyman, 548 p.

- Satarugsa, P., and Johnson, R.A., 2000, Cenozoic tectonic evolution of the Ruby Mountains metamorphic core complex and adjacent valleys, northeastern Nevada, *Rocky Mountain Geology*, v. 35, no. 2, p. 205-230, doi: 10.2113/35.2.205.
- Serra, O., 1984, *Fundamentals of Well-Log Interpretation: 2. The interpretation of Logging Data: Developments in Petroleum Science*, 15B: Amsterdam, Elsevier, p. 684.
- Schieber, J., Southard, J.B., Kissling, P., Rossman, B., and Ginsburg, R., 2013, Experimental deposition of carbonate mud from moving suspensions: Importance of flocculation and implications for modern and ancient carbonate mud deposition, *Journal of Sedimentary Research*, v. 83, p. 1026-1032, doi: 10.2110/jsr.2013.77.
- Schubel, K.A., and Simonson, B.M., 1990, Petrography and diagenesis of cherts from Lake Magadi, Kenya, *Journal of Sedimentary Petrology*, v. 60, no. 5, p. 761-776.
- Sims, J. D., 2013, Earthquake-induced load casts, pseudonodules, ball-and-pillow structures, and convolute lamination: Additional deformation structures for paleoseismic studies, *GSA Special Papers 2013*, v. 493, p. 191-201, doi: 10.1130/2012.2493(09).
- Slatt, R.M., Jordan, D.W., D'Agostino, A.E., and Gillespie, R.H., 1992, Outcrop gamma-ray logging to improve understanding of subsurface well log correlations: Geological Society, London, *Special Publications*, v. 95, p. 3-19, doi: 10.1144/GSL.SP.1992.065.01.02.
- Smith, J.F. Jr, Ketner, K.B., and Mabey, D.R., 1976, Stratigraphy of post-Paleozoic rocks and summary of resources in the Carlin-Pinon Range area, Nevada: United States Geological Survey PP 867-B, 53 p.
- Solomon, B. J., McKee, E. H., and Andersen, D. W., 1979, Stratigraphy and Depositional Environments of Paleogene Rocks Near Elko, Nevada *in* Armentrout, J.M., Cole, M.R., and TerBest, H. (eds.), *Cenozoic paleogeography of the western United States: Society of Economic Paleontologists and Mineralogists, Pacific Section*, p. 75–88.
- Solomon, B.J., 1981, *Geology and Oil Shale Resources near Elko, Nevada: United States of the Interior Geological Survey Open-File Report 81-709*, 154 p.
- Solomon, B.J., and Moore, S. W., 1982*a*, Geologic map and oil shale deposits of the Elko West quadrangle, Elko County Nevada. U. S. Geological Survey Miscellaneous Field Studies Map MF-1420, scale 1:24,000.
- Solomon, B.J., and Moore, S. W., 1982*b*, Geologic map and oil shale deposits of the Elko East quadrangle, Elko County Nevada. U.S. Geological Survey Miscellaneous Field Studies Map MF-1421, scale 1:24,000.
- Solomon, B.J., 1992, The Elko Formation of Eocene and Oligocene (?) age—source rocks and petroleum potential *in* Trexler, J.H, Jr, and others (eds.), 1992, *Structural Geology and*

- Petroleum Potential of Southwest Elko County, Nevada: 1992 Fieldtrip Guidebook, Nevada Petroleum Society, Inc., Reno, Nevada, p. 25-38.
- Svendsen, J.B., and Hartley, N.R., 2001, Comparison between outcrop-spectral gamma ray logging and whole rock geochemistry: implications for quantitative reservoir characterization in continental sequences: *Marine and Petroleum Geology*, v. 18, p. 657-670, doi: 10.1016/S0264-8172(01)00022-8.
- Surdam, R.C., and Stanley, K.O., 1979, Lacustrine sedimentation during the culminating phase of Eocene Lake Gosiute, Wyoming (Green River Formation): *Geological Society of America Bulletin*, v. 90, p. 93-110.
- Swanson, V.E., 1961, *Geology and Geochemistry of Uranium in Marine Black Shales A Review*: United States Department of the Interior Geological Survey PP 356-C, 51 p.
- Utada, M., 2001, Zeolites in burial diagenesis and low-grade metamorphic rocks *in* Bish, D.L., and Ming, D.W. (eds.), *Natural Zeolites: Occurrence, Properties, Applications, Reviews in Mineralogy and Geochemistry*, Mineralogical Society of America, v. 45, p. 277-304, doi: 10.2138/rmg.2001.45.9.
- Vandervoort, D.S., and Schmitt, J.G., 1990, Cretaceous to early Tertiary paleogeography in the hinterland of the Sevier thrust belt, east-central Nevada: *Geology*, v. 18, no. 6, p. 567-570, doi: 10.1130/0091-7613(1990)018<0567:CTETPI>2.3.CO;2.
- Wignall, P.B., and Myers, K.J., 1988, Interpreting benthic oxygen levels in mudrocks: A new approach: *Geology*, v. 6, p. 452-455, doi: 10.1130/0091-7613(1988)016<0452:IBOLIM>2.3.CO;2.
- Wingate, F.H., 1983, Palynology and age of the Elko Formation Eocene near Elko, Nevada: *Palynology*, v. 7, p.93-132.
- Yang, L., Xu, T., Wei, M., Feng, G., Wang, F., and Wang, K., 2015, Dissolution of arkose in dilute acetic acid solution under conditions relevant to burial diagenesis, *Applied Geochemistry*, v. 54, p. 65-73, doi: 10.1016/j.apgeochem.2015.01.007.

## **APPENDICES**

## APPENDIX 1: OUTCROP GAMMA RAY DATA

**Table 4: Elko Hills A**

Interval (ft.)	Dose [nGy/h]	Total[cpm]	Total[ppm]	API	K wt. %	U[ppm]	Th[ppm]
20.0	123.91	6536.90	1578.90	173.48	2.94	8.73	14.15
20.5	121.82	6475.90	1564.20	170.52	2.92	7.34	16.27
21.0	123.68	6257.30	1511.40	174.24	2.62	8.66	15.76
21.5	119.20	6578.50	1589.00	165.92	3.11	6.50	16.04
22.0	118.56	6379.00	1540.80	165.88	2.81	7.28	15.67
22.5	115.72	5982.10	1444.90	162.88	2.45	7.51	15.90
23.0	110.32	5911.30	1427.80	154.24	2.68	6.63	14.58
23.5	97.92	5241.10	1265.90	137.44	2.22	6.23	13.02
24.0	82.96	4448.00	1074.40	116.28	1.90	5.61	10.25
24.5	74.99	3925.20	948.10	105.76	1.53	5.43	9.46
25.0	78.34	3909.70	944.30	110.88	1.49	5.38	11.00
25.5	73.92	3728.30	900.50	104.16	1.55	4.93	9.98
26.0	76.96	3588.30	866.70	108.24	1.68	5.53	9.28
26.5	71.11	3521.70	850.60	99.92	1.57	4.25	10.20
27.0	82.85	3637.50	878.60	117.12	1.63	5.73	11.30
27.5	69.82	3337.50	806.10	98.12	1.55	3.98	10.37
28.0	63.44	3132.90	756.70	88.68	1.54	3.69	8.63
28.5	64.14	3002.70	725.30	90.24	1.41	3.51	9.90
29.0	65.85	2949.40	712.40	92.44	1.49	3.20	10.75
29.5	69.18	3038.50	733.90	97.24	1.51	4.08	10.11
30.0	69.30	3224.60	778.90	96.88	1.70	4.02	9.38
30.5	66.93	3270.10	789.90	92.72	1.88	3.54	8.58
31.0	81.01	3606.90	871.20	112.20	2.25	4.93	9.19
31.5	103.44	4713.60	1138.50	142.08	3.26	4.46	13.56
32.0	112.99	5094.00	1230.40	153.88	3.93	5.10	12.55
32.5	123.80	5374.20	1298.10	169.88	3.99	5.48	15.55
33.0	127.58	5619.70	1357.40	175.40	4.03	4.80	18.13
33.5	120.12	5348.00	1291.70	164.76	3.88	5.60	14.47
34.0	108.50	4862.30	1174.40	149.24	3.35	4.59	14.73
34.5	90.94	4276.80	1033.00	125.72	2.65	5.08	10.67
35.0	96.91	4304.20	1039.60	134.84	2.51	6.22	11.23
35.5	97.26	4259.70	1028.90	135.32	2.58	5.04	13.43
36.0	87.16	3940.60	951.80	121.52	2.23	5.06	11.34
36.5	81.56	3604.00	870.50	113.64	2.07	5.39	9.35

37.0	88.50	3899.10	941.80	123.32	2.25	5.54	10.75
37.5	92.91	4061.50	981.00	129.56	2.35	5.56	11.87
38.0	106.67	4635.60	1119.70	149.84	2.43	5.21	17.32
38.5	94.90	4051.80	978.70	132.40	2.40	5.29	12.92
39.0	92.16	4097.40	989.70	129.76	1.95	6.06	12.52
39.5	116.72	4987.60	1204.70	164.84	2.37	6.60	18.53
40.0	114.21	5285.40	1276.60	160.84	2.43	5.21	20.07
40.5	134.82	5990.30	1446.90	193.24	1.92	7.63	25.37
41.0	117.80	5465.00	1320.00	167.84	1.97	6.30	21.48
41.5	117.26	5304.60	1281.30	165.88	2.31	6.03	20.17
42.0	129.85	5655.80	1366.10	182.00	3.03	7.08	19.22
42.5	141.44	6137.00	1482.30	197.68	3.47	7.89	19.76
43.0	143.53	6467.10	1562.00	199.32	3.87	8.05	18.25
43.5	148.01	6816.20	1646.40	204.20	4.39	8.40	16.69
44.0	143.57	6939.00	1676.00	196.20	4.82	7.44	14.89
44.5	145.17	6735.70	1626.90	199.60	4.51	7.40	17.06
45.0	132.68	6124.40	1479.30	182.36	4.15	7.53	13.93
45.5	158.61	7265.20	1754.80	220.12	4.29	11.31	15.25
46.0	148.92	7460.40	1802.00	206.60	4.05	10.97	13.51
46.5	155.94	7698.90	1859.60	216.84	4.13	10.67	16.35
47.0	144.34	6873.30	1660.20	202.76	3.15	11.26	15.57
47.5	128.75	6265.80	1513.40	181.04	2.80	9.28	15.50
48.0	131.52	6358.80	1535.90	185.96	2.56	9.47	17.31
48.5	124.61	5474.00	1322.20	174.84	2.84	8.95	14.45
49.0	89.41	4106.30	991.80	125.16	2.13	6.24	10.29
49.5	91.42	4239.50	1024.00	128.32	2.06	7.36	9.12
50.0	96.95	4405.30	1064.10	136.20	2.12	7.51	10.55
50.5	101.28	4546.90	1098.20	142.00	2.30	7.55	11.20
51.0	112.10	4956.90	1197.30	159.20	1.94	11.10	9.84
51.0	111.84	4930.20	1190.80	157.88	2.20	11.55	7.57
51.5	105.65	4858.40	1173.50	148.76	2.19	9.58	9.27
52.0	107.30	5122.00	1237.20	150.20	2.52	8.24	10.99
53.5	90.68	4195.40	1013.30	127.08	2.10	6.56	10.25
61.0	137.65	6065.40	1465.00	190.16	4.01	9.01	13.48
62.0	151.23	6845.20	1653.40	208.24	4.58	9.63	14.48
63.0	167.51	7537.60	1820.60	228.16	5.84	9.19	15.30
64.0	136.37	6204.50	1498.60	192.24	2.87	6.00	24.58
65.0	134.94	6045.00	1460.10	190.44	2.77	7.34	21.85
66.0	147.02	6527.50	1576.60	209.08	2.57	8.02	25.95

67.0	137.57	6266.20	1513.50	194.16	2.80	7.02	23.30
68.0	136.53	6140.60	1483.20	191.24	3.21	6.79	21.39
70.0	143.02	6534.20	1578.20	199.80	3.55	6.77	22.21
71.0	164.85	7187.10	1735.90	230.12	4.10	8.63	23.87
71.5	152.33	7009.30	1693.00	212.72	3.82	7.78	22.34
72.0	147.99	6916.70	1670.60	204.84	4.22	7.59	19.15
73.0	170.56	7803.80	1884.90	236.68	4.71	6.54	27.25
74.0	150.35	6763.50	1633.60	211.56	3.24	8.37	23.19
75.0	147.65	6530.40	1577.30	208.24	2.99	10.88	18.34
76.0	131.98	6259.80	1512.00	185.56	2.88	7.80	19.27
77.0	141.86	6781.80	1638.00	198.24	3.48	7.04	21.56
78.0	145.52	6825.10	1648.50	202.44	3.87	7.02	21.09
79.0	136.76	6087.60	1470.40	191.72	3.21	6.82	21.45
80.0	123.20	5777.80	1395.50	172.32	2.98	5.46	20.24
81.0	134.04	6409.00	1548.00	187.84	3.17	6.17	21.94

**Table 5: Elko Hills B Outcrop Gamma Ray Data**

Interval (ft.)	Dose [nGy/h]	Total[cpm]	Total[ppm]	API	K wt. %	U[ppm]	Th[ppm]
0.0	64.25	3072.80	742.20	90.76	1.31	4.37	8.71
0.5	81.65	3926.60	948.40	112.56	2.48	3.48	11.26
1.0	88.49	3962.10	963.60	109.24	2.00	3.73	11.85
1.5	79.76	3888.90	907.20	104.44	1.95	3.29	11.73
2.0	64.06	3079.90	936.00	96.32	1.77	3.49	10.02
2.5	78.33	3989.50	981.40	130.36	2.31	4.75	13.85
3.0	75.00	3755.90	1032.30	131.60	2.52	5.04	12.74
3.5	69.12	3875.40	932.70	122.08	2.08	5.03	12.14
4.0	93.38	4063.10	877.90	118.52	1.94	5.73	10.41
4.5	94.67	4273.70	1002.80	131.04	2.14	5.98	12.24
5.0	87.20	3861.70	1304.50	163.92	3.36	6.93	13.68
5.5	84.55	3634.90	1361.70	181.40	3.90	7.43	14.89
6.0	93.42	4151.80	1595.10	202.28	4.59	6.29	19.63
6.5	118.51	5400.90	1599.60	210.60	4.59	7.17	19.95
7.0	131.47	5637.80	1580.80	199.68	4.46	7.27	17.54
7.5	147.12	6603.80	1553.10	203.88	4.29	7.74	18.33
8.0	152.69	6622.70	1557.30	197.36	4.16	7.57	17.56
8.5	145.02	6544.90	1559.10	198.32	4.06	7.63	18.08
9.0	147.58	6430.00	1565.50	189.16	3.83	7.65	16.67
9.5	142.90	6447.50	1642.60	174.16	3.65	6.02	16.90
10.0	143.29	6454.80	1672.80	162.44	3.53	5.06	16.37
10.5	136.48	6481.50	1817.20	229.00	4.86	9.03	19.75

11.0	125.91	6800.50	1478.60	178.08	3.76	6.61	16.26
11.5	117.76	6925.60	1236.90	139.08	2.75	5.61	12.55
12.0	165.77	7523.60	1077.30	115.72	1.93	5.30	10.61
12.5	128.84	6121.70	975.70	108.68	1.49	5.25	10.71
13.0	100.25	5120.80	866.90	85.72	1.29	3.45	9.37
13.5	82.60	4460.10	884.50	93.28	1.19	4.33	9.90
14.0	76.84	4039.40	810.10	80.76	0.98	3.31	9.65
14.0	60.91	3589.10	825.20	89.48	1.10	5.52	6.93
14.5	65.72	3662.00	754.80	72.00	0.94	3.45	7.34
15.0	56.83	3354.10	779.50	81.16	0.98	4.16	8.05
15.5	62.98	3416.50	788.10	99.16	1.56	5.13	8.29
16.0	50.78	3125.10	764.00	96.88	1.65	4.43	8.76
16.5	57.08	3227.40	747.70	93.04	1.58	4.09	8.76
17.0	70.64	3263.00	744.20	92.52	1.56	4.03	8.83
17.5	69.18	3163.30	763.70	92.96	1.70	3.01	10.42
18.0	66.39	3095.60	746.90	94.72	1.74	3.72	9.28
18.0	66.12	3081.10	712.90	91.88	1.70	4.55	7.07
18.5	66.67	3161.90	815.40	109.08	1.88	5.30	9.15
19.0	68.00	3092.50	783.10	101.96	2.00	3.51	10.47
19.5	66.02	2951.60	733.60	96.20	1.59	3.26	11.17
20.0	77.96	3376.00	697.00	93.36	1.45	3.61	10.32
20.5	73.38	3242.00	676.30	93.80	1.46	4.34	8.93
21.0	68.54	3037.10	665.80	85.08	1.20	3.45	9.57
21.5	66.42	2885.70	657.70	88.44	1.32	4.45	7.93
22.0	66.75	2800.20	692.80	90.76	1.46	4.48	7.89
22.5	60.25	2756.70	684.10	89.24	1.51	4.89	6.49
23.0	62.84	2723.00	668.30	78.32	1.69	3.01	6.80
23.5	64.75	2868.20	691.50	84.84	1.80	3.29	7.43
24.0	63.80	2832.30	779.30	105.16	2.25	3.88	9.53
24.5	56.80	2767.10	822.20	99.12	2.18	3.27	9.52
25.0	61.38	2862.90	954.90	123.52	2.46	5.79	9.46
25.5	76.12	3226.30	1203.50	160.24	2.64	6.63	16.24
26.0	71.85	3403.90	1368.10	180.76	2.80	7.73	18.53
26.5	89.08	3953.50	1329.30	182.08	2.75	8.01	18.50
27.0	114.29	4982.50	1328.50	174.52	2.83	7.86	16.59
27.5	128.54	5664.00	1364.50	180.16	3.41	7.33	16.74
28.0	129.30	5503.40	1332.70	176.04	3.25	7.79	15.43
28.5	124.47	5500.30	1350.70	176.04	3.21	8.08	15.01
29.0	129.51	5649.20	1402.50	183.00	3.73	7.96	14.91

29.5	126.38	5517.50	1416.10	184.28	3.58	8.47	14.81
30.0	126.28	5592.10	1325.20	169.88	2.87	8.08	14.83
30.5	132.23	5806.50	1314.30	173.20	3.09	7.22	16.50
31.0	132.66	5862.90	1131.90	140.40	2.35	5.92	13.86
31.5	121.35	5486.50	1191.20	156.48	2.28	7.48	15.04
32.0	124.17	5441.60	1300.80	180.60	2.51	7.99	19.13
32.5	100.26	4686.40	1046.90	139.12	2.11	6.62	13.10
33.0	110.97	4931.60	1046.30	133.40	2.27	5.86	12.55
33.5	127.76	5385.50	919.00	117.96	1.68	6.12	10.53
34.0	98.79	4334.40	857.80	112.72	1.72	5.98	9.34
34.5	95.29	4331.90	1073.30	143.80	2.27	7.68	11.51
35.0	83.61	3804.70	945.30	136.08	2.11	7.31	10.96
35.5	80.13	3551.30	1495.60	198.08	3.80	9.37	15.58
35.5	102.42	4443.40	1565.90	208.28	4.20	9.62	16.03
36.0	96.82	3913.80	1556.10	197.64	4.63	7.75	15.39
36.5	142.52	6192.10	1575.90	201.40	4.96	7.96	14.59
37.0	150.38	6483.30	1620.80	202.20	5.24	7.15	15.29
37.5	144.13	6442.40	1590.20	208.44	4.44	9.84	14.67
38.0	147.35	6524.60	1569.20	202.12	5.19	8.52	12.73
38.5	148.55	6710.40	1544.60	199.80	4.69	7.75	15.69
39.0	150.98	6583.80	1603.10	208.56	4.61	8.13	17.44
39.5	148.46	6496.90	1751.00	221.28	5.54	8.01	17.14
40.0	145.77	6395.00	1771.90	228.20	5.23	9.58	16.97
40.5	151.47	6637.00	1934.20	235.16	4.62	8.83	22.65
41.0	162.07	7249.40	1759.80	222.48	3.54	8.43	24.60
41.5	166.14	7336.00	1618.10	214.52	2.89	8.41	25.25
42.0	169.48	8007.70	1629.00	209.36	2.89	8.40	23.98
42.5	158.36	7285.90	1576.00	196.72	2.69	7.14	24.14
43.0	151.44	6699.30	1585.50	206.24	2.79	8.22	23.96
43.5	148.07	6744.40	1655.40	214.92	3.28	7.70	25.21
44.0	138.95	6524.80	1772.50	216.64	3.09	8.75	24.30
44.5	145.74	6564.10	1696.70	212.92	2.93	8.87	23.77
45.0	152.59	6853.80	1467.40	183.88	2.55	7.73	20.31
45.5	153.33	7338.60	1861.00	230.52	3.44	9.89	24.09
46.0	150.60	7024.40	1685.70	209.80	2.64	12.01	17.87
46.5	130.11	6075.20	2167.00	278.84	3.45	18.64	18.63
47.0	163.52	7705.00	2395.20	296.52	3.73	21.28	16.65
47.5	147.96	6978.90	2645.30	303.88	4.30	18.54	21.69
48.0	196.51	8971.70	2503.70	297.40	4.22	18.28	20.91
48.5	209.20	9916.50	2526.10	295.68	3.76	17.57	23.74

49.0	215.40	10952.10	2133.60	251.96	3.02	14.57	21.77
49.5	210.77	10365.90	1995.20	241.64	2.87	14.52	19.89
50.0	208.59	10458.50	1998.90	241.72	3.23	14.21	19.09
50.5	177.23	8833.40	2000.40	255.24	3.07	15.64	20.25
51.0	169.94	8260.30	1944.70	234.12	2.90	14.14	18.65
51.5	170.84	8275.90	1776.60	209.92	2.85	11.11	18.86
52.0	179.59	8281.90	2142.20	292.08	3.85	15.16	27.30
52.5	165.00	8051.40	1880.70	245.08	3.73	12.10	22.15
53.0	148.47	7355.40	1720.30	228.48	3.16	13.06	18.36
53.5	206.22	8869.00	1578.40	202.60	4.00	11.40	11.85
54.0	174.12	7786.60	1704.60	178.20	1.88	14.95	7.13
54.5	161.67	7122.50	1845.00	184.68	2.60	14.25	7.27
55.0	146.14	6534.70	1718.60	169.20	2.23	12.33	8.72
55.5	124.99	7057.10	1779.00	182.48	2.17	13.21	10.52
56.0	131.00	7638.50	1675.20	151.16	1.97	11.35	7.21
56.5	119.64	7115.40	2054.50	209.64	2.39	14.74	13.37
57.0	128.41	7365.20	2051.30	207.88	2.47	15.34	11.41
57.5	106.87	6935.50	2319.80	237.76	2.44	16.53	16.62
58.0	147.39	8505.90	2083.40	202.84	1.96	13.80	15.27

**Table 6: Coal Mine Canyon Outcrop Gamma Ray Data**

Interval (ft.)	Dose [nGy/h]	Total[cpm]	Total[ppm]	API	K wt. %	U[ppm]	Th[ppm]
34.0	104.39	4658.00	1125.10	147.32	2.10	7.61	13.21
34.5	113.65	4860.10	1173.90	160.80	2.13	9.61	12.46
35.0	92.84	4479.50	1082.00	130.92	1.91	6.85	11.39
35.5	59.69	2828.20	683.10	83.60	1.38	4.98	5.42
36.0	52.92	2515.30	607.50	74.08	1.23	4.24	5.12
36.5	50.07	2468.60	596.30	69.92	1.25	3.36	5.76
37.0	48.22	2305.80	556.90	67.76	1.07	4.09	4.48
37.5	47.58	2485.20	600.30	66.84	1.05	4.42	3.67
38.0	52.23	2997.60	724.00	73.24	1.17	3.49	6.65
38.5	61.74	3417.30	825.40	86.84	1.32	5.16	6.11
39.0	50.99	3136.00	757.40	71.48	1.21	3.10	6.83
39.5	55.43	3009.50	726.90	78.56	0.98	4.74	6.24
40.0	47.52	2519.40	608.50	67.08	0.96	3.67	5.59
40.5	42.30	2445.70	590.70	59.76	0.79	4.13	3.52
41.0	42.46	2579.50	623.00	60.04	0.78	4.02	3.85
41.5	53.74	2865.50	692.10	76.80	0.79	5.75	4.54
42.0	46.84	2884.10	696.60	66.68	0.73	4.64	4.47
42.5	67.53	3712.40	896.70	96.32	1.01	7.49	5.06
43.0	57.70	3055.10	737.90	82.92	0.65	7.38	3.37
43.5	51.83	2962.40	715.50	74.32	0.64	5.65	4.72

44.0	44.73	2612.10	630.90	64.56	0.47	5.33	3.60
44.5	46.92	2660.30	642.60	67.52	0.51	5.58	3.68
45.0	53.00	2562.90	619.00	73.40	1.45	3.63	5.29
45.5	64.35	2899.70	700.40	89.52	1.70	4.30	6.98
46.0	70.69	3177.70	767.50	98.76	1.75	3.76	10.17
46.5	74.18	3285.30	793.50	103.84	1.74	5.33	8.34
47.0	79.99	3480.60	840.70	111.72	2.00	4.86	10.21
47.5	85.37	3703.70	894.60	119.00	2.16	5.69	9.73
48.0	76.08	3339.30	806.60	106.16	1.88	5.63	7.76
48.5	71.79	3117.90	753.10	100.40	1.73	4.13	9.92
49.0	72.22	3250.30	785.10	101.00	1.70	5.27	7.91
49.5	68.37	3113.60	752.00	95.36	1.73	4.27	8.38
50.0	59.46	2872.70	693.90	83.00	1.46	4.32	6.27
50.5	55.17	2634.40	636.30	77.28	1.27	3.80	6.64
51.0	55.00	2627.70	634.70	77.24	1.23	4.15	6.09
51.5	51.54	2351.50	568.00	73.24	0.89	3.96	6.83
52.0	46.11	2309.00	557.70	65.48	0.81	4.38	4.37
52.5	53.91	2398.70	579.40	77.12	0.78	4.95	6.26
68.0	145.73	6392.00	1543.90	209.20	1.80	16.06	12.98
68.5	147.11	6890.20	1664.20	211.84	1.62	16.75	12.98
69.0	139.67	6415.60	1549.60	201.24	1.47	16.04	12.35
69.5	134.95	6211.40	1500.30	194.64	1.38	15.78	11.58
70.0	121.20	5876.20	1419.30	173.36	1.70	12.77	11.00
78.0	95.50	4885.20	1179.90	135.32	1.79	6.58	13.51
78.5	101.37	4843.00	1169.80	143.80	1.82	8.08	12.51
79.0	95.56	4731.00	1142.70	135.52	1.74	6.33	14.26
79.0	87.33	4619.00	1115.70	123.12	1.80	5.74	12.10
79.5	94.09	4754.20	1148.30	133.44	1.69	6.88	12.84
80.0	83.81	4446.00	1073.90	118.80	1.55	6.29	10.92
80.5	80.59	4519.00	1091.50	114.28	1.46	5.38	11.97
81.0	86.47	4614.30	1114.50	122.76	1.54	7.36	9.81
81.5	121.97	5107.30	1233.60	173.84	1.95	10.91	13.84
82.0	102.48	4461.90	1077.70	145.00	1.92	8.01	12.55
82.5	110.33	4788.20	1156.50	156.56	2.00	8.27	14.60
83.0	107.08	4552.50	1099.60	151.76	2.00	7.28	15.38
83.5	100.71	4558.30	1101.00	142.48	1.93	6.89	14.12
84.0	90.60	3979.80	961.30	128.56	1.65	6.13	13.28
121.0	130.68	5369.50	1296.90	188.84	1.30	12.58	16.85
121.5	103.11	4579.70	1106.20	147.72	1.40	9.68	11.97
122.0	70.98	3099.70	748.70	101.76	0.95	6.56	8.52
122.5	61.51	2645.80	639.10	88.20	0.83	4.66	9.41

123.0	46.55	2166.90	523.40	66.12	0.82	2.83	7.59
123.5	57.82	2481.60	599.40	82.36	0.96	4.50	7.75
124.0	64.27	2842.20	686.50	90.72	1.30	4.35	8.78
124.5	64.52	2848.90	688.10	91.24	1.28	3.67	10.35
125.0	64.40	2857.70	690.20	91.76	1.06	4.50	9.70
125.5	84.14	3493.30	843.80	120.12	1.27	6.56	11.83
126.0	82.63	3519.00	850.00	118.52	1.11	6.09	13.01
126.5	85.34	3266.60	789.00	122.68	1.06	6.72	12.99
127.0	75.52	3347.60	808.60	106.96	1.44	4.37	12.24
127.5	79.37	3423.50	826.90	112.72	1.42	3.88	14.74
128.0	74.38	3257.60	786.80	105.56	1.33	4.23	12.61
128.5	75.45	3349.00	808.90	107.20	1.34	4.50	12.44
129.0	73.86	3409.60	823.50	104.48	1.45	3.60	13.12
129.5	86.69	3694.20	892.30	123.16	1.51	6.17	12.41
130.0	96.09	3938.80	951.40	137.12	1.49	6.62	15.08
130.5	87.79	3871.80	935.20	124.84	1.51	5.47	14.23
131.0	84.25	3837.10	926.80	118.76	1.77	5.42	11.77
131.5	84.07	3576.60	863.90	119.60	1.42	5.43	13.36
132.0	84.23	3835.70	926.50	118.92	1.69	4.75	13.47
132.5	82.65	3799.10	917.60	117.04	1.54	5.49	12.12
133.0	75.70	3519.70	850.10	107.00	1.51	4.47	11.77
133.5	70.35	3446.60	832.50	99.40	1.40	4.01	11.23
134.0	83.54	3680.40	889.00	118.92	1.39	5.53	13.11
134.5	94.25	3923.50	947.70	135.12	1.25	7.32	14.14
135.0	94.09	3963.80	957.40	134.76	1.29	7.95	12.63
135.5	98.26	4247.30	1025.90	142.64	0.79	8.83	14.84
136.0	103.62	4335.00	1047.10	149.56	1.09	8.36	16.31
136.5	98.00	4380.20	1058.00	141.16	1.09	8.67	13.59
137.0	103.20	4370.30	1055.60	149.00	1.07	9.46	14.05
137.5	106.85	4572.70	1104.50	153.28	1.40	9.71	13.30
138.0	110.95	4774.00	1153.10	159.52	1.35	9.76	14.96
138.5	106.39	4457.70	1076.70	153.72	1.02	10.55	13.25
139.0	93.48	3856.80	931.50	135.24	0.86	9.20	11.97
139.5	78.46	3389.50	818.70	113.28	0.82	7.38	10.28
140.0	84.69	3704.90	894.90	121.84	1.01	7.98	10.46
140.5	119.48	5051.70	1220.20	172.52	1.24	9.98	18.21
141.0	121.19	5204.30	1257.00	174.96	1.26	9.99	18.72
141.5	154.01	6682.20	1614.00	224.24	1.05	13.97	23.92
142.0	169.53	7407.00	1789.10	247.32	1.00	14.29	29.25
167.0	94.55	4336.60	1047.50	135.40	1.35	6.81	14.83

167.5	91.90	3889.40	939.40	131.80	1.23	7.81	12.41
168.0	78.67	3437.30	830.20	113.68	0.80	7.03	11.16
168.5	73.10	3621.60	874.70	105.00	0.93	5.76	11.01
169.0	71.63	3589.90	867.10	102.84	0.90	6.24	9.63
169.5	84.78	3739.70	903.30	121.56	1.11	7.39	11.17
170.0	86.58	3871.00	935.00	122.64	1.62	6.29	11.60
170.5	81.10	3973.70	959.80	113.44	1.96	5.14	10.24
171.0	81.86	3768.10	910.10	115.48	1.66	5.72	10.79
171.5	82.42	3948.60	953.70	115.72	1.87	4.46	12.53
172.0	88.88	3982.30	961.90	125.64	1.72	5.80	12.93
172.5	84.93	3823.50	923.50	120.28	1.60	5.39	12.89
173.0	82.25	3782.20	913.50	116.04	1.69	5.15	11.95
183.0	77.01	3675.50	887.80	109.84	1.25	4.90	12.66
183.5	81.96	3698.30	893.30	118.20	0.93	6.03	13.77
184.0	79.38	3170.80	765.90	114.72	0.78	7.11	11.34
184.5	74.05	3026.50	731.00	106.92	0.75	6.91	9.91
185.0	72.84	3205.60	774.30	104.84	0.87	6.04	10.65
185.5	81.47	3485.20	841.80	116.52	1.19	5.76	12.85
186.0	80.04	3512.50	848.40	113.24	1.55	5.23	11.65
186.5	84.45	3781.70	913.40	120.84	1.24	5.66	13.93
186.5	88.51	3837.20	926.80	126.04	1.47	6.54	12.55
187.0	79.85	3675.60	887.80	112.96	1.53	5.44	11.24
187.5	88.77	3777.60	912.40	126.72	1.40	5.98	14.12
188.0	89.25	3801.30	918.10	126.88	1.54	6.68	12.20
188.5	89.02	3864.30	933.40	126.64	1.51	5.78	14.06
189.0	88.86	3868.30	934.30	127.36	1.22	7.26	12.44
189.5	101.37	4243.00	1024.80	145.60	1.31	7.72	15.72
190.0	89.17	3974.90	960.10	127.64	1.26	7.22	12.43
190.5	96.59	4028.40	973.00	138.08	1.44	6.47	15.82
191.0	89.13	3964.50	957.60	127.64	1.23	6.35	14.29
191.5	103.39	4230.10	1021.70	149.00	1.11	10.21	12.39
192.0	95.23	4042.80	976.50	136.24	1.34	8.77	11.16
192.5	97.40	4203.20	1015.20	139.72	1.25	8.46	13.01
193.0	117.33	4838.30	1168.60	169.48	1.22	9.13	19.23
193.5	91.70	4146.20	1001.50	132.24	1.03	6.76	15.42
194.0	89.69	3672.10	887.00	130.12	0.75	7.50	14.53
194.5	73.44	3202.40	773.50	105.72	0.88	5.14	12.63
195.0	62.84	2835.40	684.90	90.16	0.86	4.59	9.92
195.5	63.70	2705.90	653.60	91.36	0.87	4.01	11.34
196.0	61.03	2510.00	606.30	88.00	0.67	4.48	10.36
196.5	52.11	2342.10	565.70	74.68	0.71	3.87	8.09

197.0	52.10	2133.90	515.40	74.84	0.67	2.98	10.07
197.5	44.40	2002.90	483.80	63.32	0.70	2.87	7.29
198.0	42.12	1836.80	443.70	60.48	0.58	2.63	7.54
198.5	38.23	1721.10	415.70	54.32	0.69	2.33	6.16
199.0	41.86	1920.00	463.70	59.84	0.60	3.40	5.76
199.5	49.79	2125.30	513.30	71.56	0.64	3.80	7.73
200.0	47.28	2161.90	522.20	67.88	0.61	3.36	7.81
200.5	63.62	2473.30	597.40	92.08	0.63	4.94	10.62
201.0	63.32	2693.50	650.60	90.92	0.79	4.70	10.17
201.5	71.96	2976.40	718.90	103.64	0.85	5.30	11.91
202.0	78.09	3362.10	812.10	112.44	0.94	5.82	12.71
202.5	81.95	3414.40	824.70	117.80	1.02	5.35	14.67
203.0	83.89	3489.60	842.90	120.84	0.97	6.79	12.75
203.5	79.78	3371.80	814.40	114.96	0.87	6.72	11.82
204.0	76.67	3396.40	820.40	110.20	0.96	5.17	13.37
204.5	84.49	3798.40	917.40	122.20	0.90	4.60	17.75
205.0	70.60	3207.90	774.80	101.44	0.95	4.07	13.42
205.5	70.27	2984.20	720.80	101.56	0.67	5.87	10.97
206.0	68.40	2895.60	699.40	98.60	0.79	4.81	11.87
206.5	67.69	2944.20	711.10	97.84	0.66	5.11	11.60
207.0	65.03	2861.30	691.10	94.28	0.55	4.89	11.59
207.5	59.21	2512.20	606.80	85.96	0.45	5.07	9.55
208.0	49.44	2332.40	563.40	71.12	0.58	3.00	9.46
208.5	68.38	2687.30	649.10	98.72	0.70	5.70	10.48
209.0	65.78	2791.90	674.40	95.48	0.50	6.29	9.29
209.5	65.65	2734.90	660.60	95.04	0.62	5.12	11.04
210.0	69.83	3004.50	725.70	101.00	0.70	5.42	11.61
210.5	67.72	3141.90	758.90	97.72	0.72	5.35	10.85
211.0	71.18	3342.60	807.40	103.40	0.60	4.19	15.07
211.5	72.27	3560.50	860.00	104.84	0.60	5.42	12.97
212.0	71.00	3263.90	788.40	103.16	0.55	6.81	9.97
212.5	64.76	3152.90	761.50	93.20	0.78	4.89	10.40
213.0	54.15	2842.70	686.60	77.96	0.65	4.85	7.19
213.5	50.84	2767.60	668.50	73.72	0.40	5.75	5.33
214.0	48.76	2871.80	693.60	70.88	0.35	5.33	5.66
214.5	59.07	3321.40	802.20	85.60	0.46	6.48	6.60
215.0	60.99	3609.90	871.90	88.68	0.41	7.44	5.65
215.5	64.87	3793.10	916.20	94.56	0.34	8.31	5.66
216.0	60.01	3455.50	834.60	87.64	0.31	7.82	5.03

216.5	58.17	3087.30	745.70	85.24	0.18	7.45	5.69
217.0	74.13	3445.00	832.10	109.08	0.08	9.88	7.19
217.5	84.45	3834.60	926.20	124.36	0.10	11.63	7.43
218.0	85.72	3974.10	959.90	126.24	0.08	11.37	8.50
218.5	84.50	3580.50	864.80	124.64	0.00	13.27	4.62
219.0	79.14	2945.80	711.50	116.72	0.00	12.60	3.98
219.5	92.17	3425.30	827.30	135.96	0.00	14.23	5.53
220.0	83.46	3284.10	793.20	123.12	0.00	12.40	5.98
220.5	97.01	4190.10	1012.10	143.16	0.00	13.35	9.09
221.0	104.09	4228.50	1021.30	153.56	0.00	15.38	7.63
221.5	120.78	4624.10	1116.90	178.20	0.00	17.90	8.75
222.0	110.05	4371.70	1055.90	162.32	0.00	16.90	6.78
222.5	99.92	3834.50	926.20	147.44	0.00	15.09	6.68
223.0	86.55	3412.00	824.10	127.72	0.00	12.67	6.59
223.5	87.54	3178.00	767.60	129.08	0.00	14.05	4.17
224.0	75.55	3056.60	738.30	111.48	0.00	11.15	5.57
224.5	71.63	2955.10	713.80	105.68	0.00	10.67	5.08
225.0	78.04	2954.50	713.60	115.12	0.00	11.29	6.20
225.5	75.12	2867.50	692.60	110.84	0.00	11.41	4.89
226.0	69.97	3015.20	728.30	103.20	0.00	10.41	4.98
226.5	73.80	2877.90	695.10	108.92	0.00	10.77	5.69
227.0	69.20	2612.10	630.90	102.04	0.00	10.18	5.15
227.5	56.90	2141.80	517.30	83.96	0.00	8.80	3.39
228.0	59.16	2173.80	525.00	87.24	0.00	9.00	3.81
228.5	52.38	2040.70	492.90	77.32	0.00	7.43	4.47
229.0	54.55	1969.00	475.60	80.48	0.00	8.39	3.34
229.5	47.23	1767.10	426.80	69.68	0.00	7.39	2.64
230.0	52.19	1756.70	424.30	77.00	0.00	7.61	4.03
230.5	64.92	2031.90	490.80	95.76	0.00	10.20	3.54
231.0	76.84	2725.00	658.20	113.32	0.00	11.96	4.41
231.5	73.93	2580.00	623.20	109.04	0.00	11.55	4.16
232.0	72.31	2360.10	570.10	106.60	0.00	11.20	4.25
232.5	67.07	2565.50	619.70	98.92	0.00	9.95	4.83
233.0	91.91	3544.30	856.10	135.60	0.00	13.87	6.16
233.5	113.82	4758.30	1149.30	167.96	0.00	15.86	10.27
234.0	103.95	4477.00	1081.40	153.44	0.00	14.69	8.98
234.5	83.13	3806.20	919.30	122.68	0.00	11.35	7.97
235.0	78.30	3579.50	864.60	115.56	0.00	10.84	7.21

235.5	82.32	2960.80	715.10	121.40	0.00	12.00	6.35
236.0	59.63	2271.00	548.50	87.96	0.00	8.92	4.15
236.5	64.62	2236.40	540.20	95.28	0.00	10.01	3.80
237.0	63.08	2314.00	558.90	93.04	0.00	9.47	4.32
237.5	75.75	3038.00	733.80	111.72	0.00	11.25	5.43
238.0	64.91	2634.40	636.30	95.84	0.00	8.79	6.38
238.5	51.27	2214.20	534.80	75.68	0.00	7.31	4.30
239.0	50.37	2226.50	537.80	74.32	0.00	7.71	3.16
239.5	79.76	2408.70	581.80	117.56	0.00	12.94	3.51
240.0	91.57	2534.10	612.10	135.00	0.00	14.83	4.09
240.5	76.90	2241.10	541.30	113.44	0.00	11.90	4.56
241.0	85.70	2460.60	594.30	126.40	0.00	13.30	5.00
241.5	75.10	2195.90	530.40	110.68	0.00	12.42	2.83
242.0	74.15	2251.20	543.70	109.40	0.00	11.64	4.07
242.5	69.22	2038.40	492.40	102.08	0.00	10.27	4.98
243.0	71.92	2231.10	538.90	106.08	0.00	11.56	3.40
243.5	94.31	2726.00	658.40	139.08	0.00	14.91	4.95
244.0	107.02	2821.90	681.60	157.72	0.00	17.97	3.49
244.5	99.34	2497.00	603.10	146.52	0.00	16.24	4.15
245.0	71.53	2129.30	514.30	105.48	0.00	11.82	2.73
245.5	54.80	1775.90	429.00	80.88	0.00	8.55	3.12
246.0	50.37	1527.90	369.00	74.32	0.00	7.73	3.12
246.5	70.29	1994.10	481.60	103.68	0.00	11.03	3.86
247.0	96.03	2659.70	642.40	141.60	0.00	16.00	3.40
247.5	95.65	2636.70	636.90	141.00	0.00	15.71	3.83
248.0	86.28	2696.90	651.40	127.20	0.00	13.62	4.56
248.5	45.90	1846.70	446.00	67.68	0.00	6.95	3.02
249.0	37.90	1686.80	407.40	55.80	0.00	5.73	2.49
249.5	36.76	1343.70	324.60	54.24	0.00	5.50	2.56
250.0	41.22	1207.10	291.60	60.80	0.00	6.62	1.96
250.5	45.67	1492.70	360.50	67.36	0.00	7.14	2.56
251.0	37.77	1299.70	313.90	55.72	0.00	5.84	2.25
251.5	43.25	1327.10	320.60	63.80	0.00	6.59	2.77
252.0	53.50	1631.90	394.20	78.84	0.00	9.02	1.67
252.5	52.35	1571.90	379.70	77.20	0.00	7.99	3.32
253.0	32.22	1002.70	242.20	47.52	0.00	4.97	1.94
253.5	41.25	1326.60	320.40	60.80	0.00	6.66	1.88
254.0	34.49	1068.90	258.20	50.88	0.00	5.28	2.16
254.5	47.39	1635.50	395.00	69.92	0.00	7.52	2.44
255.0	49.05	1586.40	383.20	72.36	0.00	7.50	3.09

255.5	49.46	1651.60	398.90	72.96	0.00	7.72	2.80
256.0	50.48	1790.80	432.50	74.40	0.00	8.12	2.36
256.5	71.20	2165.80	523.10	105.00	0.00	11.52	3.21
257.0	94.94	2811.60	679.10	139.96	0.00	15.67	3.65
257.5	96.03	3242.60	783.20	141.56	0.00	15.40	4.59
258.0	116.53	3359.20	811.40	171.80	0.00	18.89	5.17
258.5	101.59	3438.70	830.60	149.80	0.00	16.16	5.13
259.0	91.96	3499.50	845.30	135.64	0.00	14.35	5.21
259.5	79.08	3574.50	863.40	116.20	0.14	10.79	6.91
260.0	80.62	3511.30	848.10	118.80	0.06	11.27	6.92
260.5	73.27	3404.20	822.20	108.08	0.00	10.97	5.08
261.0	67.08	3118.10	753.10	98.92	0.03	9.43	5.75
261.0	64.10	3224.10	778.70	93.92	0.21	9.01	4.62
261.5	69.04	3444.30	831.90	101.28	0.22	8.88	6.68
262.0	56.54	3431.00	828.70	82.68	0.25	7.03	5.61
262.5	71.21	3756.50	907.30	104.44	0.23	9.22	6.75
263.0	71.77	3892.00	940.10	105.76	0.05	9.42	7.40
263.5	55.03	3075.50	742.80	80.64	0.19	6.74	5.92
264.0	49.29	2942.10	710.60	72.12	0.21	5.99	5.21
264.5	53.39	3025.60	730.80	78.28	0.18	5.99	6.87
265.0	48.65	2574.70	621.90	71.40	0.11	6.34	4.73
265.5	49.62	2633.30	636.00	72.36	0.29	5.93	5.07
266.0	40.61	2361.40	570.40	58.76	0.35	4.69	3.91
266.5	40.21	2445.00	590.60	58.04	0.42	4.24	4.35
267.0	40.60	2549.90	615.90	58.12	0.54	4.11	4.15
267.5	51.49	3328.50	803.90	74.36	0.52	5.49	5.53
268.0	52.49	2909.50	702.70	76.04	0.44	6.67	3.91
268.5	50.18	2831.30	683.90	73.12	0.32	5.90	5.20
269.0	42.01	2488.30	601.00	60.88	0.39	4.00	5.66
269.5	47.07	2674.80	646.10	68.52	0.31	5.16	5.57
270.0	46.90	2659.80	642.40	68.68	0.15	5.48	5.61
270.5	45.04	2742.20	662.30	65.20	0.40	4.15	6.40
271.0	48.99	2854.60	689.50	71.56	0.27	4.76	7.29
271.5	45.27	2817.80	680.60	65.28	0.47	4.50	5.44
272.0	47.36	2729.70	659.30	67.72	0.65	4.43	5.47
272.5	51.88	2868.00	692.70	75.48	0.37	5.33	6.73
273.0	53.72	3173.40	766.50	77.52	0.56	5.25	6.64
273.5	62.32	3398.40	820.80	90.48	0.49	6.42	7.82
274.0	63.34	3397.20	820.50	91.88	0.50	7.04	6.89
277.0	64.82	3598.10	869.10	94.36	0.44	7.15	7.53

277.5	59.04	3380.90	816.60	85.28	0.56	6.78	5.52
278.0	50.09	3173.90	766.60	72.68	0.39	5.56	5.49
278.5	38.80	2497.10	603.10	55.52	0.53	3.85	4.06
279.0	31.35	1984.80	479.40	45.12	0.33	3.61	2.74
279.5	32.30	2042.20	493.30	46.64	0.29	3.62	3.26
280.0	31.26	1855.70	448.20	45.32	0.24	3.82	2.73
280.5	31.14	1892.20	457.00	45.16	0.27	3.46	3.29
281.0	61.55	3635.80	878.20	88.68	0.66	7.55	4.43
281.5	53.24	3461.80	836.10	76.96	0.49	5.83	5.62
282.0	57.69	3322.90	802.60	83.52	0.48	6.57	5.82
282.5	56.36	3406.30	822.70	81.44	0.56	6.26	5.60
283.0	47.84	2719.40	656.80	69.36	0.41	5.62	4.46
283.5	47.02	2762.40	667.20	68.00	0.40	5.87	3.66
284.0	47.80	2963.40	715.80	69.16	0.42	5.92	3.77
284.5	45.77	2971.60	717.80	66.04	0.46	4.90	4.87
285.0	59.65	3314.50	800.60	86.64	0.42	7.63	4.72
285.5	61.03	3625.60	875.70	88.36	0.52	7.14	5.73
286.0	62.35	3448.10	832.80	90.24	0.53	7.72	5.00
286.5	70.70	3867.10	934.10	102.72	0.50	8.71	6.26
287.0	51.50	3030.70	732.00	74.72	0.40	6.06	4.96
287.5	33.40	2001.40	483.40	48.44	0.30	3.26	4.39
288.0	29.20	1834.50	443.10	42.32	0.23	3.54	2.58
288.5	36.66	2030.40	490.40	53.12	0.32	4.09	3.82
290.0	35.57	2106.80	508.90	51.80	0.21	4.55	3.01
290.5	46.09	2664.90	643.70	66.80	0.37	5.60	4.02
291.0	61.09	3423.30	826.90	88.32	0.59	6.68	6.36
291.5	40.14	2466.40	595.70	57.68	0.46	4.25	4.08
292.0	40.56	2511.00	606.50	58.72	0.36	5.18	2.88
292.5	43.57	2615.70	631.80	62.76	0.48	4.76	4.25
293.0	39.87	2565.50	619.70	57.68	0.35	4.51	4.00
298.0	38.81	2433.30	587.70	55.92	0.43	3.97	4.32
298.5	51.10	2978.90	719.50	73.80	0.49	6.54	3.41
299.0	37.29	2209.10	533.60	54.16	0.26	4.25	4.00
299.5	41.97	2431.20	587.20	60.68	0.38	4.82	4.01
300.0	40.82	2450.40	591.90	58.88	0.39	5.14	2.88
300.5	45.82	2547.40	615.30	66.52	0.31	5.96	3.47
301.0	41.34	2435.40	588.20	59.96	0.32	4.88	3.95
301.5	39.01	2231.40	539.00	56.64	0.28	4.72	3.60
302.0	31.82	2167.00	523.40	45.92	0.32	3.46	3.28
302.5	43.78	2613.20	631.20	63.68	0.28	5.50	3.80
303.0	47.89	2852.60	689.00	70.04	0.23	5.74	5.11

303.5	40.08	2450.90	592.00	58.16	0.28	4.58	4.26
304.0	35.25	2067.00	499.20	50.84	0.37	3.75	3.73
304.5	41.36	2274.10	549.30	60.08	0.32	4.86	4.02
305.0	42.31	2523.40	609.50	61.28	0.33	4.83	4.34
305.5	37.24	2315.80	559.40	54.16	0.26	4.39	3.72
306.0	42.15	2595.00	626.80	61.16	0.32	4.97	4.07
306.5	43.05	2711.00	654.80	62.36	0.37	5.34	3.43
308.0	44.53	2648.30	639.70	64.56	0.32	5.26	4.34
308.5	46.08	2458.30	593.80	67.20	0.26	5.36	5.04
309.0	40.52	2270.70	548.50	58.76	0.33	4.87	3.63
309.5	34.50	1952.10	471.50	50.44	0.15	4.39	3.23
310.0	36.51	2153.50	520.10	52.88	0.29	4.33	3.40
310.5	33.04	1902.80	459.60	48.20	0.18	4.16	3.01
311.0	38.04	2051.20	495.40	55.36	0.23	4.99	2.94
311.5	43.41	2415.00	583.30	63.28	0.25	5.16	4.50
312.0	57.12	3046.70	735.90	83.44	0.24	7.77	4.36
312.5	58.15	2998.10	724.10	84.92	0.28	7.34	5.43
313.0	52.33	2953.50	713.40	76.40	0.27	7.17	3.68
313.5	51.45	2839.50	685.80	75.08	0.29	6.23	5.15
314.0	55.93	2794.50	675.00	81.92	0.19	7.98	3.76
314.5	57.29	2974.80	718.50	84.08	0.12	8.17	4.20
315.0	58.62	2910.50	703.00	86.00	0.13	8.41	4.16
315.5	59.10	3043.10	735.00	86.88	0.08	8.60	4.20
316.0	55.67	2857.20	690.10	81.28	0.21	8.54	2.40
316.5	51.77	2636.00	636.70	75.72	0.21	6.34	5.41
317.0	44.25	2545.10	614.70	64.60	0.21	5.94	3.43
317.5	50.14	2419.00	584.30	73.28	0.23	6.66	4.08
318.0	44.41	2291.30	553.40	64.88	0.22	5.58	4.18
318.5	54.62	2275.60	549.60	78.64	0.61	6.71	3.80
319.0	60.97	2609.50	630.30	87.56	0.70	7.63	3.83
319.5	59.17	2560.30	618.40	85.40	0.60	6.82	5.31
320.0	55.06	2559.80	618.30	78.76	0.79	5.91	4.71
320.5	59.28	2774.70	670.20	85.48	0.61	6.56	5.81
320.5	60.28	2710.60	654.70	86.84	0.63	7.33	4.53
321.0	46.77	2511.60	606.60	67.00	0.59	4.97	4.45
321.5	44.68	2424.00	585.50	63.64	0.65	5.29	2.73
322.0	42.21	2408.60	581.80	60.24	0.63	4.56	3.42
328.0	24.39	1451.30	350.50	35.16	0.26	2.61	2.53
328.5	24.49	1453.90	351.20	35.28	0.28	2.21	3.28
329.0	23.81	1477.20	356.80	34.28	0.28	2.45	2.55
329.5	28.50	1566.80	378.40	41.48	0.21	3.52	2.49

330.0	30.82	1668.70	403.00	45.00	0.14	4.12	2.45
330.5	38.34	2056.40	496.70	56.08	0.17	4.97	3.40
331.0	44.20	2315.00	559.20	65.16	0.00	6.03	4.23
331.5	49.07	2396.50	578.80	72.16	0.08	6.16	5.40
369.0	40.78	2021.40	488.20	60.00	0.03	5.72	3.44
369.5	44.55	1851.90	447.30	65.68	0.00	6.31	3.80
370.0	47.48	1857.10	448.60	70.04	0.00	7.57	2.37
370.5	43.24	1687.80	407.70	63.80	0.00	6.50	2.95
371.0	39.18	1686.30	407.30	57.76	0.00	5.89	2.66
371.5	42.43	1561.50	377.20	62.56	0.00	6.63	2.38
372.0	43.35	1569.80	379.20	64.00	0.00	6.51	2.98
372.5	47.83	1505.10	363.50	70.52	0.00	7.39	2.85
373.0	52.58	1515.50	366.00	77.56	0.00	7.85	3.69
373.5	44.04	1369.60	330.80	64.96	0.00	7.25	1.74
374.0	49.45	1309.50	316.30	72.88	0.00	7.87	2.48
374.5	51.80	1369.60	330.80	76.40	0.00	8.24	2.62
375.0	52.04	1313.70	317.30	76.76	0.00	8.49	2.21
375.5	48.95	1385.10	334.50	72.20	0.00	7.95	2.15
376.0	55.78	1376.30	332.40	82.20	0.00	9.63	1.29
376.5	48.60	1287.80	311.10	71.64	0.00	8.28	1.35
377.0	49.67	1222.10	295.20	73.28	0.00	7.99	2.34
391.0	66.37	2574.10	621.70	97.96	0.00	9.83	4.83
391.5	91.57	3197.50	772.30	135.08	0.00	13.42	6.93
392.0	99.47	3505.70	846.80	146.76	0.00	14.52	7.65
392.5	118.82	4644.00	1121.70	175.36	0.00	15.90	12.04
393.0	141.04	5553.70	1341.40	208.20	0.00	18.91	14.23
408.0	98.28	1859.60	449.20	144.84	0.00	17.07	2.07
434.0	145.14	3450.00	833.30	213.92	0.00	24.42	4.64
438.0	126.69	3050.30	736.80	186.72	0.00	21.66	3.36
482.0	85.10	2814.10	679.70	125.48	0.00	13.43	4.51
475.0	75.91	2981.00	720.00	112.00	0.00	10.83	6.34
490.0	38.35	1461.70	353.00	55.60	0.34	4.56	3.42

**Table 7: Tomera Ranch Outcrop Gamma Ray Data**

Interval (ft.)	Dose [nGy/h]	Total[ppm]	Total[cpm]	API	K wt. %	U[ppm]	Th[ppm]
25.0	127.43	1225.10	5072.10	185.60	0.92	7.90	26.92
26.0	109.65	1142.80	4731.50	160.24	0.65	6.45	24.56
27.0	84.23	913.90	3783.70	118.04	1.97	5.24	11.15
28.0	101.34	1081.10	4476.10	141.16	2.62	5.47	13.87
29.0	92.90	983.30	4070.90	130.24	2.13	5.94	12.16
30.0	87.03	964.80	3994.30	120.08	2.59	3.83	12.00

32.0	95.11	991.90	4106.50	133.36	2.23	5.19	14.04
33.0	80.97	896.00	3709.60	114.08	1.69	5.30	11.16
34.0	91.54	952.60	3943.80	129.88	1.62	8.70	8.59
35.0	92.28	928.60	3844.60	131.56	1.41	9.82	7.61
36.0	129.19	1352.80	5601.00	182.92	2.34	13.57	9.23
37.0	111.08	1124.70	4656.50	157.64	1.94	11.57	8.51
38.0	76.39	848.40	3512.60	107.60	1.59	6.81	6.92
39.0	57.18	605.00	2504.90	81.36	0.91	5.89	4.92
40.0	88.07	870.00	3601.80	125.36	1.39	9.23	7.32
41.0	61.23	652.80	2702.90	87.00	1.02	6.27	5.13
42.0	103.24	1086.60	4498.80	148.52	1.24	7.43	17.31
43.0	103.37	1178.80	4880.50	147.64	1.56	8.65	13.37
44.0	66.29	749.80	3104.50	93.56	1.29	5.57	7.09
45.0	58.42	696.60	2884.20	82.44	1.18	4.68	6.53
46.0	77.56	779.10	3225.50	108.92	1.67	6.78	6.99
47.0	81.82	918.30	3802.10	115.40	1.68	6.62	8.89
48.0	84.05	950.10	3933.50	118.28	1.80	5.87	10.63
49.0	85.85	911.90	3775.60	121.76	1.51	8.22	7.96
50.0	107.22	1102.80	4565.80	152.24	1.81	11.13	8.56
51.0	100.81	1032.20	4273.70	142.80	1.85	9.84	8.62
52.0	65.37	659.00	2728.40	93.76	0.80	7.96	4.32
53.0	41.67	454.20	1880.30	59.60	0.57	5.11	2.40
54.0	70.61	831.40	3442.00	100.08	1.28	6.95	6.00
55.0	74.82	929.90	3849.90	106.16	1.31	7.46	6.38
56.0	73.30	1130.20	4679.10	105.36	0.82	9.66	3.74
57.0	55.07	1030.00	4264.50	77.80	1.02	5.64	4.09
58.0	42.59	904.60	3745.10	60.44	0.74	3.77	4.61
59.0	93.86	1012.60	4192.30	134.80	1.19	6.78	15.38
60.0	96.88	1021.90	4231.00	139.72	1.06	8.56	13.57
61.0	99.01	1059.80	4387.80	141.44	1.41	10.03	9.66
62.0	77.19	847.00	3506.80	111.08	0.90	8.39	7.39
63.0	70.78	937.30	3880.80	100.96	1.08	6.79	7.34
64.0	56.47	810.80	3356.80	80.84	0.74	6.38	4.49
65.0	43.30	707.90	2930.90	62.04	0.55	5.32	2.67
66.0	32.19	652.20	2700.10	45.80	0.50	3.73	1.99
67.0	29.82	705.10	2919.20	42.40	0.50	3.41	1.78
68.0	23.41	712.20	2948.80	33.04	0.46	2.73	0.96
69.0	30.54	1089.70	4511.70	42.24	0.84	3.22	0.76
70.0	27.57	1071.20	4434.90	37.76	0.88	2.83	0.26
71.0	31.34	1030.70	4267.20	43.76	0.75	3.97	0.00
72.0	30.66	1061.50	4395.00	42.44	0.83	3.61	0.07

73.0	160.19	1616.10	6691.10	231.76	1.40	22.53	7.28
74.0	183.57	1836.10	7601.60	265.32	1.60	26.96	6.01
75.0	77.28	798.30	3305.00	111.00	0.94	9.95	4.09
76.0	94.02	990.90	4102.40	134.40	1.32	12.04	4.24
77.0	127.21	1319.60	5463.50	182.60	1.51	16.33	6.95
78.0	126.32	1278.70	5293.80	181.04	1.65	15.60	7.46
79.0	107.22	1146.90	4748.20	152.96	1.56	12.61	6.78
80.0	112.56	1187.30	4915.40	160.24	1.77	13.12	6.74
81.0	108.45	1111.70	4602.50	154.96	1.57	12.63	7.20
82.0	89.42	924.70	3828.30	127.72	1.30	10.67	5.39
83.0	61.97	644.60	2668.70	88.56	0.84	7.81	3.16
84.0	65.55	717.00	2968.50	92.84	1.20	6.69	5.03
85.0	75.35	819.20	3391.70	106.60	1.39	8.16	4.77
86.0	77.94	834.70	3455.90	109.80	1.63	7.21	6.51
87.0	61.42	717.20	2969.50	86.20	1.39	5.24	5.51
88.0	51.64	568.30	2352.80	72.56	1.12	4.34	4.98
89.0	67.31	768.80	3183.00	93.04	1.95	4.22	7.02
90.0	71.12	767.80	3178.80	99.64	1.67	5.75	6.73
91.0	61.96	686.20	2841.00	86.96	1.34	5.45	5.48
92.0	59.35	687.60	2846.90	82.84	1.45	4.30	6.31
93.0	71.31	769.10	3184.00	99.60	1.73	5.74	6.50
94.0	58.15	664.80	2752.30	81.56	1.28	4.75	5.77
95.0	64.83	687.20	2845.20	91.04	1.44	5.29	6.42
96.0	48.30	558.90	2313.80	68.08	0.99	4.41	4.24
97.0	54.28	575.10	2381.00	77.36	0.84	6.27	3.44
98.0	79.85	795.90	3295.30	113.48	1.32	8.87	5.35
99.0	48.06	540.10	2236.20	67.68	0.96	4.58	3.92
100.0	74.08	827.20	3424.80	103.28	1.86	4.78	8.82
101.0	86.78	954.80	3953.00	120.52	2.27	7.07	6.91
102.0	94.25	1012.50	4191.80	131.08	2.46	7.79	7.35
103.0	74.56	813.80	3369.30	104.92	1.54	7.49	5.09
104.0	66.30	768.50	3181.60	92.32	1.73	4.55	7.06
105.0	83.23	884.40	3661.50	116.64	1.90	6.73	8.10
106.0	89.26	979.20	4054.10	124.84	2.12	7.71	7.31
107.0	82.93	884.20	3660.80	115.88	1.98	7.68	5.69
108.0	67.83	735.60	3045.50	95.20	1.51	6.19	5.38
109.0	104.34	1101.10	4558.70	144.32	2.96	8.76	6.72
110.0	21.91	867.40	3591.10	30.68	0.47	2.87	0.05
111.0	21.87	1028.80	4259.30	30.56	0.49	2.77	0.14
112.0	22.18	967.30	4004.60	30.88	0.53	2.80	0.00
113.0	17.33	722.70	2991.90	24.72	0.24	2.61	0.00

114.0	98.37	1065.20	4410.10	132.52	3.86	5.44	6.81
115.0	118.27	1327.00	5494.10	159.28	4.65	7.19	6.84
116.0	164.84	1807.40	7482.90	227.68	4.67	16.51	5.22
117.0	163.28	1763.00	7299.10	220.48	6.17	12.01	6.42
118.0	151.66	1675.20	6935.80	207.08	5.02	12.60	6.49
119.0	97.99	1102.00	4562.30	135.64	2.72	9.62	3.79
120.0	108.99	1287.80	5331.60	150.40	3.13	10.64	3.80
121.0	124.48	1415.20	5859.30	170.04	4.15	10.08	5.75
122.0	124.22	1457.40	6033.80	168.32	4.58	8.46	6.84
123.0	106.57	1196.10	4952.00	145.24	3.67	7.48	6.67
124.0	73.27	868.30	3595.00	99.36	2.69	4.13	5.82
125.0	74.97	844.00	3494.20	102.56	2.47	4.26	7.24
126.0	67.02	797.30	3300.80	92.40	2.01	3.62	7.82
127.0	74.85	865.20	3582.10	102.28	2.53	4.60	6.25
128.0	88.20	959.90	3974.00	121.44	2.70	6.04	7.48
129.0	83.38	934.40	3868.70	113.64	2.86	5.83	5.31
130.0	113.17	1204.60	4987.30	154.00	3.97	6.86	8.90
131.0	111.88	1204.00	4984.90	152.64	3.77	8.05	6.98
132.0	102.53	1125.10	4658.00	140.56	3.24	8.58	5.02
133.0	103.55	1136.60	4705.80	142.20	3.24	8.66	5.27
134.0	114.06	1298.00	5373.90	155.68	3.82	9.02	5.60
135.0	139.98	1527.60	6324.40	190.60	4.82	10.78	6.81
136.0	140.82	1529.00	6330.20	193.96	4.23	12.14	7.29
137.0	118.00	1305.50	5405.00	162.88	3.46	9.03	8.82
138.0	115.53	1214.20	5027.20	160.40	3.08	9.91	7.96
139.0	86.74	991.10	4103.30	120.48	2.30	6.75	7.42
140.0	96.30	1083.50	4485.90	134.40	2.40	7.37	9.26
141.0	126.97	1334.50	5525.10	178.60	2.70	12.11	9.63
142.0	117.84	1263.80	5232.10	164.88	2.77	10.60	8.94
143.0	96.41	1077.80	4462.30	134.72	2.33	8.34	7.68
144.0	82.34	905.60	3749.20	115.24	1.95	6.62	7.77
145.0	95.05	1066.30	4414.70	133.88	2.01	5.32	14.79
146.0	106.22	1104.90	4574.30	150.24	2.03	6.67	16.10
147.0	105.33	1081.00	4475.50	149.68	1.85	6.96	16.10
148.0	97.90	1102.80	4565.80	138.52	1.90	6.15	14.73
149.0	101.84	1107.70	4586.20	143.32	2.24	5.00	16.87
151.0	117.27	1202.70	4979.50	165.48	2.39	6.68	18.45
152.0	117.00	1221.90	5058.70	164.64	2.55	6.33	18.30
153.0	113.72	1234.50	5110.90	159.16	2.74	5.57	17.69
154.0	107.89	1187.90	4918.30	150.44	2.72	4.94	16.85
155.0	123.19	1317.50	5454.60	172.64	2.89	5.98	19.64

156.0	126.98	1359.00	5626.40	178.72	2.76	7.11	19.42
157.0	123.96	1341.00	5552.10	174.52	2.65	7.18	18.67
158.0	120.25	1342.70	5559.20	168.80	2.73	7.46	16.36
159.0	109.42	1323.10	5478.00	153.32	2.54	6.79	14.59
160.0	108.81	1275.60	5281.10	152.92	2.40	6.27	16.09
161.0	106.85	1294.90	5360.90	149.52	2.56	6.03	15.08
162.0	113.19	1299.50	5380.20	158.92	2.57	6.25	16.95
163.0	116.04	1338.30	5540.60	162.92	2.61	6.52	17.25
164.0	107.39	1264.50	5235.40	150.36	2.52	5.61	16.29
165.0	111.44	1320.00	5465.20	155.48	2.81	6.07	15.49
166.0	106.36	1233.60	5107.50	149.80	2.20	8.67	11.31
167.0	119.34	1401.50	5802.40	167.16	2.76	7.87	15.01
168.0	106.89	1160.60	4804.90	148.32	2.97	4.60	16.00
169.0	97.08	1062.70	4399.80	135.32	2.50	4.81	14.21
170.0	114.82	1270.30	5259.10	158.96	3.26	5.12	16.46
171.0	110.22	1192.30	4936.20	153.16	2.98	5.30	15.77
172.0	103.37	1152.30	4770.80	143.64	2.79	4.77	15.21
173.0	100.78	1130.40	4680.10	140.04	2.73	4.66	14.77
174.0	107.32	1201.50	4974.60	149.48	2.77	5.74	14.81
175.0	106.52	1200.20	4969.00	148.36	2.79	4.51	16.91
176.0	102.99	1204.20	4985.80	143.68	2.59	5.32	14.92
177.0	106.38	1204.70	4987.80	149.16	2.47	5.62	16.17
178.0	97.63	1162.60	4813.20	136.96	2.30	4.36	16.32
179.0	83.18	1046.90	4334.40	117.36	1.72	3.75	14.96
180.0	69.50	961.10	3979.10	97.84	1.53	3.84	10.66
181.0	72.08	1034.70	4284.00	101.68	1.50	4.03	11.36
182.0	76.59	1173.00	4856.40	108.60	1.43	4.76	11.91
183.0	66.78	1116.90	4624.20	94.32	1.35	3.80	10.58
184.0	54.91	1064.80	4408.60	77.64	1.05	3.33	8.55
185.0	56.20	1210.00	5009.60	79.52	1.09	3.75	8.02
186.0	117.22	1244.50	5152.40	164.84	2.54	8.03	14.99
187.0	109.91	1183.10	4898.10	154.28	2.45	6.79	15.19
188.0	99.97	1120.10	4637.60	139.88	2.42	4.90	15.49
189.0	99.61	1123.60	4652.10	139.80	2.27	6.46	12.95
190.0	83.18	935.60	3873.40	117.04	1.77	5.49	11.20
191.0	95.87	1098.10	4546.20	134.84	2.13	5.02	15.15
192.0	102.63	1173.50	4858.40	144.64	2.18	6.22	15.00
193.0	96.55	1179.10	4881.70	135.48	2.21	5.24	14.55
194.0	107.25	1432.20	5929.50	144.20	4.33	4.47	9.79
195.0	105.57	1450.90	6007.10	142.96	3.94	5.63	8.72
196.0	102.18	1487.10	6156.70	140.76	3.07	7.96	6.99

197.0	75.98	1205.20	4989.80	105.12	2.14	6.63	4.46
198.0	76.67	1327.60	5496.60	104.92	2.52	5.27	5.61
199.0	70.82	1325.80	5488.80	96.64	2.38	4.99	4.66
200.0	82.59	1547.30	6406.00	115.52	1.95	8.35	4.38
201.0	76.35	1516.10	6276.80	107.72	1.50	8.68	3.57
202.0	154.15	1667.50	6903.70	215.04	3.77	15.70	7.28
203.0	87.72	933.60	3865.40	123.92	1.66	9.49	5.36
204.0	138.82	1404.90	5816.60	196.00	2.64	15.51	7.42
205.0	149.07	1511.40	6257.50	211.32	2.61	17.80	6.79
206.0	138.01	1397.20	5784.60	198.20	1.65	17.69	7.57
207.0	97.69	1018.10	4215.10	137.76	1.94	9.55	7.58
208.0	103.96	1133.70	4693.80	145.96	2.27	9.01	9.39
209.0	92.07	1047.30	4336.00	130.80	1.52	11.26	4.10
210.0	83.21	999.40	4137.50	116.08	2.02	7.03	6.88
211.0	87.03	1056.10	4372.50	121.00	2.28	7.55	6.03
212.0	93.21	1143.10	4732.70	132.00	1.66	10.65	5.06
213.0	73.67	984.90	4077.80	103.16	1.66	7.14	4.87
214.0	71.52	950.30	3934.20	100.64	1.49	6.94	5.32
215.0	55.43	799.10	3308.60	77.20	1.41	4.28	5.10
216.0	59.08	844.30	3495.70	82.68	1.42	4.61	5.77
217.0	89.87	1021.30	4228.20	125.40	2.20	7.53	7.49
218.0	110.04	1177.80	4876.40	152.80	2.91	10.22	6.12
219.0	79.33	910.50	3769.50	110.88	1.89	7.67	4.82
220.0	72.90	798.50	3306.00	101.20	1.92	6.28	5.06
221.0	74.98	824.40	3413.30	104.28	1.93	6.19	5.97
222.0	83.50	971.60	4022.60	116.96	1.94	6.94	7.60
223.0	109.89	1179.80	4884.80	156.64	1.64	13.66	5.28
224.0	102.54	1087.90	4504.20	144.20	2.13	11.02	5.49
225.0	90.29	998.00	4131.90	125.80	2.29	7.56	7.17
226.0	78.56	932.50	3860.80	107.56	2.55	5.55	5.59
227.0	71.95	797.30	3301.10	100.72	1.68	7.16	4.14
228.0	74.92	841.80	3485.10	104.36	1.88	6.17	6.23
229.0	80.04	896.30	3710.90	110.32	2.39	5.08	7.86
230.0	85.73	916.10	3793.00	118.80	2.35	7.25	5.80
231.0	89.50	998.90	4135.80	124.72	2.28	8.03	6.00
232.0	92.55	1028.00	4256.20	128.24	2.54	8.16	5.58
233.0	88.30	995.50	4121.50	123.48	2.06	7.67	7.29
234.0	112.53	1210.10	5010.10	159.88	1.88	12.48	7.49
235.0	110.75	1188.40	4920.30	157.04	1.94	12.50	6.50
236.0	108.52	1146.70	4747.50	153.84	1.88	11.75	7.44
237.0	105.44	1138.60	4714.00	147.48	2.45	10.44	6.19

238.0	111.88	1178.40	4878.60	157.76	2.21	12.09	6.42
239.0	126.89	1335.60	5529.80	178.40	2.69	12.98	7.88
240.0	115.03	1186.20	4911.20	163.44	1.88	13.74	5.86
242.0	123.86	1318.40	5458.30	176.80	1.79	13.94	9.16
241.0	100.65	1137.30	4708.60	142.88	1.69	11.90	5.16
243.0	180.54	1908.40	7901.00	257.96	2.51	23.71	7.03
244.0	150.09	1700.80	7041.80	213.68	2.32	19.33	5.48
245.0	120.28	1412.20	5846.60	171.28	1.89	14.55	6.16
246.0	143.72	1682.20	6964.50	204.88	2.14	18.60	5.46
247.0	193.48	2305.60	9545.50	280.08	1.56	30.09	3.60
248.0	207.56	2548.90	10552.70	299.56	1.94	31.53	4.07
249.0	184.84	2341.00	9692.30	267.00	1.64	27.49	5.21
250.0	124.73	1818.20	7527.70	179.44	1.35	18.11	3.24
251.0	128.48	2029.70	8403.10	184.72	1.42	19.14	2.22
252.0	241.35	2504.60	10369.60	348.40	2.24	35.91	6.32
253.0	297.47	2938.00	12163.60	431.88	1.98	47.82	4.41
254.0	251.37	2585.80	10705.70	364.36	1.85	39.30	5.09
255.0	183.10	1923.70	7964.30	263.68	1.91	27.30	3.68
256.0	186.02	2033.00	8417.00	266.32	2.43	25.83	5.20
257.0	120.80	1427.60	5910.30	171.00	2.19	14.86	4.27
258.0	86.24	1067.20	4418.50	121.04	1.92	8.68	5.22
259.0	69.95	940.60	3894.20	97.88	1.61	6.42	5.19
260.0	75.71	1022.30	4232.60	105.80	1.80	7.26	4.73
261.0	68.27	1026.30	4249.00	94.72	1.82	5.81	4.78
262.0	65.07	958.70	3969.30	90.64	1.66	5.54	4.94
265.0	102.23	1098.60	4548.50	141.84	2.72	8.53	7.52
266.0	66.97	1031.70	4271.50	93.48	1.68	5.03	6.59
267.0	65.78	1105.20	4575.90	91.44	1.74	5.30	5.30
268.0	73.04	1170.60	4846.70	102.76	1.50	7.53	4.63
269.0	165.26	1725.90	7145.30	234.68	2.75	20.83	6.01
270.0	214.32	2323.30	9618.80	304.52	3.50	27.49	7.15
271.0	141.84	1554.20	6434.50	201.84	2.23	17.32	6.90
272.0	141.99	1580.60	6543.90	201.32	2.44	16.27	8.03
273.0	190.78	2066.80	8557.00	269.52	3.54	23.86	5.50
274.0	292.70	3053.20	12640.90	417.68	4.20	39.83	7.96
275.0	419.77	4267.50	17668.10	606.88	3.52	67.14	3.36
276.0	376.08	3870.30	16023.70	542.48	3.57	59.08	3.18
277.0	342.80	3567.10	14768.20	496.40	2.68	55.08	3.22
278.0	226.57	2406.50	9963.20	329.76	1.29	35.54	6.20
279.0	142.73	1559.20	6455.40	205.16	1.68	17.05	10.47
280.0	115.39	1294.30	5358.60	162.48	2.42	10.48	9.98

282.0	148.08	1564.10	6475.80	211.20	2.18	18.85	6.38
284.0	200.20	2092.40	8662.80	287.16	2.42	27.38	7.35
286.0	281.77	2831.00	11720.60	406.00	2.86	41.48	7.10
288.0	170.67	1781.00	7373.40	240.48	3.42	19.88	6.68
290.0	95.27	1027.00	4252.00	134.04	1.99	9.70	6.15
292.0	103.85	1102.70	4565.40	146.88	1.91	11.58	5.92
294.0	92.03	1039.80	4305.00	130.04	1.77	9.29	6.85
296.0	107.90	1107.50	4585.10	150.96	2.55	9.88	7.78
298.0	66.11	716.40	2966.00	92.08	1.69	4.39	7.48
300.0	76.63	849.70	3517.80	103.84	2.83	3.74	7.16
297.0	72.00	812.20	3362.50	97.52	2.72	2.88	7.74
301.0	82.89	923.10	3821.90	111.92	3.17	4.07	7.16
302.0	77.45	897.70	3716.80	103.84	3.21	3.42	6.28
303.0	75.14	872.10	3610.70	101.84	2.76	4.85	4.72
304.0	80.38	976.50	4042.90	107.12	3.53	2.98	6.70
305.0	67.69	843.90	3493.90	91.52	2.58	2.84	6.88
306.0	61.77	811.00	3357.70	84.20	2.16	2.71	6.99
307.0	49.85	688.70	2851.40	68.68	1.54	2.70	5.61
308.0	43.99	710.40	2941.20	59.84	1.55	1.99	4.78
309.0	38.46	712.70	2950.50	52.20	1.40	1.77	3.91
310.0	32.43	657.10	2720.50	45.36	0.75	2.63	3.08
311.0	26.64	636.50	2635.20	37.20	0.61	2.39	2.08
312.0	26.28	843.10	3490.70	36.12	0.80	1.83	2.17
313.0	20.32	839.80	3476.90	28.04	0.57	1.92	0.89
316.0	15.44	738.50	3057.60	21.48	0.40	1.77	0.23
318.0	17.14	879.10	3639.50	23.84	0.41	1.93	0.46
320.0	14.40	605.00	2504.60	20.32	0.28	1.86	0.24
321.0	79.42	858.60	3554.70	107.56	2.95	3.68	7.73
322.0	68.03	793.60	3285.60	92.08	2.53	3.82	5.26
323.0	59.98	698.40	2891.40	82.16	1.93	3.52	5.78
324.0	48.76	655.80	2715.00	67.32	1.48	2.57	5.77
325.0	49.70	669.10	2770.20	68.24	1.55	2.51	5.84
326.0	47.31	694.50	2875.20	65.36	1.37	2.51	5.84
327.0	48.12	740.50	3065.90	66.20	1.47	2.28	6.11
328.0	58.02	1069.60	4428.40	80.36	1.65	3.80	5.89
329.0	35.93	875.00	3622.70	49.24	1.17	1.86	3.91
330.0	36.52	967.20	4004.40	50.60	1.04	2.15	4.19
331.0	28.87	975.80	4039.80	39.68	0.90	2.22	1.88
332.0	20.50	832.60	3447.10	28.48	0.55	1.95	1.02
334.0	15.04	585.40	2423.70	21.20	0.31	1.73	0.60
336.0	15.25	649.30	2688.00	21.36	0.33	1.92	0.18

338.0	17.60	722.80	2992.60	24.80	0.34	2.16	0.52
340.0	13.56	562.30	2327.90	19.08	0.28	1.76	0.13
341.0	16.65	509.20	2108.40	23.96	0.14	2.57	0.29
342.0	12.29	539.20	2232.30	17.28	0.28	1.47	0.26
343.0	14.87	593.80	2458.60	21.00	0.30	1.93	0.19
344.0	70.13	756.80	3133.20	95.84	2.33	4.21	6.22
345.0	72.17	807.70	3343.90	97.56	2.78	2.90	7.47
346.0	75.24	853.00	3531.60	101.20	3.05	2.82	7.46
347.0	75.53	891.50	3690.90	100.80	3.25	2.79	6.62
348.0	77.34	884.00	3659.90	103.24	3.31	2.91	6.75
349.0	88.69	1000.10	4140.70	116.60	4.37	2.98	5.71
350.0	86.98	997.60	4130.30	114.92	4.10	2.46	7.41
351.0	94.97	1038.20	4298.50	126.16	4.28	2.83	8.76
352.0	85.49	976.20	4041.80	114.04	3.71	3.46	6.75
353.0	92.99	1043.80	4321.60	122.68	4.43	3.04	6.87
354.0	80.92	932.70	3861.40	107.28	3.69	2.70	6.66
355.0	100.69	1166.90	4831.00	131.48	5.20	2.79	6.49
356.0	80.88	909.80	3766.60	109.44	3.03	4.02	7.20
357.0	87.55	938.30	3884.80	120.76	2.55	6.35	7.29
358.0	82.54	942.30	3901.40	109.80	3.68	3.45	5.83
359.0	88.78	992.20	4107.70	117.20	4.23	3.60	5.18
360.0	77.62	922.20	3818.10	102.12	3.75	2.98	4.57
361.0	61.03	686.40	2842.00	83.24	2.11	3.07	6.23
362.0	55.92	644.60	2668.90	76.16	1.98	2.56	6.00
363.0	56.89	665.80	2756.40	76.96	2.16	2.85	4.90
364.0	57.30	679.40	2812.70	77.04	2.29	1.59	6.92
366.0	50.42	563.20	2331.80	69.96	1.36	3.43	5.19
368.0	47.92	560.40	2320.00	65.64	1.57	2.92	4.29
370.0	53.36	645.10	2671.00	72.16	1.99	2.71	4.66
372.0	55.98	631.10	2613.00	76.40	1.91	2.99	5.48
373.0	66.71	683.00	2827.80	90.68	2.38	4.03	5.09
374.0	54.66	627.70	2598.70	74.32	1.93	3.08	4.70
376.0	58.88	652.20	2700.00	80.52	1.96	3.17	5.95
378.0	69.17	777.50	3218.90	93.08	2.77	3.12	5.95
380.0	79.81	974.20	4033.30	104.52	4.05	2.51	4.91
381.0	84.93	1100.00	4554.20	110.56	4.49	2.79	4.10
382.0	100.50	1322.70	5476.40	130.92	5.28	3.54	4.53
383.0	107.43	1419.40	5876.60	140.56	5.50	3.70	5.74
384.0	91.49	1283.60	5314.20	120.28	4.47	4.63	2.93
386.0	49.59	672.00	2782.30	68.92	1.34	3.05	5.77
387.0	51.46	656.40	2717.70	72.40	1.08	4.08	5.62

388.0	50.35	639.70	2648.50	70.04	1.33	3.66	4.87
390.0	36.11	555.20	2298.60	50.16	0.95	3.08	2.58
391.0	45.53	508.00	2103.10	63.24	1.22	3.38	4.17
392.0	47.13	531.30	2199.60	65.00	1.41	2.77	5.07
393.0	48.04	536.20	2220.00	65.96	1.49	3.01	4.51
394.0	54.26	624.70	2586.30	74.00	1.89	2.50	5.94
395.0	60.10	627.80	2599.20	83.20	1.68	3.19	7.70
396.0	59.04	646.70	2677.30	82.96	1.33	1.67	12.08
397.0	51.09	552.10	2285.80	71.84	1.13	2.18	9.08
398.0	53.30	579.30	2398.30	74.24	1.39	1.88	9.24
399.0	51.32	580.90	2405.10	71.48	1.33	2.89	6.77
400.0	50.55	586.80	2429.50	69.40	1.58	2.03	6.97
401.0	56.50	633.00	2620.90	77.60	1.78	3.03	6.22
402.0	65.08	727.00	3009.90	87.44	2.64	2.53	6.24
403.0	52.68	633.80	2624.00	71.44	1.90	2.57	5.12
404.0	47.00	547.00	2264.50	64.40	1.51	2.28	5.50
405.0	52.84	604.40	2502.40	73.16	1.50	2.59	7.11
406.0	69.21	826.70	3422.60	95.76	2.01	1.85	12.20
407.0	67.52	809.90	3353.00	93.68	1.88	1.42	13.06
408.0	64.48	799.30	3309.40	87.72	2.30	2.07	8.59
409.0	65.71	844.10	3494.50	88.00	2.76	2.13	6.70
410.0	70.62	803.80	3327.70	93.80	3.21	2.25	6.11
445.0	165.11	1891.20	7830.00	224.40	5.95	5.21	21.88

**APPENDIX 2: GAMMA RAY DATA SUMMARY STATISTICS**

**Gamma Ray Data K wt. %, U [ppm], and Th [ppm] and API Summary Statistics**

**Tables 8-12: Elko Hills A**

<b>API</b>					
<b>Facies</b>	<b>1/2</b>	<b>3</b>	<b>5</b>	<b>6</b>	<b>10,11,12</b>
Mean	201.85	176.73	146.20	127.66	192.22
Standard Error	7.39	5.61	5.66	9.55	4.53
Median	192.24	169.88	136.20	117.12	191.48
Mode	#N/A	#N/A	#N/A	#N/A	#N/A
Standard Deviation	16.52	16.84	38.83	25.26	20.27
Sample Variance	273.06	283.48	1507.64	638.25	410.76
Kurtosis	0.80	-1.62	-0.96	-1.75	-0.15
Skewness	1.34	0.24	0.39	0.35	0.62
Range	38.00	45.44	131.44	66.00	70.80
Minimum	190.16	153.88	88.68	96.88	165.88
Maximum	228.16	199.32	220.12	162.88	236.68
Count	5	9	47	7	20

<b>Total [ppm]</b>					
<b>Facies</b>	<b>1/2</b>	<b>3</b>	<b>5</b>	<b>6</b>	<b>10,11,12</b>
Mean	1579.54	1362.63	104.72	993.62	1566.23
Standard Error	69.82	37.02	4.12	99.99	26.83
Median	1498.60	1320.00	97.26	874.90	1564.20
Mode	#N/A	#N/A	#N/A	#N/A	#N/A
Standard Deviation	156.13	111.05	28.22	244.92	116.96
Sample Variance	24375.46	12333.09	796.34	59986.42	13679.73
Kurtosis	0.05	-0.59	-0.95	1.29	2.29
Skewness	1.17	0.75	0.41	1.42	0.87
Range	360.50	331.60	95.17	648.90	527.50
Minimum	1460.10	1230.40	63.44	778.90	1357.40
Maximum	1820.60	1562.00	158.61	1427.80	1884.90
Count	5	9	47	7	20

<b>K wt. %</b>					
Facies	1/2	3	5	6	10,11,12
Mean	4.01	2.99	2.59	2.24	3.26
Standard Error	0.57	0.29	0.14	0.23	0.12
Median	4.01	3.03	2.30	2.25	3.14
Mode	#N/A	#N/A	1.49	#N/A	3.21
Standard Deviation	1.28	0.86	0.97	0.61	0.55
Sample Variance	1.63	0.73	0.93	0.38	0.30
Kurtosis	-0.77	-2.00	-0.41	-0.60	1.15
Skewness	0.57	-0.04	0.87	0.63	1.20
Range	3.07	2.07	3.41	1.63	2.14
Minimum	2.77	1.92	1.41	1.63	2.57
Maximum	5.84	3.99	4.82	3.26	4.71
Count	5	9	47	7	20

<b>U [ppm]</b>					
Facies	1/2	3	5	6	10,11,12
Mean	8.23	6.53	6.78	5.54	7.33
Standard Error	0.68	0.39	0.34	0.46	0.30
Median	9.01	6.30	6.23	5.53	7.03
Mode	#N/A	#N/A	#N/A	#N/A	7.02
Standard Deviation	1.52	1.17	2.33	1.22	1.33
Sample Variance	2.31	1.36	5.43	1.49	1.76
Kurtosis	-0.87	-1.84	-0.57	-0.53	1.71
Skewness	-0.92	0.10	0.58	0.49	0.69
Range	3.63	2.95	8.35	3.49	6.08
Minimum	6.00	5.10	3.20	4.02	4.80
Maximum	9.63	8.05	11.55	7.51	10.88
Count	5	9	47	7	20

<b>Th [ppm]</b>					
Facies	1/2	3	5	6	10,11,12
Mean	17.94	19.16	12.61	11.88	20.35
Standard Error	2.22	1.20	0.48	1.06	0.80
Median	15.30	19.76	11.23	11.30	21.24
Mode	#N/A	#N/A	10.25	#N/A	#N/A
Standard Deviation	4.96	3.60	3.28	2.79	3.59
Sample Variance	24.55	12.96	10.75	7.81	12.91
Kurtosis	-2.26	1.16	0.27	-1.89	-0.66
Skewness	0.70	-0.28	0.87	0.38	0.00
Range	11.10	12.82	14.77	6.71	13.10
Minimum	13.48	12.55	7.57	9.19	14.15
Maximum	24.58	25.37	22.34	15.90	27.25
Count	5	9	47	7	20

**Tables 13-17: Elko Hills B**

<b>API</b>					
Facies	1/2	3	5	6	10,11,12
Mean	201.52	188.92	108.39	116.34	207.48
Standard Error	1.91	4.54	4.76	5.76	8.55
Median	201.40	183.00	99.12	120.30	209.80
Mode	#N/A	#N/A	#N/A	#N/A	#N/A
Standard Deviation	4.27	24.44	28.18	16.30	56.03
Sample Variance	18.27	597.12	794.24	265.70	3139.91
Kurtosis	1.20	0.59	1.44	-0.88	0.11
Skewness	1.12	-0.28	1.34	-0.82	-0.47
Range	10.64	111.64	117.16	40.84	210.92
Minimum	197.64	123.52	72.00	90.76	92.96
Maximum	208.28	235.16	189.16	131.60	303.88
Count	5	29	35	8	43

<b>Total [ppm]</b>					
Facies	1/2	3	5	6	10,11,12
Mean	1562.86	1528.90	76.78	899.25	1719.06
Standard Error	20.13	41.00	3.45	45.03	72.31
Median	1565.90	1576.00	70.49	940.55	1696.70
Mode	#N/A	#N/A	#N/A	#N/A	#N/A
Standard Deviation	45.02	220.81	20.12	127.36	474.15
Sample Variance	2026.48	48757.57	405.01	16219.34	224814.58
Kurtosis	1.67	0.07	1.85	-0.26	0.11
Skewness	-0.49	-0.41	1.44	-0.99	-0.40
Range	125.20	979.30	85.70	356.00	1948.30
Minimum	1495.60	954.90	50.78	676.30	697.00
Maximum	1620.80	1934.20	136.48	1032.30	2645.30
Count	5	29	35	8	43

<b>K wt. %</b>					
Facies	1/2	3	5	6	10,11,12
Mean	4.57	3.37	1.80	2.03	3.20
Standard Error	0.26	0.19	0.09	0.16	0.14
Median	4.63	3.09	1.74	2.11	3.23
Mode	#N/A	2.89	2.00	#N/A	3.73
Standard Deviation	0.58	1.02	0.55	0.45	0.92
Sample Variance	0.33	1.04	0.30	0.20	0.84
Kurtosis	-1.34	-0.56	4.36	-0.71	-0.43
Skewness	-0.28	0.65	1.28	-0.71	-0.34
Range	1.44	3.66	2.89	1.21	3.67
Minimum	3.80	1.88	0.94	1.31	1.19
Maximum	5.24	5.54	3.83	2.52	4.86
Count	5	29	35	8	43

<b>U [ppm]</b>					
Facies	1/2	3	5	6	10,11,12
Mean	8.37	9.02	4.82	4.84	10.54
Standard Error	0.48	0.42	0.26	0.28	0.74
Median	7.96	8.13	4.45	4.89	8.87
Mode	#N/A	8.01	3.45	#N/A	#N/A
Standard Deviation	1.07	2.26	1.52	0.80	4.82
Sample Variance	1.15	5.09	2.31	0.64	23.25
Kurtosis	-2.50	1.21	-0.67	-0.04	-0.96
Skewness	0.28	1.37	0.74	-0.20	0.40
Range	2.47	9.16	4.98	2.50	18.27
Minimum	7.15	5.79	3.01	3.48	3.01
Maximum	9.62	14.95	7.99	5.98	21.28
Count	5	29	35	8	43

<b>Th [ppm]</b>					
Facies	1/2	3	5	6	10,11,12
Mean	15.38	15.71	10.25	11.29	17.98
Standard Error	0.23	0.96	0.47	0.64	0.71
Median	15.39	15.69	9.57	11.70	18.36
Mode	#N/A	#N/A	#N/A	#N/A	#N/A
Standard Deviation	0.52	5.15	2.80	1.82	4.63
Sample Variance	0.27	26.51	7.85	3.33	21.43
Kurtosis	1.45	-0.37	2.13	-1.04	-0.33
Skewness	-0.58	0.13	1.29	-0.29	-0.32
Range	1.44	18.12	12.64	5.14	19.01
Minimum	14.59	7.13	6.49	8.71	8.29
Maximum	16.03	25.25	19.13	13.85	27.30
Count	5	29	35	8	43

**Tables 18-22: Coal Mine Canyon**

API								
Facies	1/2	3	4	5	6	8/13	10,11,12	14
Mean	125.95	117.61	66.07	101.76	70.36	96.86	167.05	72.40
Standard Error	2.98	4.57	1.83	2.76	1.66	8.42	11.95	2.48
Median	120.84	116.72	67.72	102.40	67.50	94.36	161.06	69.92
Mode	149.00	#N/A	60.80	#N/A	57.68	#N/A	#N/A	#N/A
Standard Deviation	27.45	35.71	15.67	27.86	12.85	22.29	33.81	9.59
Sample Variance	753.32	1275.03	245.50	776.17	165.15	496.86	1143.03	92.01
Kurtosis	1.70	2.49	0.89	0.10	-0.78	-0.15	-1.67	1.53
Skewness	1.17	1.08	0.36	0.54	0.27	0.88	0.28	1.09
Range	140.72	182.76	77.72	124.04	57.48	60.68	88.44	36.56
Minimum	71.12	64.56	34.28	54.16	45.92	74.32	125.48	59.76
Maximum	211.84	247.32	112.00	178.20	103.40	135.00	213.92	96.32
Count	85	61	73	102	60	7	8	15

Total [ppm]								
Facies	1/2	3	4	5	6	8/13	10,11,12	14
Mean	87.84	82.00	480.29	715.90	48.07	65.96	116.36	51.25
Standard Error	2.06	3.13	17.44	15.70	1.10	5.68	8.65	1.72
Median	84.45	82.25	443.10	704.35	46.77	64.82	118.82	50.07
Mode	94.09	96.03	330.80	826.90	#N/A	#N/A	#N/A	#N/A
Standard Deviation	19.02	24.47	148.97	158.55	8.42	15.03	22.87	6.68
Sample Variance	361.91	598.95	22191.80	25138.98	70.87	225.91	523.25	44.60
Kurtosis	1.66	2.29	-1.00	-0.23	-1.17	-0.15	-1.63	1.24
Skewness	1.12	1.03	0.49	0.41	0.12	0.83	-0.03	0.97
Range	97.67	124.80	561.70	733.60	30.53	41.20	60.04	25.23
Minimum	49.44	44.73	242.20	415.70	31.82	50.37	85.10	42.30
Maximum	147.11	169.53	803.90	1149.30	62.35	91.57	145.14	67.53
Count	85	61	73	102	60	7	8	15

K wt. %								
Facies	1/2	3	4	5	6	8/13	10,11,12	14
Mean	1.18	1.07	0.17	0.36	0.35	0.14	0.00	0.99
Standard Error	0.04	0.10	0.02	0.04	0.03	0.09	0.00	0.07
Median	1.23	1.25	0.00	0.22	0.32	0.00	0.00	1.01
Mode	1.40	0.00	0.00	0.00	0.28	0.00	0.00	0.79
Standard Deviation	0.36	0.79	0.19	0.42	0.19	0.25	0.00	0.28
Sample Variance	0.13	0.62	0.04	0.18	0.04	0.06	0.00	0.08
Kurtosis	-0.91	-1.56	-0.94	-0.09	-0.60	-0.32	#N/A	-0.89
Skewness	-0.11	-0.26	0.63	0.99	0.15	1.31	#N/A	0.03
Range	1.51	2.16	0.65	1.44	0.79	0.56	0.00	0.94
Minimum	0.45	0.00	0.00	0.00	0.00	0.00	0.00	0.51
Maximum	1.96	2.16	0.65	1.44	0.79	0.56	0.00	1.45
Count	85	61	73	102	60	7	8	15

U								
Facies	1/2	3	4	5	6	8/13	10,11,12	14
Mean	7.11	7.96	6.15	8.56	5.97	9.36	17.42	4.72
Standard Error	0.30	0.48	0.25	0.41	0.17	1.21	1.41	0.34
Median	6.33	6.34	5.90	7.66	5.88	7.71	16.49	4.24
Mode	6.29	5.33	7.39	4.50	7.63	#N/A	#N/A	#N/A
Standard Deviation	2.75	3.78	2.11	4.10	1.30	3.20	4.00	1.30
Sample Variance	7.54	14.29	4.44	16.78	1.68	10.25	15.99	1.70
Kurtosis	3.77	-0.75	-0.58	-0.55	-0.85	-0.28	-0.45	0.74
Skewness	1.84	0.78	0.29	0.55	0.31	1.20	0.80	1.25
Range	13.75	12.90	9.04	16.56	5.14	8.05	11.00	4.13
Minimum	3.00	3.10	2.21	2.33	3.46	6.78	13.42	3.36
Maximum	16.75	16.00	11.25	18.89	8.60	14.83	24.42	7.49
Count	85	61	73	102	60	7	8	15

Th								
Facies	1/2	3	4	5	6	8/13	10,11,12	14
Mean	12.57	9.21	3.55	6.89	4.26	4.93	6.93	4.70
Standard Error	0.22	0.64	0.17	0.29	0.22	0.61	1.51	0.25
Median	12.41	7.91	3.12	6.16	4.02	4.30	5.79	4.54
Mode	11.97	6.83	3.12	6.16	3.80	#N/A	#N/A	#N/A
Standard Deviation	2.03	4.96	1.42	2.93	1.67	1.61	4.27	0.96
Sample Variance	4.11	24.60	2.01	8.60	2.78	2.58	18.20	0.93
Kurtosis	1.16	3.93	-0.19	0.38	30.33	-0.84	-0.44	-0.63
Skewness	0.82	1.57	0.79	1.04	4.73	0.66	0.83	0.30
Range	10.71	26.04	6.00	12.69	12.70	4.37	12.16	3.28
Minimum	8.52	3.21	1.29	2.73	2.37	3.16	2.07	3.37
Maximum	19.23	29.25	7.29	15.42	15.07	7.53	14.23	6.65
Count	85	61	73	102	60	7	8	15

**Tables 23-27: Tomera Ranch**

API						
Facies	3	4	5	6	8/13	10,11,12
Mean	141.91	80.90	159.05	150.73	93.85	143.38
Standard Error	7.08	3.76	9.45	22.09	7.05	5.16
Median	127.74	76.68	137.68	127.54	96.90	148.36
Mode	#N/A	#N/A	144.20	#N/A	#N/A	#N/A
Standard Deviation	49.08	36.05	97.26	93.73	37.29	41.62
Sample Variance	2408.78	1299.76	9459.68	8785.15	1390.39	1732.59
Kurtosis	2.46	-0.22	7.35	-0.17	0.37	3.22
Skewness	1.51	0.21	2.52	0.75	0.00	1.23
Range	222.36	165.64	569.12	331.32	157.88	225.00
Minimum	77.20	17.28	37.76	33.04	24.72	79.52
Maximum	299.56	182.92	606.88	364.36	182.60	304.52
Count	48	92	106	18	28	65

Total [ppm]						
Facies	3	4	5	6	8/13	10,11,12
Mean	101.24	782.36	1272.05	109.92	66.51	102.39
Standard Error	4.88	21.87	62.68	15.70	5.00	3.62
Median	90.76	698.40	1099.85	95.27	68.17	104.16
Mode	#N/A	#N/A	#N/A	#N/A	#N/A	#N/A
Standard Deviation	33.83	208.65	645.31	64.72	26.44	28.96
Sample Variance	1144.31	43535.27	416421.27	4188.21	698.92	838.74
Kurtosis	2.00	0.52	7.65	-0.31	0.27	3.42
Skewness	1.38	1.01	2.60	0.62	0.00	1.30
Range	152.65	911.40	3813.30	227.96	109.88	158.12
Minimum	54.91	508.00	454.20	23.41	17.33	56.20
Maximum	207.56	1419.40	4267.50	251.37	127.21	214.32
Count	48	92	106	18	28	65

<b>K wt. %</b>						
Facies	3	4	5	6	8/13	10,11,12
Mean	2.29	1.86	2.28	1.81	1.31	2.51
Standard Error	0.12	0.13	0.10	0.20	0.15	0.10
Median	2.04	1.56	2.13	1.88	1.10	2.53
Mode	3.24	0.28	1.68	0.50	1.32	2.76
Standard Deviation	0.81	1.21	1.02	0.86	0.81	0.80
Sample Variance	0.66	1.45	1.03	0.73	0.66	0.63
Kurtosis	1.12	1.15	1.70	-0.39	3.44	5.31
Skewness	1.14	1.18	1.15	-0.24	1.74	1.33
Range	3.77	5.36	5.60	2.96	3.73	5.30
Minimum	1.05	0.14	0.57	0.46	0.24	0.65
Maximum	4.82	5.50	6.17	3.42	3.97	5.95
Count	48	92	106	18	28	65

<b>U</b>						
Facies	3	4	5	6	8/13	10,11,12
Mean	9.38	3.62	11.95	12.65	6.73	6.64
Standard Error	0.94	0.24	1.14	2.49	0.58	0.57
Median	7.46	2.87	8.00	9.19	6.33	5.81
Mode	7.67	2.57	#N/A	#N/A	#N/A	6.79
Standard Deviation	6.51	2.29	11.74	10.58	3.05	4.61
Sample Variance	42.33	5.24	137.77	111.98	9.31	21.21
Kurtosis	4.43	4.92	8.38	0.71	2.36	8.97
Skewness	2.13	2.18	2.81	1.16	1.18	2.76
Range	28.20	12.10	64.31	36.57	13.72	26.07
Minimum	3.33	1.47	2.83	2.73	2.61	1.42
Maximum	31.53	13.57	67.14	39.30	16.33	27.49
Count	48	92	106	18	28	65

Th						
Facies	3	4	5	6	8/13	10,11,12
Mean	7.57	5.56	6.76	5.15	4.77	12.53
Standard Error	0.50	0.33	0.28	0.53	0.48	0.66
Median	6.52	5.77	6.63	5.20	4.88	14.21
Mode	7.29	6.99	6.00	#N/A	4.09	16.10
Standard Deviation	3.47	3.12	2.84	2.26	2.53	5.36
Sample Variance	12.01	9.72	8.07	5.13	6.40	28.71
Kurtosis	0.66	2.06	2.77	-0.59	0.09	-0.61
Skewness	1.20	0.64	0.92	-0.27	-0.40	0.24
Range	13.22	17.18	15.49	8.20	9.66	22.29
Minimum	3.24	0.13	0.00	0.96	0.00	4.63
Maximum	16.46	17.31	15.49	9.16	9.66	26.92
Count	48	92	106	18	28	65

## APPENDIX 3: GAMMA RAY MEASUREMENT ACCURACY EXPERIMENTS

**Table 28: Control room**

	30 sec					1 min					2 min					3 min					5 min				
	Total	K	U	Th	API	Total	K	U	Th	API	Total	K	U	Th	API	Total	K	U	Th	API	Total	K	U	Th	API
1	1050	2.9	4.68	11.24	128.8	946.4	2.39	5.12	9.51	117.24	982.9	2.35	4.8	12.12	124.48	931.8	2.45	3.97	10.73	113.88	896.3	2.21	3.93	10.49	108.76
2	1071.1	2.9	4	15.16	139.04	945.5	2.42	5.07	11.16	123.92	965.9	2.27	4.8	10.16	115.36	922.1	2.32	3.45	11.39	110.28	892.5	2.29	3.53	10.28	106
3	1153.2	2.84	4.77	13.78	138.72	943.7	2.33	3.15	11.09	106.84	961.4	2.53	4.74	9.92	118.08	913.1	2.34	3.33	11.45	109.88	909.2	2.35	3.91	10.37	110.36
4	1103.1	3.37	4.62	13.43	144.6	928.8	2.33	4.3	11.17	116.36	946.5	2.47	5.13	10.32	121.84	917.7	2.32	3.11	12.25	111	910.5	2.33	3.99	10.46	111.04
5	1083.6	3.09	3.71	10.58	121.44	929.9	2.26	3.98	11.62	114.48	961.4	2.35	4.65	9.53	112.92	912	2.28	3.75	10.85	109.88	907	2.33	3.91	9.81	107.8
6	1104.6	3	4.89	10.93	130.84	935.4	2.05	5.03	10.49	115	970.9	2.52	4.49	11.3	121.44	895.8	2.31	3.99	10.08	109.2	911.3	2.3	4	10.26	109.84
7	1077	2.82	5.99	10.29	134.2	937.5	2.37	4.36	10.14	113.36	965.3	2.49	4.72	11.53	123.72	898.5	2.23	4.52	10.83	115.16	887.1	2.24	3.73	9.24	102.64
8	1101.1	3.6	2.31	11.7	122.88	950.6	2.44	3.81	10.84	112.88	977.1	2.52	3.99	10.36	113.68	899.5	2.13	3.92	10.39	107	929.5	2.35	3.98	10.56	111.68
9	1071.6	3.08	1.94	15.18	125.52	936.2	2.34	3.06	11.49	107.88	977.7	2.45	5.05	11.1	124	915.8	2.24	3.92	10.32	108.48	917.5	2.37	3.52	10.22	106.96
10	1077.1	2.73	4.09	12.64	126.96	907.1	2.4	4.29	11.15	117.32	992.3	2.49	4.53	11.11	120.52	919.1	2.26	3.95	8.95	103.56	930.4	2.33	4.08	10.83	113.24
11	1098.1	2.65	5.64	14.2	144.32	918.6	2.08	4.61	11.69	116.92	971.6	2.37	4.59	11.83	121.96	910.3	2.3	3.33	10.86	106.88	932.2	2.21	4.14	10.77	111.56
12	1055	3.12	5.38	10.07	133.24	919.9	2.17	5.24	12.34	126	949.7	2.17	4.78	11.39	118.52	918.6	2.36	2.76	11.66	106.48	930.3	2.39	4.21	10.46	113.76
13	1087.1	3.31	3.55	14.12	137.84	906	2.33	4.34	9.89	111.56	938.1	2.25	4.22	11.08	114.08	915.5	2.28	3.35	10.78	106.4	921.5	2.4	4.21	10.62	114.56
14	1120.6	2.72	5.22	13.23	138.2	933.5	2.22	4.95	8.93	110.84	934.3	1.94	4.77	10.68	111.92	921.5	2.13	3.1	10.34	100.24	919.4	2.33	4.19	10.81	114.04
15	1047.5	2.88	3.89	15.69	139.96	924.1	2.33	3.13	10.46	104.16	956.6	2.37	5.14	10.34	120.4	922	2.18	4.28	9.83	108.44	905.4	2.43	3.04	10.89	106.76
16	1104.6	2.88	5.48	12.65	140.52	917.9	2.38	3.21	9.67	102.44	964.5	2.31	4.1	11.21	114.6	908.2	2.2	3.12	10.07	100.44	873.7	2.25	3.33	10.78	105.76
17	1073	2.93	1.66	12.2	108.96	931.2	2.32	3.12	11.23	107	963	2.29	4.21	13.3	123.52	924.5	2.02	3.94	10.75	106.84	904.5	2.26	4.87	9.07	111.4
18	1082.1	2.95	6.49	12.99	151.08	916.9	2.24	4.87	8.94	110.56	957.9	2.37	4.08	10.37	112.04	947.8	2.29	4.39	10.41	113.4	908.2	2.24	4.02	10.86	111.44
19	1084.5	3.04	3.34	15.23	136.28	956.5	2.57	3.88	11.18	116.88	942.4	2.34	4.18	10.01	110.92	945.9	2.39	4.35	10.82	116.32	907.8	2.37	3.91	9.57	107.48
20	1127.7	2.94	8.02	10.21	152.04	944.5	2.42	3.6	11.13	112.04	934.1	2.24	4.42	10.48	113.12	923.4	2.23	4.88	10.98	118.64	895.2	2.29	3.49	10.34	105.92
21	1069.6	2.94	3.65	11.64	122.8	904.9	2.34	3.84	11.11	112.6	947	2.38	3.38	11.81	112.36	946.2	2.3	4.17	11.71	117	906.5	2.28	3.62	11.39	111
22	1097	3.2	5.37	10.05	134.36	903.6	2.19	5.35	8.8	113.04	947.2	2.3	4.32	10.93	115.08	944.3	2.38	3.56	10.98	110.48	899.3	2.26	4.67	10.17	114.2
23	1093.5	2.82	4.88	14.02	140.24	935.4	2.21	4.42	8.51	104.76	947	2.36	3.47	11.04	109.68	948.5	2.4	4.4	10.81	116.84	892.2	2.33	3.27	10.64	106
24	1097.6	3.04	5.28	9.85	130.28	943	2.32	4.66	10.61	116.84	944.4	2.23	4.13	10.97	112.6	940.9	2.37	4.02	11.51	116.12	866	2.13	3.41	10.05	101.56
25	1072	2.85	5.48	12.65	140.04	925.7	2.11	3.88	9.63	103.32	974.4	2.23	4.37	10.74	113.6	964.9	2.46	3.94	10.23	111.8	847.5	2.25	3.16	9.5	99.28
26	1081.6	2.5	7.08	11.22	141.52	959.1	2.5	3.97	10.42	113.44	949.9	2.25	4.29	9.99	110.28	928.2	2.33	3.99	11.05	113.4	888.7	2.3	3.53	10.05	105.24
27	1081.6	3.03	3.73	14.15	134.92	917.2	2.03	6.06	9.32	118.24	961.5	2.28	4.58	10.45	114.92	935.3	2.35	3.94	11.14	113.68	891.5	2.3	3.72	11.19	111.32
28	1083.1	3.13	4.86	13.2	141.76	939.8	2.52	3.4	10.89	111.08	939.8	2.34	3.42	12.39	114.36	926.3	2.21	4.37	9.58	108.64	887.5	2.34	3.08	10.98	106
29	1095.6	3.35	3.19	11.37	124.6	928.9	2.37	3.57	11.66	113.12	930.5	2.44	3.54	11.78	114.48	941.1	2.39	3.61	11.1	111.52	896.8	2.31	3.71	10.22	107.52
30	1000.9	2.72	4.87	10.49	124.44	959.7	2.52	4.49	12.37	125.72	926.3	2.34	3.87	11.37	113.88	911.2	2.08	4.19	11.12	111.28	884.6	2.22	3.15	9.46	98.56
31	1072	3.22	4.1	13.04	136.48	927.2	2.34	4.89	8.02	108.64	931.6	2.2	4.44	11.69	117.48	936.7	2.41	4.5	9.86	114	885.5	2.22	3.95	9.75	106.12
32	1087	3.12	3.67	13.63	133.8	918.7	2.31	4.42	10.27	113.4	919.7	2.35	3.41	12.58	115.2	924.5	2.39	3.71	12.23	116.84	908.5	2.36	3.63	11.02	110.88
33	1056	3	4.73	10.95	129.64	937.2	2.4	4.45	12.28	123.12	955	2.36	4.3	10.98	116.08	917.5	2.35	3.58	10.18	106.96	893.9	2.3	3.27	10.6	105.36
34	1083.1	2.99	0.73	18.69	128.44	919.1	2.47	3.28	10.28	105.84	933.3	2.28	4.69	10.11	114.44	937.1	2.57	3.8	10.35	112.92	904.2	2.36	3.6	10.59	108.92
35	1108.6	3.06	4.25	15.34	144.32	962	2.18	5.32	12.32	126.72	940.2	2.4	3.96	10.39	111.64	918.9	2.44	3.93	11.3	115.68	901.2	2.29	2.87	10.82	102.88
36	1098.1	3.12	3.22	16.5	141.68	908.1	1.96	4.3	11.76	112.8	938.5	2.38	4	9.81	109.32	921.2	2.31	4.55	11.27	118.44	932.7	2.27	4.28	10.35	111.96
37	1050.5	3.06	2.65	14.82	129.44	921.4	2.24	4.74	10.62	116.24	925.6	2.31	4.91	9.82	115.52	915.4	2.16	3.83	10.82	108.48	915.2	2.37	4.38	9.78	112.08
38	1068.6	3.1	2.53	15.34	131.2	915.8	2.14	3.36	10.66	103.76	773.4	1.94	3.16	8.12	88.8	917.5	2.36	4.3	9.86	111.6	942.4	2.52	3.75	11.63	116.84
39	1074.6	2.99	2.55	13.83	123.56	917.3	2.24	4.59	9.87	112.04	930	2.26	4.06	10.72	111.52	913.5	2.31	3.78	10.45	109	943.8	2.39	3.77	11.68	115.12
40	1068.6	2.9	7.23	9.58	142.56	907.1	2.3	4.77	9.71	113.8	949.6	2.35	4.55	11.45	119.8	956	2.5	4.03	10.88	115.76	909.4	2.31	3.36	10.97	107.72
41	1049	2.8	4.96	11.47	130.36	950	2.41	4.44	10.5	116.08	950.2	2.44	4.81	10.18	118.24	934.8	2.45	3.13	11.24	109.2	902.5	2.33	3.77	10.54	109.6
42	1049.5	2.65	7.22	11.93	147.88	938.2	2.16	5.27	12.21	125.56	924.4	2.41	3.42	11.42	111.6	954.2	2.45	4.09	10.7	114.72	891.1	2.29	3.77	10.04	106.96
43	1060.5	3.1	2.55	13.04	122.16	919.7	2.23	5.29	9.52	116.08	949.1	2.35	4.63	9.47	112.52	948.2	2.43	3.71	10.1	108.96	895.3	2.39	3.85	10.03	109.16
44	1077.6	2.8	5.37	13.19	140.52	932	2.41	4.39	9.23	110.6	938	2.35	2.91	11.83	108.2	954.1	2.44	4.67	10.38	117.92	890.1	2.31	3.38	10.1	104.4
45	1089	2.86	3.9	14.93	136.68	930.2	2.28	4.12	10.78	112.56	905.6	2.26	4.78	8.64	108.96	943.8	2.37	4.06	11.46	116.24	898.5	2.37	3.97	9.18	106.4
46	1069	2.97	3.63	13.93	132.28	916.2	2.16	3.21	8.7	95.04	916.6	2.38	3.64	9.48	105.12	921	2.22	4.77	9.43	111.4	932.5	2.41	3.66	10.49	109.8
47	1067.1	3.2	2.04	15.39	129.08	911.4	2.32	4.05	9.43	107.24	928.1	2.22	3.7	9.51	103.16	965.7	2.43	4.46	11.72	121.44	920.3	2.35	3.71	10.78	110.4
48	1107.1	2.99	3.6	11.13	121.16	915.4	2.44	2.98	10.33	104.2	918.8	2.11													

**Table 29: Granite**

	30 sec					1 min					2 min					3 min					5 min				
	Total	K	U	Th	API	Total	K	U	Th	API	Total	K	U	Th	API	Total	K	U	Th	API	Total	K	U	Th	API
1	1028.9	3.94	4.09	8.3	128.96	1180.3	4.22	5.85	10.52	156.4	1096.5	2.81	2.39	9.26	101.12	1223.8	4.62	3.94	11.07	149.72	1180.5	4.48	3.98	11.62	150
2	955.4	3.66	3.18	9.77	123.08	1161.8	4.37	3.97	8.61	136.12	1166.6	4.3	3.73	10.7	141.44	1213.9	4.63	3.77	11.73	151.16	1174	4.46	3.88	11.44	148.16
3	1027.9	3.99	3.48	9.65	130.28	1182.6	4.55	4.56	10.52	151.36	1168	4.8	2.24	10.63	137.24	1218.8	4.72	3.43	12.78	154.08	1180.8	4.41	3.9	10.5	143.76
4	993.4	3.86	3.19	7.44	117.04	1182.1	4.5	4.52	9.26	145.2	1176.6	4.55	3.52	12.08	149.28	1239.9	4.73	3.7	11.89	152.84	1176.4	4.37	4.04	11.31	147.48
5	964.4	3.62	2.49	4.29	95	1155.3	4.26	4.54	9.69	143.24	1139.7	4.48	3.25	10.86	141.12	1218	4.64	3.93	12.47	155.56	1159.2	4.25	3.92	10.54	141.52
6	966.9	3.64	2.69	10.62	122.24	1151.8	4.32	3.52	11.88	144.8	1151.6	4.45	4.65	10.53	150.52	1239.4	4.75	4.21	11.09	154.04	1162	4.54	3.27	11.23	143.72
7	989.4	3.94	2.4	10.34	123.6	1155	4.4	2.43	12.53	139.96	1154.2	4.47	2.9	11.75	141.72	1231.7	4.45	5.03	11.78	158.56	1154.1	4.4	3.61	10.29	140.44
8	967.8	3.36	2.79	8.12	108.56	1158.1	4.34	4	8.87	136.92	1149.2	4.26	3.49	12.21	144.92	1223.4	4.56	3.68	13.54	156.56	1167.7	4.55	3.24	11.82	146
9	998.4	3.63	4.67	6.5	121.44	1161.8	4.39	4.4	9.18	142.16	1155.5	4.38	4.28	10.86	147.76	1231.4	4.83	4.19	11.75	157.8	1144	4.45	3.27	10.26	138.4
10	985.4	3.45	3.21	9.05	117.08	1106	4.14	3.68	10.49	137.64	1154.3	4.29	4.47	12.38	153.92	1224	4.57	4.09	12.46	155.68	1146.8	4.56	3.82	10.02	143.6
11	938.3	3.61	2.33	9.4	114	1148.3	4.26	4.59	9.43	142.6	1159.3	4.32	4.06	11.92	149.28	1230.1	4.62	3.78	12.07	152.44	1141.7	4.31	3.83	10.21	140.44
12	957.9	3.33	2.06	11.54	115.92	1189.1	4.31	2.65	12.65	140.76	1145.4	4.28	3.9	11.19	144.44	1207.5	4.54	4.22	11.89	153.96	1166	4.61	3.89	11.45	150.68
13	967.9	3.68	1.46	9.78	109.68	1156.3	4.39	3.01	11.3	139.52	1167.4	4.39	3.64	11.65	145.96	1217.6	4.7	3.46	11.68	149.6	1175.4	4.54	4.5	11.33	153.96
14	952.9	3.48	3.16	8.54	115.12	1179.9	4.14	4.59	13.53	157.08	1147.1	4.42	3.86	10.02	141.68	1219	4.51	4.56	12.87	160.12	1154.4	4.49	3.16	10.62	139.6
15	1024.5	3.74	3.83	8.89	126.04	1165.1	4.38	3.25	10.88	139.6	1142.4	4.59	3.13	10.41	140.12	1190.4	4.59	3.77	11.4	149.2	1149.8	4.41	3.81	10.82	144.32
16	949.2	3.51	4.35	6.57	117.24	1162.3	4.48	3.85	9.5	140.48	1163.1	4.49	3.16	11.26	142.16	1186.6	4.64	3.23	11.94	147.84	1182.5	4.61	4.28	10.99	151.96
17	974.4	3.72	1.62	9.74	111.44	1153.5	4.21	3.06	12.99	143.8	1185.2	4.59	2.96	10.17	137.8	1192.2	4.86	3.38	11.36	150.24	1182.1	4.69	3.54	11.06	147.6
18	932.8	3.4	3.26	9.56	118.72	1157.6	4.47	3.09	13.05	148.44	1153	4.48	3.97	11.52	149.52	1182.1	4.69	4.21	10.25	149.72	1161.8	4.47	3.44	11.55	145.24
19	954.4	3.6	3.33	6.2	109.04	1148.6	4.29	4.03	8.75	135.88	1127.8	4.48	3.32	11.43	143.96	1181.6	4.57	4.45	10.28	149.84	1166.1	4.45	4.16	9.46	142.32
20	908.7	3.27	2.36	9.47	109.08	1147.8	4.36	4.68	10.41	148.84	1167.4	4.58	3.49	11.51	147.24	1184.7	4.54	4.22	10.41	148.04	1172.6	4.63	3.63	10.83	146.44
21	979.3	3.33	3.69	9.77	121.88	1139.5	4.11	4.06	10.18	138.96	1172.5	4.62	3.74	11.97	151.72	1178	4.47	4.87	10.96	154.32	1158.4	4.53	4.18	10.49	147.88
22	955.3	3.31	3.71	8.24	115.6	1174.9	4.54	3.94	10.49	146.12	1153.4	4.62	3.48	10.03	141.88	1208.3	4.71	3.48	12.44	152.96	1166	4.57	4.16	11.44	150.88
23	945.3	3.59	2.58	6.06	102.32	1127.5	4.21	4.51	10.6	145.84	1159	4.29	3.51	10.49	138.68	1214.8	4.7	5.04	10.76	158.56	1170.1	4.62	3.37	11.1	145.28
24	986.4	3.63	2.65	9.35	116.68	1157	4.24	4.93	11.17	151.96	1159.8	4.43	4.15	11.06	148.32	1207.6	4.6	3.9	11.76	151.84	1164.7	4.41	4.21	10.13	144.76
25	1207.4	4.29	3.39	11.39	141.32	1159.3	4.5	4.11	13.4	158.48	1151.3	4.39	2.9	11.06	137.68	1223.6	4.65	3.63	12.64	154	1174.4	4.47	4.19	10.27	146.12
26	1190.9	4.2	2.71	15.33	150.2	1144.8	4.4	3.04	10.02	134.8	1124.9	4.53	3.76	11.35	147.96	1221.6	4.74	3.89	13.56	161.2	1164.9	4.54	3.64	11.1	146.16
27	1224.4	4.48	6.31	7.85	153.56	1166.1	4.35	4.54	11.46	151.76	1160.3	4.69	3.09	11.67	146.44	1215	4.74	2.98	12.34	149.04	1171.4	4.44	3.83	11.3	146.88
28	1187.8	4.59	3.33	9.29	137.24	1169.8	4.23	3.89	12.73	149.72	1171.6	4.77	3.6	10.87	148.6	1207	4.7	3.87	11.36	151.6	1169.4	4.55	3.19	11.75	145.32
29	1139.1	4.19	3.68	10.09	136.84	1147.6	4.14	4	10.82	141.52	1165.2	4.5	4.21	11.29	150.84	1209.3	4.57	4.01	11.5	151.2	1178.5	4.54	3.8	10.75	146.04
30	909.1	3.19	5.03	6.54	117.44	1188.6	4.92	4.45	10.84	157.68	1165.4	4.51	3.22	11.5	143.92	1201.5	4.77	4.12	11.6	155.68	1169.4	4.52	3.74	11.04	146.4
31	935.7	3.36	3.12	8.07	111	1161.3	4.49	3.81	10.77	145.4	1153.9	4.49	3.44	11.21	144.2	1225.9	4.77	4.25	9.67	149	1173.9	4.6	3.47	11.72	148.24
32	953.2	3.39	3.39	7.51	111.4	1201.2	4.46	3.45	11.73	145.88	1136.3	4.42	3.26	10.11	137.24	1213.7	4.68	3.6	11.02	147.76	1177.5	4.56	4.39	9.81	147.32
33	972.7	3.57	3.79	9.19	124.2	1186.4	4.45	4.69	11.8	155.92	1162.1	4.53	4.17	9.44	143.6	1207.4	4.6	3.95	11.67	151.88	1177.6	4.53	3.53	11.4	146.32
34	908	3.54	2.27	10.44	116.56	1175.3	4.46	4.41	13.36	160.08	1169.3	4.7	3.39	9.71	141.16	1199	4.68	4.06	10.74	150.32	1172.6	4.33	3.62	12.19	147
35	927.7	4.01	2.9	7.95	119.16	1202.9	4.54	5.17	11.7	160.8	1154.4	4.35	4.41	9.51	142.92	1205.2	4.64	4.29	10.89	152.12	1185.5	4.7	4.34	10.37	151.4
36	903.6	3.27	4	6.17	109	1156.3	4.72	3.15	10.44	142.48	1169.4	4.58	3.59	11.05	146.2	1211	4.82	3.43	10.68	147.28	1180.4	4.49	4.05	10.89	147.8
37	930.7	3.65	3.38	6.69	112.2	1199.6	4.58	5.16	9.15	151.16	1187	4.7	3.44	10.91	146.36	1214.2	4.75	4.59	10.65	155.32	1171.9	4.54	3.67	10.77	145.08
38	928.1	3.86	3.76	9.89	131.4	1168.8	4.35	4.01	11.03	145.8	1186.3	4.5	3.32	11.61	145	1206.5	4.55	3.23	13.95	154.44	1156.7	4.32	3.46	11.43	142.52
39	922.2	3.44	2.73	8.36	110.32	1173.8	4.45	4.24	10.59	147.48	1178.9	4.61	4.65	10.24	151.92	1206.2	4.62	2.63	12.8	146.16	1187.9	4.53	3.02	11.32	141.92
40	908.6	3.77	3.58	7.14	117.52	1174.1	4.75	4.28	10.26	151.28	1180.5	4.51	4.43	11.7	154.4	1194.8	4.55	2.98	11.57	142.92	1166.7	4.27	3.35	11.18	139.84
41	930.7	3.83	2.12	7.35	107.64	1178.8	4.65	4.55	7.95	142.6	1185.8	4.62	3.99	10.4	147.44	1211.5	4.66	3.6	11.79	150.52	1186.2	4.66	4.1	10.95	151.16
42	947.2	3.49	3.31	9.28	119.44	1179.3	4.33	4.94	9.62	147.28	1158.3	4.44	4.72	11.48	154.72	1218.9	4.96	4.3	10.84	157.12	1184.8	4.58	3.56	10.9	145.36
43	913.6	3.18	4.87	5.8	113.04	1192.1	4.7	2.89	10.3	139.52	1172	4.45	4.68	10.59	151	1215.5	4.84	3.37	12.89	155.96	1171.6	4.51	3.21	11.83	145.16
44	921.1	3.5	3.08	5.24	101.6	1152.8	4.19	4.64	11.1	148.56	1160.8	4.5	3.66	11.31	146.52	1214.9	4.86	3.12	11.74	149.68	1176.8	4.43	4.09	10.37	145.08
45	922.7	3.64	2.35	7.1	105.44	1191.1	4.77	3.85	10.07	147.4	1168.7	4.4	3.75	10.74	143.36	1206.9	4.76	4.05	11.19	153.32	1175.7	4.41	3.91	10.65	144.44
46	985.3	3.27	3.26	10.35	119.8	1194.1	4.76	2.05	12.25	141.56	1179	4.5	3.79	11.61	148.76	1213.9	4.75	3.26	11.36	147.52	1169.5	4.44	3.8	12.17	150.12
47	937.2	3.44	2.57	8.39	109.16	1177.8	4.47	2.38	14.18	147.28	1196	4.45	3.27	12.4	146.96	1218.2	4.91	3.43	11.59	152.36	1195.5	4.6	3.89	10.69	147.48
48	904.6	3.34	2.26	7.69</																					

**Table 30: Core; 190'**

	30 sec					1 min					2 min					3 min					5 min				
	Total	K	U	Th	API	Total	K	U	Th	API	Total	K	U	Th	API	Total	K	U	Th	API	Total	K	U	Th	API
1	1050	2.9	4.68	11.24	128.8	1071.6	3	4.58	13.53	138.76	1077.4	3	3.82	10.85	121.96	1090.7	2.95	4.27	14.02	137.44	1113	2.91	5.08	13	139.2
2	1071.1	2.9	4	15.16	139.04	1113	2.83	4.28	15.01	139.56	1087.1	3.04	3.77	13.27	131.88	1069.7	2.93	4.24	12.59	131.16	1073.6	2.9	4.19	13.8	135.12
3	1153.2	2.84	4.77	13.78	138.72	1062.1	2.71	5.85	12.13	138.68	1084.7	2.94	4.02	12.68	129.92	1088.6	2.97	4.81	13.21	138.84	1076.6	2.9	4.16	13.7	134.48
4	1103.1	3.37	4.62	13.43	144.6	1092.4	2.94	4.99	12.33	136.28	1051.6	3.08	4.21	11.34	128.32	1070.5	3.09	3.18	13.09	127.24	1091.2	2.91	4.52	12.34	132.08
5	1083.6	3.09	3.71	10.58	121.44	1097.2	3.08	4.77	12.59	137.8	1089.5	2.96	4.42	12.29	131.88	1068.4	2.87	4.63	13.6	137.36	1070.5	2.85	3.72	13.9	130.96
6	1104.6	3	4.89	10.93	130.84	1109.2	3.26	4.25	11.23	131.08	1083.6	3.13	3.28	12.75	127.32	1080.5	2.95	4.6	12.86	135.44	1075.8	2.83	3.93	12.3	125.92
7	1077	2.82	5.99	10.29	134.2	1088.9	3.3	3.82	13.58	137.68	1079.7	3.08	3.77	12.69	130.2	1067.8	3.01	4.28	12.48	132.32	1067.6	2.72	3.71	12.18	121.92
8	1101.1	3.6	2.31	11.7	122.88	1083.2	3.25	4.97	11.89	139.32	1066.6	2.93	4.16	12.98	132.08	1076.9	2.98	3.94	13.85	134.6	1068.7	2.66	3.25	13.56	122.8
9	1071.6	3.08	1.94	15.18	125.52	1089.9	3.09	4.47	12.51	135.24	1070.5	3.08	3.12	12.78	125.36	1070.7	2.96	4.62	12.65	134.92	1067.9	2.61	4.07	11.51	120.36
10	1077.1	2.73	4.09	12.64	126.96	1057.1	3.04	4.74	12.73	137.48	1063.6	2.91	3.98	13.45	132.2	1076.3	3.01	4.13	13.69	135.96	1077.6	2.65	2.93	12.51	115.88
11	1098.1	2.65	5.64	14.2	144.32	1065.9	2.86	5.04	11.46	131.92	1058.5	2.86	4.25	11.32	125.04	1053.8	2.98	4.22	12.92	133.12	1075.3	2.58	3.41	12.31	117.8
12	1055	3.12	5.38	10.07	133.24	1089.2	2.97	4.48	12.15	131.96	1081.1	3.04	4.6	12.31	134.68	1070.4	2.81	4.86	11.37	129.32	1053.7	2.44	3.17	12.35	113.8
13	1087.1	3.31	3.55	14.12	137.84	1079.4	3.19	3.48	10.85	122.28	1071.7	2.87	4.79	12.07	132.52	1085.5	2.85	4.31	13.27	133.16	1099.8	3.01	4.49	12.63	134.6
14	1120.6	2.72	5.22	13.23	138.2	1089.7	3.1	6.58	11.42	147.92	1058.7	2.77	4.9	11.35	128.92	1063.5	2.95	3.96	12.66	129.52	1103.7	3	4.77	12.49	136.12
15	1047.5	2.88	3.89	15.69	139.96	1092.7	3.21	3.68	12.47	130.68	1049.6	2.98	4.49	11.77	130.68	1070.4	3	3.44	13.5	129.52	1095.3	2.97	4.11	13.87	135.8
16	1104.6	2.88	5.48	12.65	140.52	1089.4	2.99	5.06	10.91	131.96	1086	2.8	4.03	12.01	125.08	1076.1	2.84	4.02	13.06	129.84	1094.2	2.97	4.57	12.65	134.68
17	1073	2.93	1.66	12.2	108.96	1099.7	2.95	5.37	12.79	141.32	1081.5	2.88	3.23	13.7	126.72	1078.3	2.99	5.15	12.81	140.28	1085.8	3.01	4.08	13.89	136.36
18	1082.1	2.95	6.49	12.99	151.08	1087.2	2.79	4.86	13.41	137.16	1055.7	2.73	4.21	10.66	120	1062.4	2.94	3.74	12.95	128.76	1080.6	3.1	3.88	12.12	129.12
19	1084.5	3.04	3.34	15.23	136.28	1114	2.96	5.74	13.24	146.24	1067.3	2.7	3.36	12.07	118.36	1070	2.93	4.74	12.08	133.12	1075	3	4.27	12.21	131
20	1127.7	2.94	8.02	10.21	152.04	1124.5	3.11	4.85	14.74	147.52	1088.4	3.14	3.74	13	132.16	1088.2	2.97	3.84	12	126.24	1096.2	3	3.72	11.91	125.4
21	1069.6	2.94	3.65	11.64	122.8	1048.6	2.8	2.5	12.75	115.8	1081.6	2.86	5.25	11.55	133.96	1059.5	2.88	4.21	13.75	134.76	1065	2.96	3.84	11.8	125.28
22	1097	3.2	5.37	10.05	134.36	1104.2	2.86	4.58	13.94	138.16	1103.3	2.95	4.2	14.24	137.76	1059.2	2.98	3.75	13.29	130.84	1066.3	2.85	3.56	12.02	122.16
23	1093.5	2.82	4.88	14.02	140.24	1091.4	3.07	2.36	13.6	122.4	1064.3	2.71	4.95	12.33	132.28	1076.6	2.94	4.02	13.38	132.72	1049.6	2.82	3.79	13.14	128
24	1097.6	3.04	5.28	9.85	130.28	1056.8	3.03	3.92	11.84	127.2	1099.6	2.81	5.02	12.3	134.32	1058.8	3	3.41	12.91	126.92	1065.2	2.84	3.79	12.7	126.56
25	1072	2.85	5.48	12.65	140.04	1133	3.23	5.74	13.81	152.84	1081.5	2.91	3.56	12.69	125.8	1077.5	2.94	4.61	12.7	134.72	1108.3	3.15	4.08	13.2	135.84
26	1081.6	2.5	7.08	11.22	141.52	1098.7	3.19	3.83	13.6	136.08	1103.1	3.04	3.81	14.34	136.48	1100.7	3.2	4.27	13.88	140.88	1088.8	3.08	4.1	14.18	138.8
27	1081.6	3.03	3.73	14.15	134.92	1115	3.15	4.94	10.64	132.48	1104.4	3.05	4.99	14.48	146.64	1082	2.95	4.75	12.5	135.2	1085.9	3.01	4.66	12.71	136.28
28	1083.1	3.13	4.86	13.2	141.76	1101.5	3.06	4.42	12.78	135.44	1089	3.18	3.31	15.15	137.96	1078.5	2.92	4.54	13.01	135.08	1090.9	3.04	3.73	12.48	128.4
29	1095.6	3.35	3.19	11.37	124.6	1104.2	2.95	4.43	12.42	132.32	1069.3	3.01	4.78	12.23	135.32	1066	3.04	4.17	10.92	125.68	1089.8	3.04	4	13.16	133.28
30	1000.9	2.72	4.87	10.49	124.44	1093.2	3.03	4.93	12.58	138.24	1079.1	3.22	3.55	13.26	132.96	1079.2	2.97	3.22	12.94	125.04	1087.5	2.95	3.72	13.47	130.84
31	1072	3.22	4.1	13.04	136.48	1096.4	2.99	6.03	12.93	147.8	1089	3.06	3.85	11.79	126.92	1084.9	3.2	4.62	12.85	139.56	1082.6	3.01	4.7	11.66	132.4
32	1087	3.12	3.67	13.63	133.8	1081.7	3.51	3.39	15.13	143.8	1108	3.08	4.4	14.5	142.48	1105.7	3.06	4.34	13.77	138.76	1077.2	3.04	4.44	13.27	137.24
33	1056	3	4.73	10.95	129.64	1086.2	3.28	4.42	13.75	142.84	1071.2	3	4.28	13.26	135.28	1077.9	2.99	4.83	13.07	138.76	1077	2.94	4.66	12.21	133.16
34	1083.1	2.99	0.73	18.69	128.44	1103	3.16	4.56	11.33	132.36	1075.4	3.06	3.9	12.29	129.32	1103.4	3.11	4.99	12.64	140.24	1083.5	2.93	3.99	13.26	131.84
35	1108.6	3.06	4.25	15.34	144.32	1112.7	3.16	3.44	13.29	131.24	1096.9	3.03	3.54	11.97	124.68	1106.7	3	4.05	13.57	134.68	1076.1	3.05	3.86	13.86	135.12
36	1098.1	3.12	3.22	16.5	141.68	1117.7	3.2	5.35	11.97	141.88	1090.1	3.04	3.95	12.95	132.04	1104	2.96	4.11	13.45	134.04	1075	3.07	3.79	13.9	135.04
37	1050.5	3.06	2.65	14.82	129.44	1096.4	3.16	3.95	15.24	143.12	1095.4	2.94	4.5	12.48	132.96	1090.8	2.96	4.14	13.4	134.08	1066.1	2.97	4.09	13.29	133.4
38	1068.6	3.1	2.53	15.34	131.2	1071.4	3.05	4.1	12.45	131.4	1085.8	3.13	3.18	13.59	129.88	1105.7	3.12	4.55	12.88	137.84	1066.4	3.08	3.84	12.87	131.48
39	1074.6	2.99	2.55	13.83	123.56	1069.7	3.29	3.91	13.19	136.68	1075.5	3.19	4.35	12.13	134.36	1107.7	3.24	4.72	13.21	142.44	1091.4	3.12	3.98	13.58	136.08
40	1068.6	2.9	7.23	9.58	142.56	1089.2	3.12	5.14	12.66	141.68	1090.1	3.05	6.14	11.89	145.48	1100.3	3.21	3.89	11.77	129.56	1100.5	3.19	3.84	13.53	135.88
41	1049	2.8	4.96	11.47	130.36	1067.6	2.8	5.09	9.04	121.68	1080.6	2.94	4.75	12.76	136.08	1095.2	2.98	4.77	13.38	139.36	1074.5	2.97	4.57	13.44	137.84
42	1049.5	2.65	7.22	11.93	147.88	1095.9	3.22	4.49	12.35	136.84	1110.2	3.17	4.64	14.06	144.08	1108.6	3.06	4.07	13.3	134.72	1086.9	2.97	4.31	13	134
43	1060.5	3.1	2.55	13.04	122.16	1085.7	2.91	4.51	12.42	132.32	1074.7	3.06	4.22	12.62	133.2	1086.8	3.09	4.33	12.83	135.4	1078.7	2.93	5.49	12.67	141.48
44	1077.6	2.8	5.37	13.19	140.52	1076.2	3.08	4.3	10.76	126.72	1097.3	3.19	3.83	13.61	136.12	1074.8	3.12	3.12	12.35	128.28	1079.5	2.97	4.85	12.66	136.96
45	1089	2.86	3.9	14.93	136.68	1109.5	3.16	2.58	15.45	133	1075.3	3.1	4.66	12.47	136.76	1073	3.02	3.62	12.87	128.76	1076.3	3.06	4.08	12.89	133.16
46	1069	2.97	3.63	13.93	132.28	1070.6	2.76	6.99	10.8	143.28	1085.7	2.84	4.89	14.16	141.2	1072	3.01	3.88	13.13	131.72	1083.7	2.87	4.44	12.64	132
47	1067.1	3.2	2.04	15.39	129.08	1080.2	3.03	4.71	13.63	140.68	1073.7	3.05	4.03	13.86	136.48	1058.4	3.01	3.61	12.58	127.36	1080.1	3.12	3.8		

Table 31: Core; 195'

	30 sec				1 min				2 min				3 min				5 min								
	Total	K	U	Th	API	Total	K	U	Th	API	Total	K	U	Th	API	Total	K	U	Th	API	Total	K	U	Th	API
1	1158.8	2.66	5.63	14.96	147.44	1123.2	3.16	4.43	13.39	139.56	1159.2	3.12	5.65	14.68	153.84	1145.5	3.29	3.47	14.02	136.48	930.7	2.31	3.94	11.57	114.76
2	1173.7	3.11	4.22	12.53	133.64	1148.3	3.06	5.72	11.82	142	1151.8	2.92	5.14	12.96	139.68	1121.4	3.08	4.27	13.95	139.24	1153.3	3.14	4.38	14.45	143.08
3	1126.7	3.09	5.34	13.9	147.76	1147.5	3.25	4.95	12.02	139.68	1137.7	3.3	4.94	12.39	141.88	1133.8	3.31	4.21	11.91	134.28	1149.9	3.18	4.51	13.15	139.56
4	1155.2	3.31	3.36	17.2	148.64	1153.1	2.85	5.8	13.76	147.04	1147.9	3.04	4.07	15.32	142.48	1123.6	3.14	4.86	13.72	144	1144.7	3.12	4.44	14.24	142.4
5	1143.6	3.23	4.38	11.72	133.6	1103.2	3.07	3.59	15.19	138.6	1121.5	2.84	5.49	12.29	138.52	1132.5	3.1	4.41	13.54	139.04	1149.7	3.17	4.48	13.52	140.64
6	1157.2	3.29	6.74	12.37	156.04	1140.3	3.1	4.58	12.36	135.68	1165.3	2.9	5.81	13.69	147.64	1151.8	3.26	4.2	13.45	139.56	1146.4	3.18	4.64	13.49	141.96
7	1163.8	3.28	4.76	11.4	136.16	1152.8	3.21	5.21	13.01	145.08	1137.2	3.13	3.19	14.48	133.52	1146.5	3.22	4.99	13.55	145.64	1139.9	3.16	4.22	13.89	139.88
8	1143.1	2.68	7.16	12.95	151.96	1107.7	2.94	3.82	14.17	134.28	1128.1	3.13	4.71	13.55	141.96	1136	3.29	3.72	12.75	133.4	1170.7	3.19	4.71	15.39	150.28
9	1150.2	3.15	4.82	17.01	157	1131.8	3.19	4.53	11.46	133.12	1115.3	3.13	4.98	14.84	149.28	1145.1	3.25	5.11	13.36	146.32	1154.5	3.05	4.3	14.43	140.92
10	1149.1	3.28	5.29	11.83	142.12	1143.3	3.31	2.42	14.3	129.52	1144.1	2.92	5.19	14.35	145.64	1135.7	3.13	4.97	13.32	143.12	1148.5	3.21	4.56	13.77	142.92
11	1170.7	3.09	5.26	11.36	136.96	1152.5	3.14	4.76	12.96	140.16	1130.7	3.12	4.53	13.52	140.24	1127.9	3.22	3.73	14.21	138.2	1144.1	3.16	4.98	14.18	147.12
12	1182.8	3.21	5.34	18.96	169.92	1163.6	3.29	4.35	12.23	136.36	1110.9	3.06	5.12	12.61	140.36	1133.1	2.86	5.1	14.08	142.88	1154.5	3.1	5.29	13.59	146.28
13	1171.2	2.6	5.25	10.97	127.48	1143.3	3.1	6.45	10.93	144.92	1137.1	3.15	3.64	16	143.52	1111.3	3.01	4.79	12.65	137.08	1161.1	3.16	4.29	14.29	142.04
14	1161.2	3.25	3.5	13.63	134.52	1129.1	3.02	4.78	14	142.56	1110.3	3.11	4.77	12.59	138.28	1133.5	3.07	4.9	13.56	142.56	1149.2	3.22	4.85	13.75	145.32
15	1160.2	2.75	3.46	17.06	139.92	1150.3	3.35	4.11	14.03	142.6	1142.3	3.25	5	13.61	146.44	1125.6	3.07	4	13.78	136.24	1161.7	3.19	4.64	14.53	146.28
16	1182.3	2.98	4.84	16.29	151.56	1150.8	3.09	3.9	12.6	131.04	1136.9	2.98	4.45	13.94	139.04	1117.4	3.18	3.98	14.39	140.28	1147.1	3.08	4.58	13.57	140.2
17	1166.7	2.97	5.41	11.83	145.44	1119.3	3.33	2.94	12.94	128.56	1103.4	3.01	4.31	14.59	141	1138.3	3.23	4.14	13.51	138.84	1149.2	3.18	4.91	14.82	149.44
18	1159.2	3.19	4.62	15.77	151.08	1128.5	3.04	4.89	13.86	143.2	1114	2.99	4.82	10.95	130.2	1124.5	3.1	3.91	14.17	137.56	1159.3	3.3	4.23	14.39	144.2
19	1149.6	2.68	8.56	12.22	160.24	1135.3	3.3	5.12	13.38	147.28	1135.6	3.13	3.66	15.56	141.6	1125.9	2.98	4.89	14.3	144	1150.9	3.2	3.44	14.71	137.56
20	1166.2	3.4	4.52	12.43	140.28	1160.8	3.21	3.73	12.59	131.56	1131.6	3.13	3.33	13.82	132	1115.6	3.09	3.61	15.06	138.56	1151.6	3.17	4.95	13.55	144.52
21	1120.7	2.77	4.17	15.93	141.4	1142.3	3.27	5.12	13.39	146.84	1117.4	3.07	4.04	12.9	133.04	1118.2	3.22	4.33	13.36	139.6	1150.6	3.13	4.49	14.31	143.24
22	1145.2	3.27	4.05	17.61	155.16	1154	3.27	4.99	12.9	143.84	1126.2	3.22	3.69	12.79	132.2	1163.7	3.28	4.08	14.23	142.04	1158.9	3.14	4.74	13.41	141.28
23	1162.3	3.18	4.77	10.66	131.68	1134.3	3.08	4.69	12.22	135.68	1106.3	3.02	4.26	13.9	138	1153	3.17	4.21	14.79	143.56	1130.5	3.17	3.72	12.84	131.84
24	1130.2	3.16	4.55	11.71	133.8	1129.5	3.03	5.1	15.1	149.68	1101.4	3.08	4.46	12.77	136.04	1133.6	2.95	4.58	14.52	141.92	1140	3.22	3.93	14.83	142.28
25	1112.2	3.26	3.58	11.07	125.08	1134.8	3.11	3.94	13.86	136.72	1124.1	3.11	4.09	13.01	134.52	1135.1	3.28	4.6	14.03	145.4	1142.3	3.26	4.04	14.53	142.6
26	1158.2	2.87	5.12	16.52	152.96	1120.3	3.22	4.26	13.4	139.2	1103.3	3.08	3.19	13.22	127.68	1132.9	3.14	3.53	13.71	133.32	1143	3.2	4.86	13.71	144.92
27	1160.2	3.22	4.63	14.23	145.48	1119.3	3.14	4.53	11.47	132.36	1102.1	2.83	4.53	13.83	136.84	1119.4	3.23	4.18	14.65	143.72	1136.3	3.12	4.27	13.89	139.64
28	1170.7	3.29	4.95	14.17	148.92	1167.1	3	4.45	15.59	145.96	1122.1	2.94	4.41	12.17	131	1145.2	3.03	4.97	13.77	143.32	1125.9	3.16	3.79	14.36	138.32
29	1206.8	3.23	6.15	12.22	149.76	1135.8	3.11	3.6	12.89	130.12	1114.1	3.15	4.08	15.04	143.2	1126.4	3.05	5.52	12.41	142.6	1125.4	3.19	4.08	13.54	137.84
30	1126.2	3.03	6.83	10.63	145.64	1091.9	3.07	3.51	11.89	124.76	1118.3	3.16	3.37	13.62	132	1140	3.07	5.06	12.47	139.48	1143	3.15	4.81	13.67	143.56
31	1179.2	3.5	5	12.33	145.32	1104.2	3.08	5.49	12.48	143.12	1144.9	2.94	5.5	12.71	141.88	1134.5	3.07	4.52	13.53	139.4	1135.5	3.21	4.26	14.3	142.64
32	1108.6	3.33	1.38	15.46	126.16	1108	2.94	4.55	11.13	127.96	1150.3	3.28	4.13	12.52	135.6	1132.5	3.09	3.86	14.18	137.04	1142.5	3.2	4.26	14.76	144.32
33	1138.2	2.98	6.51	10.69	142.52	1117.2	2.83	4.68	12.79	133.88	1133	3.04	4.09	13.6	135.76	1150.4	3.26	4.13	14.52	143.28	1148.4	3.36	3.91	13.66	139.68
34	1125.7	2.82	5.48	12.66	139.6	1123.2	3.3	4.16	12.77	137.16	1112.1	3.12	4.16	12.87	134.68	1143.9	3.07	4.22	13.57	137.16	1159.5	3.16	5.22	14.45	150.12
35	1163.2	2.88	4.25	16.91	147.72	1085.7	3.24	3.1	11.54	122.8	1133.1	2.97	4.31	14.6	140.4	1135.9	3	4.75	15.04	146.16	1149.3	3.23	4.26	12.9	137.36
36	1128.6	2.91	6.73	10.42	142.08	1114.2	3.17	5.26	13.52	146.88	1142.3	3.26	4.67	15.5	151.52	1126.6	3.18	4.73	12.84	140.08	1148.4	3.22	4.49	13.81	142.68
37	1132.7	3.04	5.7	15.89	157.8	1150.6	3.18	4.4	13.9	141.68	1107.2	3.1	3.79	13.7	134.72	1137.2	3.22	4.41	13.73	141.72	1137.3	3.26	4.24	13.89	141.64
38	1123.1	2.6	6.38	15.88	156.16	1149.1	3.3	3.36	13.9	135.28	1103.3	2.92	5.02	12.98	138.8	1153.3	3.2	4.35	14.46	143.84	1138.7	3.19	4.31	14.61	143.96
39	1154.7	3.41	4.34	14.74	148.24	1144.1	2.93	4.83	14.15	142.12	1112.6	3.02	4.06	12.84	132.16	1130.9	3.26	3.93	12.77	134.68	1141.7	3.12	5.17	13.83	146.6
40	1141.2	3.2	2.77	17.82	144.64	1127.5	3.35	2.77	14.11	132.2	1124.2	2.99	4.6	13.79	139.8	1114.6	3.04	4.53	12.98	136.8	1123.7	3.23	4.02	13.9	139.44
41	1164.2	3.39	1.15	16.5	129.44	1150	2.96	4.48	15.08	143.52	1129.4	3.14	3.98	14.04	138.24	1147.5	2.93	4.82	13.9	141.04	1127.4	3.06	4.24	14.41	140.52
42	1133.2	3.08	6.68	9.12	139.2	1121.8	3.07	5.52	12.74	144.24	1119.1	3.11	3.36	13.12	129.12	1144.2	3.12	4.86	13.98	144.72	1138.2	3.28	4.4	13.71	142.52
43	1120.6	3.14	4.99	11.14	134.72	1129	3.05	6.09	12.65	148.12	1092.1	2.9	4.34	12.13	129.64	1142.3	3.14	3.48	15.67	140.76	1144	3.1	5.09	13.56	144.56
44	1156.2	3.41	2.64	12.45	125.48	1109	2.93	4.67	12.39	133.8	1127	3.08	4.84	11.7	134.8	1128.6	2.99	4.19	13.89	136.92	1140.2	3.22	3.99	13.99	139.4
45	1129.6	3.12	5.12	14.18	147.6	1124.3	3.13	5.12	14.57	149.32	1106.8	2.76	5.13	12.74	136.16	1141.5	3.26	4.63	13.39	142.76	1148.3	3.24	5	13.09	144.2
46	1158.8	2.91	4.22	14.87	139.8	1129.8	3.01	4.16	12.19	130.2	1094.8	2.83	4.39	11.95	128.2	1148.2	3.09	4.82	13.69	142.76	1146	3.15	4.83	13.9	144.64
47	1127.2	3.38	6.7	10.32	148.96	1153.8	2.94	6.09	13.44	149.52	1111.6	2.98	3.93	13.83	134.44	1160.5	3.17	4.81	13.5						

**APPENDIX 4: TOC ANALYSES**

**Table 32:**

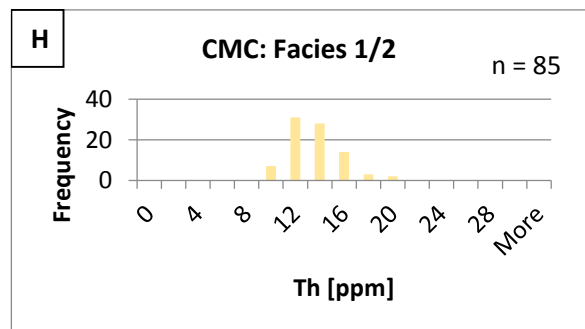
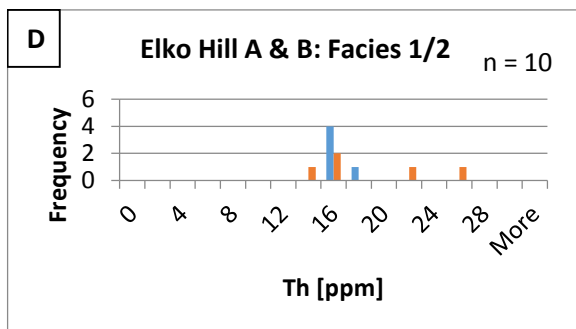
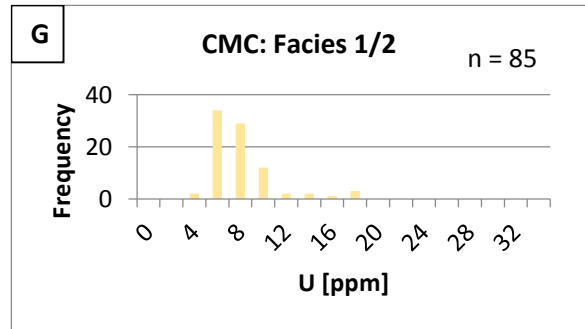
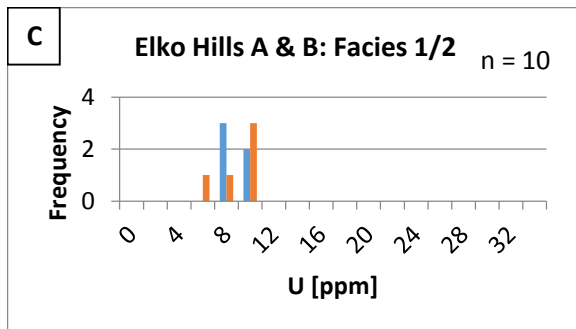
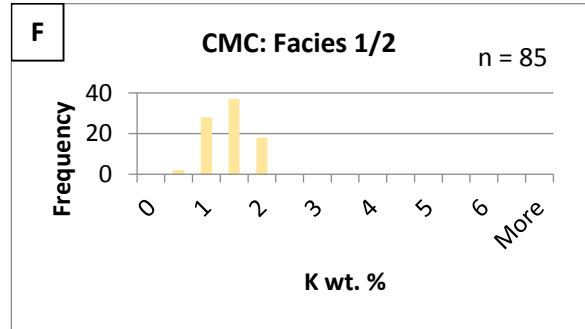
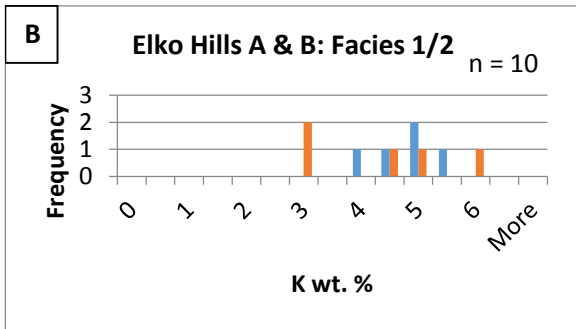
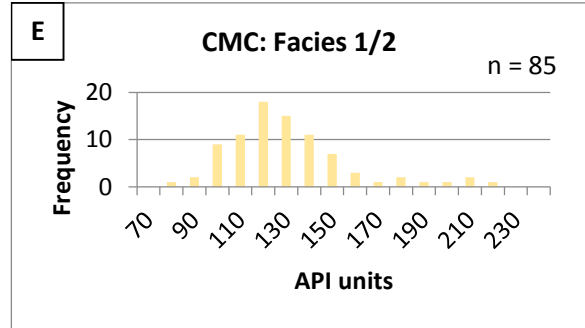
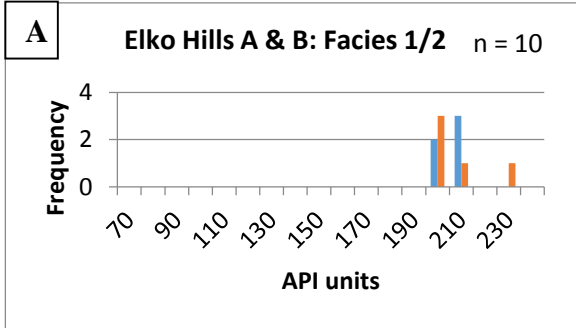
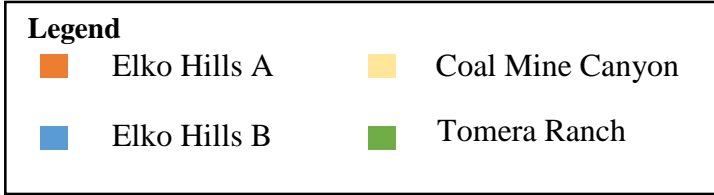
 <b>Weatherford®</b> LABORATORIES									
TOTAL ORGANIC CARBON DATA									
Company : CSU									
Client ID	Well Name	Depth ( ) Top	Sample Type	Sample Prep	*	Leco TOC	Notes Checks	Pyrogram	LAB ID
CMC-13	CMC-13	214	Rock	NOPR		5.93			3403774719
CMC-13	CMC-13	252	Rock	NOPR		0.73	TOC		3403774721
Elko Hills B-13	COS-3-13	36.7	Rock	NOPR		28.80			3403774717
Elko Hills A-13	COS-4-13	24	Rock	NOPR		24.20	TOC		3403774713
Elko Hills A-14	COS-4-13	48.5	Rock	NOPR		25.60			3403774715
TR-13	TR-13	209.5	Rock	NOPR		12.40	TOC		3403774731
TR-14	TR-14	73	Rock	NOPR		7.82	TOC		3403774723
TR-14	TR-14	122	Rock	NOPR		4.35			3403774725
TR-14	TR-14	204	Rock	NOPR		31.40	TOC		3403774727
TR-14	TR-14	275	Rock	NOPR		0.48	TOC		3403774729
<b>Notes:</b> "-1" – not measured or invalid value for Tmax TOC - Total Organic Carbon, wt. % S1 - volatile hydrocarbon (HC) content, mg HC/ g rock S2 - remaining HC generative potential, mg HC/ g rock S3 - carbon dioxide content, mg CO <sub>2</sub> / g rock					<b>Pyrogram:</b> f - flat S2 peak n - normal ltS2sh - low temperature S2 shoulder htS2sh - high temperature S2 shoulder ltS2p - low temperature S2 peak htS2p - high temperature S2 peak				
* - comments regarding contamination ** - low S2, Tmax is unreliable Meas. %Ro - measured vitrinite reflectance HI - Hydrogen index = S2 x 100 / TOC, mg HC/ g TOC OI - Oxygen Index = S3 x 100 / TOC, mg CO <sub>2</sub> / g TOC PI - Production Index = S1 / (S1+S2)					LECO – TOC on Leco Instrument RE - Programmed pyrolysis or TOC on Rock-Eval instrument SRA – Programmed pyrolysis by SRA Instrument EXT - Extracted Rock NOPR - Normal Preparation				

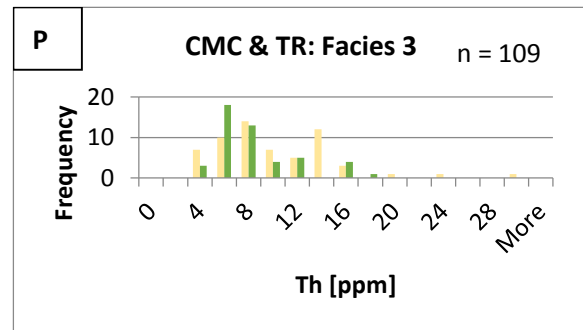
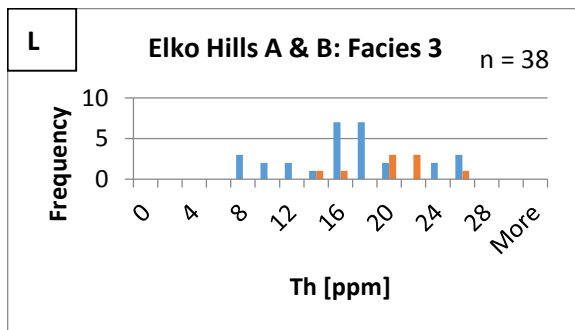
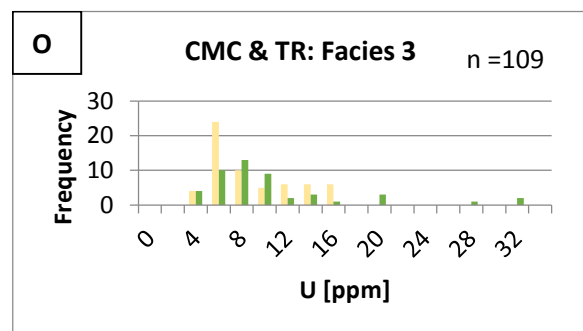
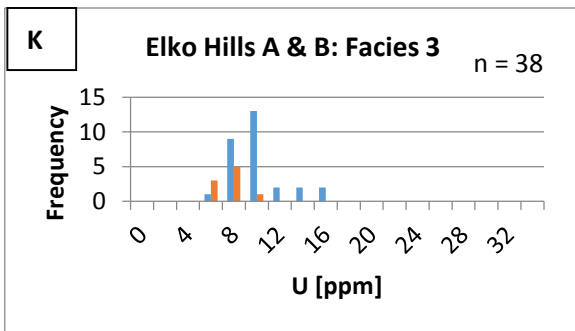
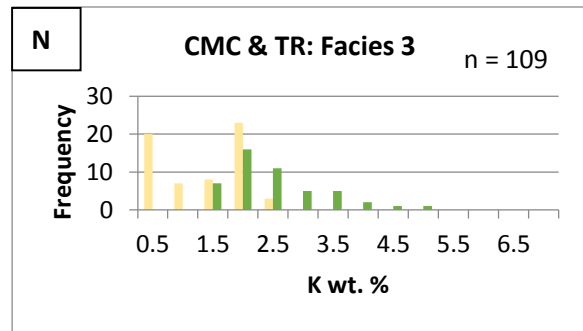
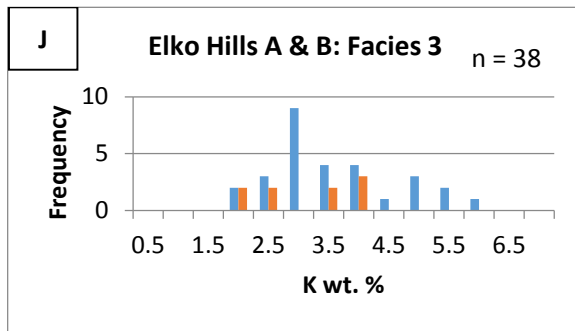
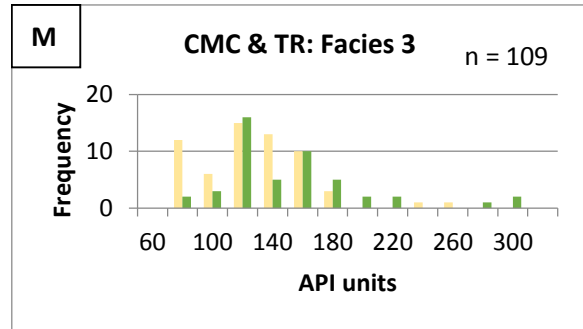
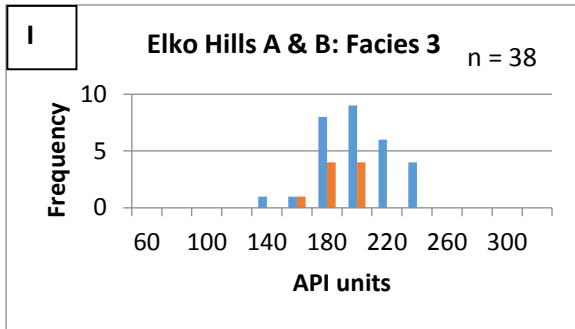
## APPENDIX 5: X-RAY DIFFRACTION ANALYSES

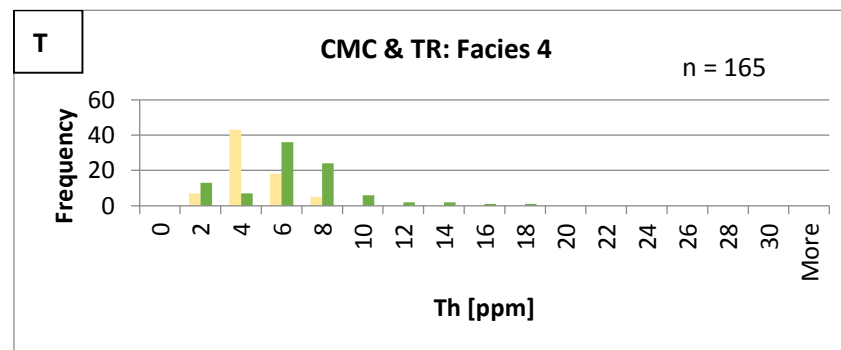
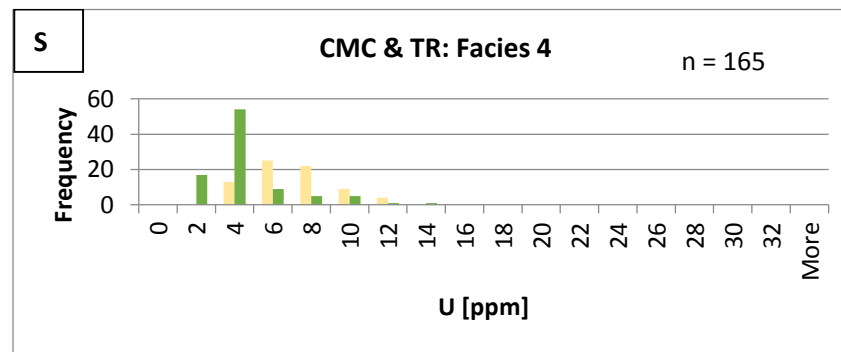
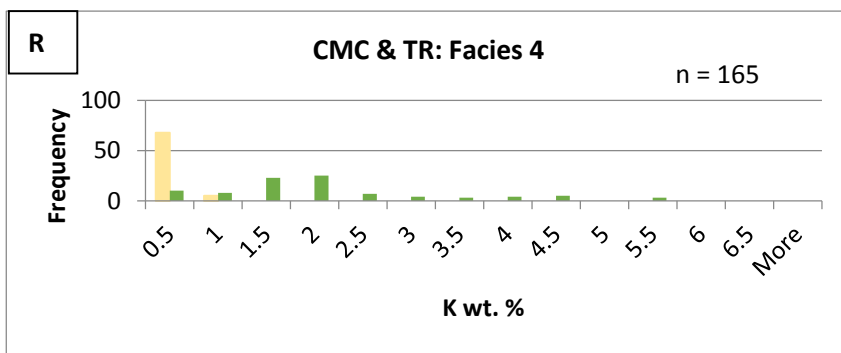
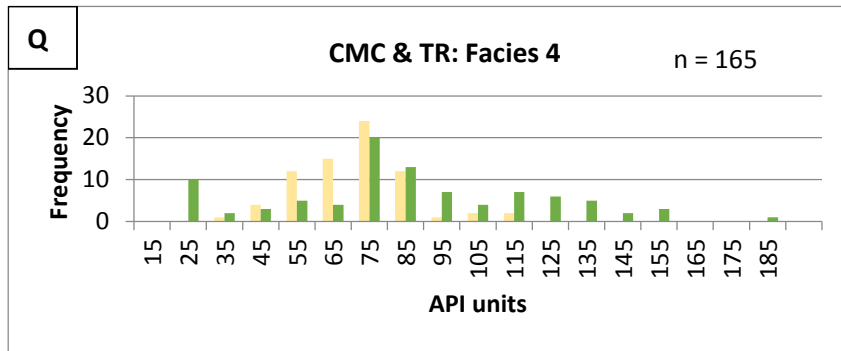
**Table 33:**

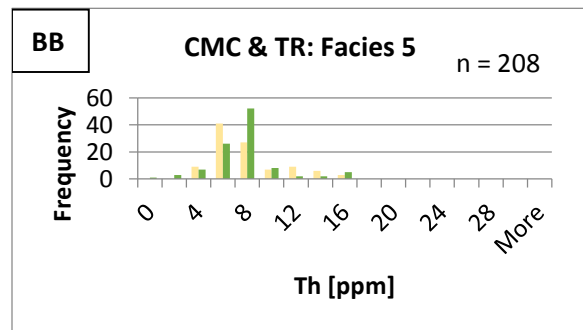
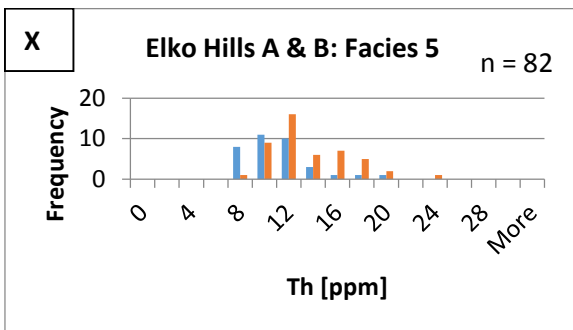
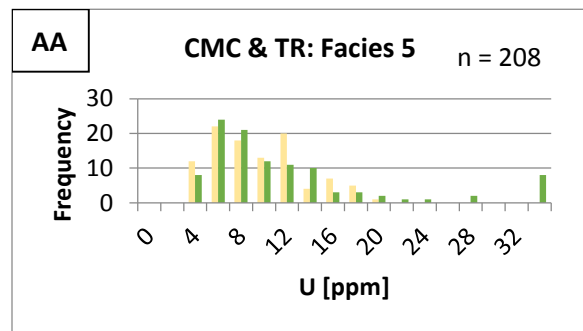
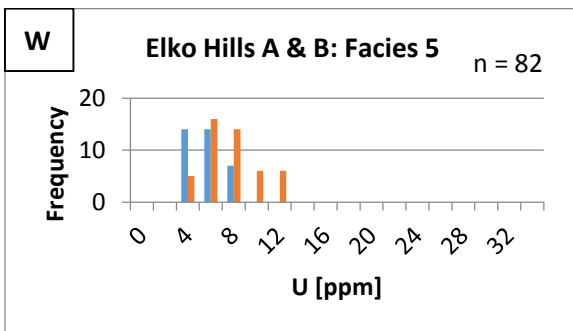
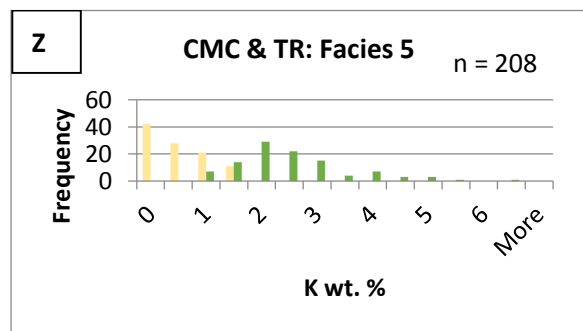
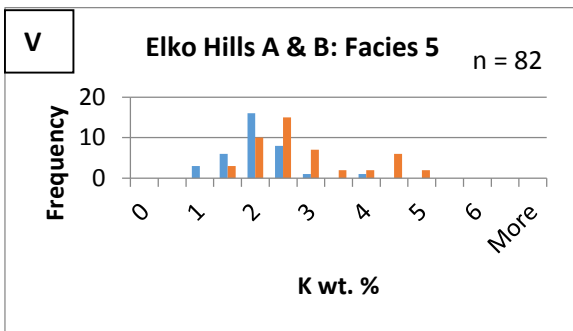
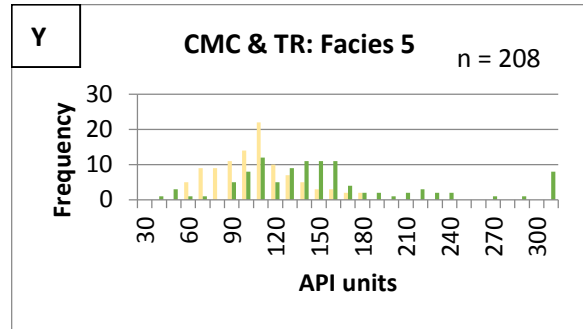
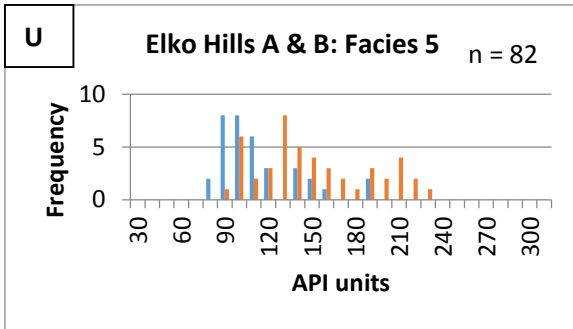
Client Name:		X-Ray Diffraction (Weight %)															Date:	
CSU																	2/13/15	
Sample #	Quartz	CLAYS				CARBONATES			FELDSPARS		SULFIDES		SULFATES			OTHERS		AMORPHOUS
		Chlorite	Kaolinite	Illite	Montmorillonite	Calcite	Dolomite	Siderite	Feldspar	Albite/Plag.	Pyrite	Galena	Barite	Gypsum	Anhydrite	Apatite	Mica	UNIDENTIFIABLE
Elko Hills B	20.7	53.1	3.1		13.3				18.9	6.5								5.0
Elko Hills B	36.7	29.3	2.2		19.2	7.3	5.1						28.7					8.1
Elko Hills B	36	7.6	6.9		19.2	0.5	3.7	2.5	10.8	29.1								19.6
Elko Hills B	41	6.7	3.5		25.7	2	0.9	2.6	13.2	19.4	0.7							23.6 (Zeolite:1.8)
Elko Hills B	10	50	3.5		16.8				18.5	6.1								5
Elko Hills B	0.7	47	17.5		27.8		1.5											6.2
Elko Hills B	37.9	29.3			25.3	0.9	11.1	4.9		5.4	1.4							10.7 (Ammonioiarosite: 11%)
Elko Hills B	51	2.1	2.7		12	0.2	1.6			2.2	0.8							20.5 (Clinoptilolite: 57.9%)
Elko Hills A	42	31.4	9.1		42.3	0.7				8.7								7.8
Elko Hills A	65	72	1.9		12.9					13.2								4.5
Elko Hills A	22	37.6	6.2		25.7	2.2	3.9	2.9	5.8	7.4	0.8							7.6
Elko Hills A	48.5	26.9	10.5		34.4	0.9	3.3	2.1		8.6	2.3							11
Elko Hills A	24	43.3	8.2		36.2	1.1	3.7											7.5
CMC-13	34.5	61.9			22.2	0.3				11								4.6
CMC-13	40	73			19.7					3.2								4.2
CMC-13	121	9.3		4.6	43.8	1.8	1.4	3.8		9.8								20.0 (Magadiite: 5.4%)
CMC-13	127	15.6	6.7		49.1	1.9				9.6								17
CMC-13	168.5	9.6	14.8		41.1	1	1.8			10.1								21.5
CMC-13	211	1.3			66.4					11.1								13.6 (Gordaitite: 7.6%)
CMC-13	231	2.4			22.4	0.5	34			26.1								12.9 (Cesium: 1.7%)
CMC-13	238.5	5.6	12.5		12.1	0.9	42.2			16.4								10.4
CMC-13	304.8	8.3	15		16.3		38.9			10.8								10.7
CMC-14	192	15	2.4		20.5	0.5	1.4	3.1	11.2	16.2								17.7 (Cristobalite: 12%)
CMC-13	252	46.2		3	15		2.5	15.4		12.2								5.7
CMC-13	214	5.1			27.5	1.1				10.6								13.1(Brannockite:42.6%)
CMC-13	392	3.3		3.2	53.9	9.4				19.4								10.9
CMC-13	490	3.9	8.6		17.4		36.9	11.9		8.5	1.3							11.4
TR-14	73	10.8	6.3		27.8	1.1	2.7	2.6		16.5								18.2 (Cristobalite: 14%)
TR-14	99				20.4		2.3	55.7		13.2								8.5
TR-14	102	6.7	2.9		20.5	0.6		41.3		12.1								9.4 (Cristobalite: 6.5%)
TR-13	152	5	5.2		13.8	0.3	3.8	2		26	0.9							22.3 (Clinoptilolite: 20.7%)
TR-13	167.5	9.9	4.2		16.1	0.4	2.2	11.8		13	21.6							18.6 (Cristobalite: 2.2%)
TR-14	204	27.8	7.2		16.4	0.7	3.1	3.4		8.8	14.6							9.3 (Zeolite:8.9)
TR-13	209.5	25.8			15.9	0.4		3		15.7	29.9							9.2
TR-13	402	1.6	2.6		5.9	0.2	1.1	0.8		17	0.7							22.6 (Clinoptilolite: 47.6%)
TR-13	69		3.8		18.7			53.9		14.6								9
TR-14	275	14.7	3.5		27.6	0.7		3.3		22.7	14.5							13.1
TR-13	259	4.6	5.3		7.5		1	1.1	0.9	17.6	0.6							23 (Clinoptilolite: 38.5%)
TR-14	199	19.1			16.9	0.6	3.8	3.2		14	30.5							11.9
TR-14	390	1.6			14.9	0.8	1.5	63		9.3								8.9
TR-14	122	23		3.9	15.4		7.7	2.5		25.9	12.1							9.5
TR-14	391	0.9	10.8		7.9	0.6	0.8	0.7		12.9	0.4							22.7(Clinoptilolite: 42.3%)

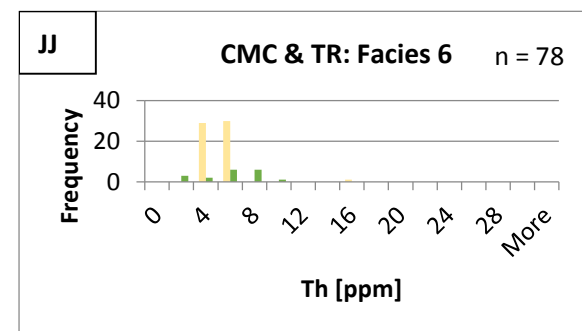
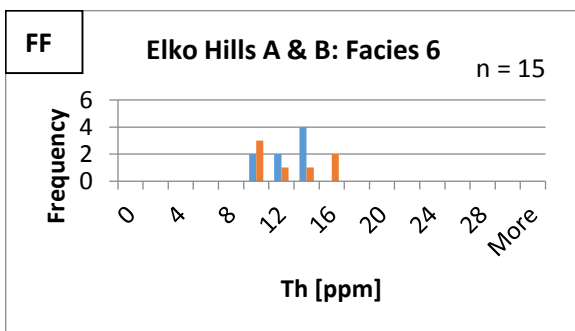
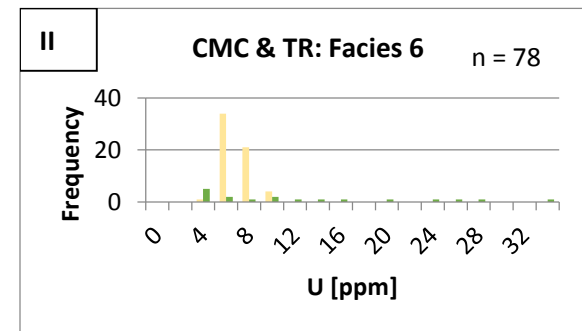
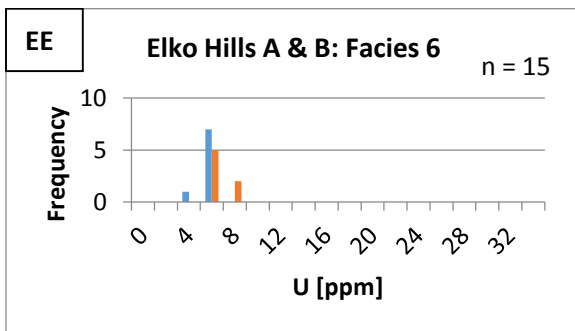
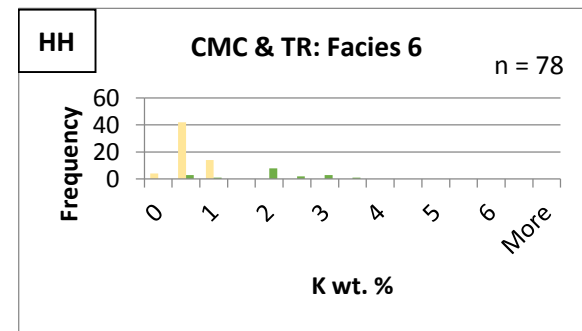
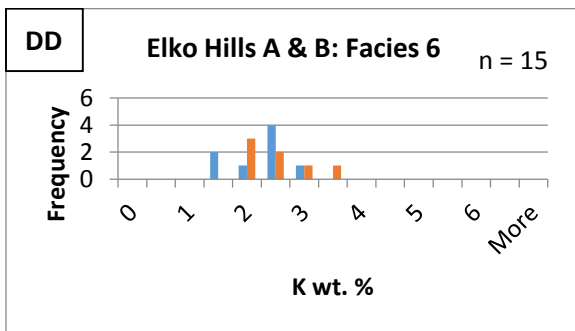
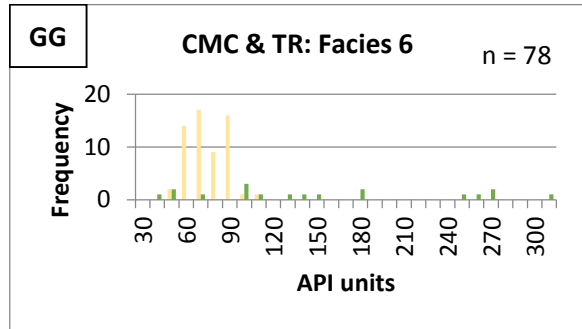
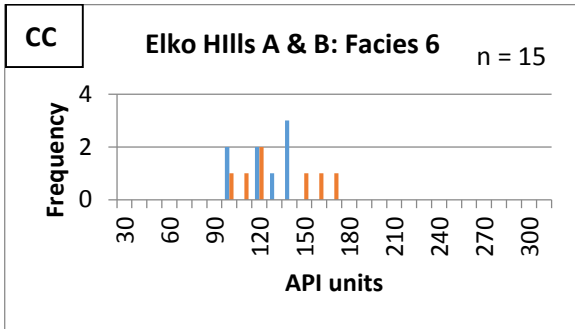
## APPENDIX 6: FREQUENCY DISTRIBUTION CHARTS

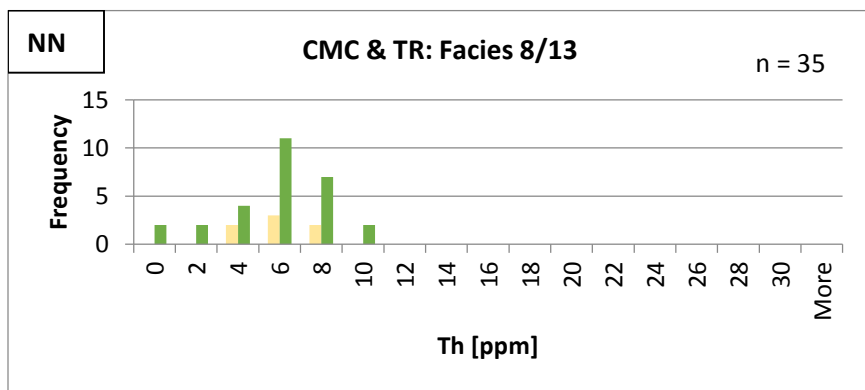
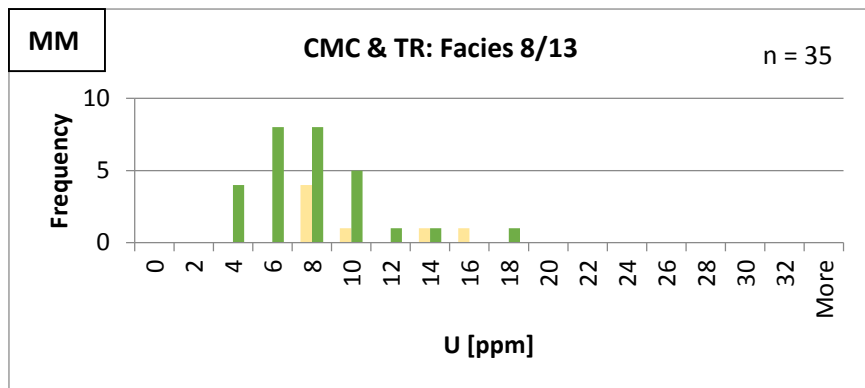
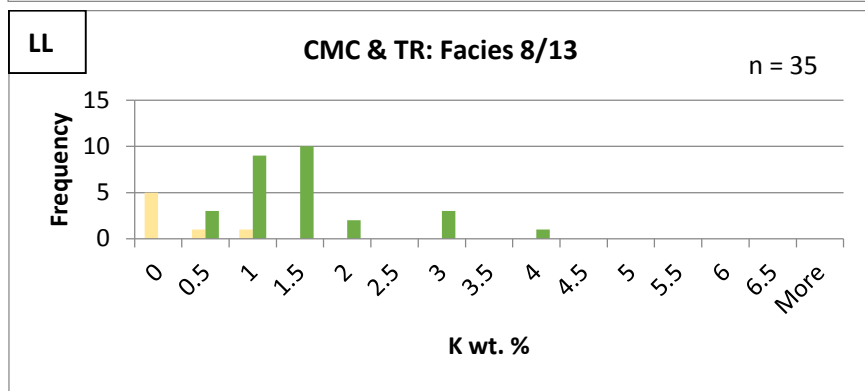
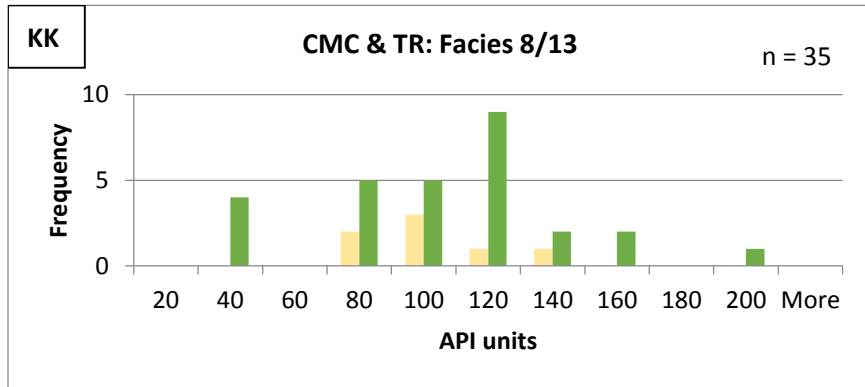


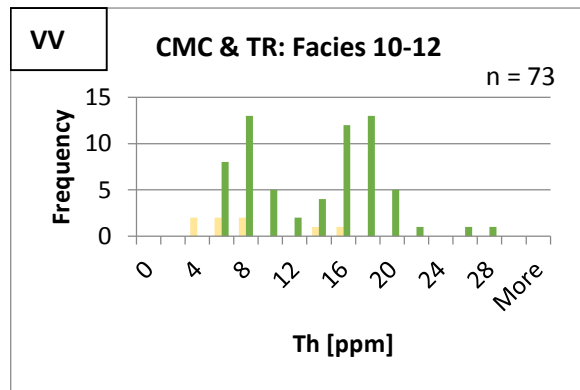
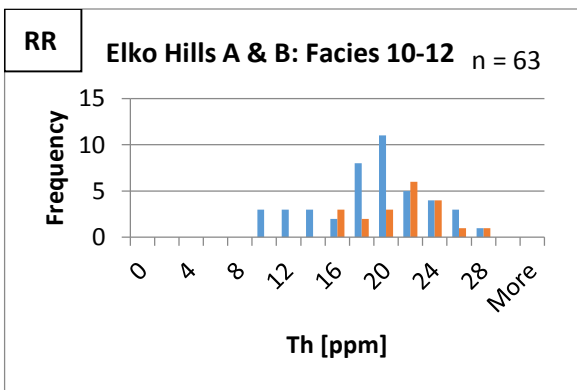
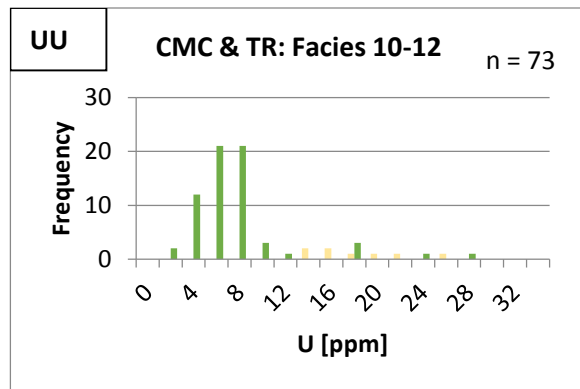
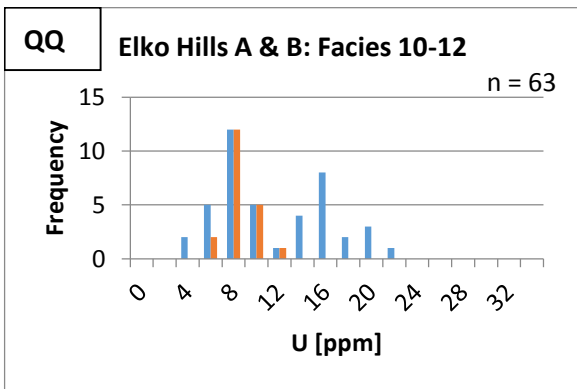
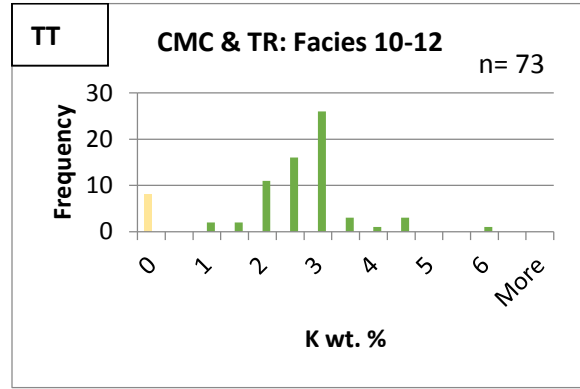
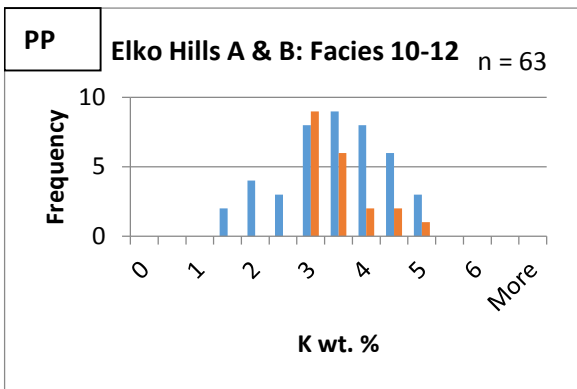
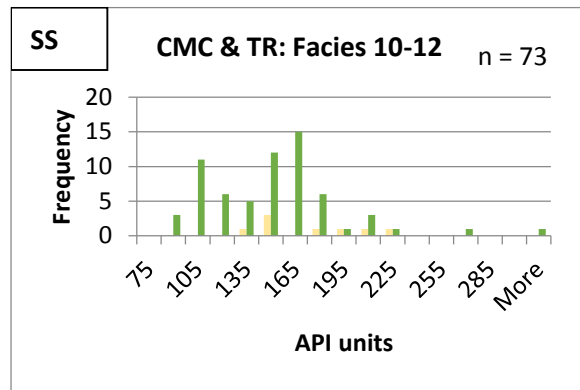
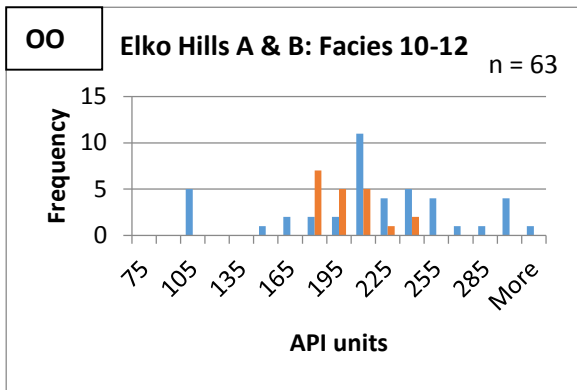


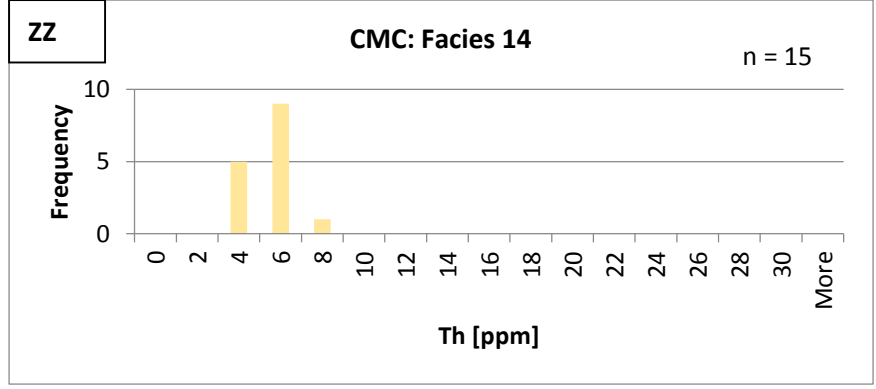
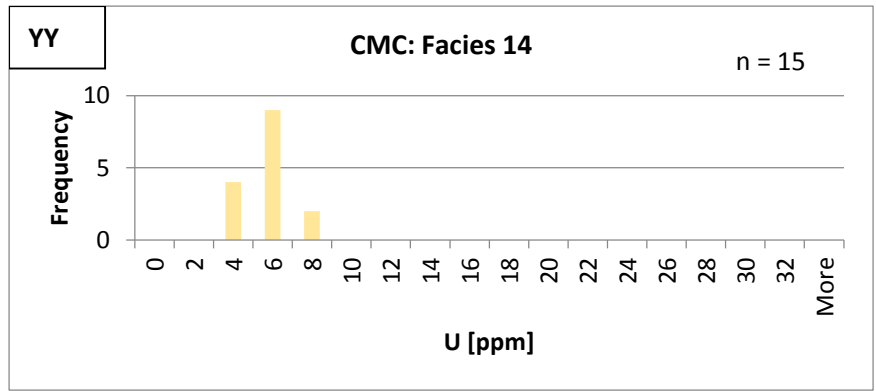
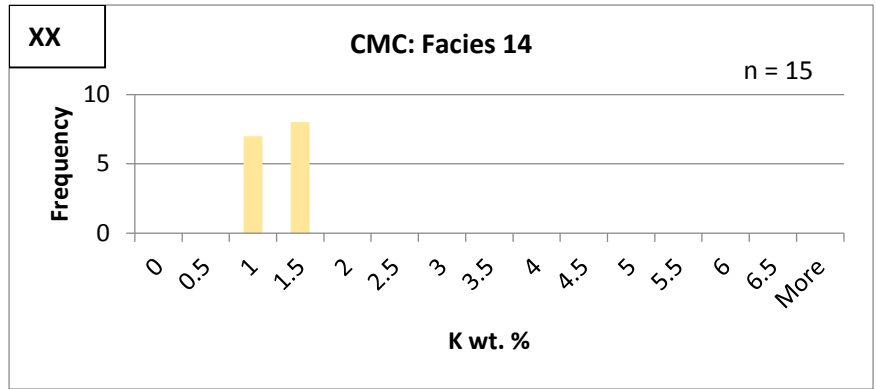
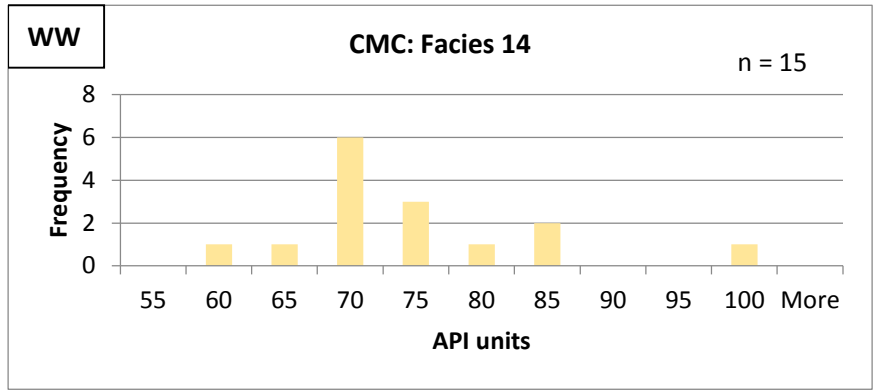












**Figures 23A-ZZ:** Frequency distribution charts labeled by outcrop and facies.

## APPENDIX 7: SCANNING ELECTRON MICROSCOPE ANALYSES

### Elko Hills B at 51ft.:

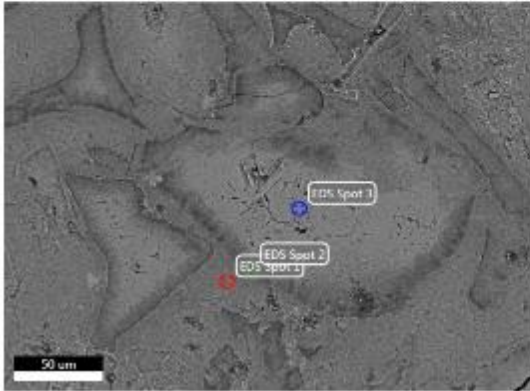
EDAX TEAM

Page 1

McGowan

Author: segenhoff  
Creation: 3/4/2015  
Sample Name: COS3-51

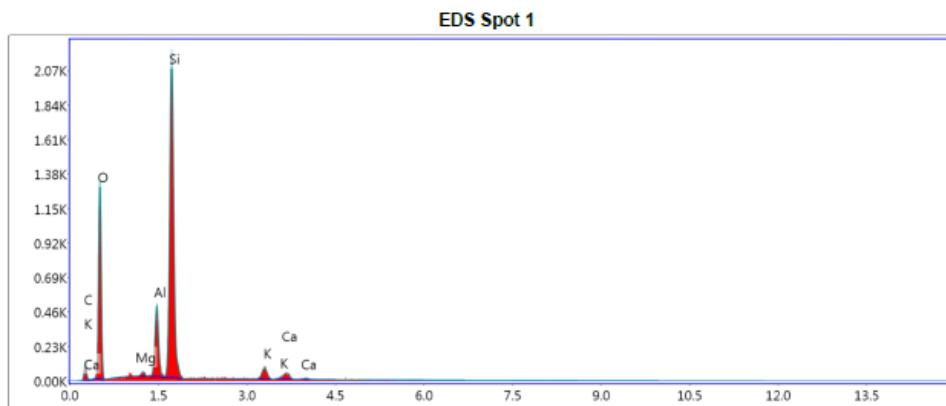
#### Area 1



Notes:

EDS Spot 1

kV: 15      Mag: 544      Takeoff: 35.5      Live Time(s): 10      Amp Time(μs): 12.8      Resolution:(eV) 126.7



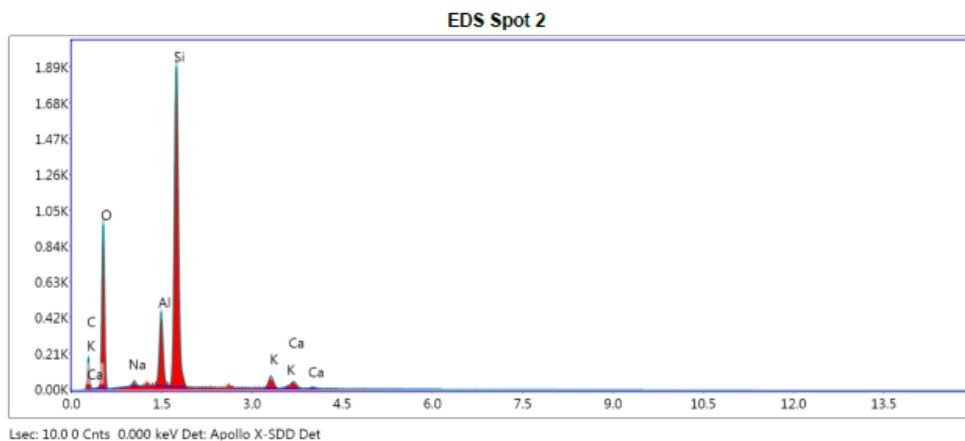
Lsec: 10.0 0 Cnts 0.000 keV Det: Apollo X-SDD Det

**eZAF Smart Quant Results**

Element	Weight %	Atomic %	Net Int.	Error %	Kratio	Z	R	A	F
C K	13.05	20.54	54.17	16.05	0.02	1.09	0.96	0.16	1
O K	42.58	50.31	706.22	9.27	0.15	1.04	0.98	0.33	1
MgK	0.47	0.36	22.74	26.02	0.00	0.96	1.01	0.7	1.02
AlK	6.63	4.64	355.04	5.36	0.05	0.92	1.02	0.82	1.02
SiK	32.46	21.85	1,693.19	3.69	0.26	0.94	1.02	0.85	1
K K	2.82	1.36	81.44	13.49	0.02	0.86	1.05	0.94	1.01
CaK	1.99	0.94	47.62	18.02	0.02	0.88	1.05	0.96	1

EDS Spot 2

kV: 15      Mag: 544      Takeoff: 35.5      Live Time(s): 10      Amp Time(μs): 12.8      Resolution(eV) 126.7



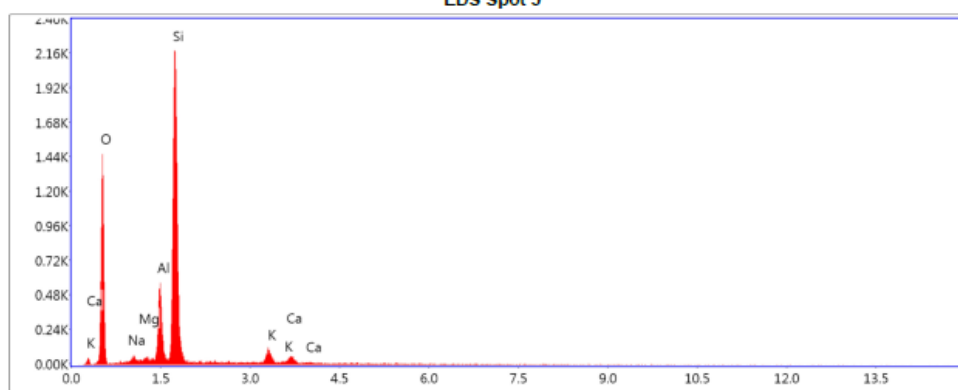
**eZAF Smart Quant Results**

Element	Weight %	Atomic %	Net Int.	Error %	Kratio	Z	R	A	F
C K	19.90	30.17	82.37	14.12	0.04	1.09	0.96	0.17	1
O K	37.77	42.99	534.75	9.78	0.12	1.03	0.98	0.3	1
NaK	0.55	0.44	16.12	28.00	0.00	0.93	1.01	0.56	1.01
AlK	6.49	4.38	332.16	5.34	0.05	0.91	1.02	0.83	1.02
SiK	30.67	19.89	1,524.76	3.85	0.25	0.93	1.03	0.86	1
K K	2.68	1.25	73.61	11.89	0.02	0.86	1.05	0.95	1.01
CaK	1.93	0.88	43.77	18.70	0.02	0.87	1.05	0.96	1

## EDS Spot 3

kV: 15      Mag: 544      Takeoff: 35.5      Live Time(s): 10      Amp Time(μs): 12.8      Resolution:(eV) 126.7

## EDS Spot 3



Lsec: 10.0 0 Cnts 0.000 keV Det: Apollo X-SDD Det

eZAF Smart Quant Results

Element	Weight %	Atomic %	Net Int.	Error %	Kratio	Z	R	A	F
O K	45.83	60.34	797.23	8.73	0.19	1.06	0.97	0.38	1
NaK	0.68	0.63	19.01	31.33	0.00	0.96	1	0.54	1.01
MgK	0.40	0.34	17.62	27.40	0.00	0.97	1	0.69	1.02
AlK	8.50	6.64	417.06	5.33	0.07	0.94	1.01	0.81	1.03
SiK	38.16	28.62	1,796.61	3.87	0.30	0.96	1.02	0.83	1
K K	3.94	2.12	103.52	11.00	0.03	0.88	1.04	0.93	1.01
CaK	2.49	1.31	54.22	15.84	0.02	0.9	1.05	0.94	1

## Elko Hills B at 36 ft.:

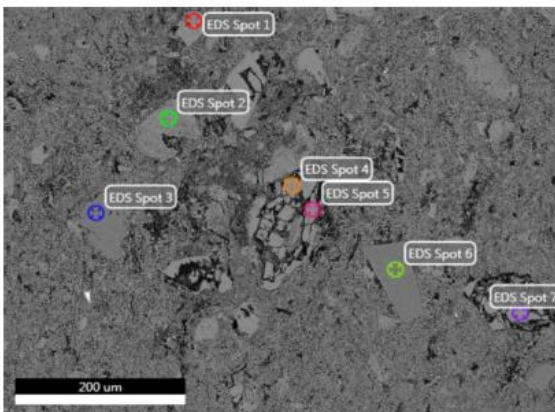
### EDAX TEAM

Page 1

McGowan

Author: segenhoff  
Creation: 3/4/2015  
Sample Name: COS3-36

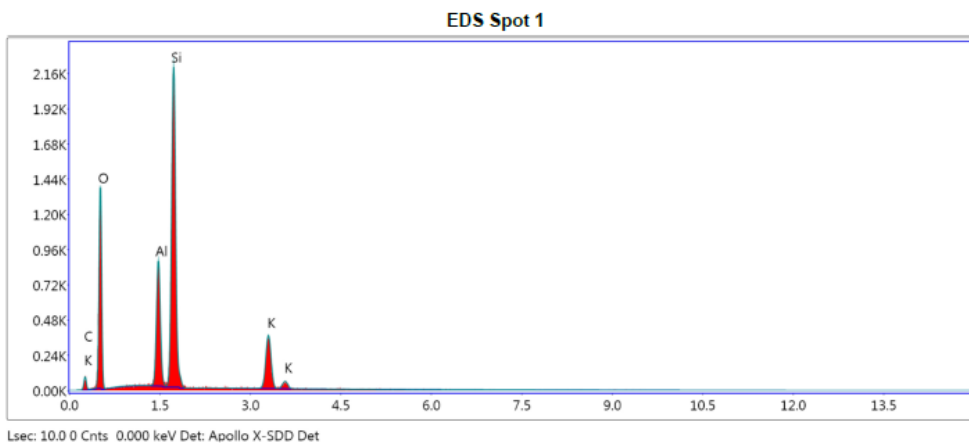
#### Area 1



Notes:

EDS Spot 1

kV: 15      Mag: 249      Takeoff: 35.5      Live Time(s): 10      Amp Time(μs): 12.8      Resolution:(eV) 126.7

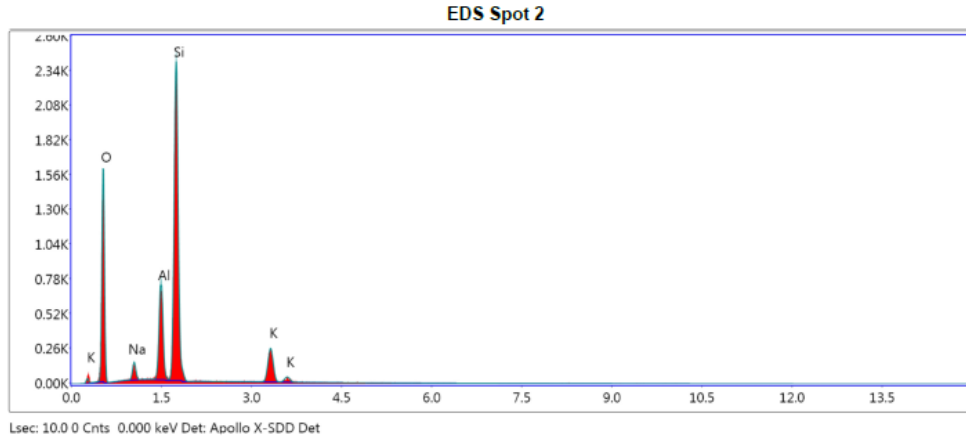


**eZAF Smart Quant Results**

Element	Weight %	Atomic %	Net Int.	Error %	Kratio	Z	R	A	F
C K	6.15	10.50	28.90	21.28	0.01	1.11	0.95	0.16	1
O K	41.72	53.47	741.93	9.43	0.14	1.06	0.97	0.31	1
AlK	10.58	8.04	643.70	4.81	0.08	0.94	1.01	0.81	1.02
SiK	30.10	21.98	1,735.12	3.99	0.24	0.95	1.02	0.82	1
KK	11.46	6.01	375.40	4.44	0.09	0.88	1.04	0.94	1

EDS Spot 2

kV: 15      Mag: 249      Takeoff: 35.5      Live Time(s): 10      Amp Time(μs): 12.8      Resolution:(eV) 126.7

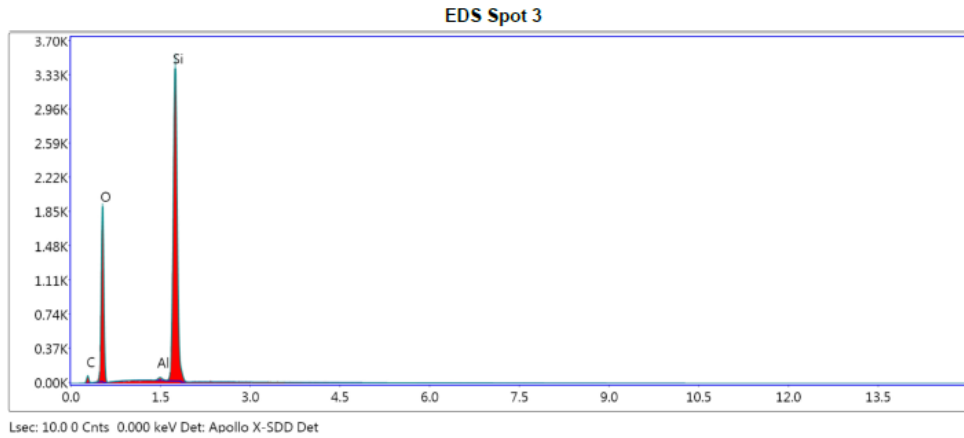


**eZAF Smart Quant Results**

Element	Weight %	Atomic %	Net Int.	Error %	Kratio	Z	R	A	F
O K	43.90	58.51	855.35	8.84	0.17	1.07	0.97	0.37	1
NaK	2.53	2.35	82.74	11.33	0.01	0.96	1	0.54	1.01
AlK	9.84	7.77	556.24	5.05	0.08	0.94	1.01	0.8	1.02
SiK	35.21	26.73	1,900.76	3.95	0.28	0.96	1.02	0.81	1
K K	8.52	4.64	260.14	5.57	0.07	0.89	1.04	0.93	1

EDS Spot 3

kV: 15      Mag: 249      Takeoff: 35.5      Live Time(s): 10      Amp Time(μs): 12.8      Resolution:(eV) 126.7

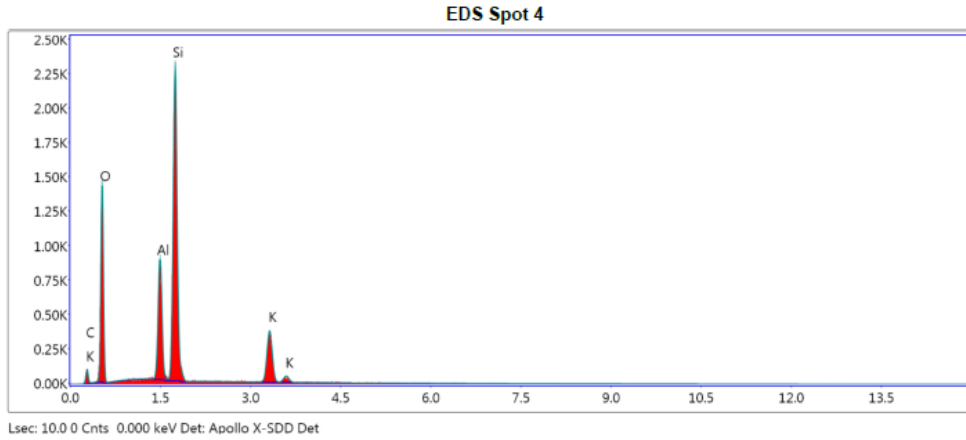


**eZAF Smart Quant Results**

Element	Weight %	Atomic %	Net Int.	Error %	Kratio	Z	R	A	F
CK	8.71	13.87	35.55	17.11	0.01	1.09	0.96	0.14	1
OK	46.62	55.71	1,038.59	8.25	0.19	1.04	0.98	0.4	1
AlK	0.48	0.34	29.58	20.41	0.00	0.92	1.02	0.82	1.04
SiK	44.19	30.08	2,750.52	2.97	0.37	0.94	1.02	0.9	1

EDS Spot 4

kV: 15      Mag: 249      Takeoff: 35.5      Live Time(s): 10      Amp Time(μs): 12.8      Resolution:(eV) 126.7

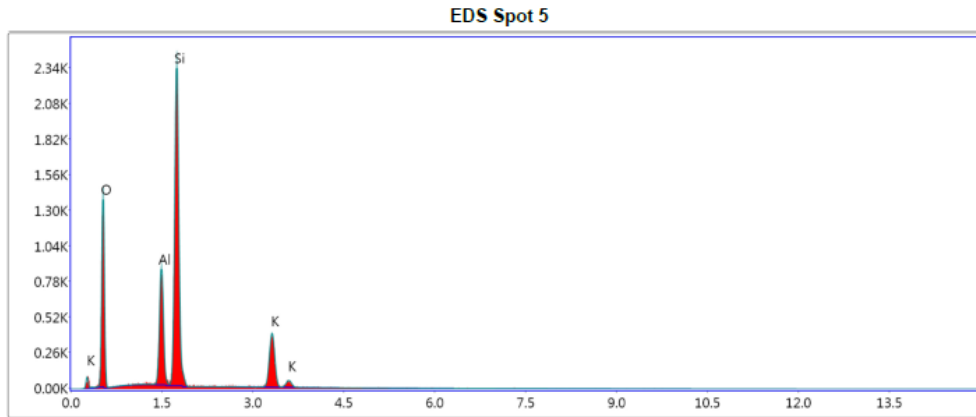


**eZAF Smart Quant Results**

Element	Weight %	Atomic %	Net Int.	Error %	Kratio	Z	R	A	F
C K	7.36	12.40	37.32	18.07	0.01	1.11	0.95	0.16	1
O K	41.84	52.93	785.39	9.41	0.14	1.06	0.97	0.31	1
AlK	10.29	7.72	662.40	4.79	0.08	0.93	1.01	0.81	1.02
SiK	29.42	21.20	1,799.10	3.95	0.23	0.95	1.02	0.82	1
K K	11.10	5.75	385.74	4.38	0.09	0.88	1.04	0.94	1

EDS Spot 5

kV: 15      Mag: 249      Takeoff: 35.5      Live Time(s): 10      Amp Time(μs): 12.8      Resolution:(eV) 126.7



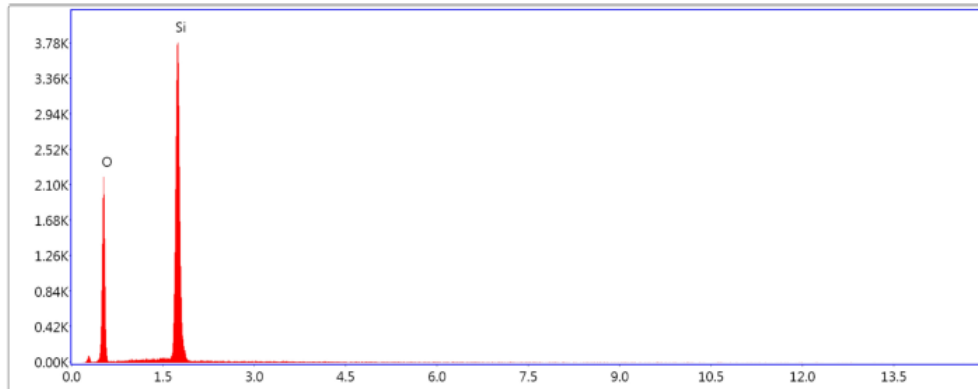
**eZAF Smart Quant Results**

Element	Weight %	Atomic %	Net Int.	Error %	Kratio	Z	R	A	F
O K	42.96	58.31	784.20	9.27	0.15	1.07	0.97	0.33	1
AlK	10.87	8.75	650.85	4.85	0.09	0.94	1.01	0.81	1.02
SiK	33.46	25.88	1,892.38	3.96	0.26	0.96	1.02	0.81	1
K K	12.71	7.06	407.58	4.44	0.11	0.89	1.04	0.93	1

EDS Spot 6

kV: 15      Mag: 249      Takeoff: 35.5      Live Time(s): 10      Amp Time(μs): 12.8      Resolution:(eV) 126.7

EDS Spot 6



Lsec: 10.0 0 Cnts 0.000 keV Det: Apollo X-SDD Det

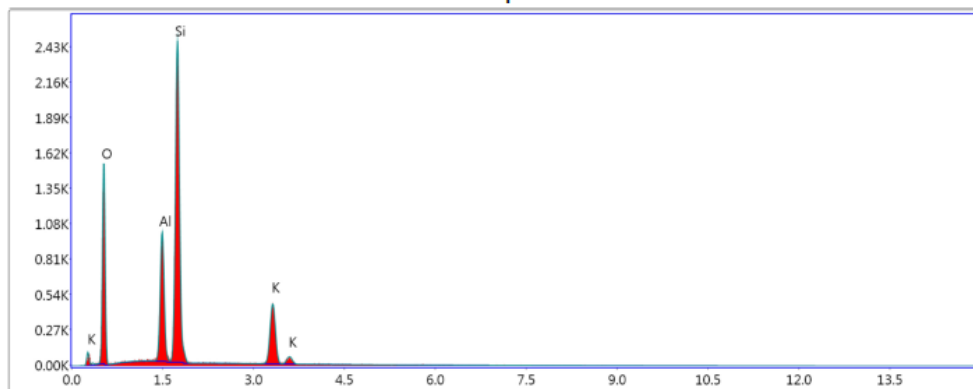
**eZAF Smart Quant Results**

Element	Weight %	Atomic %	Net Int.	Error %	Kratio	Z	R	A	F
O K	49.20	62.96	1,210.07	7.69	0.23	1.05	0.98	0.45	1
Si K	50.80	37.04	3,119.06	2.89	0.43	0.95	1.02	0.9	1

## EDS Spot 7

kV: 15      Mag: 249      Takeoff: 35.5      Live Time(s): 10      Amp Time(μs): 12.8      Resolution:(eV) 126.7

## EDS Spot 7



Lsec: 10.0 0 Cnts 0.000 keV Det: Apollo X-SDD Det

**eZAF Smart Quant Results**

Element	Weight %	Atomic %	Net Int.	Error %	Kratio	Z	R	A	F
O K	42.71	58.18	821.38	9.31	0.15	1.07	0.97	0.32	1
AlK	11.42	9.23	733.86	4.77	0.09	0.95	1.01	0.81	1.02
SiK	32.15	24.95	1,944.30	4.03	0.25	0.97	1.01	0.81	1
K K	13.72	7.65	473.80	4.30	0.11	0.89	1.04	0.94	1

TR section at 69.8 ft.:

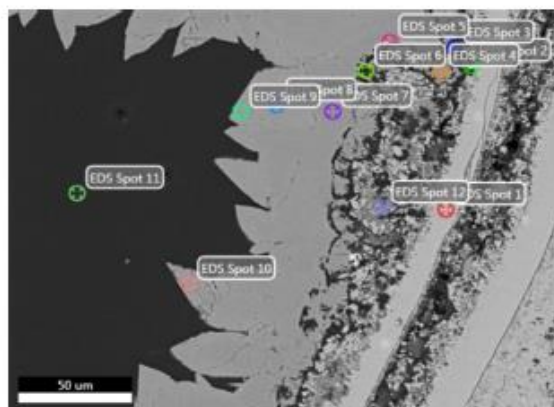
## EDAX TEAM

Page 1

### Pennsylvanian

Author: segenhoff  
Creation: 8/15/2013  
Sample Name: KH-46-377.70

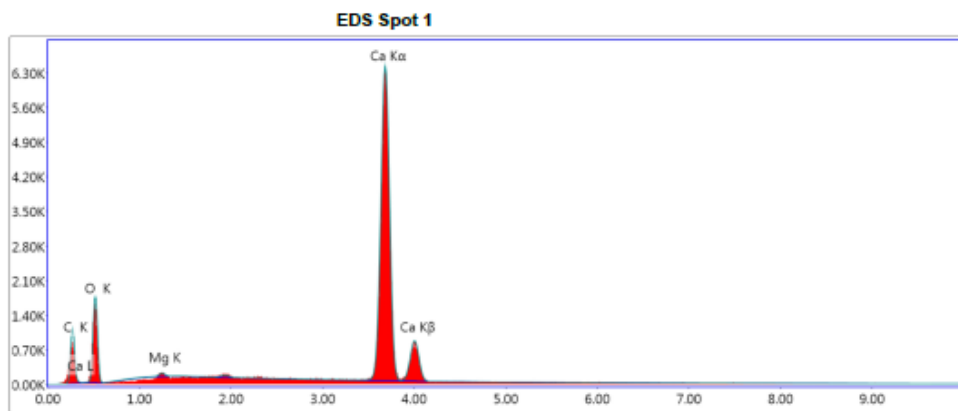
#### Area 6



Notes:

EDS Spot 1

kV: 15      Mag: 673      Takeoff: 35.6      Live Time(s): 30      Amp Time(μs): 3.2      Resolution:(eV) 128



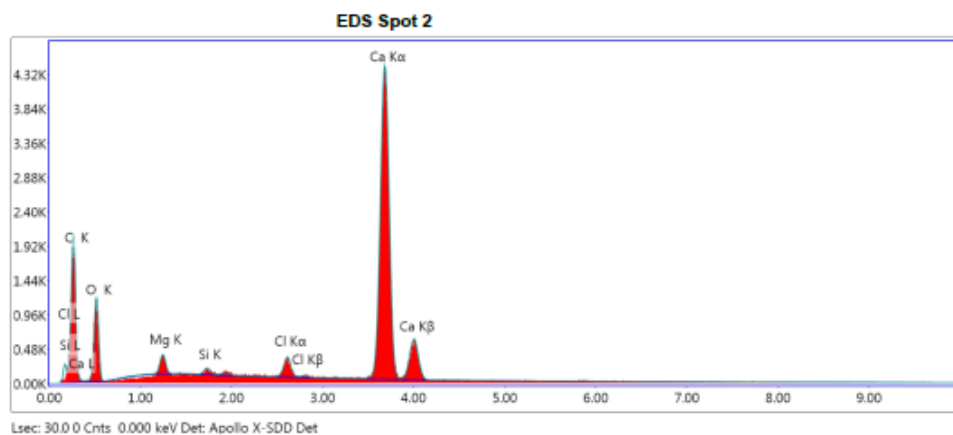
Lsec: 30.00 Cnts 0.000 keV Det: Apollo X-SDD Det

**eZAF Smart Quant Results**

Element	Weight %	Atomic %	Net Int.	Error %
C K	8.38	16.66	175.89	7.6
O K	31.97	47.71	332.11	11.02
MgK	0.23	0.22	14.15	26.99
CaK	59.42	35.4	2389.09	2.04

## EDS Spot 2

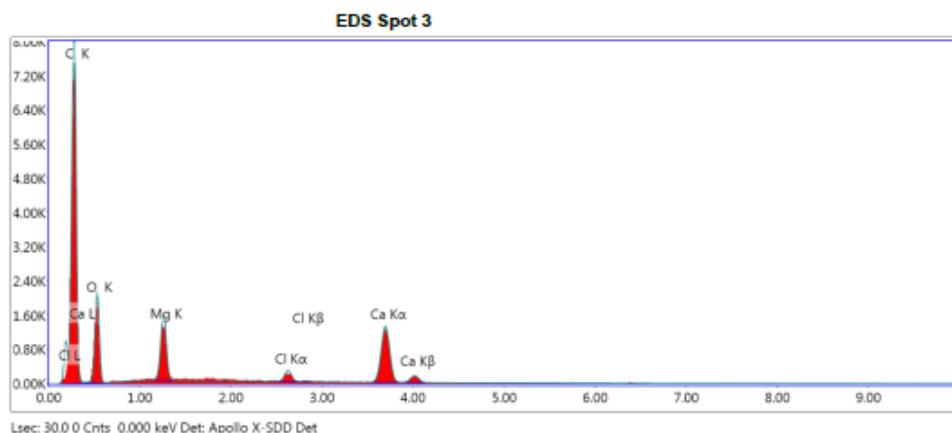
kV: 15      Mag: 673      Takeoff: 35.6      Live Time(s): 30      Amp Time(μs): 3.2      Resolution:(eV) 128

**eZAF Smart Quant Results**

Element	Weight %	Atomic %	Net Int.	Error %
C K	19.87	35.43	305.54	7.77
O K	26.34	35.25	223.44	11.51
MgK	1.15	1.01	60.88	9.78
SiK	0.3	0.23	20.24	17.74
ClK	1.6	0.97	87.72	9.44
CaK	50.73	27.11	1636.03	2.11

EDS Spot 3

kV: 15      Mag: 673      Takeoff: 35.6      Live Time(s): 30      Amp Time(μs): 3.2      Resolution:(eV) 128

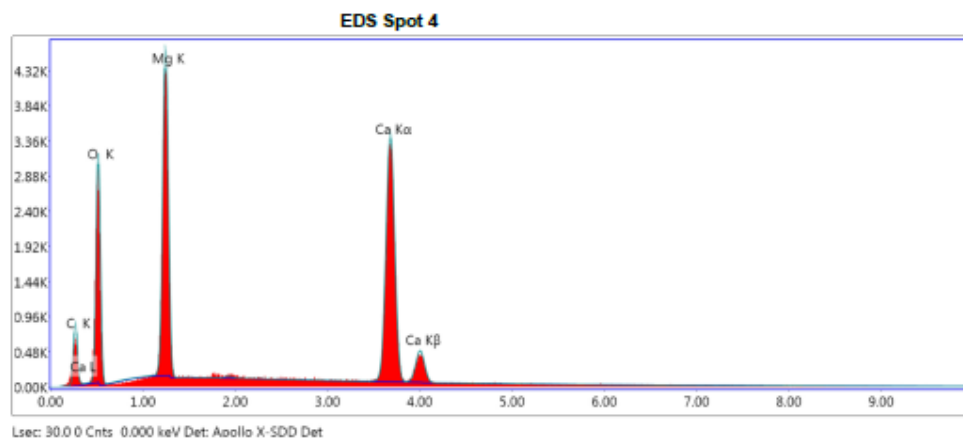


**eZAF Smart Quant Results**

Element	Weight %	Atomic %	Net Int.	Error %
C K	55.96	68.2	1274.68	6.4
O K	26.54	24.28	402.93	10.38
MgK	4.55	2.74	360.74	5.53
ClK	1.29	0.53	86.74	7.09
CaK	11.66	4.26	489	2.87

## EDS Spot 4

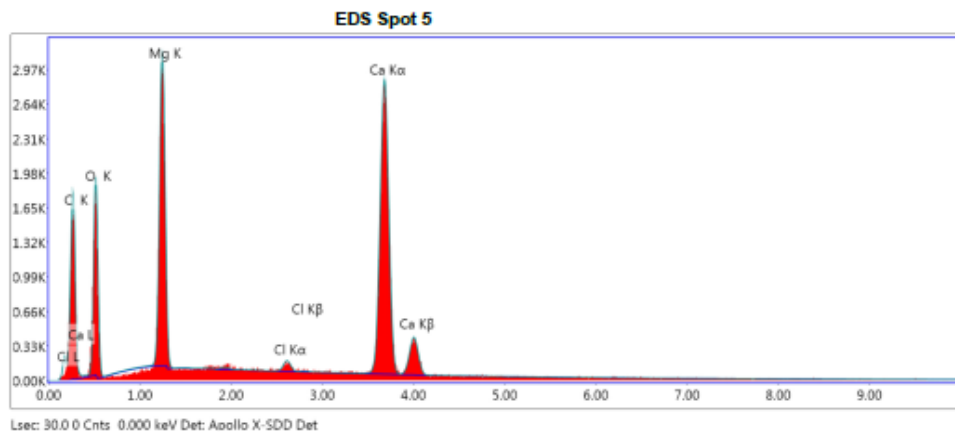
kV: 15      Mag: 673      Takeoff: 35.6      Live Time(s): 30      Amp Time(μs): 3.2      Resolution:(eV) 128

**eZAF Smart Quant Results**

Element	Weight %	Atomic %	Net Int.	Error %
C K	9.81	16.91	135.3	9.59
O K	39.73	51.42	596.71	10.04
MgK	16.72	14.24	1082.98	5.63
CaK	33.74	17.43	1265.99	2.25

EDS Spot 5

kV: 15      Mag: 873      Takeoff: 35.6      Live Time(s): 30      Amp Time(μs): 3.2      Resolution:(eV) 128

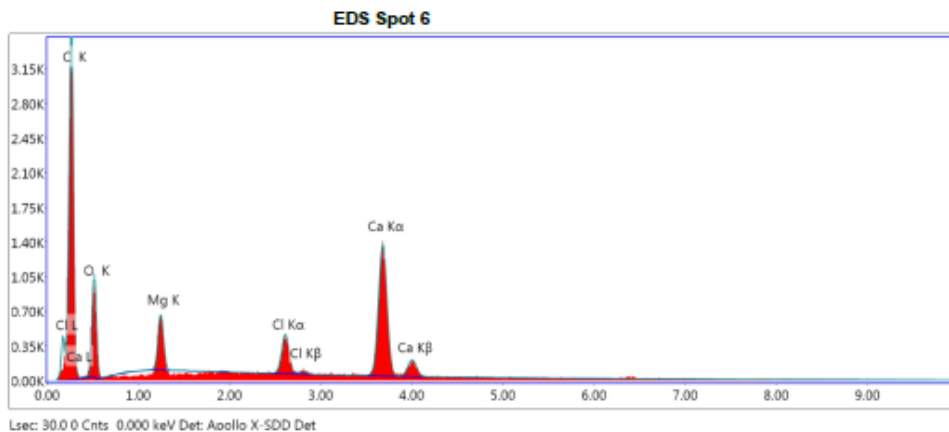


**eZAF Smart Quant Results**

Element	Weight %	Atomic %	Net Int.	Error %
C K	21.11	34.13	267.8	8.64
O K	32.27	39.16	361.55	10.51
MgK	12.98	10.37	725.86	5.63
ClK	0.62	0.34	31.87	13.18
CaK	33.01	15.99	1050.32	2.28

EDS Spot 6

kV: 15      Mag: 673      Takeoff: 35.6      Live Time(s): 30      Amp Time(μs): 3.2      Resolution:(eV) 128

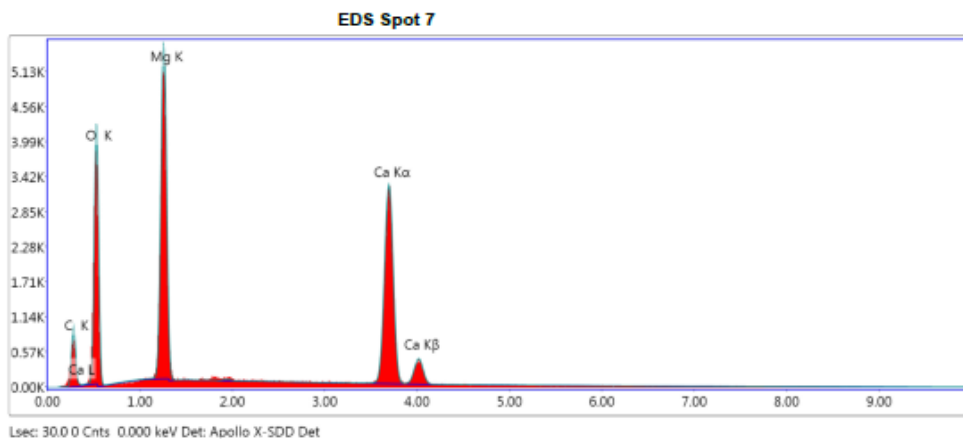


**eZAF Smart Quant Results**

Element	Weight %	Atomic %	Net Int.	Error %
C K	47.48	62.94	521.72	7.6
O K	25.5	25.38	198.9	11.26
MgK	3.01	1.97	131.8	7.02
ClK	3.31	1.49	129.19	5.46
CaK	20.71	8.23	495.05	2.81

EDS Spot 7

kV: 15      Mag: 673      Takeoff: 35.8      Live Time(s): 30      Amp Time(μs): 3.2      Resolution:(eV) 128

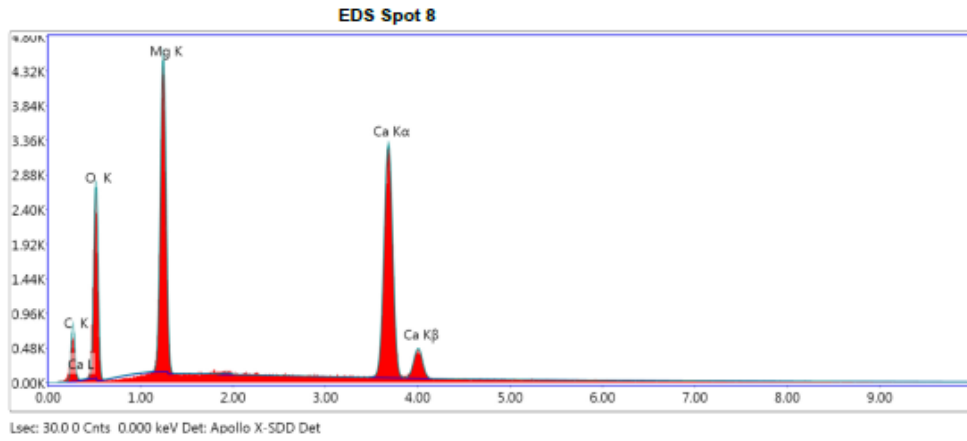


**eZAF Smart Quant Results**

Element	Weight %	Atomic %	Net Int.	Error %
C K	10.35	17.22	155.58	9.41
O K	43	53.71	806.05	9.89
MgK	17.97	14.77	1314.67	5.52
CaK	28.67	14.3	1203.65	2.28

EDS Spot 8

kV: 15      Mag: 673      Takeoff: 35.6      Live Time(s): 30      Amp Time(μs): 3.2      Resolution:(eV) 128

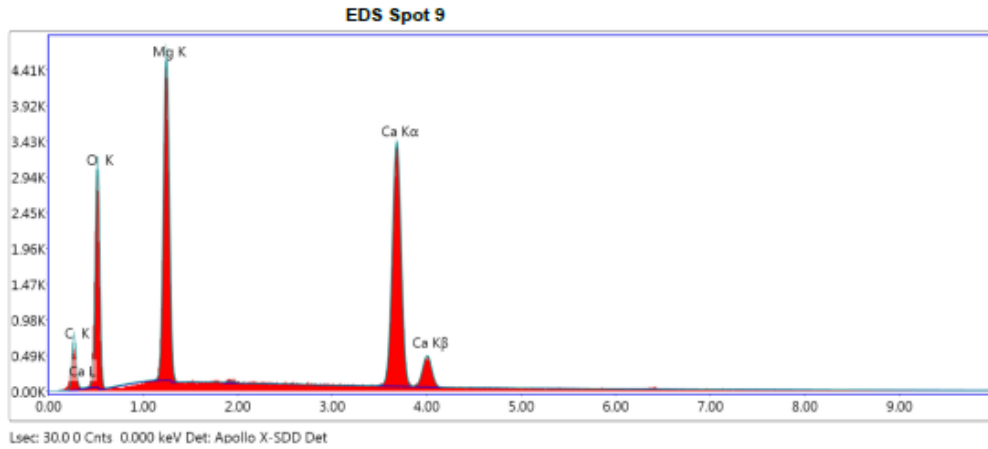


**eZAF Smart Quant Results**

Element	Weight %	Atomic %	Net Int.	Error %
C K	10.05	17.46	127.69	9.7
O K	37.92	49.47	522.36	10.13
MgK	17.65	15.16	1077	5.6
CaK	34.38	17.9	1206.99	2.27

EDS Spot 9

kV: 15      Mag: 673      Takeoff: 35.6      Live Time(s): 30      Amp Time(μs): 3.2      Resolution:(eV) 128

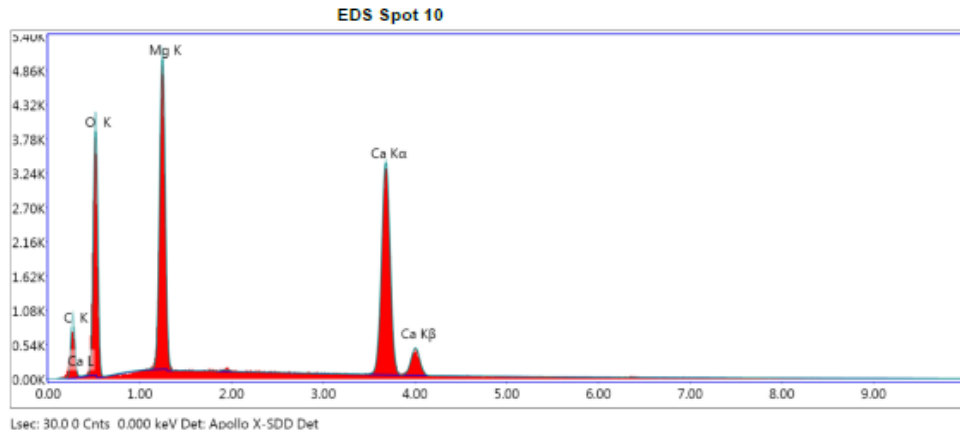


**eZAF Smart Quant Results**

Element	Weight %	Atomic %	Net Int.	Error %
C K	9.08	15.7	122.21	9.74
O K	40.07	52.1	603.08	10.01
MgK	17.25	14.76	1107.91	5.62
CaK	33.61	17.44	1249.09	2.26

EDS Spot 10

kV: 15      Mag: 673      Takeoff: 35.6      Live Time(s): 30      Amp Time(μs): 3.2      Resolution:(eV) 128



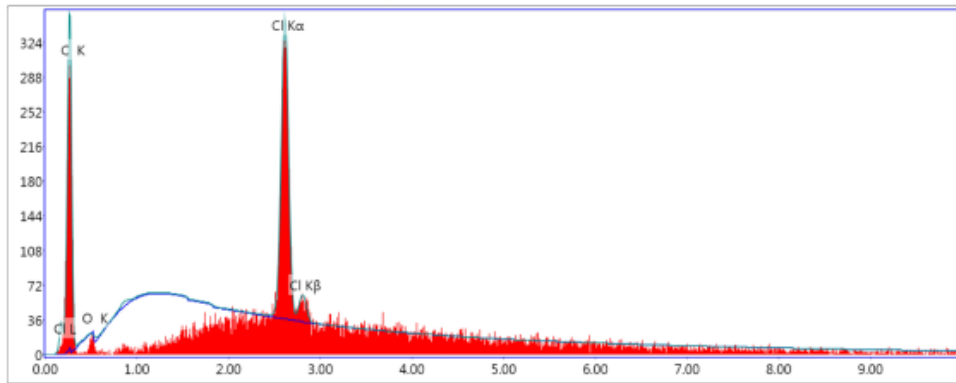
**eZAF Smart Quant Results**

Element	Weight %	Atomic %	Net Int.	Error %
C K	10.6	17.67	164.31	9.28
O K	42.95	53.72	788.94	9.75
MgK	16.74	13.78	1222.63	5.58
CaK	29.71	14.84	1254.01	2.24

EDS Spot 11

kV: 15      Mag: 673      Takeoff: 35.6      Live Time(s): 30      Amp Time(μs): 3.2      Resolution:(eV) 128

EDS Spot 11



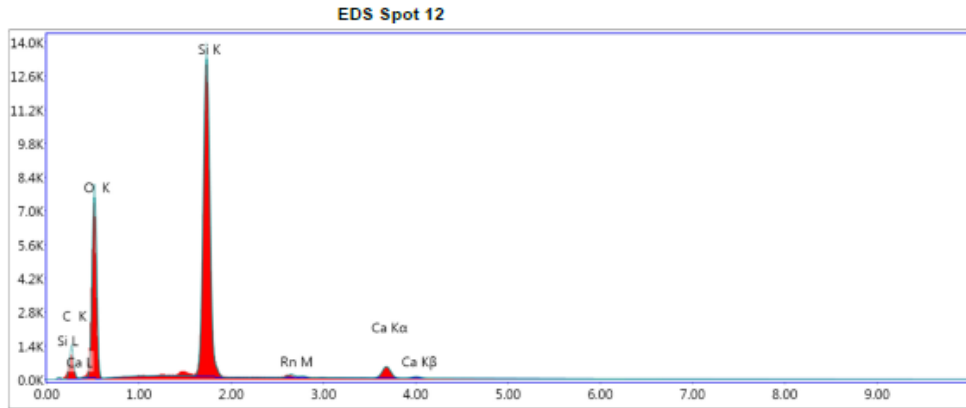
Lsec: 30.0 0 Cnts 0.000 keV Det: Apollo X-SDD Det

eZAF Smart Quant Results

Element	Weight %	Atomic %	Net Int.	Error %
C K	80.36	92.33	53.73	12.2
O K	0.04	0.04	0.04	9.85
Cl K	19.6	7.63	100.5	5.47

EDS Spot 12

kV: 15      Mag: 673      Takeoff: 35.8      Live Time(s): 30      Amp Time(μs): 3.2      Resolution:(eV) 128

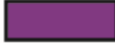
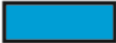


Lsec: 30.0 0 Cnts 0.000 keV Det: Apollo X-SDD Det

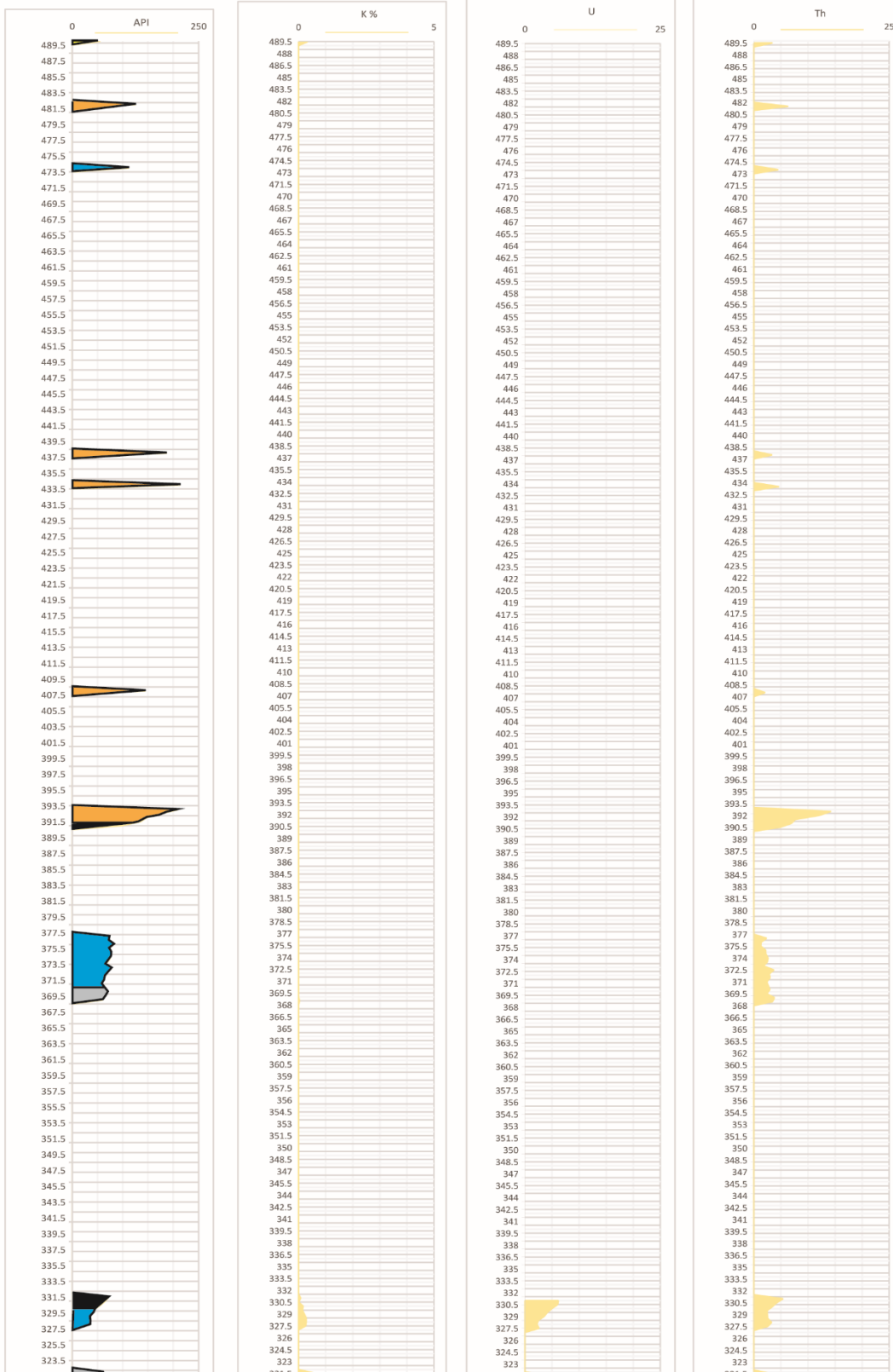
**eZAF Smart Quant Results**

Element	Weight %	Atomic %	Net Int.	Error %
C K	20.48	30.21	220.7	10.68
O K	44.03	48.76	1527.14	8.47
Si K	30.82	19.44	3691.64	2.71
Rn M	1.31	0.1	41.11	13.89
Ca K	3.35	1.48	177.1	4.81

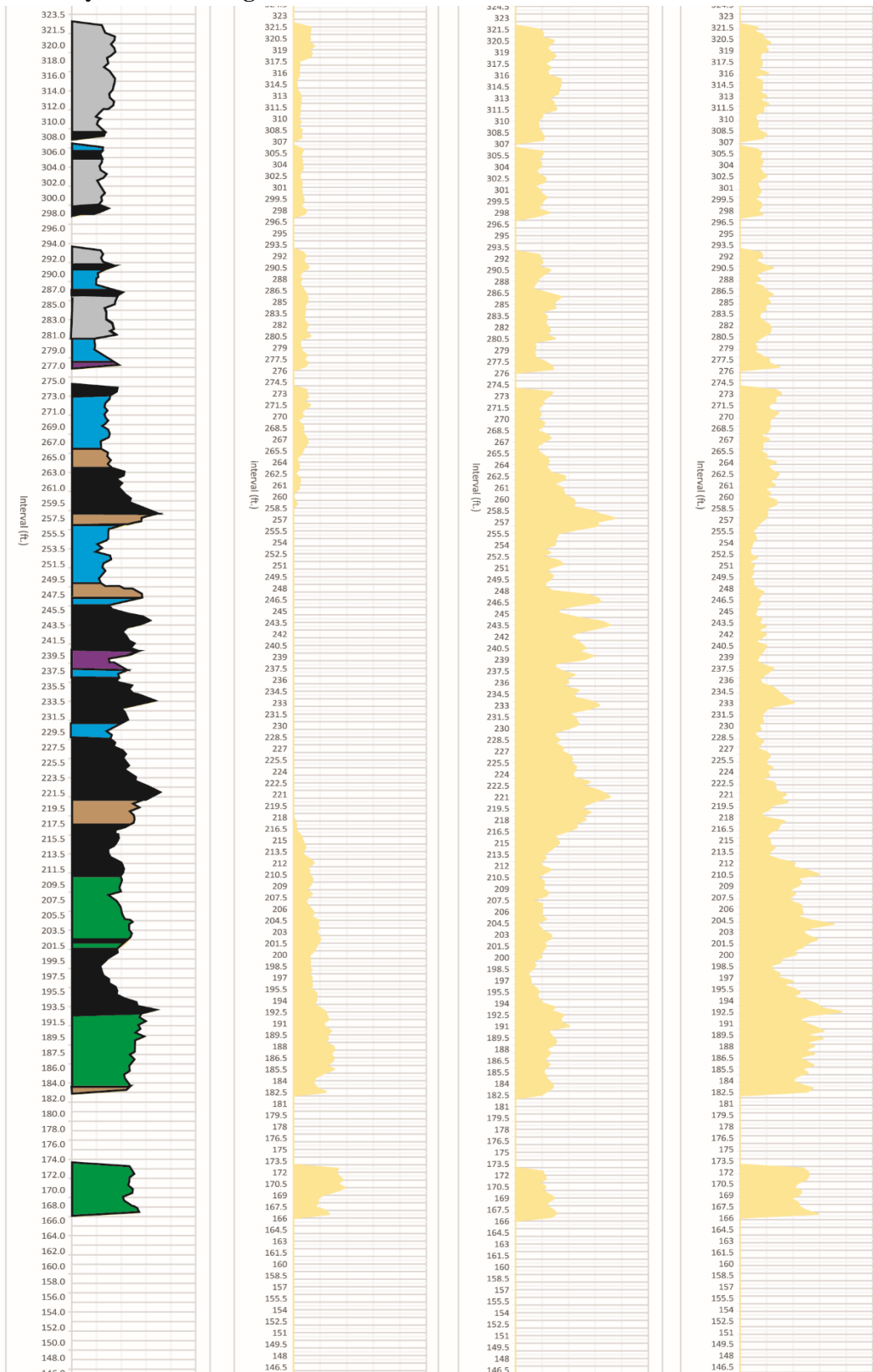
## APPENDIX 8: GAMMA RAY CURVES

Legend			
Facies 1/2		Facies 6	
Facies 3		Facies 8/13	
Facies 4		Facies 10-12	
Facies 5		Facies 14	

# Coal Mine Canyon section: Page 1 of 3



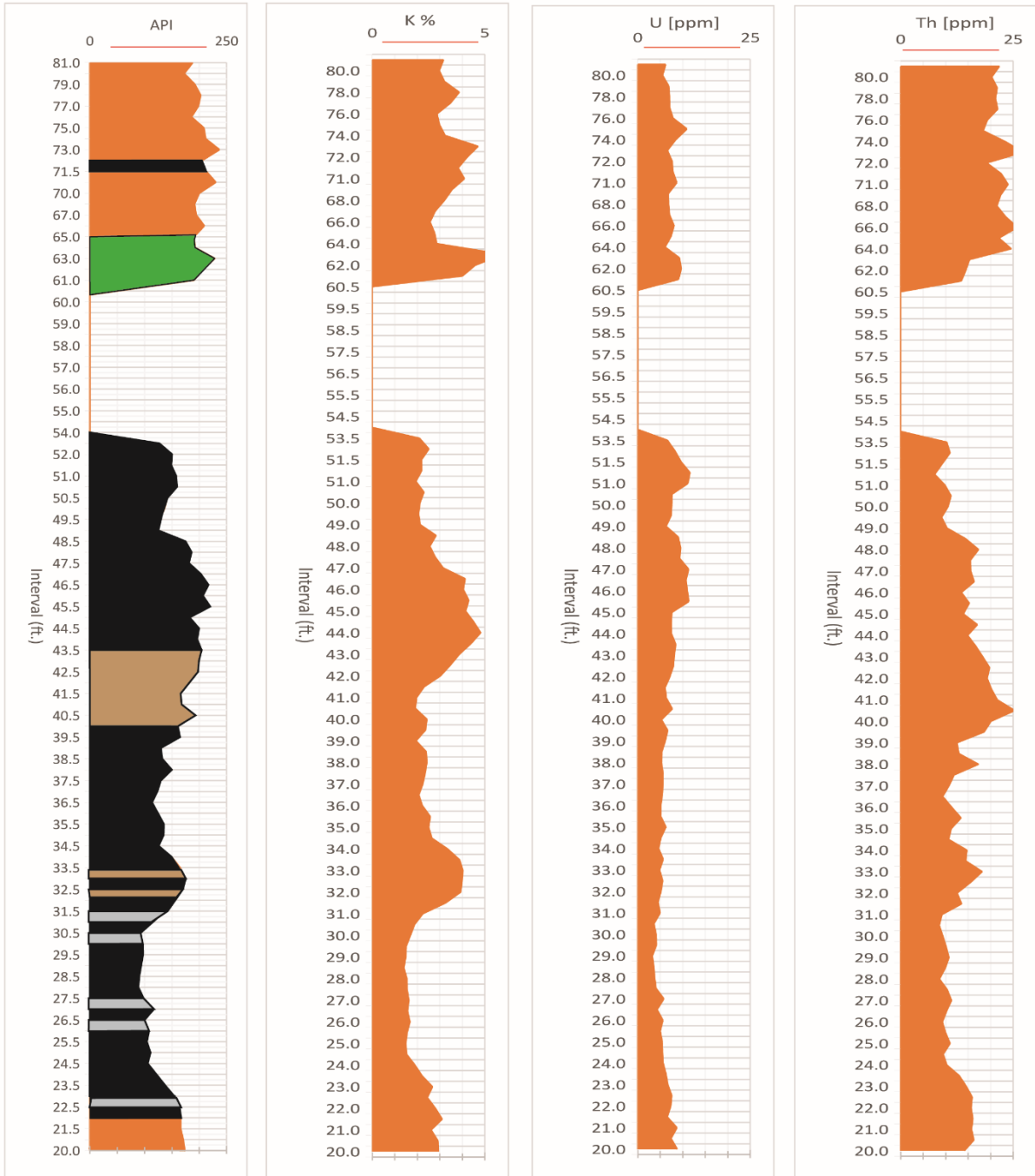
# Coal Mine Canyon section: Page 2 of 3



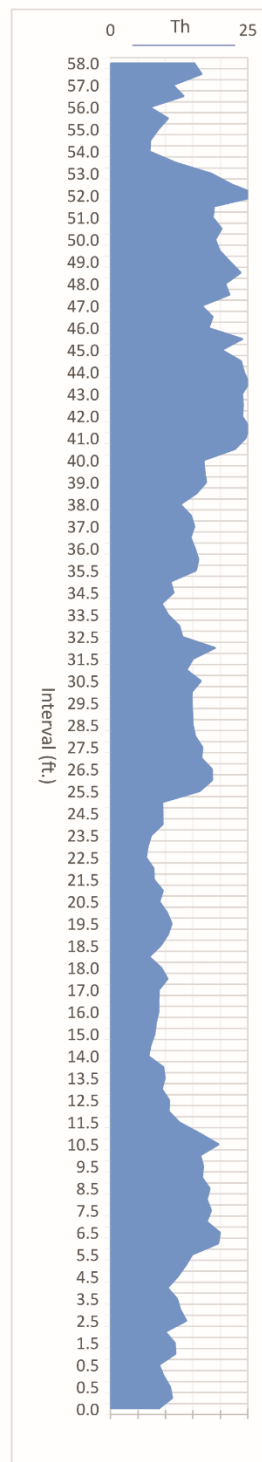
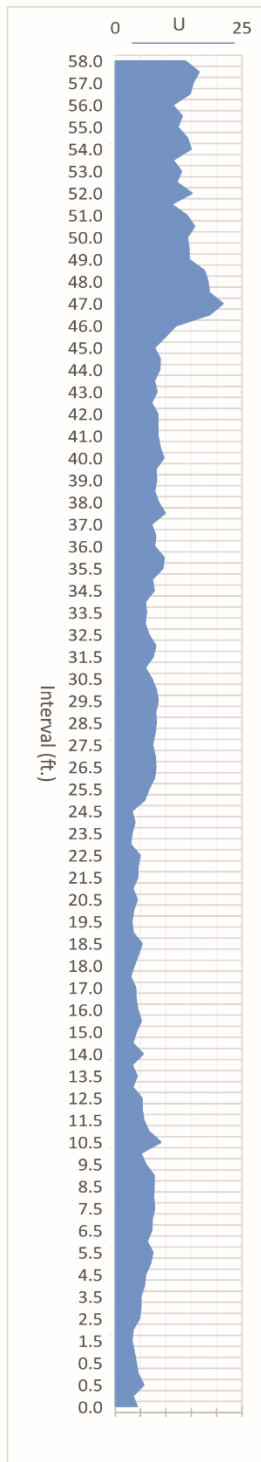
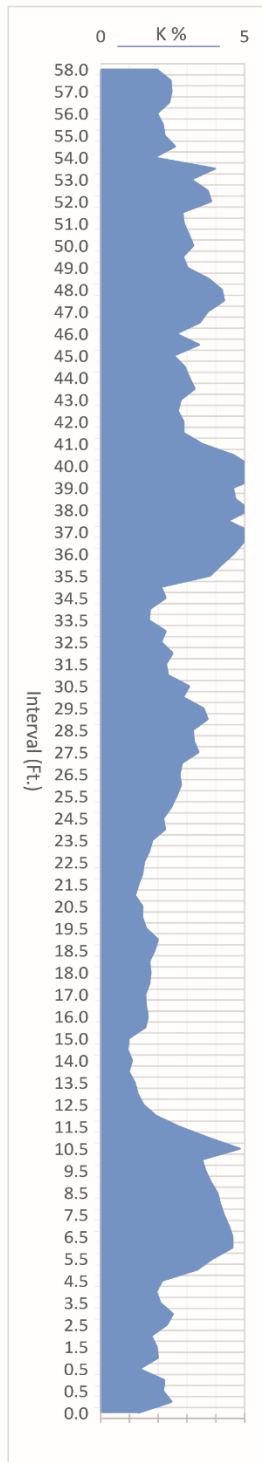
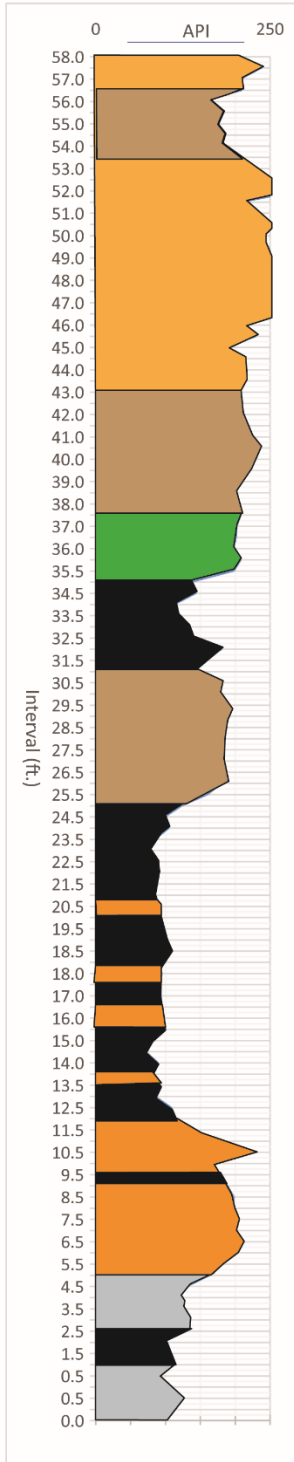
Coal Mine Canyon section: Page 3 of 3



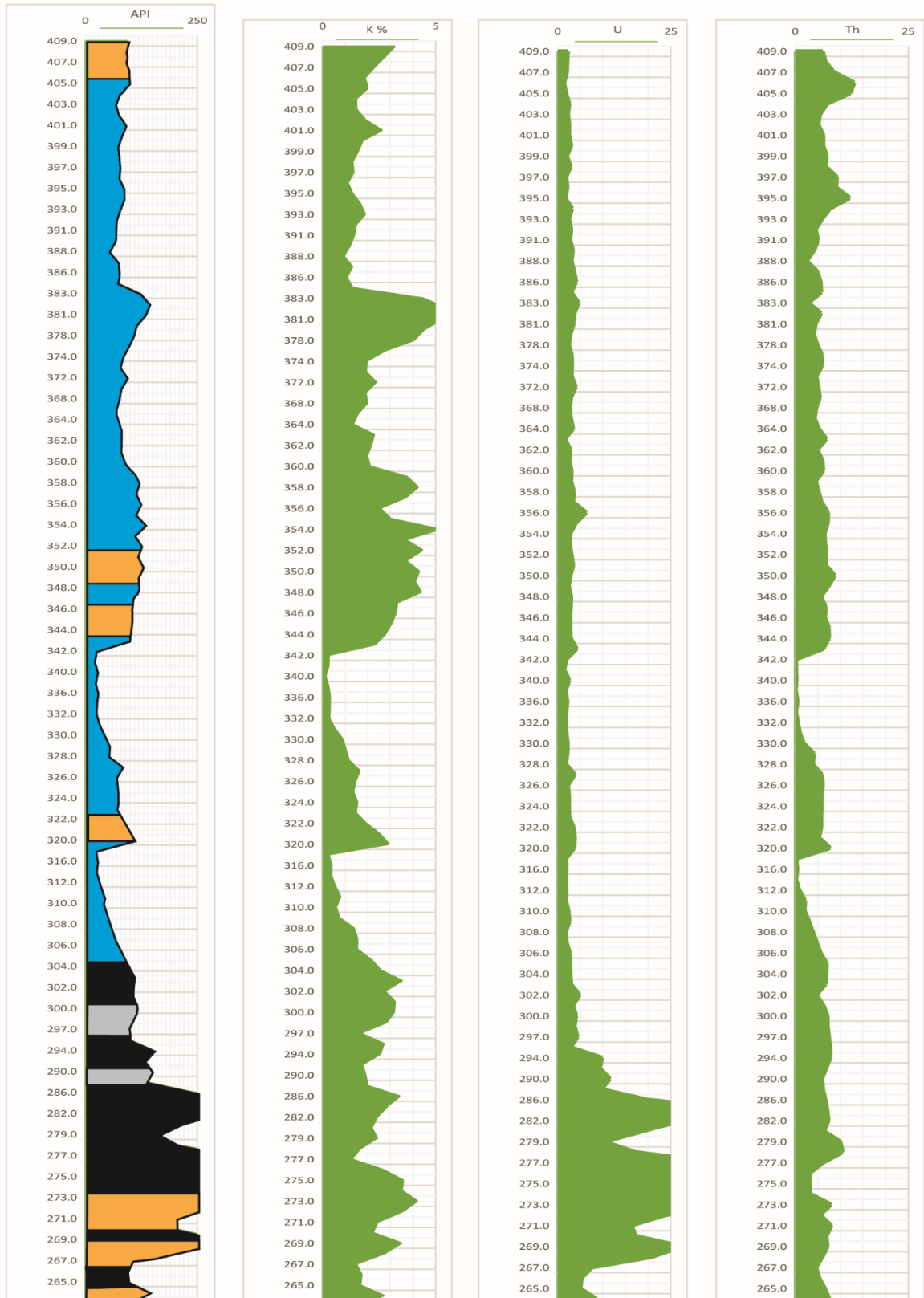
**Elko Hills A Section:**



**Elko Hills B section:**

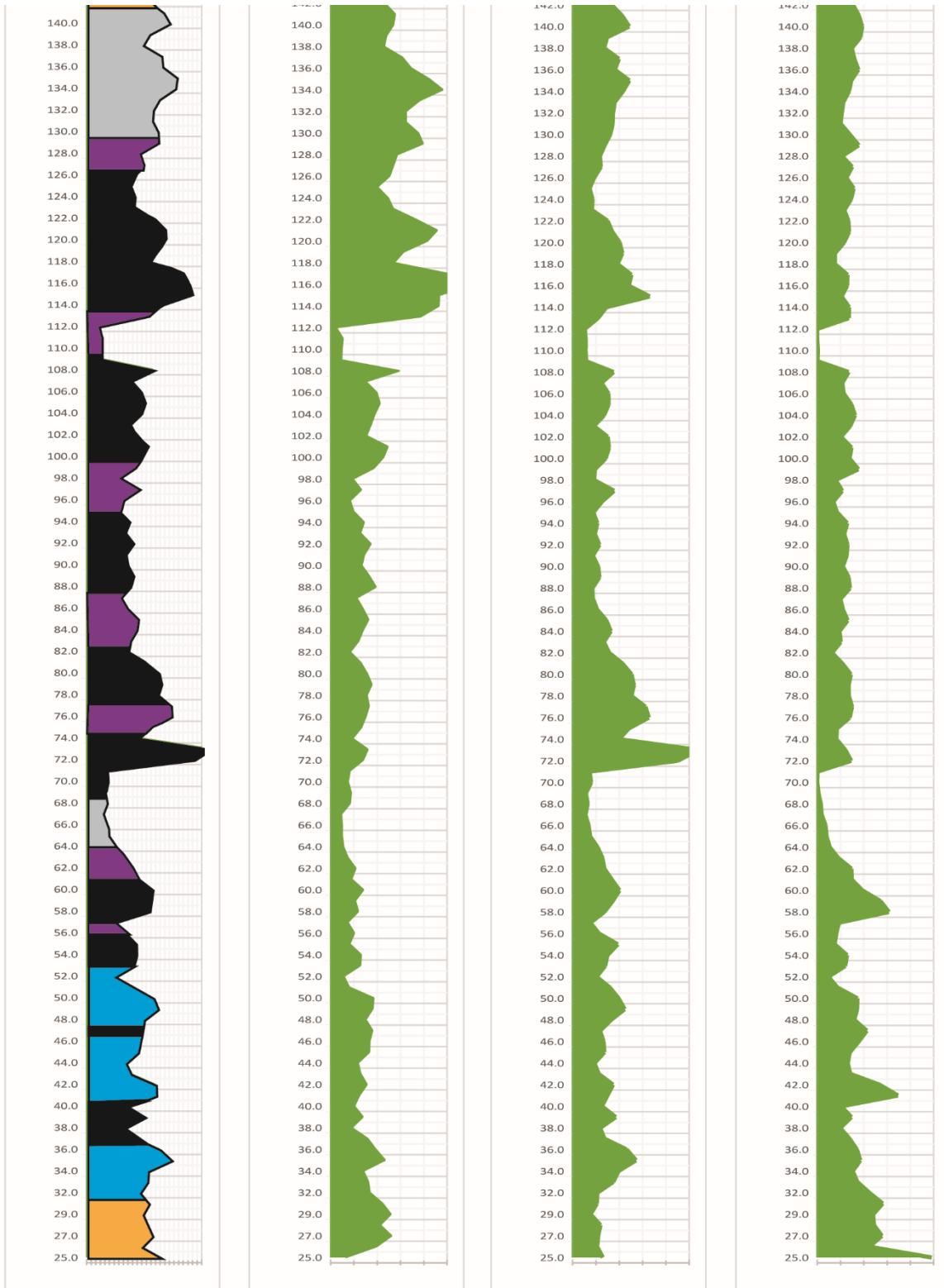


Tomera Ranch Section: Page 1 of 3

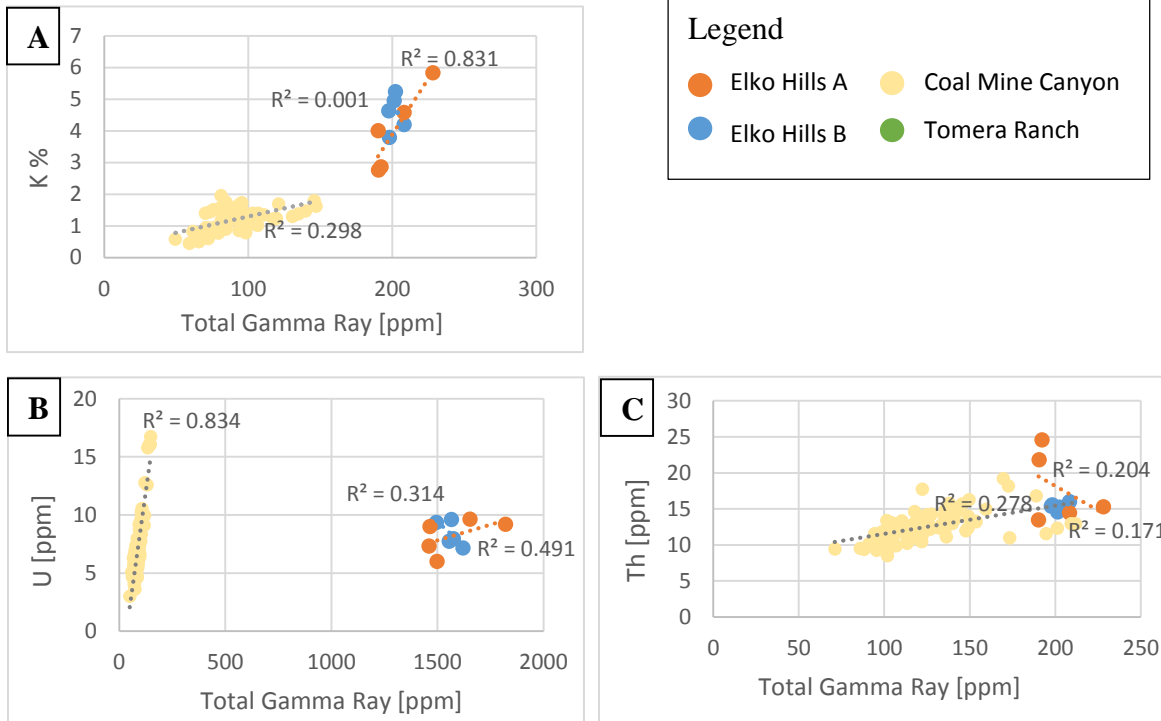




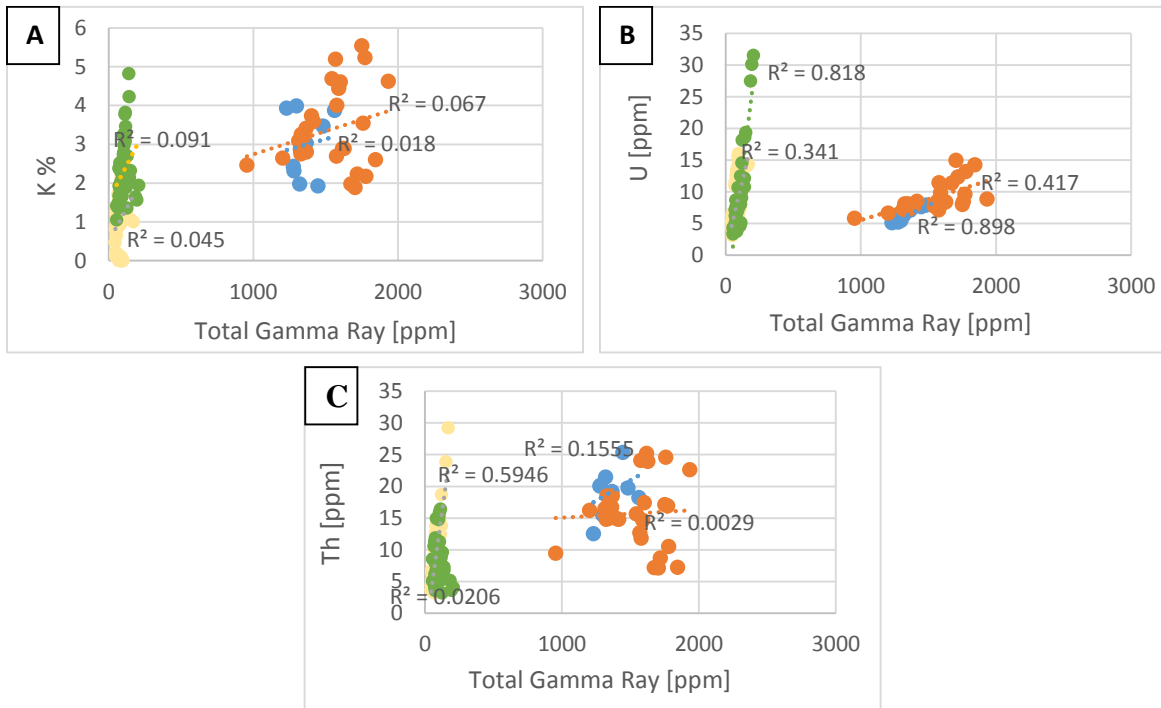
Tomera Ranch Section: Page 3 of 3



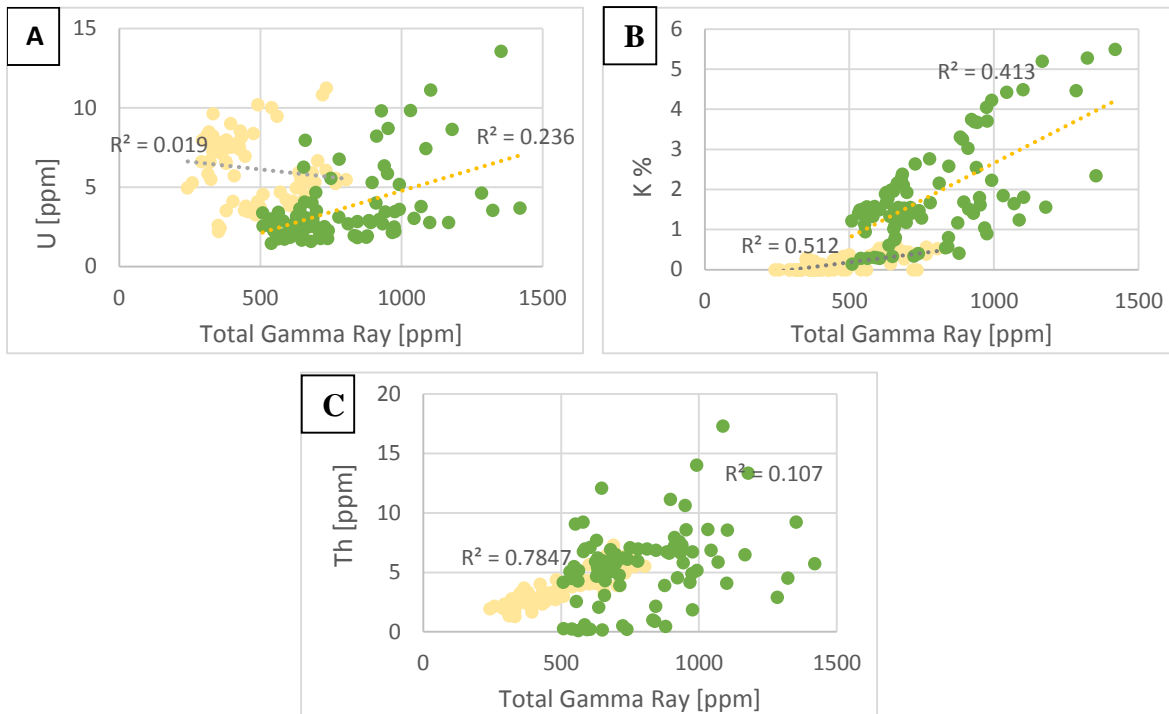
**APPENDIX 9: CROSS-PLOTS (K, U, & TH VS. TOTAL GAMMA RAY)**



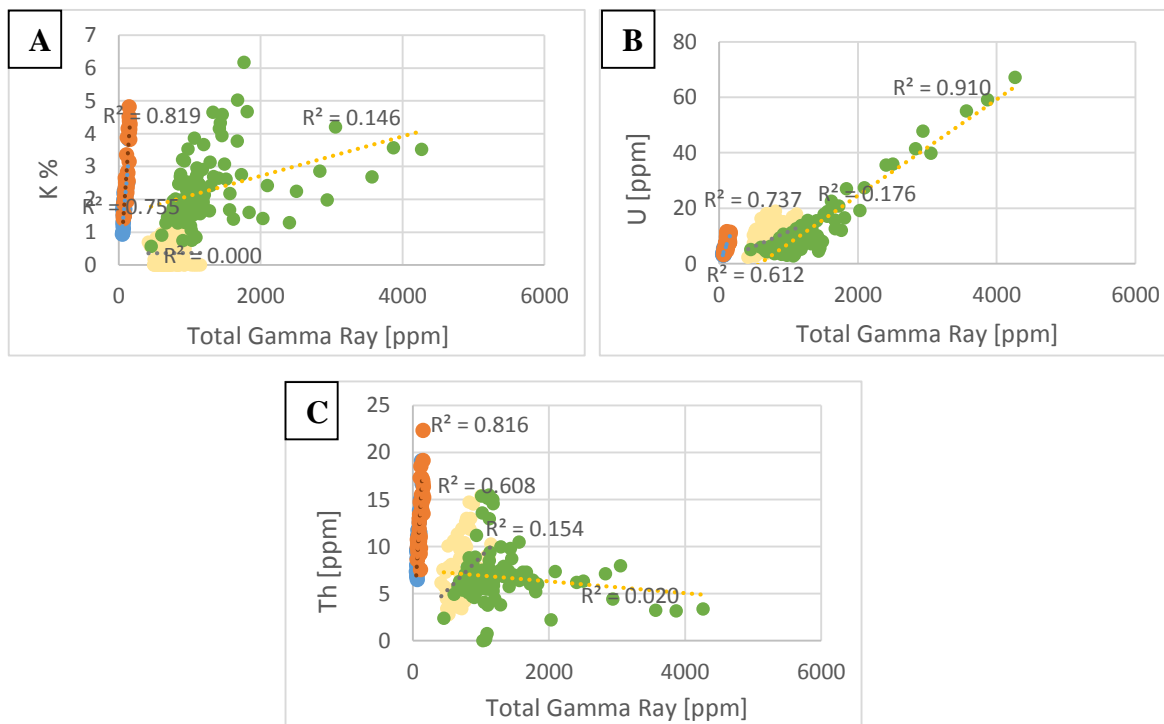
**Figures 24A-C: Facies 1/2**



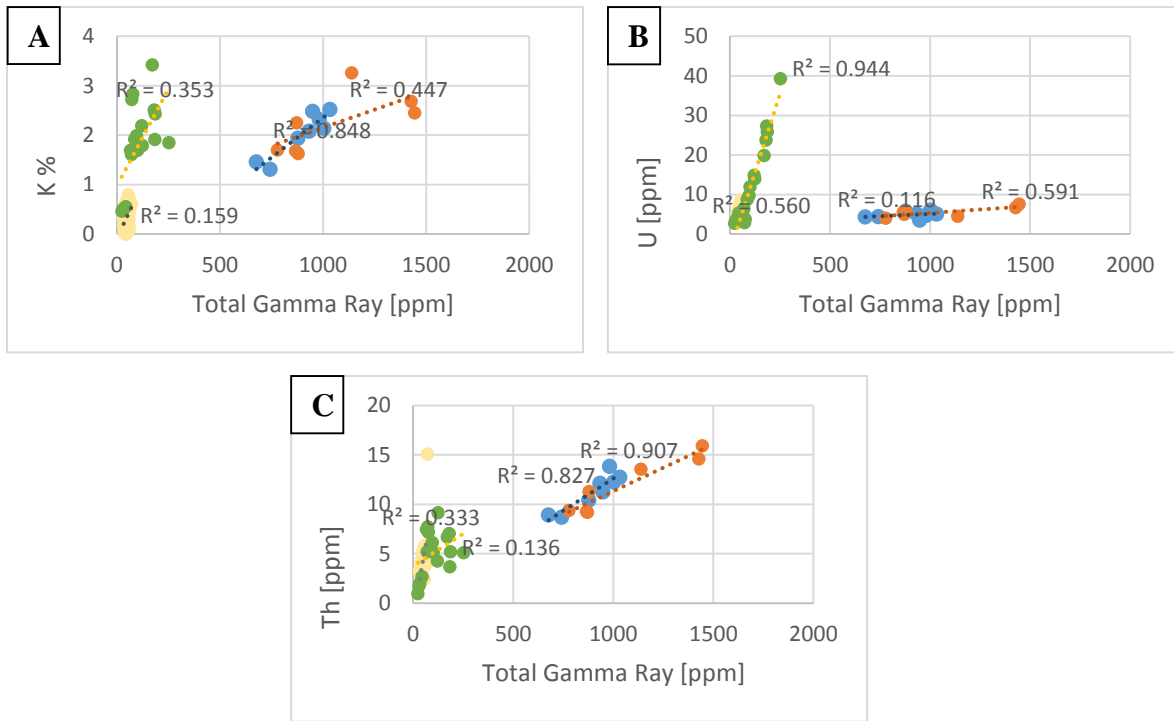
**Figures 25A-C: Facies 3**



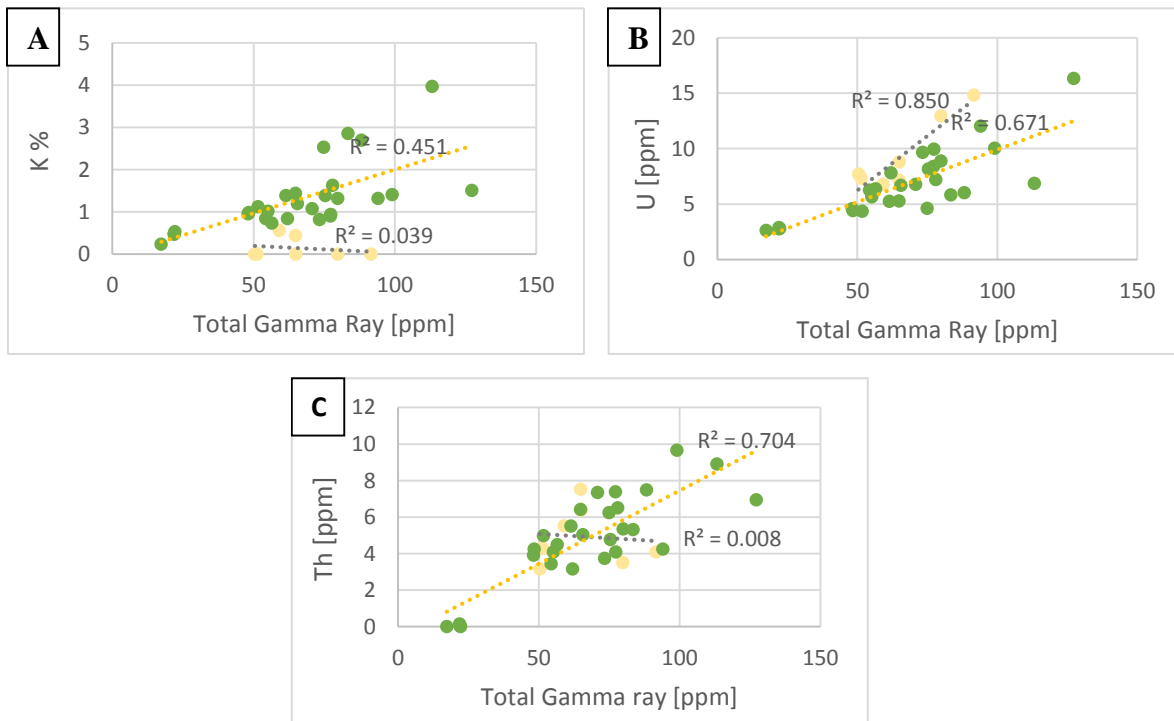
**Figures 26A-C: Facies 4**



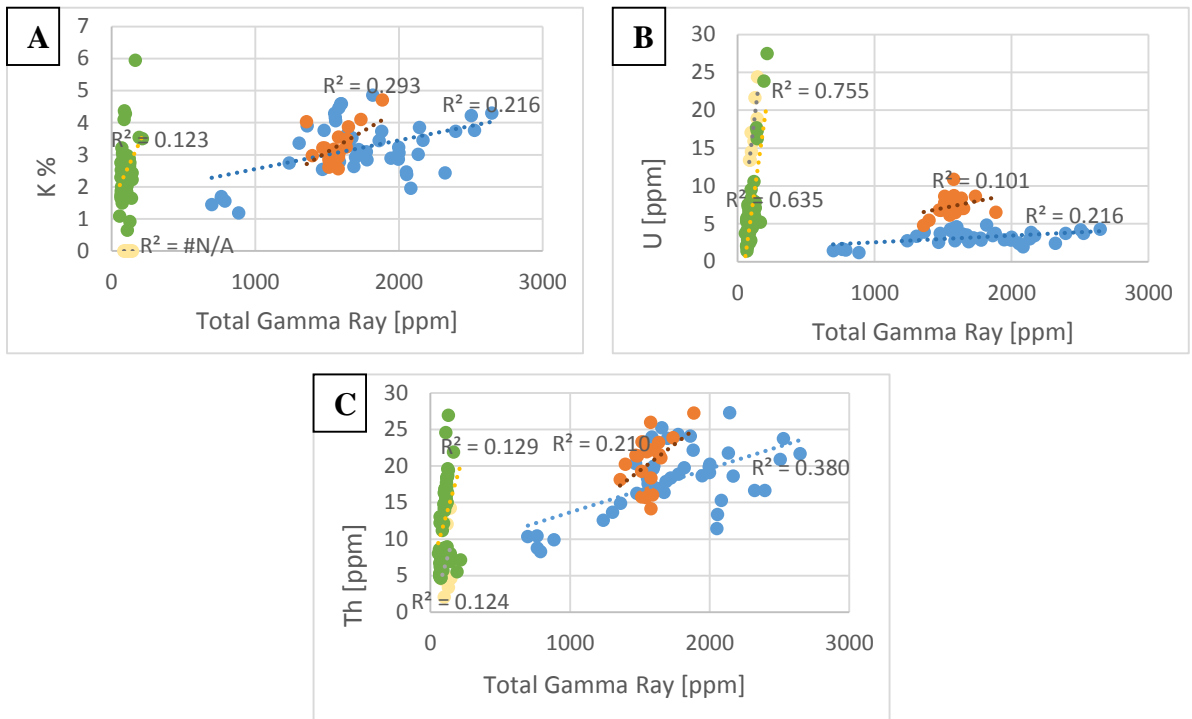
**Figures 27A-C: Facies 5**



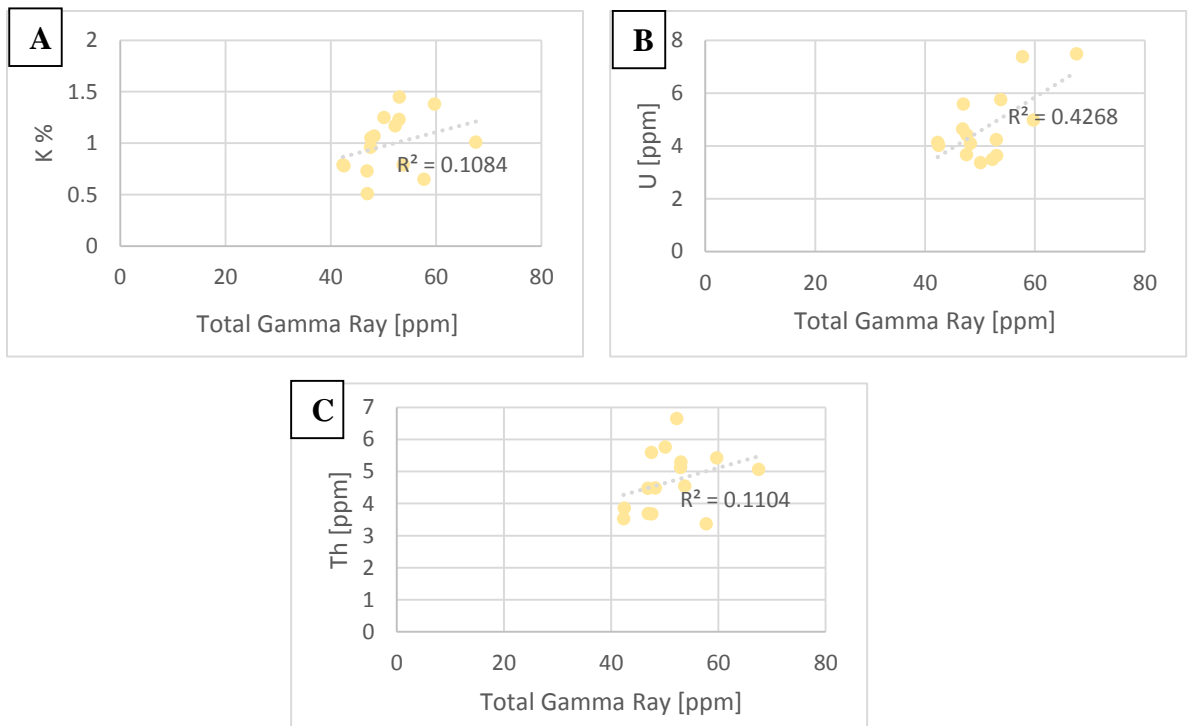
**Figures 28A-C: Facies 6**



**Figures 29A-C: Facies 8/13**



**Figures 30A-C:** Facies 10-12



**Figures 31A-C:** Facies 14